Elucidation of Novel Regulatory Pathways in Melanogenesis and Melanomagenesis





H. Matthew Berns

Supervised by:

Professor Colin Goding, Dr. Pedro Moura-Alves, and Dr. William J. Pavan

University of Oxford (UK) / National Institutes of Health (USA)

Green Templeton College / Oxford-Cambridge Scholars Program

A thesis submitted for the degree of:

Doctor of Philosophy

Hilary Term 2024

Disclaimer

I declare that this submission is my own written work. To the best of my knowledge, it contains no material that has been written by another as academic work, to this or any other university. The results presented herein derive from my own experiments, except for the TBX3 ChIP-seq experiment which was performed by Drs. Sizhu Lu and Pakavarin Louphrasitthiphol (University of Oxford) but analysed in their entirety by H. Matthew Berns.

Excerpts and/or modified text, tables, and figures featured in this thesis have been previously published in a peer-reviewed scientific journal as follows:

H. Matthew Berns, Dawn E. Watkins-Chow, Sizhu Lu, Pakavarin Louphrasitthiphol, Tongwu Zhang, Kevin M. Brown, Pedro Moura-Alves, Colin R. Goding, William J. Pavan. 2024. Single-cell profiling of MC1R-inhibited melanocytes. Pigment Cell and Melanoma Research. DOI: 10.1111/pcmr.13141

A link to the full text of the published manuscript can be found in Appendix C.

H. Matthew Berns

Trinity Term 2024

Abstract

Elucidation of Novel Regulatory Pathways in Melanogenesis and Melanomagenesis

H. Matthew Berns, Green Templeton College

D.Phil. Biomedical Sciences, Hilary Term 2024

The migration of human populations toward extreme latitudes precipitated the evolutionary selection of genetic variants which yielded skin colour alterations that maximize the absorption of ultraviolet radiation (UVR) needed for Vitamin D3 synthesis. A prime example of this phenomenon is represented by loss-of-function (LOF) coding variants in the *Melanocortin 1 receptor* (*MC1R*) associated with the Red Hair Colour (RHC) trait characterized by red hair, fair skin, high naevus count, and poor tanning ability. The human RHC trait is facilitated by high amounts of phaeomelanin (red-yellow), and reduced eumelanin (black-brown), pigment in skin and hair due to diminished MC1R function. Importantly, the RHC trait is strongly linked to increased skin cancer risk, including melanoma, a highly aggressive form of cancer arising from pigment producing cells known as melanocytes. Despite these known associations, the mechanisms surrounding the impact of RHC on skin colour and cancer are poorly understood. More specifically, it is unclear how decreased MC1R signalling drives phaeomelanogenesis and increases melanoma susceptibility. In this thesis, I first use single-cell RNA-sequencing (scRNA-seq) to define the transcriptomes of murine melanocytes which are primarily phaeomelanotic, have MC1R-inhibition and mimic the human RHC trait, or eumelanotic, have active MC1R signalling. I then defined the ‘MC1R-inhibited Gene Signature (MiGS)’ which comprises a large set of previously unidentified genes that may be implicated in melanogenesis and oncogenic transformation. Using this new dataset, I further

investigated one such candidate MiGS gene, *Tbx3*, which encodes a well-known anti-senescence transcription factor (TF) implicated in melanoma progression and showed that TBX3 can bind E-box and T-box elements to regulate genes associated with melanogenesis and senescence bypass. Furthermore, I show that TBX3, and its subfamily member TBX2, bind and regulate (B&R) unique target genes in melanoma despite the high degree of homology that exists between their DNA binding domains. Collectively, these results provide key insights into previously unidentified mechanisms by which individuals with the RHC phenotype produce phaeomelanin and are predisposed to melanoma.

Acknowledgements

To Bill, Colin, Dawn, and Pedro, I cannot thank each of you enough for your continued support throughout this journey. This has been a remarkable time made most by your eagerness and love of science which has fostered an immensely successful collaboration. Your support provided a remarkable learning environment across two fantastic institutions of biomedical research. Most importantly, each of you, in your own unique ways, instilled valuable lessons which I will continue to implement and convey throughout my career as a physician-scientist.

To members of the Pavan and Goding labs, thank you for both welcoming me with open arms and supporting me both in and outside of the lab.

To the support and core facility personnel at the National Human Genome Research Institute, especially Abdel Elkahloun (Microarray Core), Stacie Anderson and Martha Kirby (Flow Cytometry Core), and Ludwig Institute for Cancer Research, for assisting me immensely with experiments.

To my family and friends, thank you for your unwavering encouragement and support. None of this would be possible without you.

To Dr. Steve Brule, a sincere thanks for your clinical expertise and knowledge which has transformed the way I aim to approach medicine.

Last, but not least, a special thanks to Gregg Turkington and, reluctantly, Tim Heidecker, for their (Greg's) insightful movie expertise which has greatly influenced my viewpoint on film, art, and life. The run time of this thesis is incalculable; however, one can only hope that my effort will merit four, possibly even five, bags of popcorn from each of them.

Table of Contents

Disclaimer i

Abstract ii

Acknowledgements iv

Table of Contents v

List of Abbreviations x

Chapter 1: Introduction 1

Overview 2

Melanocyte Development 2

Formation and Emergence of the Neural Crest 3

NCC Migration and Acquisition of the Melanocyte Fate 4

Immature Melanoblast to Differentiated Melanocyte 6

Melanocyte Function 10

Tanning Response 10

Melanosome Maturation and Melanin Synthesis 11

Core Pathways and Molecular Regulators of Melanogenesis 15

Melanoma 18

Incidence 18

Risk Factors 19

Disease Onset and Progression 23

Treatment 29

Aims and Goals of the Thesis 31

Figures 33

Figure 1. Melanocyte Development: Neural Crest to Melanocyte Differentiation and Colonization. 33

Figure 2. Melanogenesis: Function of a Melanocyte. 36

Figure 3. Melanoma Evolution. 37

Chapter 2: Materials and Methods 38

Animal Use and Methods 39

Ethics Statement, Animal Husbandry, and Breeding Scheme 39
Tissue Harvest, Digestion, and Immunostaining 40
Fluorescence-Activated Cell Sorting (FACS) 44
Cell and Molecular Biology Techniques and Methods 45
Cell Culture 45
Immunofluorescence 48
Brightfield Microscopy 51
Single-cell RNA-sequencing of FACS Enriched Cell Population 52
Bulk RNA-sequencing of 501mel Cells (TBX3 Knockdown vs Control) 52
Western Blot Procedure 53
Bioinformatics 56
Single-cell RNA-seq Analysis 56
Gene Ontology and Pathway Analysis 57
Gene Set Enrichment Analysis 58
TBX3 ChIP-seq Analysis 58
Bulk RNA-seq Analysis 60
Analysis of TBX2 Datasets 60
Other 61
Figure Construction 61
Data Availability 62
Chapter 3: Transcriptomic Profiling of MC1R-inhibted Melanocytes Identifies Novel Mediators of Pigment Cell Biology 63
Introduction 64
Results 67
Optimising Tissue Digestion 67
FACS Selection of an Enriched Melanocyte Pool 70
Single-cell RNA-sequencing of FACS Isolated Cells 73
Melanocyte Classification 74
Defining the MC1R-inhibited Gene Signature (MiGS) 75
TGFβ superfamily a Predicted Upstream Regulator of MiGS 78
MiGS Comprises Known and Novel TF/co-TFs of Melanocyte and Melanoma Biology 78
Discussion 81

Novel Pathways within MiGS *82*

Literature Review of TF/co-TFs Found Within MiGS *87*

Conclusions and Future Work *101*

Figures and Tables *103*

Figure 1. Overview of Tissue Digestion and Melanocyte Capture. *103*

Figure 2. Positive Cells selected by FACS are Melanocytes. *105*

Figure 3. Overview of Single-cell Sequencing of Positive Selected FACS Population. *106*

Figure 4. Identification and Classification of Sequenced Cells. *108*

Figure 5. Identification of Analysis Ready Melanocytes. *109*

Figure 6. Heatmap of Scaled Expression Data from the 216 DEGs in Each Cell Grouped by Sample. *111*

Figure 7. Enriched Processes and Pathways Found in the MiGS. *112*

Figure 8. Predicted Upstream Regulators of MiGS Includes TGFβ Superfamily. *114*

Figure 9. Annotated TF/co-TFs Expressed in MiGS. *115*

Figure 10. MiGS TF/co-TF Expression from the Hair-GEL Database. *117*

Figure 11. MiGS TF/co-TF Expression in Melanoma Cell Lines and Patient Samples. *118*

Table 1. Pigmentation Associated Genes Found Within the MC1R-inhbited Gene Signature (MiGS). *120*

Chapter 4: TBX3 Binds and Regulates Genes in Melanogenesis and Senescence Bypass 121

Introduction *122*

Results *125*

TBX3 Binds Genes Associated with Hypopigmentation *125*

TBX3 ChIP Peaks Most Strongly Associate with T-box and E-box Motifs *129*

Pigmentation Genes Regulated by MITF are also Bound by TBX3 ..... *131*

Transcriptional Regulation by TBX3 Includes Both Activation and Repression *132*

MiGS and Cell Cycle Genes and Regulated by TBX3 ..... *134*

Comparison of TBX2/3 Bound and Regulated Genes in Melanoma Cells *135*

Discussion *138*

Figures *145*

Figure 1. Validation of the Inducible TBX3 Cell Line. *145*

Figure 2. Chromatin Binding Analysis Implicates TBX3 as a Regulator of Melanogenesis. *147*

Figure 3. TBX3 Exhibits Enriched Binding at E-box Motifs. *148*

Figure 4. TBX3 Binds E-boxes of Pigmentation Genes Regulated by MITF. *149*

Figure 5. TBX3 Binds and Regulates MiGS genes. *151*

Figure 6. Motif enrichment by fold change direction in TBX3 KD studies. *152*

Figure 7. TBX2 and TBX3 Rarely Target the Same Cis-Regulatory Elements. *153*

Chapter 5: Discussion **155**

Summary of Major Findings *156*

Proposed Mechanism of TBX3 ..... *162*

Limitations and Future Directions *164*

Translation to Humans *164*

Functional Validation of TBX3's Proposed Role in Melanocytes *166*

Conclusion *175*

Figures *178*

Figure 1. Summary of Work and Findings. *179*

Figure 2. Expression and Proposed Role of TBX3 in Melanocytes. *180*

Figure 3. In vivo Models for Future Functional Studies of TBX3 Function in Melanocytes *183*

Figure 4. Future Experimental Techniques to Identify TBX3 Cofactors. *184*

Appendix A: **185**

Supplemental Tables Associated with Chapter 3. ..... *185*

Table S1: Gene Signature of Murine Skin Cells from Rezza et al., 2016 (Hair-GEL.net) *185*

Table S2: Significant Differentially Expressed Genes Between Lethal Yellow and Nonagouti Melanocytes *185*

Table S3: Significant Differentially Expressed Genes Between Recessive Yellow and Nonagouti Melanocytes *185*

Table S4: MC1R-inhibted Gene Signature *185*

Appendix B: **186**

Supplemental Tables Associated with Chapter 4. ..... *186*

Table S1: GREAT Output for TBX3 ChIP Dataset *186*

Table S2: GREAT Output for MITF ChIP Dataset.....186

Table S3: Human to Mouse Conversion of TBX3 Target Genes 186

Table S4: Human to Mouse Conversion of MITF Target Genes.....186

Table S5: Significant Differentially Expressed Genes from TBX3 Knockdown186

Table S6: Significant Differentially Expressed Genes from TBX3 Knockdown which are also Associated with TBX3 ChIP-seq Peaks 186

Table S7: GREAT Output for TBX2 ChIP Dataset.....186

Table S8: Significant Differentially Expressed Genes from TBX2 Knockdown186

Table S9: Mouse to Human Conversion of Significant Differentially Expressed Genes from TBX2 Knockdown.....186

Table S10: Significant Differentially Expressed Genes from TBX2 Knockdown which are also Associated with TBX2 ChIP-seq Peaks 186

Table S11: Bound and Regulated Genes Which are Shared by TBX2/3 186

Table S12: Bound and Regulated Genes Which are Shared by TBX2/3 and Split by Action of Activation or Repression 186

Appendix C:.....187

Manuscript by Berns et al., 2024. Downloaded from Pigment Cell and Melanoma Research.....187

References 188

List of Abbreviations

A	Agouti
AKT	AKT Serine/Threonine Kinase 1
ALX3	ALX Homeobox 3
APS	Ammonium Persulfate
AR	Androgen Receptor
ARD1A	AT-Rich Interaction Domain 1A
ARID2	AT-Rich Interaction Domain 2
ASIP	Agouti Signaling Protein (Human)
ASP	Agouti Signaling Protein (Mouse)
ATF4	Activating Transcription Factor 4
B&R	Bind/bound and Regulate/regulated
BAM	Binary Alignment Map
BED	Browser Extensible Data
bFGF	basic Fibroblast Growth Factor
bHLH	basic Helix-Loop-Helix
bHLH-LZ	basic Helix-Loop-Helix-Leucine Zipper
BMP	Bone Morphogenic Protein
BRAF	B-Raf Proto-Oncogene, Serine/Threonine Kinase

BRAFi	B-Raf Proto-Oncogene, Serine/Threonine Kinase-inhibitor
BRN2(POU3F2)	POU Class 3 Homeobox 2
BSA	Bovine Serum Albumin
cAMP	cyclic Adenosine Monophosphate
CBFA2T3	CBFA2/RUNX1 Partner Transcriptional Co-Repressor 3
cCRE	ENCODE Annotated Candidate cis-Regulatory Element
CD117	'See KIT'
CD45	'See PTPRC'
CDH1	Cadherin 1
CDK2	Cyclin-dependent Kinase 1
CDK2	Cyclin-dependent Kinase 2
CDK4	Cyclin-dependent Kinase 4
CDKN2A	Cyclin-dependent Kinase Inhibitor 2A
ChIP	Chromatin Immunoprecipitation
CM	Cutaneous Melanoma
MYC	MYC Proto-Oncogene, BHLH Transcription Factor
COL12A1	Collagen Type XII Alpha 1 Chain
COL14A1	Collagen Type XIV Alpha 1 Chain
COL4A1	Collagen Type IV Alpha 1 Chain

COL5A2	Collagen Type V Alpha 2 Chain
co-TF	co-Transcription Factor
CPM	Counts Per Million
CREB	cAMP Responsive Element Binding Protein
DAPI	4′,6-diamidino-2-phenylindole
DCT	Dopachrome Tautomerase
DEG	Differentially Expressed Gene
DF	Dermal Fibroblast
DHI	5,6-Dihydroxyindole
DHICA	5,6-dihydroxyindole-2-carboxylic acid
DMEM	Dulbecco's Modified Eagle Medium
DP	Dermal Papilla
DQ	Dopaquinone
dsiRNA	Dicer-substrate Small Interfering RNA
e	Extension
E	Embryonic Day
E2F	E2F Transcription Factor
EDN3	Endothelin 3
EDNRB	Endothelin Receptor Type B

EMT	Epithelial-to-Mesenchymal Transition
ENCODE	The Encyclopedia of DNA Elements
Epi	Epidermis
ERK	Extracellular Signal-regulated Kinases
EYA1	Eyes Absent Homolog 1
FACS	Fluorescence-Activated Cell Sorting
FC	Fold Change
FDA	U.S. Food and Drug Administration
FDR	False Discovery Rate
FGF	Fibroblast Growth Factor
FISH	Fluorescence In Situ Hybridization
FOXD3	Forkhead Box D3
FPKM	Fragments Per Kilobase of transcript per Million mapped reads
FSC	Forward-scatter
GABA	Gamma-Aminobutyric Acid
GABA-A	Gamma-Aminobutyric Acid Type A
GABA-B	Gamma-Aminobutyric Acid Type B
GABRA1	Gamma-Aminobutyric Acid Type A Receptor Subunit Alpha1

GABRB2	Gamma-Aminobutyric Acid Type A Receptor Subunit Beta2
GABRB3	Gamma-Aminobutyric Acid Type A Receptor Subunit Beta3
GAPDH	Glyceraldehyde-3-Phosphate Dehydrogenase
GBC	Graph-based Cluster
GDF2	Growth Differentiation Factor 2
GDRB	Genetic Disease Research Branch
GEO	Gene Expression Omnibus
GFP	Green Fluorescent Protein
GLI2	GLI Family Zinc Finger 2
GO	Gene Ontology
GPCR	G Protein-coupled Receptor
GREAT	Genomic Regions Enrichment of Annotations Tool
GRN	Gene Regulatory Network
GSEA	Gene Set Enrichment Analysis
GSK3	Glycogen Synthase Kinase 3
HA	Hemagglutinin
HDAC	Histone Deacetylase
HDAC9	Histone Deacetylase 9

HF + ORS	Hair Follicle + Outer Root Sheath
HH	Hamburger-Hamilton
HMGA2	High Mobility Group AT-Hook 2
HRP	Horseradish Peroxidase
IC	Iliac Crest
ID1	Inhibitor of DNA Binding and Cell Differentiation 1
ID2	Inhibitor of DNA Binding and Cell Differentiation 2
ID3	Inhibitor of DNA Binding and Cell Differentiation 3
ID4	Inhibitor of DNA Binding and Cell Differentiation 4
IPA	Ingenuity Pathway Analysis
IRF1	Interferon Regulatory Factor 1
IRF4	Interferon Regulatory Factor 4
ISH	In Situ Hybridization
ITF2 (TCF4)	Transcription Factor 4
JUN	Jun Proto-Oncogene, AP-1 Transcription Factor Subunit
KD	Knockdown
KEGG	Kyoto Encyclopedia of Genes and Genomes
KIT	KIT Proto-Oncogene, Receptor Tyrosine Kinase
KITL	KIT Ligand

KRT14	Keratin 14
LacO	Lac Operon
LacR	Lac Repressor
L-DOPA	L-3,4-dihydroxyphenylalanine
LEF1	Lymphoid Enhancer Binding Factor 1
LMO2	LIM Domain Only 2
LOF	Loss-of-Function
LRO	Lysosome-related Organelle
MACS2	Model-based Analysis of ChIP-seq 2
MAPK	Mitogen-activated Protein Kinase
Mc	Melanocyte
MC1R	Melanocortin 1 Receptor
MC4R	Melanocortin 4 Receptor
MDM2	MDM2 Proto-Oncogene
MEF2C	Myocyte Enhancer Factor 2C
mGlur1	Metabotropic glutamate receptor 1
MiGS	MC1R-inhibited Gene Signature
MITF	Microphthalmia-associated Transcription Factor
MSC	Melanocyte Stem Cell

NC	Neural Crest
NCC	Neural Crest Cell
NDS	Normal Donkey Serum
Neg	Negative
NF1	Neurofibromatosis 1
NGS	Next Generation Sequencing
NHGRI	National Human Genome Research Institute
NIH	National Institutes of Health
NMDA	N-methyl-D-aspartate
NR4A	Nuclear Receptor Subfamily 4 Group A
NR4A2	Nuclear Receptor Subfamily 4 Group A Member 2
NRAS	NRAS Proto-Oncogene, GTPase
NT	Neural Tube
OCA2	Oculocutaneous Albinism type 2
P	Post-natal Day
PADI2	Peptidyl Arginine Deiminase 2
PAX3	Paired Box gene 3
PBS	Phosphate Buffered Saline
PCA	Principal Component Analysis

PCBD1	Pterin-4 Alpha-Carbinolamine Dehydratase 1
PCR	Polymerase Chain Reaction
PD-L1	Programmed Death-Ligand 1
PFA	Paraformaldehyde
PGR	Progesterone Receptor
PI3K	Phosphoinositide 3-Kinase
PKA	Protein Kinase A
PMEL	Premelanosome Protein
POMC	Pro-opiomelanocortin
POT1	Protection of Telomeres 1
PRRX1	Paired Related Homeobox 1
PRRX2	Paired Related Homeobox 2
PTEN	Phosphatase and Tensin homolog
PTPRC	Protein Tyrosine Phosphatase Receptor Type C
QA/QC	Quality Assurance / Quality Control
RALY	RALY Heterogeneous Nuclear Ribonucleoprotein
RB1	RB Transcriptional Corepressor 1
RHC	Red Hair Colour
RIPA	Radio-Immunoprecipitation Assay

RNA-seq	RNA-sequencing
RORB	RAR Related Orphan Receptor B
RPMI	Roswell Park Memorial Institute
RSK	Ribosomal s6 Kinase
RT-qPCR	Reverse Transcription-quantitative Polymerase Chain Reaction
rtTA	Reverse Tetracycline-controlled Transactivator
RUNX1T1	Runt-related Transcription Factor 1, Translocated to 1
SAM	Sequence Alignment Map
SCC	Side-scatter
SCP	Schwann cell precursor
scRNA-seq	Single-cell RNA-sequencing
SDS	Sodium Dodecyl Sulfate
SDS-PAGE	Sodium Dodecyl Sulfate–Polyacrylamide Gel Electrophoresis
siRNA	Small Interfering RNA
SLC7A11	Slc7a11 Solute Carrier Family 7, Member 11
SMAD1	SMAD Family Member 1
SMAD4	SMAD Family Member 4
SNAI1	Snail Family Transcriptional Repressor 1

SNAI2	Snail Family Transcriptional Repressor 1
SOX10	Sry-related High Mobility Group Box-containing Transcription Factor 10
SOX2	Sry-related High Mobility Group Box-containing Transcription Factor 2
STAR	Spliced Transcripts Alignment to a Reference
STAT3	Signal Transducer and Activator of Transcription 3
SWI/SNF	SWItch/Sucrose Non-Fermentable
TAC + Mx	Transit Amplifying Cells + Matrix
TBS-T	Tris Buffered Saline with Tween-20
TBX2	T-Box Transcription Factor 2
TBX3	T-Box Transcription Factor 3
TBX4	T-Box Transcription Factor 4
TBX5	T-Box Transcription Factor 5
TCGA	The Cancer Genome Atlas
TEMED	Tetramethylethylenediamine
TERT	Telomerase Reverse Transcriptase
TF	Transcription Factor
TFAP2A	Transcription Factor AP-2 Alpha
TFAP2B	Transcription Factor AP-2 Beta

TFE3	Transcription Factor E3
TFEB	Transcription Factor EB
TGFβ	Transforming Growth Factor Beta
tNCC	trunk level Neural Crest Cell
TPA	12-O-Tetradecanoylphorbol-13-acetate
TRE	Tetracycline Response Element
TSS	Transcription Start Site
TWIST	Twist Family BHLH Transcription Factor
TYR	Tyrosinase
TYRP1	Tyrosinase-Related Protein 1
UCSC	University of California Santa Cruz
UMAP	Uniform Manifold Approximation and Projection
USF1	Upstream Stimulatory Factor 1
UTR	Untranslated Region
UVR	Ultraviolet radiation
WNT1	Wnt Family Member 1
ZEB1	Zinc Finger E-box Binding Homeobox 1
ZFHX4	Zinc Finger Homeodomain 4
ZIC1	Zic Family Member 1

ZNF652	Zinc Finger Protein 652
α-MSH	alpha-Melanocyte Stimulating Hormone

Chapter 1: Introduction

Overview

Melanin is a pigmented macromolecule which colours vertebrate skin/scales, hair/fur, and eyes, and, importantly, mitigates cellular damage caused by UVR (Mort et al., 2015; Pavan & Sturm, 2019). In humans and mice, the production of melanin, known as melanogenesis, almost exclusively takes place in specialised cells known as melanocytes (D'Mello et al., 2016). More specifically, melanin synthesis is restricted to the melanosome, a lysosome-related organelle (LRO) which is unique to pigment producing cells (Raposo & Marks, 2007). Importantly, two distinct types of melanin are produced: eumelanin, a photoprotective black-brown pigment, and phaeomelanin, a red-yellow cytotoxic pigment (Pavan & Sturm, 2019). Following their production, melanocytes transfer pigment containing melanosomes to neighbouring keratin-rich cells in the eye, hair, and skin (Benito-Martinez et al., 2021). This action results in the pigmentation of these tissues and, in the case of eumelanosomes, confers protection against UVR (Benito-Martinez et al., 2021). Importantly, UVR is a Grade I carcinogen and is a primary mediator of most cutaneous cancers, including melanoma, the most lethal form of skin cancer (Saginala et al., 2021). This introductory chapter will highlight the current understanding and knowledge gaps which surround melanocyte development, function, and disease, with a specific emphasis on melanoma.

Melanocyte Development

Melanomas exhibit various transcriptomic profiles which mirror distinct stages of melanocyte development (Hoek et al., 2006; Hoek, Eichhoff, et al., 2008; Hoek & Goding, 2010; Karras et al., 2022; Rambow et al., 2019; Tsoi et al., 2018).

Furthermore, high-resolution studies have highlighted the importance of developmental pathways, as well as melanocyte stem cell (MSC) formation, in driving melanomagenesis (Centeno et al., 2023). The implications of these findings can be further extrapolated to include diseases of the melanocyte which fall outside the context of cancer. Therefore, an understanding of melanocyte development, especially the Gene Regulatory Network (GRN) and signalling pathways implicated in the development and ultimate differentiation of the melanocyte lineage is fundamentally important to understanding melanocyte function and disease states.

Formation and Emergence of the Neural Crest

Melanocytes originate from the neural crest (NC), a transient embryonic feature found in all vertebrates which forms during neurulation (Lin & Fisher, 2007). The NC, both as a molecular and morphologic definitive entity, emerges at the dorsal neural tube (NT) upon delamination from the neuroepithelium (Ernfors, 2010). This process occurs through an epithelial-to-mesenchymal transition (EMT), whereby neural crest cells (NCCs) lose cell-cell adhesion and then emigrate away from the neuroepithelium and into the surrounding mesenchymal tissue, most typically in anterior-to-posterior fashion (Ernfors, 2010). The timing of this event in development varies across species and anatomical position (Theveneau & Mayor, 2012a). For example, the appearance of NCCs in mouse and frog often occurs *before* neural tube closure while they appear *after* closure in chick (Nikolopoulou et al., 2017)

Although emergence of the definitive NC varies across species, the preceding landmark events of EMT and delamination from the neuroepithelium are

conserved. The advent of EMT is initiated by extracellular signalling cues from secreted ligands, such as FGF and TGFβ family members, and extracellular matrix proteins, such as collagens (Sauka-Spengler & Bronner-Fraser, 2008). The combined action of these signals together with the PAX3 and ZIC1 TFs leads to expression of critical EMT regulatory TFs including *Snail1/2* and *FoxD3* (Sauka-Spengler & Bronner-Fraser, 2008). Consequently, these TFs initiate essential changes towards EMT which include alteration of polarity, rearrangement of the cytoskeleton, down-regulation of cell adhesion molecules (e.g., E-cadherin), and increased expression of matrix-modifying substances, such as matrix metalloproteases (Sauka-Spengler & Bronner-Fraser, 2008; Vandamme & Berx, 2019). In total, these alterations allow for NCC delamination and create cellular competence which allows for subsequent migration, proliferation, and differentiation toward definitive terminal cell fates (Figure 1A).

NCC Migration and Acquisition of the Melanocyte Fate

There are at least four unique sub-populations which comprise the newly formed NC (cranial, vagal, trunk, and sacral) and these are largely defined by anatomical position (i.e., the axial level from where they emerge), fate restriction (i.e., the limit of possible terminal cell types they can become), and specification (i.e., initiation of a molecular identity toward the cell type they will become), which takes place before migration (Bronner & LeDouarin, 2012; Hutchins et al., 2018; Mort et al., 2015). The NCCs of these populations migrate extensive distances through the developing embryo and then differentiate into an array of diverse cell types and tissues including, neurons and glia of the peripheral nervous system, craniofacial bone and cartilage, and melanocytes (Bronner & LeDouarin, 2012). To

achieve this, NCCs must survive, proliferate, migrate, and then differentiate into appropriate cell fates at various anatomical locations across the developing embryo. Following their emergence from the neuroepithelium, NCCs face two key decisions: (1) when to migrate and (2) by which route. The events that dictate these decisions are well-studied across several model organisms, nevertheless, these choices are complex and exhibit interspecies variability (Bronner & LeDouarin, 2012). The ramifications of these decisions are consequential; however, the particulars lay outside the scope of this thesis. Therefore, for clarity and brevity, the following text will explore the actions of trunk level NCCs (tNCCs) of two model organisms, mouse and chick, which are destined toward the melanocyte lineage.

tNCCs utilize two possible routes of migration: a ventral route, through the somite, or a dorsolateral route, between the somite and the surface ectoderm (Mort et al., 2015) (Figure 1B). This begins shortly after delamination from the NT which occurs at E9 and Hamburger-Hamilton (HH) stage 12-13 in mouse and chick, respectively, and these cells are primarily restricted toward a neurogenic fate (i.e., neurons and glia) (Mort et al., 2015). In contrast, cells which migrate via the dorsolateral pathway, considered the ‘classical’ path of melanocyte migration, exhibit a predominantly melanogenic fate and are therefore thought to contribute most of the pigment producing melanocytes of the skin and hair follicles (Colombo et al., 2011). Chick and mouse might use the same migratory paths; however, the time of migration onset differs between them. For example, murine tNCCs delaminate and then immediately enter both migratory routes. On the other hand, chick tNCCs do not directly enter the dorsolateral route, instead the future melanogenic population accumulates and waits at a ‘migration staging area’, between the neural tube and somite. tNCCs in the migration staging area only enter

the dorsolateral route approximately 7-8 HH stages after the onset of ventral migration (Erickson et al., 1992; Weston, 1991). The reasoning and molecular mechanisms which facilitate these differences are unclear. Furthermore, the potential implications of these decisions in fostering eventual melanocyte development are unknown and, therefore, further work is needed to unravel these inter-species complexities and their impact on fate identification and differentiation in these organisms.

A study led by the lab of Patrik Enfors has come to question whether the 'classical pathway' is indeed the primary contributing source of melanocytes (Adameyko et al., 2009). In their work, they identified a population of ventrally migrating cells, called Schwann Cell Precursors (SCP), which exhibit a bi-potent glia/melanocyte potential fate (Adameyko et al., 2009). Furthermore, they proposed that this SCP cell population not only contributes to the first wave of melanocytes, which come to being pre-natally, but also that SCPs serve to produce post-natal melanocytes (Adameyko et al., 2009). However, this work faces many technical limitations, especially related to appropriate lineage tracing models which clouds the clarity of these findings (Vandamme & Berx, 2019). Regardless, this work, in conjunction with other studies, has made it clear that tNCCs destined toward the melanocyte lineage first exist as a bi-potent precursor which is restricted to the glial-melanogenic fate.

Immature Melanoblast to Differentiated Melanocyte

Following specification into the bi-potent glial-melanogenic fate, cells destined toward the melanocyte lineage are transformed into melanoblasts.

Acquisition of melanoblast identity coincides with expression of *Microphthalmia-associated transcription factor* (*Mitf*), the first definitive melanocyte marker gene (Vandamme & Berx, 2019). MITF is a basic-helix-loop-helix-leucine-zipper (bHLH-LZ) TF and is expressed in numerous cell/tissue types (Goding & Arnheiter, 2019). Multiple protein isoforms exist; however, the MITF-M isoform is specific to melanocytes and is essential for their development (Goding & Arnheiter, 2019). Furthermore, MITF is often considered the 'master melanocyte regulatory factor' because it is crucial for cell survival, proliferation/cell cycle progression, differentiation and it modulates the expression of key genes in melanogenesis (Levy et al., 2006). Corroborating this notion, more than 20 *Mitf* mutants have been identified in mouse and all of these exhibit pigmentation defects of varying severity (Opdecamp et al., 1997). The timing of *Mitf/mitf* expression, and therefore acquisition of melanoblast identity, begins by E10.5 in mouse, and by HH stage 12-13 in chick (Larue et al., 2013; Loring & Erickson, 1987).

Interestingly, this suggests that acquisition of melanoblast identity occurs in mouse *after* migration onset but occurs *before* these cells enter the dorsolateral pathway in chick. The reasons for this are unclear; regardless, expression of *Mitf / mitf* in early melanoblasts is influenced by a dose-dependent response to WNT and BMP signalling whereby increased exposure to WNT ligands and downstream activation of β-catenin, with a concomitant decrease in exposure to BMP ligands, leads to synergistic action of Sry-related high mobility group box-containing transcription factor 10 (SOX10) and Paired box transcription factor 3 (PAX3) in the upregulation of *Mitf/mitf* (Mort et al., 2015). Together, these three TFs are crucial for defining the melanocyte lineage as loss of any one of them results in developmental failure of melanoblasts (Hou & Pavan, 2008). *Sox10* and *Pax3* are expressed in the

presumptive NC and assume prominent roles in the NC GRN (Sauka-Spengler & Bronner-Fraser, 2008). Beyond this, these two factors are implicated in specification of the glial lineage; therefore, downregulation of glial lineage genes, controlled by SOX10/PAX3, is needed to confer melanoblast identity. Melanoblasts subjected to overexpression of FOXD3 switch toward a glial lineage with subsequent loss of MITF though this decrease does not occur from direct repression of *MITF* transcription but rather by FOXD3 preventing binding of PAX3 to the *MITF* promoter (Thomas & Erickson, 2009). It was found that SOX2 directly represses *Mitf* by binding at its proximal promoter; however, overexpression of *Mitf* in turn lead to repression of *Sox2* (Adameyko et al., 2011). In total, MITF/SOX10/PAX3 activity needs to be well-coordinated in order to direct melanoblasts further down the melanocyte lineage.

Acquisition of the melanoblast identity occurs as early as E10.5 in mice (Larue et al., 2013). At this time in development, fewer than 100 melanoblasts exist in the trunk population; however, this number will increase in time to about 20,000 cells by E15.5 (Luciani et al., 2011). The proliferating melanoblasts continue their migration and begin to enter the dermis by E11.5, in fact, by E12.5 half of all melanoblasts have trans-migrated from the dermis to the epidermis (Larue et al., 2013). The migration and survival of these melanoblasts is highly dependent on at least two cell surface receptors, EDNRB and KIT, and their ligands, KITL and EDN3, as evidenced by pigmentation deficiencies from LOF of either of these genes, including piebaldism, with white spotting of the forehead and abdomen (Hou & Pavan, 2008).

KIT is a receptor tyrosine kinase which acts as a critical regulator of melanoblast proliferation, migration, and survival as signalling through that pathway

leads to phosphorylation and increased activity of MITF (Goding & Arnheiter, 2019). Its ligand, KITL, comes in two forms, a soluble and secreted form, and a membrane-bound form, which is found on the surface of keratinocytes within the developing epidermis and this receptor plays a key role in melanoblast homing (Wehrle-Haller, 2003; Wehrle-Haller & Weston, 1995). The G protein-coupled receptor (GPCR), EDNRB, and its ligand, EDN3 are essential for migration and proliferation of mouse melanoblasts in the dermis from stages E10.5-12.5 (Mort et al., 2015).The effect of EDN3 on EDNRB has been demonstrated *in vitro* to be dose-dependent; increasing doses promote mass melanocyte differentiation while Schwann cells cultured with EDN3 dedifferentiate toward the bi-potent glial-melanocyte precursor cell type (Dupin & Douarin, 2003).

Mouse melanoblasts continue their migration into the epidermis up through at least to E15.5 by which time colonization is complete (Larue et al., 2013). From this point, melanoblasts distribute throughout the epidermis and give rise to three separate populations: (1) interfollicular melanocytes, of which there are few in mouse, (2) follicular melanocytes, which reside in the lower portion of the hair bulge, and (3) MSCs of the hair follicle bulge, which serves as a reservoir for future melanocytes (Vandamme & Berx, 2019) (Figure 1C). The following section will describe the functional role of terminally differentiated melanocytes and their contribution to pigmentation.

Melanocyte Function

Tanning Response

Human skin comprises one of the largest organs in the body, and, as the outermost layer, is constantly interacting with the surrounding environment (Dąbrowska et al., 2018). As such, it provides a barrier to maintain homeostasis, through regulation of body temperature and water content, and protects humans from harmful microorganisms and environmental insults, such as solar UVR (Dąbrowska et al., 2018). UVR is a Grade I carcinogen which is known to induce cutaneous tumour formation and growth (D'Orazio et al., 2013). The ill effects of UVR are mitigated by melanin pigments which are arranged in a manner so that they absorb and block UVR penetration of skin cells (D'Orazio et al., 2013). Keratinocytes are the most prominent cell type in the skin; however, keratinocytes themselves do not produce melanin pigment; instead, a specialized cell type, the melanocyte, produces and packages melanin into melanosomes and then transfers these organelles to neighbouring keratinocytes (Benito-Martinez et al., 2021) (Figure 2A). Melanocytes are in contact with, and subsequently transfer melanin to, upwards of 40 keratinocytes in what has been described as the epidermal melanin unit (Nordlund, 2007). In the absence of sunlight and UVR, keratinocytes primarily secrete TGFβ to maintain melanocyte quiescence and reduce melanin synthesis (Vandamme & Berx, 2019).

Keratinocytes lacking sufficient pigmentation are prone to UVR-mediated DNA damage and when injury occurs there is a tanning response whereby melanocytes increase the production and transfer of melanin to keratinocytes which darkens them and mitigates further UVR mediated harm (Lin & Fisher, 2007).

Following UVR insult, keratinocytes increase expression of *p53*, which in turn binds to, and up-regulates, expression of the *Proopiomelanocortin (POMC)* gene (Cui et al., 2007). The preproprotein encoded by the *POMC* gene undergoes further post-translational modification to form several active protein derivatives, including alpha-Melanocyte Stimulating Hormone (α-MSH), which is secreted by keratinocytes and binds to the Melanocortin 1 receptor (MC1R), a GPCR, located on the cell surface of melanocytes (Rousseau et al., 2007). α-MSH binding to MC1R triggers a cell signalling cascade which leads to the synthesis, packaging, and transfer of photoprotective eumelanin to keratinocytes (Hida et al., 2020) (Figure 2A).

Melanosome Maturation and Melanin Synthesis

Melanin synthesis, known as melanogenesis, is restricted to a specialized organelle known as the melanosome (Le et al., 2021). Successful melanogenesis requires integration of complex cellular signalling inputs to establish a competent biological and biochemical landscape within the melanocyte and the melanosome (D'Mello et al., 2016). The first step of melanogenesis involves successful development and maturation of the melanosome organelle itself (Figure 2B). The melanosome is a LRO which shares many commonalties with lysosomes, such as low luminal pH and expression of lysosomal-associated membrane proteins (Le et al., 2021). Multiple LROs exist and they are typically restricted to specific cell types, for example, melanocytes, platelets, lymphocytes, and Type II alveolar epithelial lung cells contain their own unique LROs (Huizing et al., 2008). Melanosomes, despite their similarity to lysosomes, and other LROs, significantly differ in morphology and protein composition and it is in part these differences which allow for melanogenesis (Le et al., 2021).

Classically, there are two phases, comprising four characterized stages, of melanosome development. The first two stages (stage I-II) define an early and unpigmented premelanosome phase, while the latter two stages (stage III-IV) are defined by the presence of pigmentation, which is noticeable by stage III and is fully matured by stage IV (Le et al., 2021). Two different melanosomes exist: the eumelanosome, which largely produces eumelanin, and the cysteine-rich phaeomelanosome, which almost exclusively produces phaeomelanin (D'Alba & Shawkey, 2019). The aforementioned stages of development appear to be similar between the two; however, only eumelanosome development has been well-described while phaeomelanosome development is not as well understood.

All melanosomes originate from early endosome precursors (Raposo et al., 2001). Likewise, stage I eumelanosome and phaeomelanosome exhibit a spherical shape and possess intraluminal vascular compartments which begin to accumulate a fibrillar protein specific to melanocytes called Premelanosome protein (PMEL) (D'Alba & Shawkey, 2019; Le et al., 2021). Parts of stage II maturation are shared by both types of melanosomes, including the arrival of melanogenic-specific proteins, such as Tyrosinase (TYR), an enzyme which regulates the rate-limiting steps of melanin synthesis (D'Alba & Shawkey, 2019; Le et al., 2021). However, this stage also marks a divergent point with eumelanosomes becoming more ellipsoidal in shape whereas phaeomelanosomes retain a spherical identity (D'Alba & Shawkey, 2019; Le et al., 2021). The shape alteration of eumelanosomes is largely due to increasing accumulation of PMEL which forms organized parallel sheets of fibrils when in sufficient quantities (D'Alba & Shawkey, 2019; Le et al., 2021). Strengthening PMEL fibrils distend the melanosome membrane into the elongated ellipsoid shape (D'Alba & Shawkey, 2019; Le et al., 2021) In contrast,

phaeomelanosomes lack robust amounts of PMEL, do not produce proper fibrils, and, therefore, retain a rounded shape (D'Alba & Shawkey, 2019; Le et al., 2021) (Figure 2B).

Stage III of melanosome maturation coincides with the earliest phase of melanogenesis (D'Alba & Shawkey, 2019; Le et al., 2021). In eumelanosomes, the PMEL rich fibrils thicken and appear darker due the deposition of newly synthesized melanin granules (D'Alba & Shawkey, 2019; Le et al., 2021). In contrast, matrices of phaeomelanosomes, which lack robust amounts of PMEL, remain amorphous and fail to accumulate melanin (Le et al., 2021; D'Alba and Shawkey, 2018). In eumelanosomes, stage IV is reached once the fibrils are saturated with melanin, this event marks the point at which fully mature melanosomes are ready to be delivered to neighbouring keratinocytes (D'Alba & Shawkey, 2019; Le et al., 2021). In the skin, this could be one or more of the of the neighbouring keratinocyte cells which is in contact with dendrites of interfollicular melanocytes or, for follicular melanocytes, this could be one or more of the surrounding cortical and medullary keratinocytes of the hair shaft (Benito-Martinez et al., 2021). Skin, hair, and eye colour are dependent on the successful transfer of melanin containing melanosomes to these tissues. The molecular mechanisms underlying melanosome transfer is hotly debated, and several hypotheses exist; however, this process is outside the scope of this thesis. An excellent review of this topic was published in 2021 and can be found in *Integrative and Comparative Biology* (Benito-Martinez et al., 2021).

Melanin synthesis can proceed once appropriate melanosome formation has been achieved. As mentioned previously, the enzyme TYR is shuttled to the melanosome during melanosome formation and maturation. The enzyme serves to

first convert the amino acid Tyrosine converted to L-3,4-dihydroxyphenylalanine (L-DOPA), and then secondly to Dopaquinone (DQ) (Fernandes et al., 2023; Hida et al., 2020). This reaction marks a rate-limiting step in melanin synthesis and is the only shared feature of eumelanin and phaeomelanin production (Fernandes et al., 2023; Hida et al., 2020). Importantly, LOF of TYR leads to complete absence of pigmentation and results in Oculocutaneous albinism type I (Hida et al., 2020). The proceeding steps of melanin synthesis are highly influenced by the physiological and biochemical properties of the melanosome and by the presence or absence of the amino acid cysteine (Fernandes et al., 2023; Hida et al., 2020). DQ is a highly reactive and unstable intermediate which rapidly undergoes intramolecular cyclization to form dopachrome, an intermediate which is essential for eumelanin synthesis, in an environment lacking cysteine. When melanosomes have ample cysteine, DQ can spontaneously incorporate the cysteine to form cysteinyldopa, a precursor of phaeomelanin. The newly formed cysteinyldopa is readily oxidized to produce benzothiazine molecules which are further oxidized to form mature phaeomelanin molecules. Similarly, dopachrome undergoes spontaneous conversion to the eumelanin intermediate compound 5,6-dihydroxyindole (DHI) through decarboxylation when in the right physiologic conditions. However, eumelanin synthesis more readily proceeds through enzymatic intervention by TYR and two other enzymes, dopachrome tautomerase (DCT) and tyrosine-related protein 1 (TYRP1), whereby DCT converts dopachrome to 5,6-dihydroxyindole-2-carboxylic acid (DHICA) and TYRP1 catalyses DHICA into mature eumelanin pigment (Fernandes et al., 2023; Hida et al., 2020). LOF of these proteins leads to Oculocutaneous albinism types VIII and III, respectively, with hypopigmentation and

nystagmus being two shared clinical features (Hida et al., 2020).The steps of melanosome biogenesis and melanogenesis are summarized in (Figure 2B).

Core Pathways and Molecular Regulators of Melanogenesis

To date, there are over 650 genes which are associated with pigmentation phenotypes (Baxter et al., 2019). A fraction of these are well-characterized pigmentation loci with two of the most influential being *MC1R* and *MITF* (Levy et al., 2006). As stated previously, *MC1R* encodes a G_sPCR which is responsive to the α-MSH agonist (Rousseau et al., 2007). Once bound by α-MSH, MC1R activates adenyl cyclase, which in turn increases the intracellular levels of cAMP (Mountjoy et al., 1992). The rise in cAMP leads to phosphorylation of PKA which then binds the cAMP response element-binding protein (CREB) TF and in turn targets genes which have a cAMP response element (CRE). One of the most crucial genes induced by this mechanism in melanocytes is MITF, a master melanocyte regulatory TF, which targets and induces expression of genes which encode melanogenic enzymes, such as *TYR*, *TYRP1*, and *DCT* (Levy et al., 2006)

MITF has a bHLH-LZ DNA binding and dimerization domain and exists in several protein variants, thanks to different alternative splicing and transcription initiation sites, with the MITF-M form being found exclusively in melanocytes (Goding & Arnheiter, 2019). The expression of the MITF-M isoform in melanocytes is in large part due to CREB mediated, and SOX10 dependent, activation (Huber et al., 2003). Other activators include PAX3, which is repressed by TGFβ signalling, FOXD3, WNT/β-catenin, and ONECUT2 (Goding & Arnheiter, 2019). In contrast, repressors of MITF include ATF4, JUN, GLI2, BRN2, and ALX3 (Goding & Arnheiter,

2019). Following protein synthesis, the activity of MITF can be altered through post-translational modifications, such as phosphorylation, by ERK, RSK, GSK3, AKT, p38, SUMOylation, and ubiquitination (Goding & Arnheiter, 2019). Likewise, MITF interacts with several cofactors, such p300, β-catenin, and SWI/SNF complex subunits, to regulate expression by binding the E-box motif (CACGTG) of target genes (Goding and Arnheiter, 2019).

MC1R is a key mediator in pigment-type switching, the system which dictates whether melanocytes produce eumelanin or phaeomelanin (Walker & Gunn, 2010). Eumelanin synthesis occurs when the MC1R-cAMP-CREB-MITF signalling cascade is active, such as when MC1R is bound by its agonist α-MSH (Walker & Gunn, 2010). In contrast, inhibition, or signalling loss through the MC1R-cAMP-CREB-MITF axis, leads to an environment favouring phaeomelanin synthesis (Ito & Wakamatsu, 2008) (Figure 2C). Much knowledge of this system derives from mouse studies. In the 20th century, several alleles, including the *extension* (*e*) locus, were identified which extended, or restricted, the amount of eumelanin produced by mice, and *e/e* mice, known as recessive yellow, were found to be completely yellow in colour (Searle, 1968; Silvers, 1979). Functional studies discovered that the *extension* locus mapped to mouse chromosome 8 and encoded a receptor, dubbed initially as Melanocyte-stimulating hormone receptor, which was responsive to α-MSH and stimulated eumelanin synthesis; however, recessive yellow mice did not respond to the ligand and remained yellow (Robbins et al., 1993; Tamate & Takeuchi, 1984). The recessive yellow mouse mimics the human RHC phenotype which is due to homozygous LOF variants in *MC1R* (García-Borrón et al., 2014). RHC is most strongly associated with six *MC1R* variants, p.D84E, p.R151C, p.R160W, p.D294H, p.R142H, and p.1155T (Raimondi et al., 2008). These variants

lead to reduced, or non-functional, protein products which greatly limit eumelanin production and instead promote the synthesis, and accumulation, of cytotoxic phaeomelanin (Mort et al., 2015; Pavan & Sturm, 2019; Schiöth et al., 1999).

α-MSH is not the only ligand which preferentially binds MC1R. Historic genetic mouse studies found that the agouti signalling protein (ASP), encoded by the *Agouti* gene, has a strong affinity for MC1R (Ollmann et al., 1998). ASP binding fosters phaeomelanogenesis and inhibits eumelanogenesis by two distinct actions: first, it competes with α-MSH for MC1R and inhibits activation of the MC1R-cAMP-CREB-MITF axis, thus acting as a competitive antagonist. Second, ASP not only inhibits α-MSH induced MC1R signalling but it itself reduces signalling of this axis below constitutive levels (Blanchard et al., 1995; Ollmann et al., 1998; Sakai et al., 1997). The dermal papilla cells of wildtype *Agouti* (*A/A*) mice secrete robust amounts of ASP during days 2-7 in the first hair cycle, leading to the agouti coat colour phenotype characterized by a mostly black hair follicle with a subapical yellow band (Bultman et al., 1992; Millar et al., 1995). In contrast, the nonagouti mouse (*a/a*) exhibits black hair, lacking a subapical yellow band, due to the LOF of ASP and thus has constant signaling through the MC1R pathway, even in the absence of α-MSH (Slominski et al., 2005).

Humans do not demonstrate the agouti banding phenotype; however, they do possess an ASP orthologue, ASIP, and variants of this locus are associated with hair and skin pigmentation phenotypic traits, including RHC (Kanetsky et al., 2002; Kempf et al., 2022; Sulem et al., 2007, 2008; Voisey et al., 2006). The lethal yellow (A^y/a) mouse has a large deletion which places it under the control of the *Raly* promoter, which is upstream of *agouti*, and therefore has ubiquitous overexpression of ASP, leading to a yellow coat colour due to constitutive binding of MC1R by ASP

(Duhl et al., 1994). The effects of ASP are pleiotropic, as evidenced by metabolic phenotypes, including obesity and insulin-resistant type II diabetes, and the development of spontaneous tumours in lethal yellow mice (Michaud et al., 1994). The metabolic phenotypes are largely explained by ASP-mediated inhibition of MC4R in the hypothalamus, a place where ASP is not normally expressed (Walker & Gunn, 2010). Although humans do not present with agouti banding, there are several identified patients that have constitutive overexpression of ASIP and mirror the lethal yellow phenotype comprising red hair and severe metabolic disease (Kempf et al., 2022).

Melanoma

Incidence

Melanoma arises from melanin-producing melanocytes following malignant transformation. These melanocytes primarily reside within cutaneous tissues, both in the hair follicle and interfollicularly within the basal layer of the epidermis; however, these cells are also found in the eyes, ears, mouth, and anogenital track (Castro-Pérez et al., 2023). Melanoma may arise in any of the forementioned tissues; however, cutaneous melanoma (CM) is the most common form, comprising 90% of all melanoma diagnoses (G. V. Long et al., 2023). In 2020, CM accounted for 1.7% of all cancer diagnoses across the globe. Furthermore, CM was the 5th most diagnosed cancer in the United States (Saginala et al., 2021).

Interestingly, CM constitutes less than 4% of all dermatological cancers; however, ~80% of deaths associated with skin cancer are due to CM (Saginala et al., 2021). Given this, CM is considered the most dangerous form of skin cancer (J.

Liu et al., 2023; Miller & Mihm, 2006). Worryingly, disease incidence has continued a steady rise over the last 50 years with disproportionately higher rates in fair-skinned populations of European origin (Centeno et al., 2023; Raimondi et al., 2020). Furthermore, in developed countries, the incidence rates of CM have greatly outpaced that of all other cancers (Saginala et al., 2021). For instance, between 1982 and 2011, the number of occurrences of invasive melanoma doubled in Australia and quadrupled in the United Kingdom (Whiteman et al., 2016).

Thankfully, the mortality rate has not mirrored the same rate of increase and is only slightly higher than it was fifty years ago (Berwick et al., 2009). Regardless, the rise of cases, and the mortality accompanying CM, remains far too high. The limited rise in mortality rates is most attributable to recent therapeutic advances. For example, between 1986 and 2013, melanoma-related deaths rose by 7.5%; however, following the introduction of several target-based therapies the mortality rate dropped by 17.9% between 2013 and 2016 (Saginala et al., 2021). Despite this large drop in mortality, CM remains the most lethal form of cutaneous cancer. Thus, scientific research, medical care, and government policies should work cooperatively to address the unprecedented burden of this disease through preventative care and advancement of therapeutic modalities.

Risk Factors

Several risk factors, including age, sex, geographic location, anatomical location, ethnicity, pigmentation phenotype, genetics, and exposure to environmental hazards, are associated with CM development (Berwick et al., 2009). The primary extrinsic risk factor is UVR exposure with two major sources being solar

radiation and tanning beds (Raimondi et al., 2020). This is not inherently surprising as UVR is classified as a Group 1 carcinogen to humans by the International Agency for Research on Cancer (Raimondi et al., 2020). From a mechanistic standpoint, UVR impacts biological systems in several ways. For example, UVR induces DNA lesions, most commonly in the form of pyrimidine-dimers, which lead to DNA replication errors if not correctly restored by the nucleotide excision repair pathway (Raimondi et al., 2020; Saginala et al., 2021). Furthermore, UVR impairs local immune function, alters the production of local growth factors, and promotes the production of reactive oxygen species (ROS) (Miller & Mihm, 2006). Thus, cumulative UVR-induced biological alterations are thought to drive the malignant transformation of healthy melanocytes into melanoma.

Given the impact of UVR on biological systems, it is believed that the CM incidence rise over the last 50 years is directly attributable to increased durations of exposure to UVR (C. Chang et al., 2014; Cust et al., 2011). However, no data exists which suggests that people are more exposed to UVR now than at any previous point in the history of *Homo sapiens* (Berwick et al., 2009). This explanation is therefore insufficient. Regardless, an excellent study by Armstrong and Kricker found that 68 to 98 percent of melanomas are associated with sun exposure (Armstrong & Kricker, 1993). In fact, melanoma appears most frequently in individuals who had several sunburns and/or were intermittently exposed to long durations of intense UVR (Miller & Mihm, 2006). Regardless, the Armstrong and Kricker study suggests that upwards of 30% of melanomas are UVR-independent, though recent studies have put the number closer to 15% (Armstrong & Kricker, 1993; Centeno et al., 2023). Therefore, UVR exposure, and more specifically dose-dependent UVR exposure, is one of the primary extrinsic factors driving melanoma

development, especially in people who already possess other intrinsic risk factors, but other carcinogens can clearly contribute to melanomagenesis.

Melanoma is associated with several intrinsic risk factors with genetics, phenotypic traits, such as light-skin and naevus count, family history of melanoma, and previous occurrence of melanoma being the strongest influences of disease development (E. Long et al., 2022; Miller & Mihm, 2006). Familial melanomas represent 10% of all melanoma cases and 40% of these patients have coding variants which lead to aberrant function of *Cyclin-dependent kinase N2A* (*CDKN2A*) encoding proteins (Berwick et al., 2009). The *CDKN2A* locus is a highly penetrant susceptibility region which comprises four exons that encode two tumour suppressor proteins, $p16^{INK4A}$ and $p14^{ARF}$, through alternative splicing (Rossi et al., 2019). Both of these proteins regulate cell cycle progression, but they work through different means. For instance, $p16^{INK4A}$ induces G_1-phase cell cycle arrest by preventing cyclin-dependent kinase 4 (CDK4) mediated phosphorylation of the tumour suppressor protein retinoblastoma protein 1 (RB1) which in turn preserves the RB1/E2F complex (Serrano et al., 1993). In contrast, $p14^{ARF}$ interacts with Mouse double minute 2 (MDM2), an E3 ubiquitin ligase, to inhibit proteasomal degradation of a tumour suppressor, p53, and thereby promote cell cycle arrest (Y. Zhang et al., 1998). Importantly, heritable coding variants in *CDKN2A*, as well as *CDK4* and *RB1*, are often found in familial melanomas suggesting particular importance of this pathway in melanoma development; however, LOF of this pathway on its own is not sufficient enough to induce melanoma and therefore senescence bypass, through inactivation of cell cycle regulators (e.g., CDKN2A/INK4A), and activation of pro-oncogenes (e.g., BRAF, NRAS) is needed

for melanomagenesis (Bennett & Medrano, 2002; Ha et al., 2008; Miller & Mihm, 2006; Tsao et al., 2012; Vredeveld et al., 2012; Wagstaff et al., 2022).

RHC is a well-described phenotypic trait which encompasses red hair, pale skin, high naevus count, and an inability to tan (D. L. Duffy et al., 2019; Healy et al., 2000; Rees, 2000; Schiöth et al., 1999). Critically, individuals exhibiting the RHC phenotype are at a considerably higher risk of developing melanoma as compared to persons with a non-RHC disposition (D. L. Duffy et al., 2019; Rayner et al., 2019; Rhodes et al., 1987; Schiöth et al., 1999). As previously mentioned, the *MC1R* gene encodes a GPCR which is found on the cell surface of melanocytes and functions as a major regulator of pigmentation (Lin & Fisher, 2007). In RHC associated *MC1R* variants, melanocytes produce high levels of phaeomelanin which exacerbate DNA damage through the amplification of free radicals, and this effect is worsened when cells are exposed to UVR; however, phaeomelanin can contribute to melanomagenesis independently of UVR (Mitra et al., 2012; Napolitano et al., 2014). Although the influence of *MC1R* RHC variants on melanin composition may play a role in melanoma predisposition, *MC1R* mutation status may also have an impact on melanoma initiation unrelated to its role in pigmentation. For example, individuals with *MC1R* variants fail to activate PTEN upon UVR exposure, resulting in increased PI3K/AKT signalling and oncogenic transformation (Cao et al., 2013). Relatedly, inheritance of *MC1R* and *CDKN2A* variants increases the penetrance of familial-associated melanomas (Fargnoli et al., 2010). Whether MC1R signalling plays additional roles in the prevention of melanoma initiation remains unknown. In part, this may be because, by definition, a molecular mechanism underlying melanoma predisposition must already be operating prior to the acquisition of the ultimate trigger for melanoma initiation. What is clear, is that this genotype-phenotype

relationship represents a unique situation whereby the heritable risk gene confers some of the strongest phenotypic traits, including light-skin and naevus count, associated with disease development.

Disease Onset and Progression

Melanoma can arise from any tissue containing melanocytes. Relatedly, the tissue of origin delineates the major disease types which consist of CM, found in non-glabrous skin, acral melanoma, found in glabrous (non-hairy) skin, such as the soles of the feet and palms of the hands, uveal melanoma, found in the choroid, iris, and or ciliary body of the eye, and mucosal melanoma, the least prevalent subtype which can be found in the mucosal lining of the gastrointestinal tract (Rabbie et al., 2019). The major forms of melanoma are further broken down into subtypes, for example, CM, classically contained four subtypes: superficial spreading melanoma, lentigo maligna melanoma, nodular melanoma, and acral lentiginous melanoma, which were defined by Wallace Clark (Miller & Mihm, 2006). Since then, more have been identified and as of 2018 there are seven distinct subtypes of CM (Ferrara & Argenziano, 2021). The various intricacies which delineate these various forms of melanoma lay outside the scope of this thesis; therefore, the following subsections will evaluate the key factors which contribute to the initiation and progression of the most common form of melanoma, CM. Following his initial work in defining CM subtypes, Clark developed a histopathological model which described a stepwise series of observable phenotypic changes that occur in evolution of normal melanocytes toward malignant CM (Miller & Mihm, 2006). This model has been updated and refined to incorporate molecular, genetic, clinical, and pathological

information which more accurately reflects an individual's disease state and is summarized in Figure 3 (Ferrara & Argenziano, 2021; G. V. Long et al., 2023).

The first phenotypic change noted by Clark encompasses the formation of a naevus (mole) due to hyperproliferation of melanocytes (Miller & Mihm, 2006). Genetic and molecular level studies have determined that this state of hyperproliferation is due to acquisition of a driver mutation in a proto-oncogene, most often in the MAPK signalling pathway, and almost always either *BRAF* or *NRAS* but extremely rarely both (Bauer et al., 2007; Pollock et al., 2003; Sensi et al., 2006). Melanocytes of most nevi have a restricted state of hyperproliferation which leads to a limited size mole that never progresses past an initial growth phase (Miller & Mihm, 2006). An outstanding question is what exactly leads to the abrupt end of this hyperproliferative state? The overwhelming consensus in the field is that melanocytes most likely enter a state of oncogene-induced cell senescence (Miller & Mihm, 2006). In brief, cellular, or replicative, senescence is achieved when a cell has a stable exit from the cell cycle and thus has limited proliferative ability. In oncogene-induced senesce, oncogene induced proliferation causes over-stimulation and this leads to a state of irreversible growth arrest (X. Liu et al., 2018). However, studies have shown that melanocytes within certain nevi do retain proliferative capacity and therefore it is likely that multiple cell autonomous and non-cell autonomous features, such as immune cell mediated regulation, lead to a state of quasi-senescence (Shain & Bastian, 2016).

Acquisition of a single driver mutation, and subsequent formation of a naevus, is not sufficient to drive malignant transformation. Consequently, the transition of benign to dysplastic naevus requires accumulation of additional genetic mutations which lead to the dysregulation of cellular activities such as proliferation,

differentiation, DNA repair, and apoptosis (Eddy et al., 2021; G. V. Long et al., 2023; Miller & Mihm, 2006). Cutaneous tissue is often exposed to UVR, a Group 1 carcinogen considered the primary mediator of mutagenesis in melanoma, and therefore it is not surprising that the mutational burden is greater in CM as compared to any other cancer type (Eddy et al., 2021). The negative impact of UVR is exacerbated in fair skinned people who lack a robust amount of photoprotective eumelanin pigment (Brenner & Hearing, 2008). Relatedly, people with the RHC trait not only have limited eumelanin but also produce robust amounts of phaeomelanin which itself is mutagenic both in the presence and absence of UVR (Mitra et al., 2012; Morgan et al., 2018; Napolitano et al., 2014). Interestingly, the typical nucleotide alteration, a T → A pyrimidine-to-purine transversion, which leads to the amino acid change observed in *BRAF*^{V600E} is almost never mediated by UVR (Shain & Bastian, 2016). This observation begs the question, does UVR directly lead to genetic alterations governing *BRAF*^{V600E} or do other carcinogens act as primary mediators? Pyrimidine dimers, an indicator of UVR mutagenesis, are almost always found in high numbers in nevi which have the *BRAF*^{V600E} genotype. Thus, UVR might be a primary external risk factor associated with naevus formation but other carcinogens, such as phaeomelanin which is prevalent in the RHC trait, might be equally as important in promoting the necessary genetic mutations which propel melanocyte transformation toward melanoma.

Dysplastic nevi can form from previously benign nevi; however, most familial melanomas are associated with *de novo* lesions which bypass the benign phase associated with senescence (Shain & Bastian, 2016). Several secondary mutations and molecular mechanisms are associated with this stage of progression and include *Telomerase reverse transcriptase (TERT)* and *Protection of telomeres 1*

(POT1) as well as the previously mentioned cell cycle progression regulators *CDKN2A* and *CDK4* (Shain & Bastian, 2016). TERT and POT1 proteins function in the maintenance of telomers whereby TERT maintains telomere length through the addition of TTAGG repeats and POT1 binds to those repeat elements to prevent degradation (Aramburu et al., 2020). Mutations within the *TERT* promoter are commonplace in dysplastic nevi (Shain & Bastian, 2016). A study by Chiba and colleagues showed that *TERT* promoter mutations facilitate naevus to invasive melanoma transition by facilitating cell immortalization and genomic instability that leads to uncontrolled cell proliferation (Chiba et al., 2017). Acquisition of cell immortalization, coupled with sustained and unregulated growth, is a hallmark governing the transition to melanoma *in situ* (Eddy et al., 2021). Histologically, the term melanoma *in situ* is used to describe lesions which comprise several atypical melanocytes, containing enlarged nuclei, within the epithelium. Importantly, this point marks the last phase of pre-malignancy (Shain & Bastian, 2016).

In general, tumour malignancy is achieved when cells leave the tissue of their origin and invade or spread to other parts of the body (Seyfried & Huysentruyt, 2012). Thus, the transition of melanoma *in situ* to invasive CM is marked by the movement of atypical melanocytes from the skin epithelium into the mesenchymal components of the dermis (Shain & Bastian, 2016). Molecularly, this invasive state is achieved upon sufficient accumulation of driver mutations, most frequently in *BRAF, NRAS, NF1, CDKN2A, TERT, TP53, PTEN,* and genes which encode the SWI/SWF chromatin remodelling complex, such as *ARID1A* and *ARID2* (Eddy et al., 2021; Shain & Bastian, 2016). Collectively, these mutations alter the function of prominent signalling pathways, including WNT, MAPK, and PI3K/AKT, which lead to

subsequent dysregulation in cell proliferation, growth, survival, and apoptosis (Eddy et al., 2021).

The final stage of disease development is marked by the movement of primary tumour cells from the localized region and successful colonization of another tissue (Shain & Bastian, 2016). Importantly, risk of metastatic disease is directly correlated with the depth of an invasive melanoma lesion (Shain & Bastian, 2016). The first tissue to be colonized is most typically the proximal lymph nodes which act as the primary site of drainage for the tissue of origin (Shain & Bastian, 2016). However, this is not an exclusive first step as evidenced by observations of circulating tumour cells and distant metastases irrespective of proximal lymph node colonization (Shain & Bastian, 2016). Grossly, metastasis comprises a multi-step process involving (1) separation of malignant cells from the primary tumour, most typically through EMT, (2) invasion of surrounding tissue through the basement membrane, (3) intravasation and subsequent survival in to the lymph and/or circulatory systems, (4) extravasation out of the vasculature and (5) colonization of a distant tissue, most typically through mesenchymal-to-epithelial transition (Dujon et al., 2021; K. W. Hunter et al., 2008). Most tumours can trace their origin back to a single cell which accumulated enough genetic alterations to become cancerous; however, the environment of primary tumours are incredibly complex and there is a substantial degree of intra-tumour heterogeneity (Marusyk et al., 2012). This heterogeneity is multifaceted and encompasses phenotypic, metabolic, and gene expression differences which alter several cellular properties including motility, proliferative capacity, cytokine secretion, and metastatic potential (Marusyk et al., 2012).

The cellular heterogeneity which exists in melanoma can be, in part, explained by phenotype-switching and this phenomenon provides further insights into disease progression and metastasis. Two broad cellular phenotypes, proliferative and invasive, exist and are described by the MITF rheostat model where the levels of MITF activity, a melanocyte master regulatory TF, determine the phenotypic state of melanoma cells; for example, $MITF^{high}$ cells are proliferative, whereas $MITF^{low}$ cells are more quiescent and invasive in nature (Hoek et al., 2006; Hoek, Schlegel, et al., 2008; Hoek & Goding, 2010; Rambow et al., 2019). These phenotypes, thanks to Next Generation Sequencing (NGS) studies, can be further divided into four subtypes: undifferentiated, neural crest-like, transitory, and melanocytic, which exist and recapitulate various stages of melanocyte development (Belote et al., 2020; Karras et al., 2022; Tsoi et al., 2018). Cells in the proliferative state are most melanocytic in nature, expressing genes associated with melanocyte differentiation, such as those involved in pigmentation, and exhibit the highest levels of MITF expression (Hoek et al., 2006; Tsoi et al., 2018). In contrast, cells of the invasive phenotype have low levels of MITF, are in a dedifferentiated state, and are mesenchymal in nature or are primed for EMT (Hoek et al., 2006; Rambow et al., 2015; Tsoi et al., 2018). As mentioned, multiple transcriptional programs have been identified in melanoma cells which mimic those found normally during development (Belote et al., 2021; Karras et al., 2022; Tsoi et al., 2018). Accordingly, melanoma cells which mirror the neural crest-like state express EMT inducing TFs, such as SNAIL, TWIST, and ZEB family members, which are largely responsible for driving delamination of NC from the NT (Tang et al., 2020). Following migration, local environmental cues promote phenotype-switching and foster successful metastatic colonization (Hoek & Goding, 2010; Rambow et al., 2019).

Treatment

By the early 1970s, Wallace Clark and Alexander Breslow independently devised two similar, but distinct, methods for staging growth and invasiveness of primary CM tumours (Breslow, 1970; Rebecca et al., 2012). These two approaches are still largely in use today; however, they have been expanded upon to incorporate the American Joint Committee on Cancer TNM staging system which not only assesses the histological attributes of a primary tumour (T), but also includes the presence of disease in lymph nodes, as well the number involved (N), and queries the extent of metastatic disease and organs affected (M) (Davis et al., 2019). Wide surgical resection remains the gold-standard for non-metastatic disease and is associated with a 5-year survival rate of 92% (Torre et al., 2015). The extent of surgical resection is dependent on lesion depth and invasive melanomas which are ≥ 1 mm qualify for sentinel lymph node biopsy to assess for the presence of metastatic disease (Kunishige et al., 2013). If malignant cells are detected, the remaining lymph nodes, which surround the sentinel node, are also removed by excision (Kunishige et al., 2013). Any new case of invasive melanoma should be followed-up with systemic staging, regardless of lesion depth and biopsy results (Davis et al., 2019). The proximal drainage lymph nodes of the tissue of origin are the most likely place for initial metastatic spread, thus the first clinical evaluation should assess for local lymphadenopathy by palpation (G. V. Long et al., 2023; Shain & Bastian, 2016). Additional imaging studies, such as ultrasound, CT, or MRI may be indicated, especially in high grade tumours (G. V. Long et al., 2023). If the disease has spread to more distant regions, then non-surgical means of intervention are necessary (Davis et al., 2019).

Drug based therapies for melanoma have evolved considerably over the last fifteen years. In 1975 the United States Food and Drug Administration (FDA) approved the first chemotherapy drug, dacarbazine, for metastatic melanoma (C. Lee et al., 2013). This systemic based drug therapy proved woefully ineffective as evidenced by the less than 10% survival rate of patients with advanced disease (G. V. Long et al., 2023). In 2011 three different FDA approved targeted therapies, pegylated interferon, ipilimumab, and vemurafenib, which work to combat specific molecular defects, were introduced, and have greatly altered disease outlook with 50% of treated patients showing significant disease regression (C. Lee et al., 2013; G. V. Long et al., 2023). However, these drugs are not globally effective as exampled by vemurafenib and dabrafenib which are only effective in BRAF-mutated melanomas, and many patients develop resistance shortly after therapy initiation (Castellani et al., 2023). The Marine lab demonstrated that BRAF-inhibitor (BRAFi) resistance is inversely correlated with the degree of differentiation (Rambow et al., 2018). Likewise, the Galibert lab showed that the ligand induced Aryl hydrocarbon receptor TF is bound by BRAFis and competition with canonical ligands fosters resistance to BRAFi treatment (Corre et al., 2018). Although recent drug discoveries have greatly improved prognosis, quality of life, and survival outcomes of people with advanced disease, it is clear that a better understanding of the mechanisms governing melanomagenesis and disease progression is critical in guiding development of the next generation of targeted therapies.

Aims and Goals of the Thesis

The MC1R is a primary mediator of melanin production and subsequently regulates pigment switching (Walker & Gunn, 2010). Furthermore, LOF coding variants in *MC1R* are associated with the RHC phenotype which comprises pale skin, high naevus count, an inability to tan, and red hair colour due to an abundance of phaeomelanin (Kanetsky et al., 2002; Kempf et al., 2022; Sulem et al., 2007, 2008; Voisey et al., 2006). Cellular responses downstream of active MC1R signalling are complex but it is known that MC1R activation facilitates cAMP/PKA signalling with subsequent MAPK activation and expression of MITF, as well as other gene expression changes, which promote eumelanin synthesis (Levy et al., 2006). Despite the RHC-MC1R connection, the molecular pathways underlying the regulation of phaeomelanogenesis are not well-described. Furthermore, it is not entirely clear how MC1R LOF coding variants or RHC trait contributes to melanomagenesis and disease progression despite their well-described association with the disease. Given this, it is crucial that we investigate how this protein, and its signalling axis, modulate melanocyte gene expression, and the associated GRN, to facilitate phaeomelanogenesis as these insights might prove invaluable in understanding the molecular mechanisms which drive melanomagenesis, especially in the predisposed RHC population.

Thus, a major aim of this thesis is to use scRNA-seq to profile the transcriptomes of, and identify genes that are differentially expressed between, melanocytes which are actively synthesizing one of the two different pigment types: phaeomelanin or eumelanin. To do this, I will use *in vivo* derived melanocytes from mice which almost exclusively produce eumelanin (nonagouti) and compare these to phaeomelanin (lethal yellow, A^{y}/a; recessive yellow, $Mc1r^{e}/^{e}$) producing

melanocytes which genotypically mimic known causes of the RHC phenotypic trait. I hypothesize that significant changes in melanocyte gene expression will be present and that they will in part drive the eumelanotic and phaeomelanotic states. I expect that the observed shift in the transcriptomic signature of these states (eumelanotic versus phaeomelanotic) are, at least in part, altered by the MC1R-PKA-cAMP-CREB-MITF axis; however, I also expect to identify new target genes and signalling pathways which might be responsible for phaeomelanin production and melanoma predisposition. Furthermore, I aim to follow-up on one or more identified genes/pathways to confirm the validity of my findings and gain new insights into melanogenesis and melanomagenesis. Collectively, I hope that the findings from this study will enhance our current knowledge of molecular regulators and GRNs which function to regulate development, differentiation, proliferation, survival, and disease of melanocytes. Relatedly, I expect that discoveries from this study, coupled with future follow-up work, will provide a better intellectual foundation to drive the next generation of therapeutic modalities aimed toward the treatment of pigmentary disorders and melanoma.

Figures

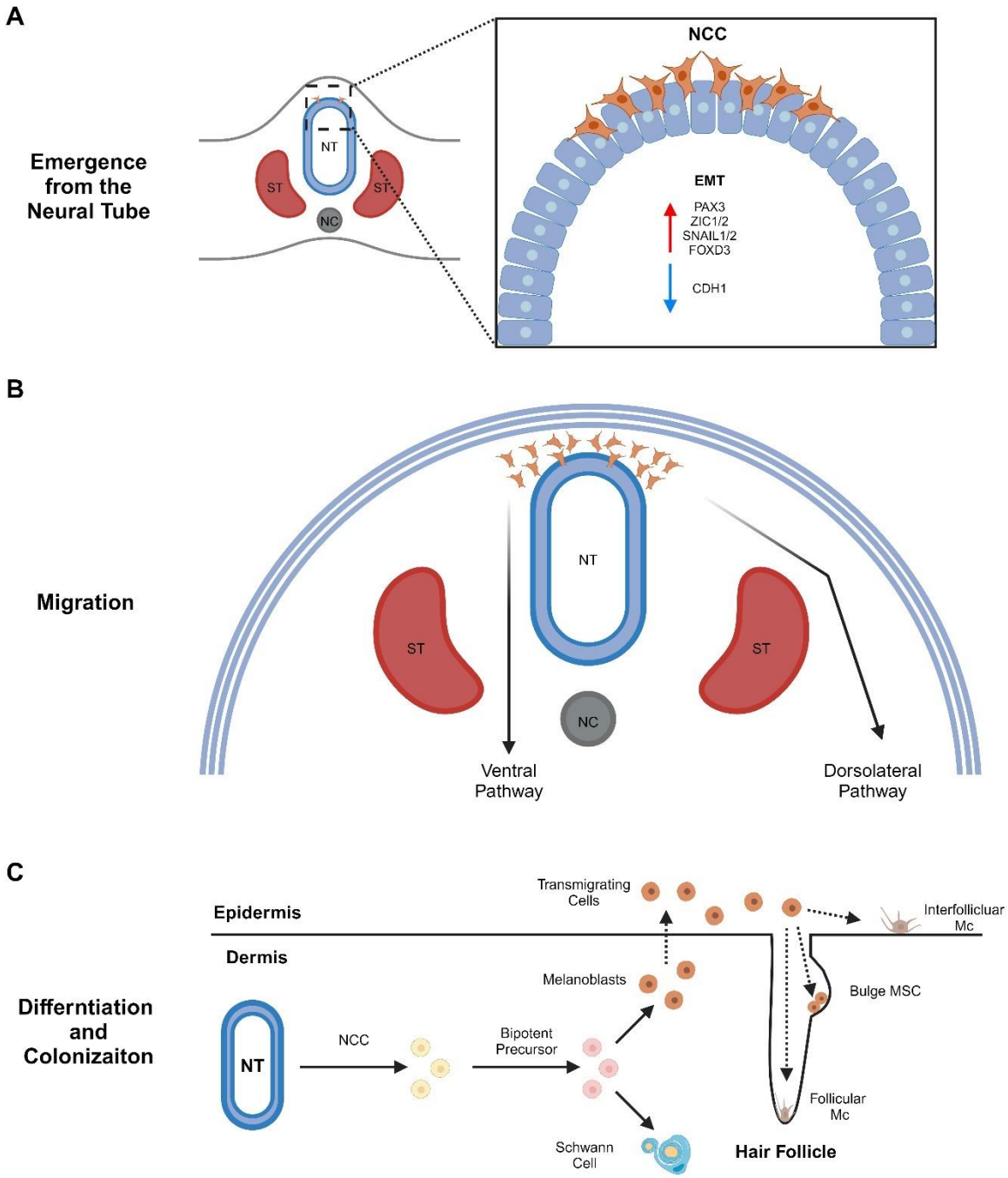


Figure 1. Melanocyte Development: Neural Crest to Melanocyte Differentiation and Colonization. (A) Schematic depicting formation of neural crest cells (NCCs) from the dorsal aspect of the neural tube (NT) with associated changes in specific genes which foster NCC development and emigration; ST = somite, NC = notochord, EMT = epithelial-to-mesenchymal transition. (B) Following delamination and

emigration from the NT, NCCs follow one of two primary paths of migration, a ventral or dorsolateral route. (C) Schematic depicting the stepwise transition of NCCs to post-natal populations of melanocytes. NCC destined to be melanocytes first exist as a bi-potent progenitor cell type. They are then specified into melanoblasts and migrate through the dermis and into the epidermis. These cells continue their migration until they reach one of three locations: (1) the epidermis, giving rise to interfollicular melanocytes, (2) the lower portion of the hair follicle, where they become follicular melanocytes, or (3) the hair bulge where they retain a stem cell status and serve as reservoir for all future melanocytes; Mc = melanocyte. This figure is based on several figures from (Vandamme & Berx, 2019)

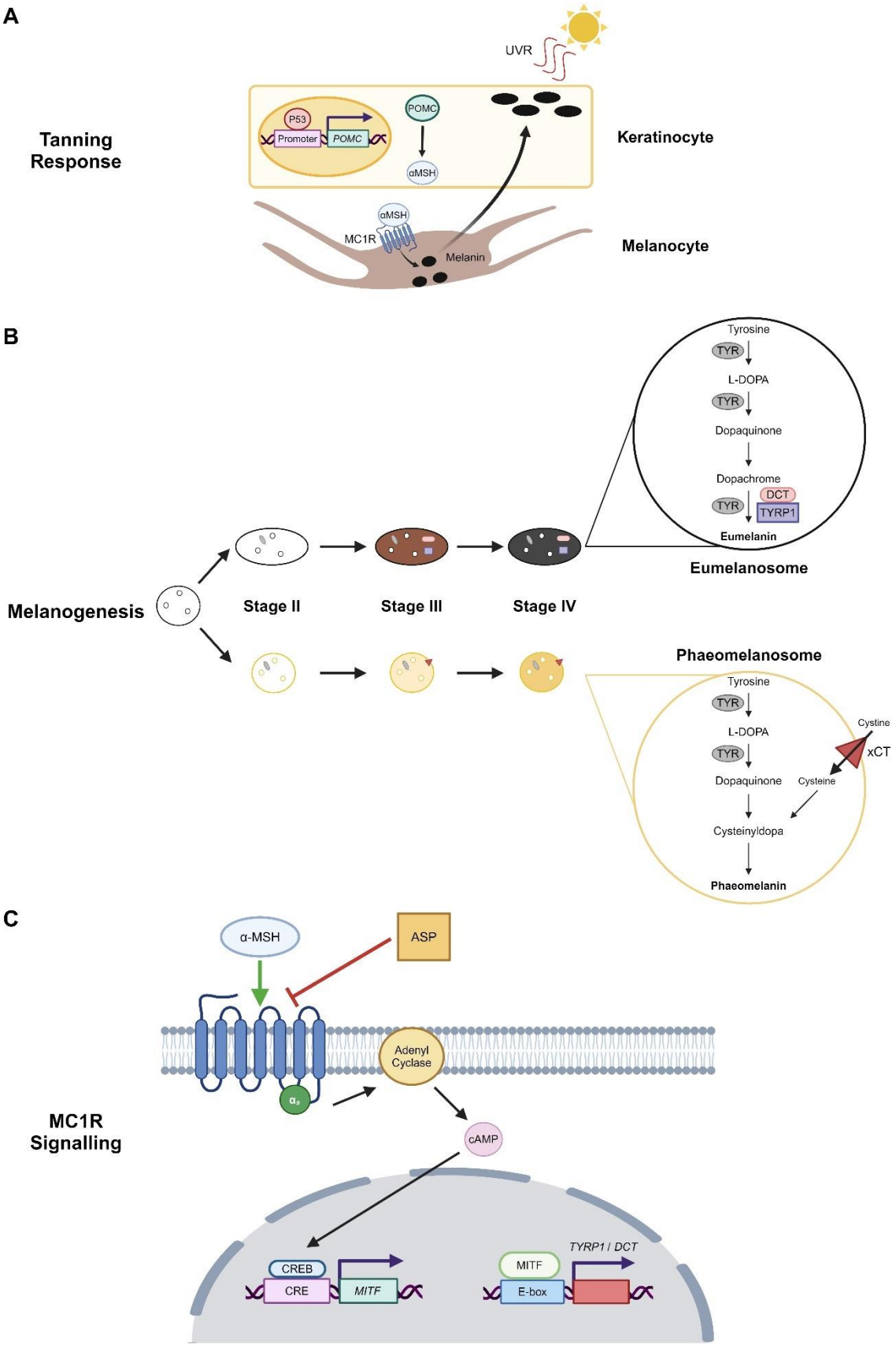

A
Tanning Response
UVR
P53
Promoter
POMC
POMC
αMSH
Keratinocyte
αMSH
MC1R
Melanin
Melanocyte
B
Tyrosine
TYR
L-DOPA
TYR
Dopaquinone
Dopachrome
TYR
DCT
TYRP1
Eumelanin
Eumelanosome
Melanogenesis
Stage II
Stage III
Stage IV
Phaeomelanosome
Tyrosine
TYR
L-DOPA
TYR
Cystine
xCT
Dopaquinone
Cysteine
Cysteinyldopa
Phaeomelanin
C
α-MSH
ASP
Adenyl Cyclase
cAMP
MC1R Signalling
CREB
CRE
MITF
MITF
E-box
TYRP1 / DCT

Figure 2. Melanogenesis: Function of a Melanocyte. (A) Following UVR-insult, keratinocytes signal to melanocytes to produce and transfer melanin. Keratinocytes, through p53, induce expression of *POMC* which is cleaved to form αMSH which binds to MC1R on the surface of melanocytes. This induces a secondary messenger system which leads to melanin production and transfer. (B) Melanogenesis takes place inside the melanosome which undergoes a stepwise series of maturation steps in order to create melanin. Importantly, synthesis of eumelanin largely takes place inside eumelanosomes while phaeomelanin is produced inside phaeomelanosomes. The production of both pigments is dependent on the enzyme TYR. Eumelanin can be produced spontaneously from DQ (Dopaquinone); however, it proceeds more readily when under the influence of two enzymes, DCT and TYRP1. In contrast, phaeomelanin synthesis occurs when DQ is in a melanosome with abundant cysteine, an amino acid which is mainly brought into the cell by the xCT antiporter in the form of cystine. (C) Schematic depicting signalling through the MC1R axis. When α-MSH binds to MC1R it leads to induction of MITF which in turn induces expression of eumelanin synthesising enzymes such as *TYRP1* and *DCT*. In contrast, Agouti (ASP) inhibits binding of α-MSH to MC1R and therefore blocks the induction of MITF and its downstream targets; CREB = cAMP Response Element-binding Protein, CRE = cAMP Response Element.

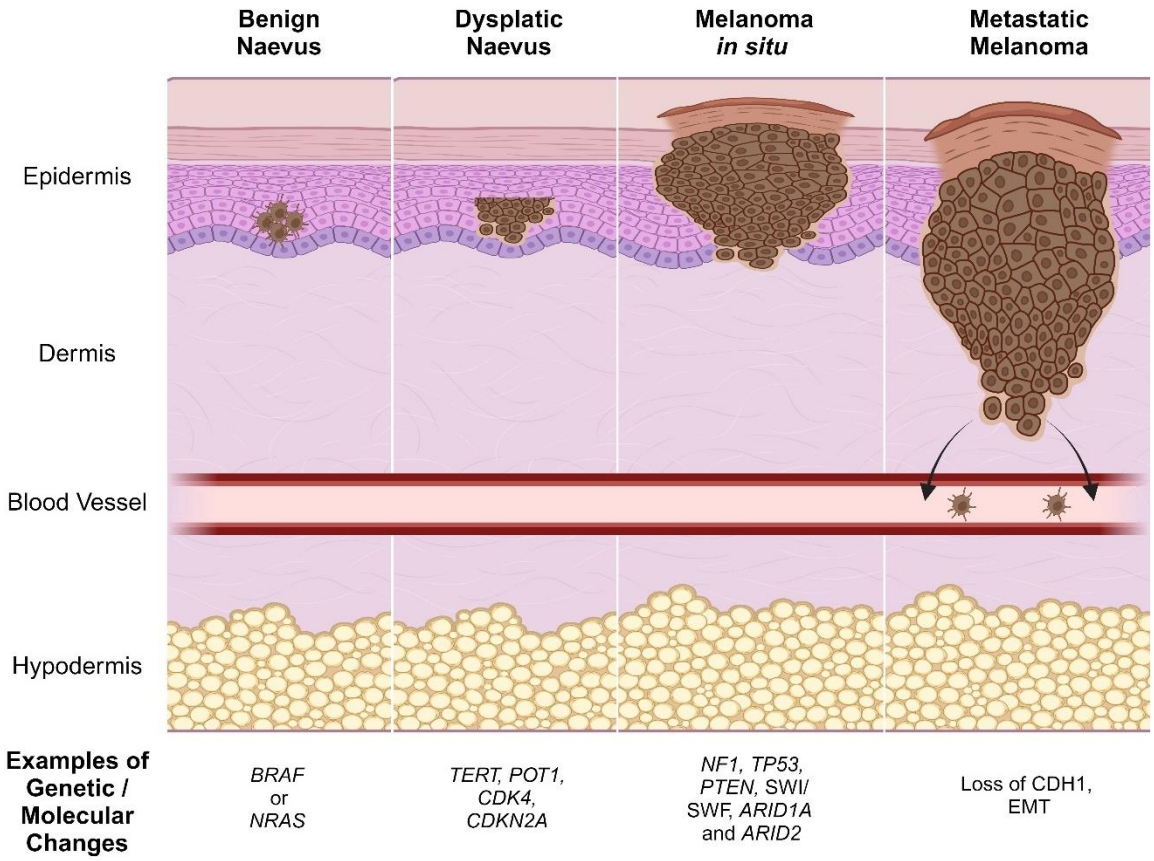


Figure 3. Melanoma Evolution. Following acquisition of a driver mutation by a melanocyte, namely *BRAF* or *NRAS*, a state of limited hyperproliferation exists which yields a benign naevus. Additional somatic variants subsequently lead to cellular dysplasia and atypia. Accumulation of driver mutations leads to the development of Melanoma *in situ* and continued unrestricted growth leads to expansion of the lesion beyond the epidermis with metastatic disease being achieved once primary tumour cells enter the vasculature and colonize tissues outside that of the tissue of origin.

Chapter 2: Materials and Methods

Animal Use and Methods

Ethics Statement, Animal Husbandry, and Breeding Scheme

Routine animal care was performed in accordance with the standards of practice set forth by the Institutional Animal Care and Use Committee at the National Institutes of Health (NIH) (Bethesda, MD, United States of America). Experimental procedures involving animals were approved, and carried out in accordance with the guidelines set forth, by the National Human Genome Research Institute (NHGRI) animal study protocol G-94-7, 'Genetic and Embryological Studies of Murine Models for Neural Crest Disorders', assigned to principal investigator Dr. William J. Pavan of the Genetic Disease Research Branch (GDRB). Routine care and colony maintenance was administered by animal technicians within the NHGRI Office of Laboratory Animal Medicine, as well as myself. All mice in this study were fed a routine diet of standard chow.

Nonagouti *(a/a*) (C57BL/6J; JAX Mice #000664), lethal yellow (*A^y/a*) (B6.Cg-A^y/a; JAX Mice #000021), and recessive yellow (*$Mc1r^{e/e}$*)(C57BL/6J-Mc1r^e/J; kindly provided by Dr. Jonathan Zippin (Weill Cornell), equivalent to JAX Mice #000060) mice were used for data generated in this thesis. All mutant alleles were maintained on a C57BL/6J genetic background.

To generate experimental samples for *in vivo* melanocytes, breeding age nonagouti and lethal yellow mice were bred (*a/a* x *A^y/a*) to produce sex and age matched littermate samples comprising one male of two genotypes*, a/a* (nonagouti) or *A^y/a* (lethal yellow). The recessive yellow mice were maintained as homozygotes for *Mc1r* (*$Mc1r^{e/e}$*) and nonagouti (*a/a*) therefore a different breeding strategy, described next, was used to generate samples for the pairwise comparison of

recessive yellow and nonagouti melanocytes. Sexually mature nonagouti (*a/a*) animals of both sexes were moved into a single cage so that they would mate with one another (*a/a* x *a/a*) on the same day, and at the same time, as breeding age recessive yellow mice (*Mc1r*$^{e/e}$ x *Mc1r*$^{e/e}$), to generate aged matched male samples which were not littermates. In total, this breeding strategy generated two litters of mice, born the same day from which males of the following genotypes were selected: *a/a*; *Mc1r*$^{+/+}$ (nonagouti) and *a/a*; *Mc1r*$^{e/e}$ (recessive yellow).

On postnatal day 3 (P3), mice were euthanized and skin samples were harvested for tissue digestion and Fluorescence-Activated Cell Sorting (FACS) enrichment optimisation experiments, as well as for scRNA-seq. Pups from all litters were phenotypically distinguishable by P2, due to differences in their coat colour, black or yellow; however, the final genotype of samples used in the scRNA-seq experiments was confirmed in the sequencing results.

Tissue Harvest, Digestion, and Immunostaining

To isolate *in vivo* derived melanocytes, P3 pups were euthanized, in an animal use designated fume hood, by decapitation with sterile scissors. To remove the dorsal skin, a scalpel was first used to make four incisions along anatomically defined margins as follows: two transverse cuts, one between each axilla and another between the anterior pelvises as well as two bilateral incisions, which were made along the midline from the axilla to the anterior pelvis. This dissected tissue was removed from the animal using sterile forceps and then subsequently placed, hair side facing up, in a 6 cm petri dish containing ice-cold 1x PBS (Phosphate Buffered Saline). Following 15 mins of incubation in PBS, the excised skin was

moved and placed, hair side down, on the lid of a 6 cm petri dish so that the hypodermal layer, comprising subcutaneous fat, could be removed. Using curved forceps, broad brush strokes were run along the entire length of the tissue until the entire hypodermis was removed.

The remaining tissue now comprised two layers, the epidermis and dermis. To facilitate separation of these layers, samples underwent an enzymatic-based digest with trypsin. All samples were moved into 6 cm petri dishes, hair side up with one sample per dish, containing 3 mL 0.25% Trypsin-EDTA (ThermoFisher #25200-056) and then set to incubate for 30-45 minutes at 37˚C and 10% CO_2. Following this incubation, the epidermis of each sample was manually removed using forceps with the assistance of a benchtop microscope at 1.5x magnification. The epidermal Flayer of each sample was then discarded into a designated animal waste receptacle. The remaining tissue of each sample, comprising the dermal layer only, were moved to their own respective 6 cm petri dish and then briefly incubated in 2 mL of ice-cold Dulbecco's Modified Eagle Medium (DMEM) (ThermoFisher #12491015) to naturalize the residual trypsin. While in the petri dish containing media, the dermis was cut into fine pieces, using fine scissors, to increase the amount of exposed surface area for the next enzymatic digest step.

Once all samples were processed, they were moved into 15 mL Falcon tubes, one for each sample, using 5 mL plastic Pasteur pipettes for another round of enzyme digestion. Liberase (Roche #05401119001) was added to each sample until a final concentration 0.3 mg/mL was reached. The Falcon tubes, containing the samples, were then moved to a rotating platform, and allowed to incubate for 45 mins at 37°C. Following incubation, 10 mL of DFD solution (DMEM / 20% FBS / 0.5

mg/ml DNase (Sigma DN-25)) was added to each sample and then tubes were inverted several times to allow for adequate mixing and enzyme inactivation.

After enzyme inhibition, the digested tissue and solution was then poured into a 6 cm petri dish, with one sample per dish. Next, 10 mL of ice-cold Wash Solution (1X PBS / 5% FBS / 25 mM HEPES / 2 mM EDTA) was added to each dish. The samples were then mechanically digested, one sample at a time, as follows: the digested tissue solutions were first, drawn into a sterile 60 cc syringe (Covidien #8881560125), and then forcefully expelled, through a 70 µm Falcon syringe filter (BD Biosciences #340605), back into the petri dish from which the sample originated. This process was repeated three times to provide adequate mechanical digestion and further facilitate separation of the tissue/cell mix into single cells. The contents of each sample were drawn into their own respective syringe for a 4th time except this time the solutions were expelled into 50 mL Falcon tubes with one sample per tube.

After mechanical digestion, Wash Solution was added to each sample until a total solution volume of 50 mL was achieved. Samples were then centrifuged, at 1250 rpm (300 g) for 7 minutes and 4°C, to form a pellet of cells. The resultant supernatant was removed carefully by vacuum aspiration so as not to disturb the cell pellet. Pellet cells were resuspended, and thoroughly mixed, in 25 mL of Wash Solution. To facilitate further mechanical digestion, the entire solution of each sample was drawn into a sterile 60 cc syringe and then forcefully expelled into a 50 mL Falcon tube with one sample per tube. The samples were then centrifuged at 1250 rpm (300 g) for 5 minutes and at 4°C to separate the cells from the solution. The residual supernatant was removed by aspiration with care so as to not disturb

the pelleted cells. The cells of each sample were then resuspended in 150 µL of Wash Solution and placed on ice until the start of the immunostaining procedure.

To create appropriate gating parameters for FACS, single marker controls are necessary. Thus, 20 µL of resuspended dermal cells were taken from each sample and pooled into a new 50 mL Falcon tube and additional Wash Solution was added to achieve a total volume of 1000 µL. This pool was then distributed into three new 50mL Falcon tubes, four tubes total with 250 µL / tube, to create a no stain control as well as single stain controls, CD45 Only, KIT Only, and Cell Viability (Table 1).

Table 1. Antibodies Used for FACS Experiments.

Condition	**Antibody**	**Dilution**	**Host Species**	**Catalogue No.**
CD45 Only	CD45.2 - FITC	1:400	Mouse	BD Pharmingen #553772
KIT Only	CD117 -PEcy7^{+},	1:100	Rat	BD Pharmingen# 558163
Cell Viability	LIVE/DEAD™ Fixable Aqua Dead Cell Stain	1:200	N/A	Invitrogen #L34965
No Stain Control	N/A	N/A	N/A	N/A

For the experimental samples, all three markers (CD45.2-FITC, CD117-PEcy7, and LIVE/DEAD™ Fixable Aqua Dead Cell Stain) were added to their respective dilution factor listed above. After addition of the markers, all Falcon tubes were wrapped in aluminium foil, to protect from light degradation, and then set to incubate for 30 mins at RT. Following incubation, 30 mL of Wash Solution was added to all samples and controls and then the tubes were centrifuged at 1250 rpm (300 *g*) for 5 mins at 4°C. The residual supernatant was carefully removed by vacuum aspiration and then the cell pellets of all samples and controls were resuspended using 200 µL of Wash Solution. After this, 70 µm cup filters (Corning #352350) were pre-wetted with 100 µL of Wash Solution and then the total volume of each sample and control condition were passed through the filter into their own respective polystyrene FACS tube (BD Falcon #352058). Last, additional Wash Solution was added to each FACS tube to achieve a final total volume of 1200 µL / sample or control.

Fluorescence-Activated Cell Sorting (FACS)

The *in vivo* derived cells, used for protocol optimisation and sequencing, were isolated using a FACSAria™ Fusion Flow Cytometer (BD Biosciences) equipped with BD FACSDiva software. This was done with help from the NHGRI Flow Cytometry Core as follows: the no stain control samples were used to delineate intact single cells from cellular debris and doublets. This was achieved using orthogonal lasers to detect cell size (forward scatter, FSC) and shape (side-scatter, SSC). Once the voltage parameters were defined, a gate was drawn to segregate

the single cells from cellular debris and doublets. Next, the single stain control cell viability control, containing LIVE/DEAD™ Fixable Aqua Dead Cell Stain, was used to refine the gate of single cells to exclude any cells which were deemed non-viable. Briefly, the LIVE/DEAD™ Fixable Aqua reagent contains a probe which emits an intense fluorescent signal when bound to free amines, which are abundant in cells with compromised integrity of their cell membrane, and, therefore, a strong signal indicates non-viability. With this, I refined the gates to only include viable single cells. I then used the remaining single stain antibody control samples to detect and define appropriate voltage for my two cell-surface markers of interest, CD117-PEcy7 (KIT) and CD45.2-FITC (CD45). Following this, each experimental sample was briefly subjected to flow cytometry in order to define a positive gate, containing melanocytes ($CD117^+$ / $CD45.2^-$), and a negative gate ($CD117^-$). Once the final gates were set, the cells from each experimental sample were subjected to FACS mediated isolation with samples being collected into microcentrifuge tubes containing a solution of 1xPBS + 0.04% FBS.

Cell and Molecular Biology Techniques and Methods

Cell Culture

Routine Culturing and Maintenance

Cell lines used in this study were maintained as follows: at NHGRI, the human melanoma cell line, 501mel, was grown in DMEM (ThermoFisher #12491015) which contained 10% FBS, 1 mM sodium pyruvate (ThermoFisher #1136007), and 4 mM L-Glutamine (ThermoFisher #25030081). At the LICR, the human melanoma cell line, 501mel, was grown in Roswell Park Memorial Institute

(RPMI) 1640 media (ThermoFisher #11875093) and supplemented with 10% FBS. The 501mel-iTBX3-3xHA-PuroR cell line was maintained in RPMI-1640 containing 10% FBS and 1µg/mL of Puromycin (ThermoFisher #A1113803). Antibody was used to select for cells which had stable integration of transfected plasmids.

Regardless of institution, all cell lines were regularly passaged when 80-90% confluent. To passage cells, all medium was first removed by aspiration. Next, flasks, or tissue culture plate wells, were washed three times with 1xPBS. All cell lines used were adherent; therefore, to facilitate detachment, 0.25% Trypsin-EDTA was added, after aspiration of the final PBS wash, and the cells were incubated until detachment occurred. The enzyme was inactivated by adding culture medium directly to the cells at 2:3 times the volume of trypsin used. This resultant solution of cells was collected into a Falcon tube, mixed thoroughly by inversion, and then seeded at appropriate densities for routine passaging (1:6-1:12) or as needed for experimental use.

Cell line maintenance and all routine cell culture techniques were done in a laminar flow cabinet, under sterile conditions, with grade-certified tissue culture materials and reagents. To cryopreserve cell lines for long term storage, the cells within 90% confluent flasks were first detached using trypsin. Culture media, at 3x the volume of trypsin, was added to the cell culture flask and then the entire solution was transferred to a Falcon tube. The Falcon tube was then centrifuged (300 g, 5 min) to pellet the cells. The resultant supernatant was removed by aspiration and cells were resuspended in a freezing medium, comprising their base media (i.e., DMEM, RPMI) with 10% DMSO. The freezing medium, containing the resuspended cells, was moved into Nunc™ Cryovials™ (ThermoFisher #374081). The vials were then transferred to a Mr. Frosty™ Freezing Container (ThermoFisher #5100-000) and then placed at -80 °C to allow for gradient colling (-1°C / minute) to achieve -

80°C. Subsequently, vials were transferred into liquid nitrogen tanks for long-term storage. Before storage, after thawing, and during routine passaging, cell lines were tested for the presence of mycoplasma by PCR and were maintained negative throughout the entirety of the study. Cell lines were subject to authentication using short tandem repeat profiling.

Culturing of FACS Isolated Primary Cells

Using FACS, primary murine cells were sorted into two populations, positive and negative, with each being captured in a solution of in 1xPBS + 0.04% FBS. After FACS, the contents of each microcentrifuge were transferred to their own respective 1.5 mL Eppendorf tube which contained 500 µL RPMI-1640. After this, cells were counted with a TC20™ Automated Cell Counter (BioRad #1450102) so that 50,000 cells / population could be seeded onto a Thermo Scientific™ Nunc™ Lab-Tek™ Chamber Slide™ (ThermoFisher #177402). Next, 300 µL of medium, containing RPMI-1640 with 5% Heat Inactivated FBS (ThermoFisher # 10082147), 200 pM Cholera Toxin (Sigma-Aldrich #C8052), 50 ng/mL Recombinant Mouse Stem Cell Factor Protein (R&D Systems #455-MC), 200 nM 12-O-Tetradecanoylphorbol-13-Acetate (TPA) (Sigma-Aldrich #79346), 0.6 ng/mL Recombinant Human bFGF (R&D Systems #233-FB-010/CF), 2 mM L-Glutamine, and 500 U/mL Penicillin-Streptomycin (ThermoFisher #15070063), was added to each well. Cells were cultured for 24 h and then fixed for immunofluorescence, this procedure is described in detail in the next section.

Immunofluorescence

Primary Cells at NHGRI

After 24 h in culture, wells containing primary cells isolated by FACS analysis of murine skin samples were washed 3x times with 1x PBS, and then fixed with 4% paraformaldehyde (PFA) by incubating them for 10 mins at RT. Following fixation, PFA was removed and then the cells were washed 3x times with 1x PBS. To allow for intracellular recognition of target proteins by antibodies, cells were permeabilized with 1xPBS + 0.5% Triton X-100 for 10 mins. The media was removed by aspiration and then cells were blocked with a blocking solution (1xPBS containing 5% Normal Donkey Serum (NDS)) for 30 mins at RT. Primary antibodies (Table 2) were diluted in blocking solution, added to the wells, and then set to incubate for 24 h at 4°C. Following incubation, the primary antibody solution was removed by aspiration and the wells were then washed 3x times with 1xPBS. Secondary antibodies, with conjugated fluorophores, were diluted in blocking solution, to their respective working concentration and then added to the wells (Table 2). Samples were then wrapped in aluminium foil, to protect from light degradation of the fluorophores, and then set to incubate for 1 h at RT. Following secondary antibody exposure, the solution was removed by aspiration and then wells were washed 3x times with 1x PBS. The chamber portion of the slide was removed, ProLong™ Diamond Antifade Mountant with DAPI (ThermoFisher #P36966) was added, and then the slides were sealed with a coverslip and set to dry, away from direct light, for 24 h. Samples were imaged using ZEISS LSM 980 microscope with an objective piece set at 10x.

Table 2. Antibodies Used for Immunofluorescence Experiments of Primary FACS Sorted Cells.

Antigen	Primary / Secondary	Dilution	Host Species	Catalogue No.
PAX3	Primary	1:350	Mouse	DSHB PAX3, RRID:AB_528426
DCT	Primary	1:250	Goat	Santa Cruz #sc-10451
KRT14	Primary, conjugated Alexa Fluor® 647	1:200	Rabbit	Abcam #ab206100
Mouse	Secondary	1:500	Donkey	Invitrogen #A-10037
Goat	Secondary	1:1000	Donkey	Invitrogen #A-11055

iTBX3-3xHA-PuroR at LICR

Immunofluorescence experiments for the inducible TBX3 (iTBX3-3xHA-PuroR) 501mel cells were performed Dr. Sizhu Lu. iTBX3-3xHA-PuroR cells were seeded into wells containing glass cover slips. After this, doxycycline (Sigma #D9891) was added, to achieve the desired experimental concertation, and induce the expression tagged-TBX3. Following 24 h of exposure, the medium was aspirated, cells were washed once with 1x PBS, and then fixed with 4% PFA for 10 mins at RT. Following fixation, the PFA was removed, and the cells were then

washed 2x times with 1x PBS. Cells were permeabilized and blocked at the same time with a solution of 1xPBS containing 5% Bovine Serum Albumin (BSA) and 0.1% Triton X-100 for 20 mins at RT. Primary antibodies (Table 3) were diluted in blocking solution (1x PBS + 5% BSA) and then added to the wells and set to incubate for 1 h at RT. Following primary body incubation, the solution was removed by aspiration and wells were then washed 2x times with 1x PBS. Secondary antibodies, with conjugated fluorophores, were diluted in blocking solution to their respective dilution factor, listed below; DAPI (0.5 µg/mL) was then added; and finally, the solution was added to the wells. Samples were wrapped in aluminium foil and then set to incubate for 30 mins at RT. The secondary antibody solution was removed by aspiration and then wells were washed 3x times with 1x PBS. The secondary antibody solution was removed and then the cover slips were mounted on VWR® Polysine® microscopy slides (VWR, 631-0107) with 2 µL of VECTASHIELD mounting medium (Vectorlabs, H-1000-10). Coverslips were sealed by administration of nail polish to the edges of the coverslip. Samples were then imaged using a Zeiss 710 microscope with a 20x objective.

Table 3. Antibodies Used for Immunofluorescence Experiments of iTBX3-3xHA-PuroR Cells.

Antigen	Primary / Secondary	Dilution	Host Species	Catalogue No.
HA	Primary	1:500	Mouse	Roche #11583816001
TBX3	Primary	1:250	Rabbit	Abcam #ab99302
Mouse	Secondary	1:1000	Donkey	Invitrogen #A-10036
Rabbit	Secondary	1:1000	Donkey	Invitrogen #A-21206

Brightfield Microscopy

To assess for the presence of melanin, and observe cellular morphology, of the positive and negative FACS isolated cell populations, brightfield images were obtained with an Axio Observer A1 microscope which had an AxioCam MR R3 camera. Images depicted in this thesis were taken at 20x magnification.

Single-cell RNA-sequencing of FACS Enriched Cell Population

FACS-isolated cells were analysed for cell viability and concentration using a Luna-FX7 cell counter (Logos Biosystems). Gel Bead-in-Emulsions were prepared by loading 5,000 cells/sample onto a Chromium Chip G (10x Genomics #1000127) and run using the Chromium controller (10x Genomics #1000204). cDNA libraries were generated with the Chromium Single Cell 3' GEM, Library and Gel Bead Kit V3.1 (10x Genomics #1000128) by following the manufacture's suggested protocol. The cDNA libraries of each sample were indexed and then pooled for sequencing using the NextSeq 500/550 Hi Output KIT v2.5 (Illumina #20024907) on an Illumina NextSeq550. Cell Ranger (10x Genomics) was used to align reads to Mus musculus genome build mm39 as well as perform barcode and UMI counting. Downstream processing of the data was performed with Partek Flow™ Genomic Analysis Software.

Bulk RNA-sequencing of 501mel Cells (TBX3 Knockdown vs Control)

501mel cells (140,000/well) were plated in a 12-well plate (1.2 mL/well). dsiRNAs (Negative Control 1 (NC1), TBX3 13.6, TBX 13.8; Table 4; Integrated DNA Technologies) were diluted in 300 µL of Opti-MEM (final concertation of 20 nM). Lipofectamine RNAiMAX (6 µL/100 µL); Invitrogen #13778075) was then diluted in 300 µL of Opti-MEM. Diluted dsiRNA and Lipofectamine were mixed and set to incubate at RT for 5 minutes. 200 µL of dsiRNA-Lipofectamine mix was added to each well. At 24 h, cells were lysed with TRIzol™ Reagent and processed for RNA isolation following the manufacturer's suggested protocol (Zymo Research #R2053).

RNA purity was assessed, via Agilent tapestation by the NHGRI Microarray Core, with all samples having a RIN purity of ≥ 9.0. RNA samples were submitted to Omega Bioservices (Norcross, GA, USA) for bulk RNA-sequencing (bulk RNA-seq). RNA purity was again assessed, via an Agilent tapestation, with all samples having a RIN ≥ 9.0. Library construction was completed using NEBNext® Ultra™ II Directional RNA Library Prep Kit for Illumina®. Samples were sequenced using NovaSeq 6000 (Illumina) PE150 with ~40 M (20 M in each direction) base read throughput for each sample. Phred Mean Quality scores for all samples was ≥ 38.86.

Table 4. Sequences of DsiRNAs Used for Knockdown of TBX3.

DsiRNA ID	Sense (5' → 3')	Antisense (5' → 3')
hs.Ri.TBX3.13.6	GAAUUUAUUAUAUCUAAG	UACAGAGCUUAGAUAUAA
hs.Ri.TBX3.13.8	AAAAGAAAUUGCAACUGU	AAACCUGACAGUUGCAAU

Western Blot Procedure

Cell Lysis

Wells containing iTBX3-HA-PuroR cells were washed once with 1x PBS. 200 µL of RIPA lysis buffer was added to each well and then plates were rotated for 10 mins at 4°C. The residual whole cell lysates were collected and transferred to 1.5 mL Eppendorf tubes. 2x Laemmli sample buffer (125 mM Tris-HCl pH 6.8, 4% Sodium dodecyl sulphate (SDS), 0.01% bromophenol blue, 10% β-mercaptoethanol, and 20% glycerol) was added to the Eppendorf tube, after which the lysate was

boiled at 95 °C for 5 mins. Samples were removed from heat, allowed to cool to RT, and then further processed by SDS-PAGE (see below).

SDS-PAGE

To assess the levels of TBX3 protein, sodium dodecyl sulphate polyacrylamide gel electrophoresis (SDS-PAGE) was first performed to resolve total protein by molecular weight. Resolving gel mix was made by creating a solution with the following components: 12% acrylamide (Severn Biotech), 375 mM Tris, 0.1% SDS, pH 8.8, 0.1% Ammonium persulfate (APS), and 0.1% tetramethylethylenediamine (TEMED). The gel solution was poured into a gel cassette, topped with 1 mL of isopropanol to prevent desiccation and to create a smooth edge, and set to incubate until acrylamide polymerisation was complete.

After complete polymerization of the resolving gel, the stacking gel mixture was prepared. Stacking gel solution was made and comprised 4% acrylamide, 125 mM Tris, 0.1% SDS, pH 6.8, 0.17 % APS, and 0.083% TEMED. The isopropanol phase was discarded and then the stacking gel solution was added to the top of the resolving gel. A well comb was inserted and then the stacking gel was left to polymerize. Following polymerization of the stacking gel portion, gels were moved into a blotting tank containing 1x running buffer (25 mM Tris, 192 mM glycine, 0.1% SDS. Samples, alongside Precision Plus Dual Colour Protein Standard ladder (Bio-Rad), were loaded into the gel and then subjugated to electrophoresis at 100 V for 2 h.

Immunoblotting and Membrane Reveal

Shortly before the completion of electrophoresis, sponges, Whatman filter papers (Cytiva #3030-917), and nitrocellulose membranes (Amersham #106000002) were immersed in 1x transfer buffer (25 mM Tris, 192 mM glycine, and 20% methanol) to allow for equilibration. Directly following electrophoresis, proteins from the gel were prepared for direct transfer to a nitrocellulose membrane by creating a transfer module in the following layers: sponge, filter paper, gel, nitrocellulose membrane, filter paper, and sponge. The entire transfer module was then moved to a tank containing 1x transfer buffer, with an ice pack, and then subjected to constant electric current (0.5 Amp) for 1 h.

Membranes were carefully removed from the transfer modules and then placed into a blocking solution of 5% milk, in 1x TBS-T (0.1% Tween; ThermoFisher #BP337-500), and set to incubate for 1 h at RT. Primary antibodies were diluted, to the desired concentration (see below), in a solution of 5% Bovine Serum Albumin (BSA), in 1x TBS-T, and placed on a roller for overnight incubation at 4 °C (Table 5). After 16 h of incubation, the membranes were washed 3x times with TBS-T. During the last wash, secondary antibodies were prepared at a concentration of 1:5000 in 5% milk in TBS-T (Table 5). Following removal of the wash solution, secondary antibodies were added to the blots and set to incubate for 2 h at RT. Membranes were then washed 3x times with TBS-T. Following the last wash, ECL western blot detection reagents (Cytiva #GERPN2106) were administered to the blot and set to incubate for 5 mins at RT. After incubation, excess ECL was removed, membranes were placed into a cassette, and X-ray films (Fujifilm) were developed in the dark room.

Table 5. Antibodies Used for Western Blot Experiments.

Antigen	Primary/ Secondary	Dilution	Host Species	Catalogue No.
GAPDH	Primary	1:1000	Rabbit	Sigma-Aldrich #G9545
TBX3	Primary	1:1000	Rabbit	Abcam #ab99302
Rabbit-HRP	Secondary	1:5000	Goat	ThermoFisher #31460

Bioinformatics

Single-cell RNA-seq Analysis

Single cell QA/QC included steps to filter out cells which did not meet the following parameters defined in the two pairwise experiments (lethal yellow / recessive yellow) as: barcode count 600-32,000/3,000-45,000, number of genes detected 500-6000/500-7000, and % ribosomal counts 12-43%/12-39%. Of the 31,017 annotated murine genes, 16,793 (54.14%)/20,060 (64.7%) passed an exclusion cut-off where genes were excluded if they had zero counts in at least 99.9% of the cells. The remaining read counts were normalized using a $\log_2$-based method

on Counts Per Million (CPM). Normalized counts underwent dimensional reduction via a Principal Components Analysis (PCA) on the first 100 principal components and unsupervised, non-biased, Graph-based clustering through a Louvain algorithm on the first 20 principal components. Graph-based clusters underwent further dimensional reduction for visualization on a Uniform Manifold Approximation and Projection diagram. Postnatal mouse skin cell types including dermal fibroblasts, dermal papilla, transit amplifying cells, matrix cells, and epidermal cells were identified by utilizing published signature gene lists (Rezza et al., 2016). The most highly expressed genes (top 10%) from the signature gene lists were overlayed on the UMAP and the graph-based clusters which coincided with expression overlay were assigned to each cell type. All non-melanocyte cell types were subsequently filtered out, leaving only clusters classified as melanocytes for downstream analysis. The melanocyte only population underwent a further iteration of PCA, graph-based clustering, and UMAP display. To eliminate the variable of cellular heterogeneity as influenced by the mitotic state, I selected for cells within the G_0 phase using a gene expression overlay established by Hsiao et al (Hsiao et al., 2020). The melanocytes within the G_0 phase underwent a further iteration of PCA, graph-based clustering, and UMAP analysis.

Gene Ontology and Pathway Analysis

Genes comprising the MiGS were uploaded to the Gene Ontology Resource for GO Enrichment Analysis via PANTHER v18.0 for Overrepresentation Tests (GO Ontology database DOI:10.5281/zenodo.6399963; Released 2022-03-22). The MiGS was run against a reference list comprising all *Mus musculus* genes in the database. Fisher's Exact test was performed with a False Discovery Rate correction

for GO Biological Process Complete, GO Cell Component Complete, and GO Molecular Function Complete with significant results being those with an FDR < 0.05. To identify predicted upstream regulators, I utilized QIAGEN's Ingenuity® Pathway Analysis (Winter Release 2023 (Released: 2023-12-15). Testing was done via Expression Core Analysis on the observed experimental fold change of the MiGS for both pairwise experiments.

Gene Set Enrichment Analysis

Gene lists comprising the significant differentially expressed (DE) +FC and -FC genes regulated by TBX3 were uploaded to the Molecular Signatures Database (MSigDB) for gene set enrichment analysis (GSEA) utilizing the Kyoto Encyclopaedia of Genes and Genomes (KEGG). For the +FC list, the top 500 genes by fold change for TBX3_13.8 were used as the maximum input value is 500 genes. Each list was tested independently with significant terms being those with an FDR q-value < 0.05.

TBX3 ChIP-seq Analysis

Prior to mapping to the human reference genome (hg38) with Bowtie2 (v.2.3.5) (Langmead & Salzberg, 2012), quality of the raw sequencing data was evaluated using FastQC (v.0.11.7), with adapter contamination removed using CutAdapt (v.2.8). Peak calling was performed using MACS2 (v.2.1.2) (Y. Zhang et al., 2008) with a 0.01 q-value threshold. Bowtie2-generated SAM files were compressed to BAM files, indexed using SAMtools (v.1.9), and sequentially converted to bigWig files using UCSCtools (v.373). The BED files of both replicates

were intersected using the UCSC Table Browser to pull out common peaks from replicate 2 (40,974) that had ≥80% overlap with replicate 1 (32,479), which yielded a group of 20,449 common peaks. For simplicity of downstream analysis, the 20,449 peak coordinates used were derived from the BED position parameters of replicate 1.

The Genomic Regions Enrichment of Annotations Tool (GREAT v4.0.4) in the “Basal plus extension” mode was used to analyse the functional significance of cis-regulatory regions of the TBX3 bound ChIP peaks. Each annotated gene was assigned a basal regulatory domain of 5 kb upstream, and 1 kb downstream, of the transcriptional start site (TSS). The regulatory domain of that gene was then extended in both directions to the nearest gene's basal domain but with no more than a 100 kb extension in one direction (McLean et al., 2010). Discovery of enriched binding motifs was done using the MEME-ChIP DNA binding motif analysis tool (Bailey et al., 2015). 250bps were added up and downstream of the chromosomal coordinates corresponding to the absolute summit of all overlapping peaks. A FASTA file was generated using the usegalaxy.org bedtools application ‘GetFastaBed’ (Quinlan & Hall, 2010). This was run against the default settings in MEME-ChIP, except for maximum width for ‘What width motifs should MEME and STREME find?’ which was increased to 20 bases. Peak distributions were obtained from GREAT and ChIPseeker (Yu et al., 2015), via usegalaxy.org. The histogram was produced by GREAT, while the Venn diagram was created with ChIPseeker.

Bulk RNA-seq Analysis

Data were analysed by ROSALIND® (https://rosalind.bio/), with a HyperScale architecture developed by ROSALIND, Inc. (San Diego, CA) as follows: reads were first trimmed using the cutadapt tool (Martin, 2011). Quality scores were then assessed using FastQC tool (Andrews 2010). Reads which passed QC were aligned to the Homo sapiens genome build hg19 using the STAR aligner tool (Dobin et al., 2013). Next, the individual sample reads were quantified using HTseq and normalized by Relative Log Expression (RLE) using DESeq2 (Love et al., 2014). DEseq2 was also used to calculate fold changes and p-values and perform optional covariate correction. Following this, the raw FASTQ, BAM, Count Matrix, and differential expression files were transferred to NHGRI. Significant Differentially Expressed Genes (DEGs) were defined as those with a padj < 0.05. Last, Partek Flow™ was used to generate expression heatmaps.

Analysis of TBX2 Datasets

BED files containing the coordinates of significant called peaks from the B16-F10-Tbx2-cl9 biological replicates were uploaded to the *Mus musculus* genome build (mm10) in UCSC Genome Browser. To compare the TBX2/3 ChIP datasets more easily, I used the UCSC Liftover tool to move the BED coordinates from mm10 to the hg38 (Homo sapiens) assembly with the most appropriate alignment Then, these peaks were intersected using the UCSC Table Browser tool to define common peaks from replicate 2 (6,677) which had ≥ 80% overlap with replicate 1 (2,787), which yielded a total of 2150 common peaks. For simplicity, all downstream analysis was done with 2150 peak BED coordinates of replicate 1. Like the TBX3 ChIP

dataset, GREAT, in “Basal plus extension” mode, was used to determine peak associations with cis-regulatory elements of annotated genes. Each annotated gene was assigned a basal regulatory domain of 5kb upstream, and 1kb downstream, of the TSS. The regulatory domain of that gene was then extended in both directions to the nearest gene's basal domain but with no more than a 100kb extension in one direction (McLean et al., 2010). In total, 1,705 peaks (1705/2150) were located at cis-regulatory elements of 1,807 genes. The TBX2 bulk RNA-seq dataset (Supplemental_Table_S2A.xlsx) was downloaded from doi:10.1101/gad.348746.121 on Genes and Development’s website (S. Lu et al., 2021). Significant DEGs were defined as those with a padj < 0.05. The DEGs were converted from their mouse to human homologs using ‘g:Profiler’ (Kolberg et al., 2023), yielding a total of 3,969 peaks out of a possible 4,286.

Other

Figure Construction

Figures were assembled and/or created with BioRender.com. UMAPs were generated with Partek Flow. Venn diagrams were produced using DeepVenn. Binding distribution, Chapter 4: Figure 2A, was modified from original GREAT output, while Figure 2B was modified from the ChIP seeker output from usegalaxy.org. Motif position distribution for Chapter 4: Figure 3E is modified from the MEME CentriMo tool.

Data Availability

The original data created for this study has been deposited in the Gene Expression Omnibus (GEO) data repository as follows: TBX3 ChIP-seq (GSE223256), TBX3 bulk RNA-seq (GSE236917), and single-cell RNA-seq (GSE236918).

Chapter 3: Transcriptomic Profiling of MC1R-inhibted Melanocytes Identifies Novel Mediators of Pigment Cell Biology

Introduction

Downstream signaling of MC1R, a melanocytic G_s-protein coupled receptor, is a major regulator of melanin production and pigment switching with LOF leading to red hair and fair skin which defines the RHC trait (Kanetsky et al., 2002; Kempf et al., 2022; Sulem et al., 2007, 2008; Voisey et al., 2006). However, precisely how *MC1R* genetic LOF variants can lead to alterations in pigment composition, and why reduced MC1R signalling is linked to melanoma predisposition remains unclear. To address this question, I chose to use high-resolution scRNA-seq to transcriptionally profile, and elucidate potential differences between melanocytes actively synthesizing one of the two main pigment types, phaeomelanin (red-yellow) and eumelanin (black-brown) (Pavan & Sturm, 2019). To do this, an appropriate model is needed to compare melanocytes which exhibit active MC1R signalling versus those which have inhibited or non-functional MC1R. The use of human samples would be ideal for identifying direct changes which may impact melanocyte function and health. However, at present, and to the best of my knowledge, there are no robust commercially available human cell lines which would best address this question. Furthermore, access to primary human samples is both limited and challenging. Fortunately, MC1R signalling is highly conserved among mammals and well-characterized mouse strains exist which possess both active MC1R signalling (nonagouti; *a/a*), and suppressed MC1R signalling (recessive yellow, $Mc1r^{e/e}$; lethal yellow, A^{y}) (Switonski et al., 2013) (Reviewed in Chapter 1). Thus, I selected to characterize melanocytes from these mice with the goal of identifying candidate genes whose transcriptional regulation is, at least in part, mediated through MC1R signaling.

Previous work in the field has attempted to address similar questions relating to MC1R signalling. However, these studies have been limited by various factors, including technical limitations, and have not fully resolved this significant and outstanding gap in knowledge in the field. For example, an excellent previous study identified a set of novel genes with potential implications in the regulation of phaeomelanogenesis (April & Barsh, 2006). That study utilized NGS, in the form of bulk RNA-seq, of whole skin layers to define gene expression of mice with functional and non-functional MC1R. The work uncovered a new set of candidate genes in the skin which are influenced by MC1R signalling and implicated the action of previously underappreciated genes in the regulation of phaeomelanogenesis. However, they utilized bulk RNA-seq to assess expression at, and between, various layers of the skin. This approach allowed broad characterization of the response of specific genes to MC1R signalling but lacked the ability to determine which cell types are responsible for the observed changes. Since melanocytes comprise a minimal fraction of the total skin cells, any melanocyte intrinsic changes could be completely masked by unchanged or increased expression in a different and more numerous cell type (e.g., keratinocytes). The expression of MC1R in the skin is almost exclusively limited to melanocytes and gene expression changes driven by MC1R signalling could potentially be melanocyte specific (Guida et al., 2021). Consequently, a bulk RNA-seq approach of skin sub-layers would likely not uncover all significant differentially expressed genes within melanocytes. Importantly, the experimental design was highly limited by the available techniques at that time. Nevertheless, one important conclusion that can be drawn from the April and Barsh study is that signalling through MC1R may be important in the paracrine effect of melanocytes on other components of the skin.

Another important study related to this question was previously addressed by Haltaufderhyde and Oancea (Haltaufderhyde & Oancea, 2014). In this work, the authors utilized a bulk RNA-seq approach to assess transcriptomic differences of human epidermal melanocyte cultures which were 'light', which could be amelanotic or contain cells possessing a gradient of phaeomelanin, or 'dark', containing robust amounts of eumelanin (Haltaufderhyde & Oancea, 2014). Unlike the gene list identified in heterogenous tissue by April and Barsh, the entirety of the Haltaufderhyde and Oancea differential list, 16 genes, can be directly attributed to expression changes within melanocytes as no other cell types were present. However, this *in vitro* approach ignores the influence of other skin cells, such as keratinocytes, paracrine factors, or systemic factors (e.g., hormones) on the regulation of melanocyte gene expression, and vice a versa. The comparison of 'light' and 'dark' melanocytes was novel; however, the authors had no guarantee that these cells were predominantly composed of one pigment type over the other. In fact, many darkly pigmented melanocytes contain a large amount of phaeomelanin (Dzierżęga-Lęcznar et al., 2017). This issue is further exacerbated by the fact that the genotypes of the samples were unknown and the state of melanogenesis was not characterized.

Although studies have explored the role of pigment profile (light vs. dark), and genetic regulators of pigment regulation (i.e., MC1R), on melanocyte gene expression, none have done so using a focused and high-resolution approach. Nevertheless, such studies have established important foundational knowledge on the influence of pigmentation, and the pathways which regulate pigment production, on global melanocyte gene expression. Moreover, these works highlight a major gap in our knowledge and highlight the need for a high-resolution genomics

approach. Therefore, in this chapter, I used one of the most advanced NGS approaches, scRNA-seq, to address this by comparing *in vivo*-derived murine melanocytes with either active or suppressed MC1R signalling. The results identify robust gene expression differences between both RHC (lethal yellow, A^{y}/a; recessive yellow, $Mc1r^{e}/^{e}$; phaeomelanin producing) mouse models and their nonagouti (eumelanin producing) counterparts. Importantly, the gene expression signature of each RHC variant overlap significantly and this intersection was used to derive the MiGS. I further identified TF and co-TFs which were differentially expressed in the MiGS. A thorough literature review and analysis identified both new and novel TF/co-TFs with implications in melanocyte biology and melanoma. Collectively, the results in this chapter highlight key transcriptomic differences between eumelanin and phaeomelanin producing melanocytes which may act in the regulation of melanogenesis and melanomagenesis within, as well as beyond, the MC1R axis.

Results

Optimising Tissue Digestion

To assess the transcriptome of RHC melanocytes, I first obtained viable primary melanocytes. A previous post-doctoral fellow in the Pavan lab successfully isolated primary melanoblasts from mice at post-natal day 1.5 (P1.5) using a series of enzymatic and mechanical digestions as well as FACS to enrich for melanocytes (Harris et al., 2018). This protocol provided a starting point for my study; however, to produce reliable and meaningful scRNA-seq results, a significant amount of time and trial experiments were needed to fully optimize the tissue digestion. There are

two important differences between that study and mine, (1) age of the mice and (2) anatomical location from which the melanocytes are to be sourced. For this study, I elected to use older mice, P3 as compared to P1.5, and restricted the tissue area to the dorsal skin. These changes were made for multiple biological and technical reasons. To best address the aim of the study, I wanted mature melanocytes which were actively producing pigment. Therefore, P3 is appropriate because at that time melanocytes have fully colonized the hair follicle of the dorsal skin region and are actively engaged in melanin synthesis during the first hair cycle (Mort et al., 2015). However, by P3 the skin has rapidly matured and grown to better provide barrier function thus complicating separation of the various skin layers (i.e., hypodermis, dermis, epidermis (Dekoninck et al., 2020). This is a significant challenge to address as the overall burden of digestion, both mechanical and chemical, impacts both cell stress and viability within the *ex vivo* environment and thus potentially elicits undesired transcriptional changes. Therefore, addressing these issues with protocol optimisation was necessary to minimize unwanted consequences and thereby create the most optimal sequencing dataset.

The procedure of obtaining primary melanocytes from the dorsal skin requires multiple steps of mechanical and enzymatic digestion (Figure 1). Over treatment of the tissue by either of these processes greatly hinders cell survival and integrity. The first step of the protocol requires dissection. I used easily identifiable anatomical landmarks, the axilla and anterior superior pelvis (iliac crest), to guide this dissection and increase reproducibility between animals. To isolate the dorsal skin, I made four incisions consisting of: two transverse cuts, with one between each axilla, and the other between the anterior pelvises, and two bilateral incisions along the midline from the axilla to the anterior pelvis (Figure 1A). This not only created

reportability in tissue size, but it also further facilitated optimisation of all downstream digestion steps by providing consistent surface area for the enzymes to act on, as discussed below.

Mature melanocytes of the P3 mouse are found in the hair follicle which mostly resides in the dermis (H. Chang & Nathans, 2013). Therefore, I needed to separate the dermis from the other layers. To do this, the skin is subjected to an enzymatic bath with Trypsin-EDTA to facilitate the breakdown of matrix and junctional proteins, such as desmogleins, and thus encourage separation of the epidermis from the dermis (Figure 1B). After incubation, the epidermis is removed with forceps *en masse* and discarded (Figure 1C). As mentioned, the skin, especially the epidermis, is more developed by P3 as compared to P1.5. Therefore, the time of exposure with the enzyme needed optimisation. The original protocol called for a 15-minute incubation time as further exposure caused precipitous cell death. However, and not surprisingly, this length of time proved woefully insufficient for the more developed skin of P3 animals. To address this, I performed several experiments in which I increased the time of exposure in 5-minute intervals up to the final 30 minutes. This represented the first point at which the epidermis could be easily removed and was subsequently used for all future experiments.

The residual dermis which harbours the hair follicles is significantly tougher to digest enzymatically at the later P3 timepoint. The digestion phase utilizes Liberase, a defined enzyme mixture which contains class I (C1) and class II (C2) collagenases, to break down the extracellular matrix holding the cells together (Figure 1D). Much like the trypsin step, over subjugation of the tissue to this enzyme limits cell viability. Therefore, an optimal time of exposure needed to be devised which provided sufficient digestion without hindering cell survival. In a similar

manner as before, I increased the length of exposure stepwise in 5-minute intervals from the original 30 minutes to a final time of 45 minutes. This timepoint provided consistent digestion which did not hinder overall cell survival but allowed for sufficient mechanical digestion to take place in the next step of the protocol (Figure 1E). Collectively, these optimisation steps proved essential in providing a source of viable single cells for subsequent scRNA-seq.

FACS Selection of an Enriched Melanocyte Pool

Melanocytes comprise a minimal fraction of all skin cells (<5%). scRNA-seq would allow us to differentiate melanocytes from other single cells during data analysis; however, at this proportion sequencing a heterogenous mixture of skin cells would greatly reduce the potential power of the experiment. Therefore, I aimed to enrich the pool of melanocytes for sequencing by using flow cytometry and FACS to select and sequester melanocytes from the other and more numerous cell populations present within the skin. With immunostaining, I targeted two cell surface proteins, KIT and CD45, to differentiate melanocytes ($KIT^+/CD45^-$) from other cell types. The majority of skin cells are $KIT^-/CD45^-$; however, one other cell population, dendritic, resident immune, cells express both KIT and CD45 (KIT^+ / $CD45^+$) (Harris et al., 2018) (Figure 1F). Therefore, these two markers appropriately delineate melanocytes from all skin cell types.

Given the importance of cell viability in gene expression analyses, I further elected to incorporate LIVE/DEAD™ Fixable Aqua Dead Cell Stain in the FACS to confirm, and select for, intact and living cells. When in contact with free amines this probe emits an intense fluorescent signal. Baseline intensity can be established in

viable cells where the probe interreacts with sparse free amines at the membrane surface, while a true positive signal occurs when the probe binds to abundant free amines in the interior of the cell (Perfetto et al., 2010). Using flow cytometry, single viable cells were identified from debris using side-scatter, forward-scatter, and Aqua (LIVE/DEAD™) and gated for with a representative experiment presented in Figure 1G. After gating on live cells, the fluorescent probe intensity of single-stained samples comprising KIT (CD117, PEcy7), CD45 (CD45.2-FITC), was contrasted against a negative stain control (Figure 1H). Gates were devised for positive cells, melanocytes (KIT^+ / $CD45^-$), and negative cells, a mixture of all cells which did not express KIT (KIT^-) (Figure 1I). After gating, these two populations were selected for and sequestered by FACS (Figure 1J). Isolation of melanocytes by FACS using $KIT^+/CD45^-$ has been done previously by our lab (Harris et al., 2018). I therefore felt confident that the positive gated cells which were sorted by FACS consisted of melanocytes. However, the signal intensity along the CD117-PEcy7 axis in my experiments did not resolve a definitive 'positive' population (Figure 1I). Furthermore, I wanted to ensure that I captured as many melanocytes as possible. Consequently, I was less stringent in gating on the CD117-PEcy7 axis. Given this, I next wanted to ensure melanocyte enrichment with FACS before collecting the final samples for NGS.

The primary cells from positive and negative FACS populations, of multiple samples, were cultured to assess for the presence of melanocytes by two microscopy-based assays; brightfield, to assess for the presence of melanin, and fluorescence, to confirm enrichment of cells expressing melanocyte specific proteins (Figure 2). FACS sorted cells were seeded at the same density, cultured for 24 h, fixed, and then immunostained. Melanocytes are highly dendritic in nature

while nonagouti melanocytes also produce eumelanin. Therefore, using brightfield imaging, I queried whether the two populations had melanin rich dendritic processes (Figure 2A,B). As expected, the positively-selected population was comprised of cells with dendrites and robust melanin deposition (Figure 2A). In contrast, the negative cell population lacks these melanocyte specific phenotypes (Figure 2B). The melanocytes of RHC mice, lethal yellow and recessive yellow, do not produce significant amounts of eumelanin and are therefore not as easily identifiable by brightfield microscopy. Therefore, I used immunostaining and confocal microscopy to examine the presence of melanocyte specific proteins, DCT, a melanin synthesizing enzyme (Hida et al., 2020), and PAX3, a survival transcription factor (Kubic et al., 2008), in the positive and negative populations. As seen in the representative experiment from a lethal yellow sample, DCT and PAX3 are expressed exclusively in the positive cell population. (Figure 2C). In contrast, the negative cells lack expression of DCT but exhibit diffuse staining of the keratinocyte marker, KRT14 (Figure 2D). A potential limitation in the experimental design exists within the culture conditions. The medium used during the 24 h culture contains compounds which favour melanocyte survival (e.g., Cholera toxin, TPA) and therefore it is possible that the culture environment promotes significant survival of melanocytes over other cell types. However, I did not observe any increase in cell death in the negative cell population. Likewise, total cell numbers between positive- and negative-selected populations appeared similar by brightfield microscopy (Figure 2A,B). Given the gating parameters it is possible that other cell types were present in the selected population, however, in total, these results showed successful enrichment of melanocytes and provided confidence in moving forward with the scRNA-seq experiments.

Single-cell RNA-sequencing of FACS Isolated Cells

We performed scRNA-sequencing to better understand global gene expression changes in eumelanin (nonagouti, *a/a*) and phaeomelanin (lethal yellow, A^{y}/a; recessive yellow, $Mc1r^{e/e}$) producing melanocytes. The process by which primary melanocytes were isolated is discussed in detail in Chapter 2 (pgs. 40 – 44) and the previous results portion of this chapter (pgs. 66 - 72). In brief, the dorsal skin was digested into a solution of single cells using enzymatic and mechanical techniques and the melanocytes from the solution were immunolabeled (KIT+/CD45-), defined as 'positive' by flow cytometry and selected for capture with FACS (Figure 3A). Of note, the lethal yellow and recessive yellow samples were collected on different days, with a nonagouti animal being harvested in parallel each time (A^{y}/a, n=1; $Mc1r^{e/e}$, n=1; *a/a*, n=2). Once sorted, the 'positive' cells were processed for library construction via the 10x Genomics Chromium pipeline and then subsequently sequenced by the NHGRI Microarray Core.

In total 11,058 sequenced cells, comprising all four samples, passed quality control (QC) checks (lethal yellow, n=1; recessive yellow, n=1; nonagouti, n=2). The data corresponding to cells which failed QC were discarded from further analysis. The sequencing data comprising cells which did pass QC first underwent dimensional reduction via non-biased PCA. This was followed by graph-based clustering analyses for graphical display of both pairwise experiments (lethal yellow vs. nonagouti; recessive yellow vs nonagouti) on Uniform Manifold Approximation and Projections (UMAP) (Figure 3B,C).

Melanocyte Classification

For this study, I used FACS to enrich the pool of sequenced melanocytes. However, enrichment does not necessarily mean exclusion of the other cell types. Therefore, I utilized published murine skin cell gene signatures, in conjunction with the identified graph-based clusters (GBC), to identify the possible presence of other cell types in an unbiased manner. In brief, GBCs which exhibited a significant expression score on the heatmap for a given cell type were subsequently labelled as such (Figure 4A,B). For example, the cells from the nonagouti / lethal yellow pair which I classified as melanocytes correspond to GBCs 1, 5, 7, and 9 (Figure 4A). For the nonagouti / recessive yellow pair, I found 1 GBC (number 1) which corresponded to melanocytes (Figure 4B). In total, I confirmed the presence of seven cell populations melanocytes, dermal fibroblasts, dermal papilla cells, epidermis, hair-follicle and outer root sheath, transit amplifying and matrix cells, as well as negative cells which did not fit into anyone category (Rezza et al., 2016) (Appendix A: Table S1). Given my primary interest in melanocytes, I wanted another method to validate this classification scheme. Therefore, I used the same heatmap based expression score approach but with highly specific bona fide melanocyte markers, *Mitf* and *Dct* (Figure 4C,D). All cell types outside of melanocytes were filtered out from further analysis.

The remaining melanocyte only population underwent a round of GBC analysis with the results displayed as a graphical projection by UMAP (Figure 5A,B). Cell cycle state exhibits a significant and influential effect on gene expression. To reduce the noise that this may exert on downstream analysis all melanocytes outside the G_0/G_1 phase were removed. Cells outside of these phases were identified by overlaying a signature which consisted of well-identified cell cycle

marker genes (Belote et al., 2021; Hsiao et al., 2020) (Figure 5C,D). Cycling cells were removed and subsequent analysis was limited to the refined population of non-cycling melanocytes. GBC analysis was once again performed but only on the populations of non-cycling melanocytes. Interestingly, the UMAPs of both RHC mouse models, which primarily synthesise phaeomelanin, exhibit a bifurcation pattern from the nonagouti, eumelanin producing, cells (Figure 5E,F). Consistent with this notion, clustering of melanocytes by genotype was unique to melanocytes and not observed in the other cell types, suggesting that the effects of intrinsic MC1R signalling loss, through ligand antagonization or LOF, are indeed restricted to melanocytes (Guida et al., 2021) (Figure 5G,H). Collectively, these results highlight the successful capture and scRNA-seq of primary murine melanocytes.

Defining the MC1R-inhibited Gene Signature (MiGS)

We next used the newly identified melanocyte populations to perform differential gene expression analysis with Partek Flow's differential analysis toolkit to identify DEGs between the two pairwise groups comparing lethal yellow to nonagouti melanocytes (Appendix A: Table S2) as well as recessive yellow to nonagouti melanocytes (Appendix A: Table S3) (ANOVA; FDR < 0.05 and fold change (FC) ±2). The method of MC1R inhibition is different for each RHC model mouse. However, both mice predominately produce phaeomelanin. Given this, I next intersected the differential lists from each experiment to identifying shared genes/pathways which are most likely to reflect the transcriptomic profile of phaeomelanin producing melanocytes regardless of how MC1R signalling loss is achieved. These two lists share a total of 219 genes, including three which exhibited anti-directional FC and were thus removed from further analysis. In total, this

resulted in a set of 216 genes which I have identified as the MiGS (Figure 6) (Appendix A: Table S4).

RHC and nonagouti mice primarily synthesize two different forms of melanin; therefore, I next asked whether any MiGS genes are associated with pigmentation. To do this, I queried the MiGS genes against a compiled list of annotated genes which are considered causative for pigmentation phenotypes (Baxter et al., 2019). Surprisingly, only 5% of MiGS genes overlap with the pigmentation causative gene set (Table 1). However, this list includes include prominent pigmentation genes, such as *Pmel* and *Tyrp1*. For example, *Tyrp1* encodes an enzymatic protein which functions in the synthesis of eumelanin (Hida et al., 2020). *Pmel* encodes a glycoprotein, often referred to as PMEL or silver, which plays an extensive role in melanosome maturation and melanin polymerization (Le et al., 2021). These data suggests that the MC1R signalling axis, at least in melanocytes, regulates a substantial network of genes which fall outside canonical pigmentation factors.

The majority of MiGS genes do not associate with pigmentation phenotypes. Given this, I next wanted to categorize and predict biological meaning for the entirety of DEGs. To do this, I first utilized PANTHER Gene Ontology (GO) to identify significantly over-represented processes and pathways. I performed GO analysis on the entire MiGS set and identified enrichment of significant terms (FDR < 0.05) terms. The top 15 terms encompass three major themes including: ‘morphogenesis’, ‘melanin processes’, and ‘neurogenesis’ / ‘neurotransmitter regulation’ (Figure 7A). Only one gene, *Tbx3*, is common amongst the ‘morphogenesis’ related terms, which include ‘semicircular canal morphogenesis’ and ‘branching involved in mammary gland duct morphogenesis’. Terms related to ‘melanin processes’ had equally high fold-enrichment; for example, 4 out of the 15 genes associated with ‘melanin

biosynthetic process' are present in the MiGS (*Tyrp1, Mc1r, Oca2,* and *Pmel*). I further sub-divided the gene lists by direction of expression (i.e., higher expression (+Fold Change (FC)) or lower expression (-FC) and repeated the analyses. The higher expressed genes of MiGS drive the enrichment of the 'neurogenesis' / 'neurotransmitter regulation' theme (Figure 7B). In contrast, the lower expressing genes are the main component governing enrichment of 'melanin processes' (Figure 7C). Overall, GO identified the presence of three major biological themes within MiGS, one encompassing known melanocyte function, such as pigmentation, and two were not necessarily expected findings.

Gene ontology analysis is a powerful tool for interrogating large gene sets. However, the findings are not necessarily all encompassing. Therefore, I used another bioinformatic based analysis, Ingenuity® Pathway Analysis (IPA), to further extrapolate potential biological significance of MiGS expression. The analysis was performed in the same manner as GO where the entire gene list was assessed and then the directional gene expression sets were analysed. IPA of the entire MiGS highlighted canonical pathways related to 'Neuroinflammation, 'Synaptogenesis' and 'Neuron receptor signalling' (Figure 7D). This result reinforces the findings from the GO analysis which included terms related to 'neurogenesis' / 'neurotransmitter regulation'. Like GO, these terms were found to be primarily driven by a host of receptors and ligands within the GABA and N-methyl-D-aspartate (NMDA)/Glutamate) families; however, IPA also identified enrichment of the Ephrin and Semaphorin families with the latter two being strongly associated with the lower expressing gene set (Figure 7F). Interestingly, IPA analysis identified four terms, 'Collagen chain trimerization', 'Collagen degradation', 'assembly of collagen fibrils and other multimeric structures', and 'collagen biosynthesis and modifying enzymes'

in the higher expressing gene group (Figure 7E) with the following genes being found in each of those terms *Col12a1, Col14a1, Col4A1,* and *Col5a2*. In contrast, GO identified one collagen biology related term (Figure 7A). In total, bioinformatic analyses of MiGS consisting of GO and IPA identified enrichment of novel pathways outside of canonical terms associated with melanocyte biology.

TGFβ superfamily a Predicted Upstream Regulator of MiGS

The *in vivo* signalling environment surrounding the hair follicle is complex; therefore, I next used IPA to predict upstream molecular regulators driving MiGS expression. There are three molecules (SMAD4, GDF2, and SMAD1) within the top 10 activated regulators that are related to TGFβ/BMP signalling (Figure 8). Importantly, multiple factors within this family are expressed by melanocyte neighbouring cells within the hair follicle (Rezza et al., 2016; Vandamme & Berx, 2019). It is important to note that, TGFβ signalling regulates melanin synthesis, whereby activation of the pathway leads to hypopigmented state (Murakami et al., 2009). This data highly suggests an active role for TGFβ/BMP signalling in RHC melanocytes which have inhibited MC1R signalling.

MiGS Comprises Known and Novel TF/co-TFs of Melanocyte and Melanoma Biology

Transcription factors play an essential role in the regulation of gene expression. The most well-characterized TF in melanocytes is MITF. This protein is encoded by *Mitf* and is considered a master regulator of melanocyte specificity, proliferation, survival, migration, differentiation, and melanogenesis (Goding &

Arnheiter, 2019). Furthermore, the expression of the *Mitf* gene is controlled by multiple signalling pathways, with signalling downstream from MC1R being considered one of the most important (Goding & Arnheiter, 2019; Levy et al., 2006). Interestingly, *Mitf* does not exhibit differential expression in this study (Appendix A: Table S4). Likewise, many post-transcriptional/translational modifiers of MITF, such as MAPKs, *Gsk3b*, *p300*, and *Stat3* do not exhibit differential expression (Appendix A: Table S4). Similarly, other well-characterized TFs in melanocyte biology, including *Sox10, Pax3, Lef1,* and *Creb*, which can all regulate *Mitf*, show no DE. Given the role of MITF in melanocytes, as a master regulator of cell fate, proliferation, survival, migration, differentiation, and, importantly, melanogenesis, I was slightly perplexed by this finding. Given this, and the assumption that the observed DEGs identified by scRNA-seq are due to regulation of transcription, I posited that other TFs were acting as primary contributors to the differential expression of MiGS genes; therefore, I next aimed to identify which TF/co-TFs were expressed in MiGS as these could be potential regulators of MiGS expression itself.

To do this, I intersected the MiGS genes against the Animal Transcription Factor DataBase (AnimalTFDB) and identified 22 annotated TF/co-TFs (H. Hu et al., 2019) (Figure 9A). I next performed a thorough literature review to determine which of these had known or novel relationships with melanocyte and pigment cell biology. Of the 22 MiGS TF/Co-TFs there are 10 known and 12 novel relationships to melanocytes (Figure 9B). Within the known group, I further delineated their association into 5 sub-categories which include neural crest development (*Hmga2, Id4, Mef2c, Tbx3*, and *Tfap2b* (J. Hu et al., 2015; Kee & Bronner-Fraser, 2001; Macrì et al., 2016; Seberg et al., 2017; Vega-Lopez et al., 2018)) melanocyte differentiation (*Mef2c* (Agarwal et al., 2011)), pigmentation (*Eya1, Id4, Irf4,* and

Tbx3 (Chhabra et al., 2018; DiVito et al., 2015; Imsland et al., 2016; C. Wang et al., 2020; J. J. Zhou et al., 2017)), oxidative stress protection (*Nr4a2* (Jagirdar et al., 2013)) and melanoma (*Ar, Eya1, Hmga2, Irf4, Nr4a2, Tbx3,* and *Zeb1* (Boyd et al., 2013; Chen et al., 2017; Heppt et al., 2018; J. Lu et al., 2010; J. Ma et al., 2021; H. Moon et al., 2017; Peres et al., 2010, 2021; Perrot et al., 2013; Rodriguez et al., 2008; Samarkina et al., 2023; Smith et al., 2011; T. Zhang et al., 2018; Q. Zhou et al., 2017) (Figure 9C).

To determine the potential biologic significance of these findings, I first wanted to validate expression of these genes in normal melanocytes in an unbiased way using an established dataset. Using the Hair-GEL database, which comprises transcriptomic data of normal murine melanocytes at age P5, I confirmed that all 22 TF/co-TFs are indeed normally expressed (Hair-GEL.net) (Rezza et al., 2016) (Figure 10). Furthermore, five TF/co-TFs found in the MiGS, *Eya1, Irf4, Hmga2, Tbx3,* and *Tfap2b* were previously identified as 'melanocyte signature genes' (Figure 10A). Of note, most known factors (Figure 10A) exhibit higher levels of expression as compared to novel ones (Figure 10B). To the best of my knowledge, the melanocytes from their study all have functional MC1R signalling and therefore provide further evidence that these genes: (1) are normally expressed in melanocytes and (2) that the differential expression found in the RHC melanocytes from my study can be, at least in part, attributed to MC1R signalling loss.

The RHC trait is strongly associated with an increased risk for developing melanoma. Therefore, an outstanding question in the field is how MC1R loss promotes melanoma development. Given the role of TF/co-TFs in regulating gene expression and participation in oncogenesis I further queried whether MiGS TF/co-TFs are expressed in melanoma. To this end, I utilized the 'Melanoma Database' to

assess relative expression in a multitude of melanoma cell lines and The Cancer Genome Atlas (TCGA) samples (Graeber Lab, 2015) (Tsoi et al., 2018) (Figure 11A). For ease of visualization, I divided them into two groups: known (Figure 11B) and novel (Figure 11C). The PCA projections further delineate the melanoma cell lines and samples by degree of differentiation consisting of 'undifferentiated', 'neural crest-like', 'transitory', and 'melanocytic' (Figure 11A). With this, I identified in which subtypes, if any, these TF/co-TFs were expressed (Figure 11D). Together, these data highlight differential expression of 22 TF/co-TFs which are all found to be normally expressed in murine melanocytes. Furthermore, 55% of these have, to the best of my knowledge, no known associations with melanocyte biology. Importantly, a plethora of these genes are expressed at various stages of melanoma. In total, these TF/co-TFs represent a set of known and novel genes which may have serious implications in the regulation of melanocyte function and melanomagenesis.

Discussion

The RHC trait is associated with *MC1R* coding variants; however, the mechanism linking these two is not clear. Likewise, the GRNs which function downstream of MC1R are poorly understood. In this chapter, I isolated primary melanocytes from MC1R-inhibited and WT melanocytes and then used a high-resolution, scRNA-seq approach to identify the MiGS. This, to the best of my knowledge, is the first study of its kind at this sort of resolution. Bioinformatic analyses of the DEGs elucidated enrichment of pathways which are traditionally not associated with canonical melanocyte biology. To my surprise, the master melanocyte regulator, *Mitf*, did not exhibit DE. However, I identified both known and

novel candidate genes, such as TF/co-TFs, which may regulate important and overlooked biological processes in melanocytes, including aspects of melanoma biology, which have MC1R signalling loss. Collectively, the MiGS establishes a new set of genes which merit further investigation toward a fuller understanding of normal melanocyte function, disease progression, and prevention and treatment of melanoma.

Novel Pathways within MiGS

Only 5% of genes comprising the MiGS are affiliated with pigmentation. Therefore, enrichment of GO terms outside of pigmentation was expected. Despite this, enrichment of several terms related to 'morphogenesis' came as a surprising result. Only one gene, *Tbx3*, is common amongst the 'morphogenesis' related terms, which include 'semicircular canal morphogenesis' and 'branching involved in mammary gland duct morphogenesis'. The *Tbx3* gene encodes for a TF of the same name (TBX3) and is a member of the T-box family. Many T-box family members play significant roles in embryonic development. For example, a mutation in *Brachyury*, the first identified family member, is the cause of the short-tailed mouse (Wansleben et al., 2014). TBX3 itself is implicated in organogenesis of many organs including lung (Lüdtke et al., 2016), heart (Hoogaars et al., 2004, 2008), mammary gland (Cho et al., 2006), limb (Frank et al., 2013), eye (Motahari et al., 2016), and the inner ear (Kaiser et al., 2021; Song & Morrow, 2023). Interestingly, TBX3 is associated with various aspects of melanocyte biology, such as neural crest development and melanoma; however, a role in melanogenesis is unclear. TBX3 regulates the process of EMT in melanoma invasion (Rodriguez et al., 2008). Furthermore, TBX3 is an anti-senescence transcription factor and facilitates

increased cellular proliferation (Bennett & Medrano, 2002; Ha et al., 2008; Khan et al., 2019; Lingbeek et al., 2002; Peres et al., 2010; Vredeveld et al., 2012; Wagstaff et al., 2022). Coding variants in *TBX3* have been implicated in the altered pigmentation of Dun horses (L. Andersson, 2020; Imsland et al., 2016); however, the mechanism by which TBX3 might govern this phenotype is unclear. Regardless, the ubiquitous presence of TBX3 across the terms related to 'morphogenesis' is an intriguing result. Collectively, the presence of 'morphogenesis' terms could indicate that phaeomelanin producing melanocytes are in a lesser state of differentiation compared to their eumelanin producing counterparts.

The final category of GO terms related to 'neurogenesis' / 'neurotransmitter regulation' and these were also present in the IPA assay. Further analysis identified three genes, *Gabra1, Gabrb2,* and *Gabrb3*, present in all the terms of this category. These genes encode three different subunits of the gamma-aminobutyric acid type A receptor (GABA-A) (Ghit et al., 2021). Common mutations of these genes are associated with an array of neurodevelopmental and psychiatric disorders including epilepsy and schizophrenia (Achkar et al., 2021; Snodgrass, 1992; Steudle et al., 2020). Despite its prevalence in the terms identified by GO analysis, the role of GABA signalling in melanocytes is not well-studied. Adjeround and colleagues showed that exposure of GABA to melanotrophs within the frog pituitary temporarily increases the amount of α-MSH production (Adjeround et al., 1986). Much like the action potential of a neuron, this action leads to a refractory period of inhibition. Despite the increase in α-MSH production, they did not query whether this impacted melanogenesis in the peripheral pigment producing cells. Upon addition of GABA, Molagoda and colleagues noted decreased pigmentation (decreased eumelanin production) in B16F10 mouse melanoma cells (Molagoda et al., 2021). In that study,

they show that GABA binds directly to melanocytes at GABA-A/B receptors and inhibits the action α-MSH-induced melanogenesis through the α-MSH-MC1R-cAMP–CREB axis by reducing cAMP and CREB dependent intracellular Ca^{2+}. Importantly, GABA can only reduce the action of α-MSH in a dose-dependent manner and does not reduce cAMP levels below the unstimulated condition independently. Contrasting this, Diazepam, a benzodiazepine which enhances GABAergic function through allosteric binding of GABA receptors, increases both melanogenesis and melanocyte dendricity (Enkhtaivan & Lee, 2021). A recent study showed that inhibition of GABA-A receptors in developing larval zebrafish induces mass proliferation of melanocytes (Allen et al., 2019). In contrast, agonising these receptors on MSCs prevents melanocyte regeneration. The authors did not interrogate the action of GABA on the MC1R-cAMP-CREB axis therefore it is unclear whether the effects are due to direct or indirect GABAergic actions.

Melanocytes are neural crest derivatives and share a common developmental lineage with neurons and glial cells of the peripheral nervous system (Mort et al., 2015). In fact, the NCCs that ultimately differentiate into melanocytes first exist as a bi-potent precursor which can adopt a glial or melanogenic fate (Mort et al., 2015). Interestingly, mature melanocytes share multiple characteristics with neurons, such as dendricity (M. Li et al., 2020). In humans, the long dendritic processes of melanocytes within the epidermis transfer melanosomes to upward of 40 neighbouring keratinocytes (Moreiras et al., 2021). Previous GO term enrichment analysis of normal human melanocytes highlighted neuronal like gene expression as exampled by significant terms such as, ‘neuron ensheathment and synapse’ (Belote et al., 2021). In the presence of the MC1R antagonist agouti, phaeomelanin-producing melanocytes in culture show marked reduction of dendricity (Pape et al.,

2008). Ni and colleagues showed that inhibition of glutamate signalling through NDMA receptors prevents the attachment of melanocyte filipodia to keratinocytes and therefore diminishes proper transfer of melanosomes (Ni et al., 2016). A recent study by the lab of Richard White convincingly showed the existence of GABAergic signalling between keratinocytes and melanoma cells through neuronal like synapses (Tagore et al., 2023). They further show that this cell-cell communication can promote the initiation of melanoma. Interestingly, in that study, it is the keratinocytes which have increased GABA receptor expression and not the melanoma cells. Expression of GABA-A by epidermal keratinocytes has been corroborated and likely functions in skin barrier homeostasis and regulation (Denda et al., 2002). Collectively, these results further support a role for GABAergic signalling in regulating melanocyte biology. Furthermore, an interesting hypothesis is that higher expression of GABA-A receptor subunits on RHC melanocytes increases the action of direct or indirect GABAergic signalling and thereby inhibits eumelanogenesis and/or promotes phaeomelanogenesis.

Outside of GABA, IPA analysis revealed enrichment of other neuronal-like terms. One example of this is glutamatergic signalling. The NMDA receptor is a mediator of glutamatergic signalling and when activated it promotes melanin synthesis in cuttlefish (*Sepia officinalis*) by enhancing tyrosinase activity (Palumbo, 2003). In addition, other glutamate receptor genes, especially *Grm1*, are expressed in human melanomas (Enkhtaivan & Lee, 2021). For example, ectopic expression of *mGluR1* in melanocytes leads to melanoma transformation and subsequent metastatic spread with complete penetrance (Eddy & Chen, 2021). The Eph/Ephrin signalling pathway is a critical player in many biological processes including, but not limited to, cell-cell attachment, cell shape, and motility (Janes et al., 2014).

Semaphorins, as well as Ephrins, are key regulators of axonal guidance in developing neurons (S. Hu & Zhu, 2018). Relatedly, developing NCCs express these proteins which act to modulate their migration (Theveneau & Mayor, 2012b). Interestingly, many genes within these families exhibit differential expression in melanocytes when treated with ASIP, a primary antagonist of MC1R signalling. The authors propose that treatment with ASIP induces dedifferentiation of melanocytes towards a more multipotent and neural crest-like state (Pape et al., 2009). These findings provide evidence that MC1R signalling loss, through LOF or ASP antagonization, may mediate MiGS expression in RHC murine melanocytes.

The following genes were found in each of the collagen-associated terms *Col12a1, Col14a1, Col4A1,* and *Col5a2*. The first two, *Col12a1* and *Col14a1*, are members of the Fibril Associated Collagens with Interrupted Triple helices (FACIT) type of collagens. This subgroup comprises 8 known members, Collagens IX, XII, XIV, XVI, XIX, XX, XXI, and XXII. Compared to other collagens, their function(s) are not fully understood. They appear to modulate other collagen fibrils by direct binding, or indirectly through altering the ECM, to guide tissue-specific fibril pattern formation (Olsen, 2014). Recent studies suggest *Co12a1* is a bona fide marker gene of MSCs (Palmer et al., 2023; Sun et al., 2023). However, any function within MSCs or melanocytes has never been explored. Collagen IV is major component of the basement membrane and further functions in intracellular signalling events to promote cell survival and proliferation (Khoshnoodi et al., 2008). A recent study by Shin et al. showed that high expression of COL14A1 is associated with poor survival outcomes in a multitude of cancers including cutaneous melanoma (Shin et al., 2022). Relatedly, the amount of collagen, and its interaction with the tumour-

microenvironment, appear to regulate melanoma phenotype switching (Miskolczi et al., 2018).

In total, these findings highlight several unexplored genes and pathways which may play important functions in melanocyte biology and span various aspects including development, dendrite formation, melanogenesis, melanosome transfer, and oncogenesis.

Literature Review of TF/co-TFs Found Within MiGS

An important finding from this study is that *Mitf*, which encodes a master regulatory TF of melanocyte biology, did not show differential expression. Likewise, known post-transcriptional/translational modifiers, such as MAPKs, *Gsk3b*, *p300*, and *Stat3*, do not exhibit DE. Similarly, other well-characterized TFs in melanocyte biology, such as *Sox10*, *Pax3*, *Lef1*, and *Creb,* which can all regulate *Mitf*, also do not show DE. However, activity of these signalling molecules may not be apparent in the RNA expression profiles. Likewise, the function of MITF is often regulated at a post-translational level and therefore differential expression could be inconsequential (Goding & Arnheiter, 2019). That being said, NGS studies which assess RNA expression have shown that significant DEGs do in fact strongly correlate with changes in the amount of total protein product as compared to non-DEGs (Koussounadis et al., 2015). Without proteomic and enzymatic studies it is impossible to know whether the activity of the aforementioned molecules is altered between eumelanotic and phaeomelanotic melanocytes; however, the absence of these genes from the MiGS supports the notion that primary transcriptional changes driving MiGS expression, and phaeomelanin synthesis, in the MC1R-inhibited

signalling state are not necessarily mediated through MITF but are instead a consequence of transcriptional regulation by other factors. With that in mind, I identified 22 TF/co-TFs which were differentially expressed in my study. Of the 22 MiGS TF/Co-TFs there are 10 which I could establish known relationships to melanocyte and pigment cell biology. Likewise, there 13 which appear to have no known ties to melanocytes. I performed a thorough literature review to better understand the meaning of these relationships and identify the potential significance of their presence in MiGS.

Known

Ar encodes the Androgen receptor (AR), a ligand-dependent nuclear transcription factor and member of the steroid hormone nuclear receptor family which mediates the actions of testosterone and dihydrotestosterone (Davey & Grossmann, 2016). *Ar* shows low expression in melanocytes and that expression is further reduced in the MC1R-inhibited melanocytes of my study (Figure 10; Appendix A: Table S4). There are two studies from the same lab which implicate AR in melanoma (M. Ma et al., 2020; Samarkina et al., 2023). One showed that decreased activity of AR in melanoma cells prevents proliferation and further induces senescence. In contrast, increased levels, or activation of the receptor, leads to the opposite. They propose therefore that AR inhibition suppresses melanomagenesis . The follow-up study further implicates the AR in BRAFi-resistant melanoma cells where higher expression/activation increases resistance (Samarkina et al., 2023). They show that inhibition of AR leads to inhibition of proliferation and tumorigenesis of BRAFi-resistant melanoma cells. Agreeing with this, AR shows high levels of expression in undifferentiated melanoma subtypes

(Figure 11). Collectively, this would suggest that AR is not an oncogenic driver in RHC melanocytes.

Eya1 is a member of eyes absent (EYA) family and functions in a wide array of biological functions ranging from organogenesis to DNA damage repair (Tadjuidje & Hegde, 2013). It is expressed in normal murine melanocytes and is a 'melanocyte signature' defining gene but shows highly reduced levels of expression in RHC melanocytes (Figure 10; Appendix A: Table S4). EYA1 is expressed in melanoma but is restricted mainly to neural crest-like and transitory subtypes (Figure 11). Furthermore, Zhou et al. showed that EYA1 drives proliferation and melanomagenesis (J. J. Zhou et al., 2017).

Hmga2 encodes high-mobility-group protein AT-hook 2 (HMGA2), a small DNA-binding protein which serves several biological functions, including adipogenesis, and is linked to a plethora of diseases, including cancer (Su et al., 2020). Hmga2 is found in *Xenopus* NCCs and coordinates the activities of critical NCC TFs, such as Snail2 and Pax3, in EMT. Furthermore, developing *Xenopus* with reduced Hmga2 have severe developmental abnormalities such as facial malformations from aberrant cartilage formation (Macrì et al., 2016). In contrast, increased HMGA2 expression has been shown to activate MSCs (H. Moon et al., 2017). *Hmga2* has nearly 5-fold higher levels of expression in RHC melanocytes (Appendix A: Table S4). It is therefore plausible that elevated *Hmga2* represents an attempt to drive RHC melanocytes toward a more differentiated state.

In humans, high levels of HMGA2 is associated with an increased risk of cancer development (Mansoori et al., 2021). Likewise, *HMGA2* is found at higher levels in primary and metastatic melanomas as compared to normal tissue

(Mansoori et al., 2021; Raskin et al., 2013). Corroborating this, HMGA2 exhibit high levels of expression across multiple melanoma phenotypes spanning undifferentiated, neural crest-like, and transitory states (Figure 11). Expression of *HMGA2* is regulated by several signalling pathways including MAPK/ERK, TGFβ/Smad, and PI3K/AKT/mTOR. Outside of EMT, other roles include regulation of cell cycle progression, survival, and DNA damage repair (Mansoori et al., 2021). Relatedly, UVB induced expression of *HMGA2*, and DNA damage repair genes, not only activates MSCs but also appears to promote oncogenesis (H. Moon et al., 2017). High amounts of phaeomelanin exacerbate DNA damage, even in the absence of UVR, and could therefore be a driver of *Hmga2* expression in RHC melanocytes (Mitra et al., 2012; Napolitano et al., 2014).

Id4 is one of four members comprising the inhibitor of cell differentiation/DNA-binding (ID) family. Collectively, these family members, ID1, ID2, ID3, and ID4, exhibit numerous functional roles in cell and developmental biology (Kee & Bronner-Fraser, 2001). More specifically, each of these show tightly regulated temporal and spatial expression in the developing nervous system and NCCs (Kee & Bronner-Fraser, 2001). However, it is unknown whether ID4 functions directly in later stages of development toward a melanocyte fate. It is broadly expressed in skin cell types but has relatively high expression levels in P5 melanocytes (Figure 10). Likewise, it is more highly expressed in the RHC melanocytes of my study (Appendix A: Table S4). Interestingly, ID4 appears more elevated in melanoma cell lines and TCGA samples which are in a spectrum comprising transitory-melanocytic phenotypes (Figure 11). Furthermore, ID4 induction in melanoma cells leads to nuclear localization of MITF and an increase in total melanin (DiVito et al., 2015). It would be interesting to assay whether higher

ID4 in RHC melanocytes does in fact lead to MITF nuclear localization, especially as this would, at surface level, promote melanogenesis, like in the DiVito study. Therefore, it is difficult to postulate why this would consequently lead to phaeomelanogenesis in RHC unless other MiGS TFs counteract the function of MITF in this situation.

ID proteins are known to interact with bHLH proteins, form a heterodimer, and in turn, prevent binding of the bHLH TFs to DNA at E-Box domains and consequently mitigate transcription of bHLH target genes (Patel et al., 2015). Therefore, outside of melanoma, ID4 may inhibit MITF mediated transcription. However, a decisive role for ID4 in melanocytes is difficult to extrapolate. Regardless, these findings strongly suggest some sort of functional role in melanocytes. Of note, the literature review found known affiliations of ID4 to various aspects of melanocyte biology, such as NCC development, pigmentation, and melanoma; however, it is not found within the pigmentation gene list as it most likely did not meet the inclusion criteria (Baxter et al., 2019).

Irf4 encodes a key TF, Interferon regulatory factor 4, in blood cell development and oncogenesis (Nam & Lim, 2016; Wong et al., 2022). This TF gene is strongly expressed in P5 murine melanocytes and is considered a 'melanocyte signature' gene (Figure 10) (HairGEL.net). In contrast, *Irf4*, has diminished expression in RHC P3 melanocytes (Appendix A: Table S4). A single nucleotide polymorphism (SNP), rs12203592, in *IRF4* is strongly associated with human hair, skin, and eye colour with the rs12203592-T variant being causal for freckles, brown hair, and increased sensitivity to sun exposure (Chhabra et al., 2018; Praetorius et al., 2013). This variant impairs binding of the TFAP2A and MITF TFs to the *IRF4* locus. IRF4 acts in concert with MITF to induce expression of *Tyr/tyr* in mouse and

zebrafish, respectively (Praetorius et al., 2013). Therefore, diminished expression of *Irf4* could hinder MITF mediated gene regulation in RHC melanocytes. IRF4 is found at elevated levels in several cancers, including melanoma (L. Wang et al., 2014). This finding is backed by high levels of *IRF4* in more differentiated melanoma cell lines and samples (Figure 11). The function of IRF4 in the context of melanoma is unclear; however, Yokoyama and colleagues recently identified a role for IRF4 in immune resistance of cancer cells. They showed that IRF4 decreases the level of PD-L1 (CD274) through a SOX10-IRF4-IRF1-PD-L1 axis (Yokoyama et al., 2021). The extent to which this axis functions in healthy melanocytes or participates in melanomagenesis remains unclear.

Mef2c encodes for a MADS box transcription factor family member and its expression is regulated by endothelin signalling in NCCs (J. Hu et al., 2015). Active signalling through this pathway enhances *Mef2c* expression by removal of HDACs at the Mef2c-F1 enhancer. This creates a positive-feedback loop that further increases MEF2C which then binds and regulates important NC developmental genes (J. Hu et al., 2015). To the best of my knowledge, MEF2c is the only MiGS TF/co-TF which bridges the differentiation of NCCs into melanocytes. MEF2C is a direct target, and binding partner, of SOX10 and it is this partnership which facilitates a role for MEF2C in melanocyte development and differentiation (Agarwal et al., 2011). Conditional inactivation of *Mef2c* in NCCs prevents appropriate expression of melanocyte genes during development which in turn prevents differentiation and therefore reduces the total number of $DOPA^{+}$ melanocytes in the dermis and epidermis (Agarwal et al., 2011). However, these conditional mice die at birth, and therefore it is difficult to know the full extent of their pigmentation phenotype. Given this, it is equally plausible that melanoblasts/melanocytes are, in

fact, developmentally delayed in mutant animals and are therefore DOPA^{-} at that time point. MEF2C is also highly expressed in melanomas comprising the neural crest-like through melanocytic phenotypes (Figure 11). Collectively, these results support a role for MEF2C in melanocyte maturation and the higher expression found in RHC melanocytes may be an attempt to drive the cells toward a state of higher maturity.

Nr4a2 is one of three Nuclear Receptor subfamily 4 group A (NR4A) members (Herring et al., 2019). The proteins encoded by these genes share high degree of homology and are expressed in various tissues. Despite their structural similarities, they appear to have cell type specific functions (Safe et al., 2016). *Nr4a2*, has elevated levels of expression in RHC melanocytes. Interestingly, NR4A2 is implicated in DNA damage response and repair in melanocytes as Smith and colleagues showed high levels of expression of *Nr4a2*/NR4A2 upon activation of MC1R by α-MSH (Smith et al., 2008). Furthermore, WT primary melanocytes grown *in vitro* have 5x higher expression by Reverse transcription-quantitative polymerase chain reaction (RT-qPCR) as compared to RHC melanocytes (Smith et al., 2008). My result, which derives from MC1R inactivation, is therefore in direct contrast to this finding (Appendix A: Table S4). However, their finding has been validated in several follow-up studies. For example, they have shown that MC1R not only induces NR4A2, but also facilitates the recruitment of NR4A2 to damaged nuclear regions so that it can interact with DNA repair proteins to induce the double-stranded break repair mechanism (Jagirdar et al., 2013; Yin et al., 2014, 2017). Collectively, my results would then suggest strongly that *in vivo* regulation of *Nr4a2* is mediated by pathways outside the MC1R axis.

Tbx3 has a relatively large increase in expression compared to many of the other TFs in the MiGS (Appendix A: Table S4). *Tbx3* knockout mice have severe developmental abnormalities which lead to lethality by late gestation. It is thought more specifically that loss of TBX3 in the NCCs, which leads to cardiac outflow tract abnormalities in these animals due to failure of cell extrinsic patterning of cardiac tissue by NCCs, is the main mechanism of lethality (Mesbah et al., 2012). In contrast, mice with a neural crest specific deletion of *Tbx3*, via *Wnt1-Cre*, appear to have normal heart structure at P0 (López et al., 2018). Curiously, these mice do not survive more than 24 h and therefore cardiac issues cannot be ruled out; however, other independent factors could also lead to early death in the perinatal period. Regardless, in their conditional deletion model, these mice present with neural crest developmental defects including cleft palate malformation and hypoplasia of enteric glia (López et al., 2018). Unfortunately, the authors did not assess melanocyte development in their conditional mutants. Interestingly, expression of TBX3 in follicular hair cells is associated with the dilute colour phenotype of the Dun horse. In contrast, regulatory mutations which decrease levels of TBX3 are associated with the dark coat colour phenotype of the non-Dun horse (L. Andersson, 2020; Imsland et al., 2016). They propose that TBX3 reduces the level of KITLG and therefore reduces melanocyte migration and survival. However, this mechanism is unproven.

As stated previously, TBX3 is a known regulator of EMT and is associated with melanoma invasion potential (Rodriguez et al., 2008). Interestingly, this is attributed in part to TBX3 induction of ID1 which prevents MITF induced expression of E-cadherin by preventing DNA binding at the E-box motif (CACGTG) (Peres et al., 2010). The invasive melanoma program is associated with the most de-differentiated phenotypes, and this is further exhibited by *TBX3* expression in the

‘Melanoma Database’ (Figure 11). Furthermore, TBX3 regulates suppression of senescence and subsequent promotion of cellular proliferation (Bennett & Medrano, 2002; Ha et al., 2008; Khan et al., 2019; Lingbeek et al., 2002; Peres et al., 2010; Vredeveld et al., 2012; Wagstaff et al., 2022). TBX3 is regulated by c-MYC and CDK2 to promote transition from S-phase. C-MYC induces *TBX3* expression by binding multiple E-box motifs approximately 1 kb upstream of the *TBX3* transcription start site (TSS) (Willmer et al., 2015). Importantly, and as previously stated, this motif is recognized by MITF, the master melanocyte regulatory TF (Levy et al., 2006). It is therefore possible that MITF regulates *TBX3/Tbx3*; however, it is not known if MITF can bind this site.

Tfap2b is one of five family members which encodes a Transcription factor family activator protein 2 (TFAP2) protein. These family members are known to regulate gene expression during embryonic development and differentiation (Jin et al., 2023). For example, a select population of *tfap2b*$^{+}$ MSCs in zebrafish are multipotent and can give rise to all pigment producing cell types (melanocytes, iridophores, and xanthophores) as well as cells of the neuronal lineage (Brombin et al., 2022). In mice, dual deletion of TFAP2 paralogs (*Tfap2a/b*) causes a complete failure of melanocyte formation (Seberg et al., 2017). TFAP2A binding peaks identified by ChIP-seq associate with pigment genes and co-occupy many MITF binding sites (Seberg et al., 2017). Furthermore, Kenny and colleagues showed that TFAP paralogs (*TFAP2A* and *TFAP2C*) modulate chromatin to facilitate MITF mediated activation of target genes (Kenny et al., 2022). Interestingly, TFAP2B levels are both low and unchanged across the four melanoma subtypes defined by the ‘Melanoma Database’ (Figure 11). An increase of *Tfap2b* in RHC melanocytes could be a compensatory mechanism to assist MITF binding. Alternatively, TFAP2B

mediated chromatin modulation could promote binding of TFs which promote expression of genes favouring phaeomelanin synthesis.

Zeb1 is one the three known genes, the others being *Hmga2* and *Tbx3*, which encode for TFs that promote EMT. However, only ***Zeb1*** is expressed at relatively lower levels in RHC melanocytes (Appendix A: Table S4). In melanoma cells, GLI2 interacts with ZEB1 at the *CDH1* promoter to prevent expression and formation of E-Cadherin (Perrot et al., 2013). A recent study identified ZEB1 as a key regulator governing various states of melanocyte differentiation with higher expression in the less differentiated neural crest-like state (Durand et al., 2023). This result is not entirely surprising given the known role of ZEB1 in NC development. Furthermore, I found that *ZEB1* is most highly expressed in undifferentiated and neural crest-like melanoma states (Figure 11). The reduced levels of *Zeb1* in RHC present an interesting result which is difficult to interpret.

Novel

Cbfa2t3 encodes a co-TF which is a member of the Myeloid translocation gene family and this protein forms a complex with DNA-bound TFs to facilitate transcriptional repression and is implicated as a tumour-suppressor in breast cancer (Kochetkova et al., 2002). In contrast, loss of this protein leads to hypoplasia of breast acinar cells (Rossetti et al., 2010). It is further associated with cancer, more specifically B-cell lymphomas which have a chromosomal translocation t(14;16)(q32;q24) (Salaverria et al., 2012). Interestingly, a CBFA2T3-ZNF652 complex functions in the inhibition of E-box targeted DNA binding of *TCF12*, which encodes HEB, human B-HLH factor, that exhibits an almost exact identity as the E-

box recognizing B-HLH domain found in the immunoglobulin enhancer binding proteins encoded by the E2A and ITF2 genes (J.-S. Hu et al., 1992; Kumar et al., 2008). RHC melanocytes in my study show high levels of fold-enrichment (Appendix A: Table S4); therefore, it would be worth investigating a potential role for CBFA2T3 in modulating E-box mediated transcription, such as whether it interacts with and inhibits DNA binding by MITF. High levels of CBFA2T3, which are tumour promoting in B-cells, could therefore have the potential to be tumour promoting in other cell types, such as melanoma. However, human melanoma cell lines and samples show low levels of expression across the various subtypes (Figure 11).

Hdac9 encodes for the Histone deacetylase 9 (HDAC9) protein which functions, like other HDACs, in the removal of acetyl groups from lysine residues at the amino termini of histones, as well as other non-histone proteins (Park & Kim, 2020). HDAC9 regulates diverse biological processes and functions in a tissue-specific manner, such as cardiac muscle development, bone formation, adipocyte differentiation and innate immunity (C. Yang et al., 2021). It exhibits diffuse levels of expression across melanoma subtypes (Figure 11). Furthermore, RHC melanocytes in my study show enrichment of *Hdac9* (Appendix A: Table S4). It is perfectly plausible then that an increase of HDAC9 leads to significant alterations of the epigenetic landscape which in turn might be consequential for MiGS expression.

Lmo2 encodes the LIM-onlyprotein2, a co-TF, which functions in blood stem cell development, haematopoiesis, and promotes the development of acute myelogenous leukaemia (L. Lu et al., 2023). Interestingly, *Lmo2* is one of the most highly expressed TF/co-TF genes in the Hair-GEL P5 melanocytes (Figure 10). Despite this fact, there is no relevant literature retaining to LMO2 function in melanocytes or melanoma. LMO2 is a significant mediator of hematopoietic

development and is therefore associated with several forms of leukaemia (L. Lu et al., 2023; Orkin, 1995). To that point, the promoter for *LMO2* is located near a translocation cluster and is therefore considered an archetypical chromosomal translocation oncogene in blood tumours (Chambers & Rabbitts, 2015). Interestingly, *Lmo2* exhibits one of highest relative fold changes as compared to other TF/co-TFs in the MiGS. The significance of this is difficult to decipher; however, this finding suggests a potentially significant role for LMO2 which, as it stands, is unknown.

Padi2 encodes a member of the Peptidyl arginine deiminase family of enzymes and functions to create post-translational modifications of proteins through deamination, a process that converts arginine residues into citrullines when in the presence of calcium ions (Cicek et al., 2022). PADI2 is implicated in several diseases ranging from various autoimmune conditions to cancer (Zhu et al., 2023). Within P5 mouse skin cells, *Padi2* expression is mostly restricted to melanocytes (Figure 10). A function for PADI2 in the context of my study is difficult to speculate though it is possible that PADI2 functions as a non-canonical post-translational modifier of melanocyte specific proteins.

Pcbd1 is part of the Pterin-4-alpha-carbinolamine dehydratase family. These enzymes primarily function in the recycling and synthesis of tetrahydrobiopterin (BH_4), an important cofactor in the catalytic conversion of phenylalanine to tyrosine by phenylalanine hydroxylase (Ferrè et al., 2014). Therefore, an increase of *Pcbd1* could facilitate more conversion of phenylalanine to tyrosine and subsequently tyrosine to DOPA, The conversion of tyrosine to DOPA is a rate-limiting step in melanogenesis, thus RHC melanocytes might increase levels of PCBD1 to foster production of phaeomelanin.

Pgr is expressed at low levels; however, the total amount is much higher in the melanocytes of RHC mice (Appendix A: Table S4). The *Pgr* gene encodes the Progesterone receptor (PGR), part of the steroid receptor superfamily, and is therefore the primary mediator of physiological actions exerted by progesterone (Akison & Robker, 2012). There is little to no expression of PGR in the 'melanoma database' (Figure 11). Subsequently, a role for PGR is difficult to interpret at this point.

Plagl1 encodes a homonymous zinc finger protein which functions to promote cell cycle arrest and apoptosis through multiple pathways (Vega-Benedetti et al., 2017). PLAGL1 is implicated in several pathologies, including cancer, where it is known to promote oncogenesis and tumour formation of lipoblastoma, hepatoblastoma, and acute myelogenous leukaemia (Dyck et al., 2007; Vega-Benedetti et al., 2017). PLAGL1 appears elevated in several undifferentiated and neural crest-like melanoma cell lines and samples (Figure 11). However, a role in melanoma has not been described. Regardless, PLAGL1 could be a player in oncogenesis and melanoma formation.

Curiously, both Paired related homeobox encoding genes, ***Prrx1*** and ***Prrx2***, are found in the MiGS. These are both strongly associated with Agnathia-Otocephaly Complex, a rare disease which leads to disruption of 1st branchial arch derivatives leading to mandibular hypoplasia or agnathia, melotia, synotia, and microstomia with oroglossal hypoplasia or aglossia (Dubucs et al., 2021). PRRX1 has been identified as a master regulatory TF which directs the fibroblast lineage toward a myofibroblastic phenotype. Interestingly, this process is tightly regulated by TGFβ signalling, a pathway which was predicted to be active in my RHC melanocytes (K.-W. Lee et al., 2022). PRRX1 is also considered an important

regulator of EMT under the influence of multiple pathways, including TGFβ (Du et al., 2021). Relatedly, *Prrx1*$^{+}$ melanocytes were found to promote a pool of metastatic initiating cells in primary melanoma tumours (Karras et al., 2022). A PubMed search for PRRX2 elicits 4x fewer results as compared to PRRX1. However, TGF-β-also induces expression of this factor and it functions to enhance invasion and migration of epithelial cells (Juang et al., 2016). Furthermore, their expression roughly mirrors each other across multiple melanoma samples with strongest expression in neural crest-like subtypes (Figure 11).

Like AR and PGR, ***Rorb*** encodes a nuclear ligand bound TF, Retinoic acid-related orphan receptor (ROR)β, and functions in a host of physiological functions and pathologies (Feng et al., 2015). One of the primary functions is thought to be in repression of bone formation. It is also implicated as a regulator of circadian rhythm (Feng et al., 2015). Expression in melanoma is restricted to the more differentiated melanocytic subtype (Figure 11).

Runx1t1 encodes for Runt-related transcription factor 1, translocated to 1 which often forms a fusion protein with RUNX1. Together, this complex works in the recruitment of HDACs to DNA to inhibit transcription (N. Hu et al., 2022). RUNX1T1 has a large influence on cell fate and development and has been implicated in several processes such as haematopoiesis, neuronal differentiation, microglial activation, intestinal development, adipogenesis, angiogenesis, and carcinogenesis (N. Hu et al., 2022). Binding partners outside of RUNX1 are unclear. Therefore, despite increased expression in melanocytes from both RHC mice, it is difficult to know whether RUNX1T1 can mediate physiologic changes. However, given that this protein is found to function in an array of tissue and cell types it is not an

impossibility that it can work with other binding partners to mediate similar effects in melanocytes.

Human **ZFHX4** is implicated in congenital bilateral ptosis (McMullan et al., 2002). Furthermore, microdeletions in 8q21.11, with subsequent loss of ZFHX4, leads to neuro and cardiac developmental issues (Ayed et al., 2021). Deletion of *Zfhx4* in mice leads to early postnatal lethality due to respiratory failure (M. Zhang et al., 2021). RHC melanocytes have diminished expression of *Zfhx4* (Appendix A: Table S4). Interestingly, this gene is found to be highly expressed in melanoma, with the highest expressing subtypes being undifferentiated and neural crest-like (Figure 11).

Conclusions and Future Work

In this chapter, I profiled the transcriptome of melanocytes which were eumelanotic, with active MC1R signalling, and phaeomelanotic, with inhibited-MC1R signalling and mimic the human RHC trait. To this end, using scRNA-seq, I identified a set of DEGs, the MiGS, which may be subjected to further biological investigation. This work illuminates the complex biology, including previously unidentified genes and signalling pathways, which participate in the GRN of melanocytes that are in a state of active, and inactive, MC1R signalling. More specifically, the MiGS identified several TF and co-TFs which could serve as key potential regulators of melanocyte function, including melanogenesis, melanomagenesis, and cancer progression. Furthermore, the collective data presented above provides a more refined set of candidate TFs which exhibit the most compelling evidence for follow-up. All MiGS TF/co-TFs warrant further

exploration; however, our future work will prioritize TFs which lie downstream of TGFβ/BMP signalling.

For follow-up efforts, detailed in Chapter 4, I chose one of the MiGS identified factors, *Tbx3*, a T-box family member, which is activated by TGFβ signalling pathway (Khan et al., 2019; J. Li et al., 2013). Importantly, *Tbx3* showed significant increased expression in phaeomelanotic melanocytes of both RHC (lethal yellow, A^{y}/a; recessive yellow, $Mc1r^{e}/^{e}$) samples as compared to the eumelanotic nonagouti melanocytes. Additionally, TBX3 is associated with pigmentation (e.g., Dun horses); however, it is unclear as to how TBX3 mediates this phenotype (L. Andersson, 2020; Imsland et al., 2016). As mentioned previously, TBX3 plays key roles in human melanomas as a regulator of epithelial-to-mesenchymal transition in melanoma invasion (Rodriguez et al., 2008). Furthermore, TBX3 acts as an anti-senescence transcription factor thus promoting cellular proliferation (Bennett & Medrano, 2002; Ha et al., 2008; Khan et al., 2019; Lingbeek et al., 2002; Peres et al., 2010; Vredeveld et al., 2012; Wagstaff et al., 2022). For these collective reasons, TBX3 was selected for further exploration as a candidate transcription factor for the regulation of MiGS and canonical melanocyte genes.

Figures and Tables

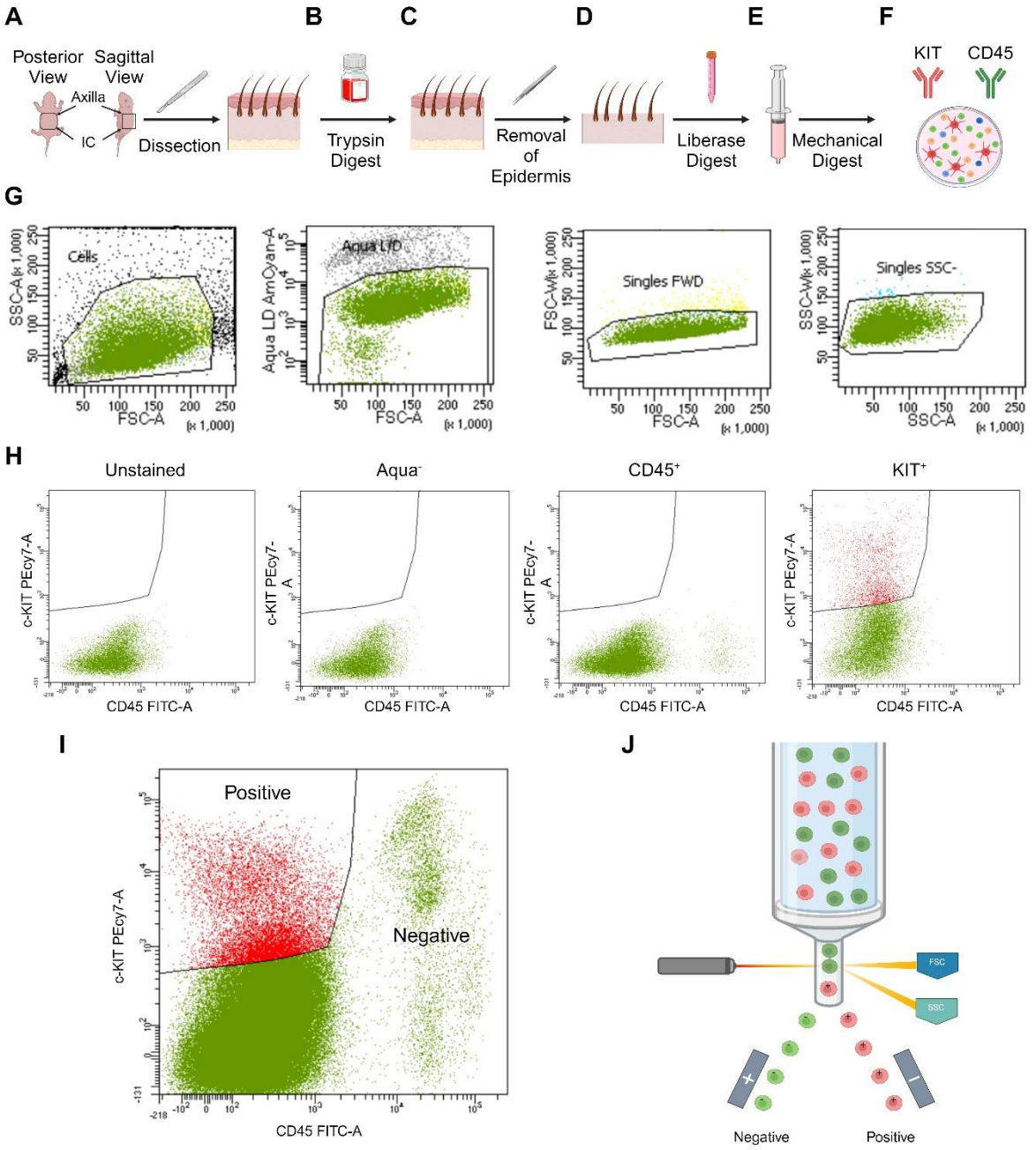


Figure 1. Overview of Tissue Digestion and Melanocyte Capture. (A-F) Schematic depicting tissue harvest and digestion. (A) Anatomical perspective with labelled landmarks used for defining the dorsal skin region; Iliac crest (IC). (B) Trypsin digestion to breakdown matrix proteins between dermis and epidermis. (C) Removal of epidermal layer with forceps. (D) Liberase digest of dermis. (E)

Mechanical digestion by repeated syringe expulsions. (F) Immunostaining of single cells with KIT-PEcy7 and CD45.2-FITC. (G-I) Flow cytometry charts which define positive and negative cell populations. (G) Identification of viable cells with Aqua, side-scatter (SSC), and forward-scatter (FSC). (H) Single and unstained samples used to define the voltage parameters for each channel. (I) Defining positive and negative gates for FACS. (J) Depiction of FACS sorter and cell collection with separation of positive and negative cell populations.

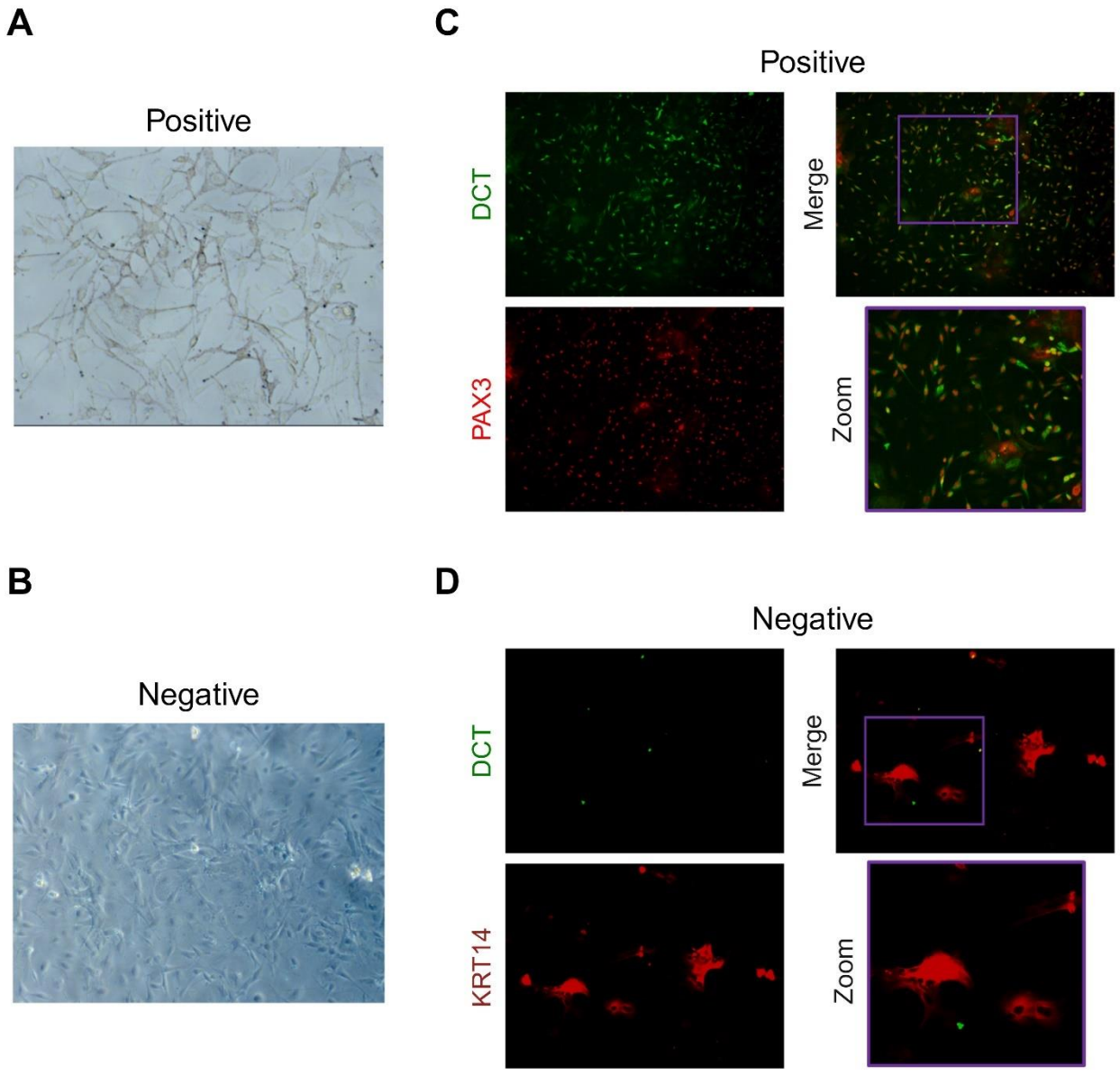


Figure 2. Positive Cells selected by FACS are Melanocytes. (A-B) Brightfield images at 20x magnification of FACS sorted positive ($KIT^+/CD45^-$) (A) and negative (KIT^-) (B) cell populations. (C-D) Immunofluorescence images at 10x magnification depicting melanocyte enrichment ($DCT^+/PAX3^+$) in the FACS sorted positive cells (C) and absence of melanocytes ($DCT^-/PAX3^-/KRT14^+$) in the negative sorted population (D).

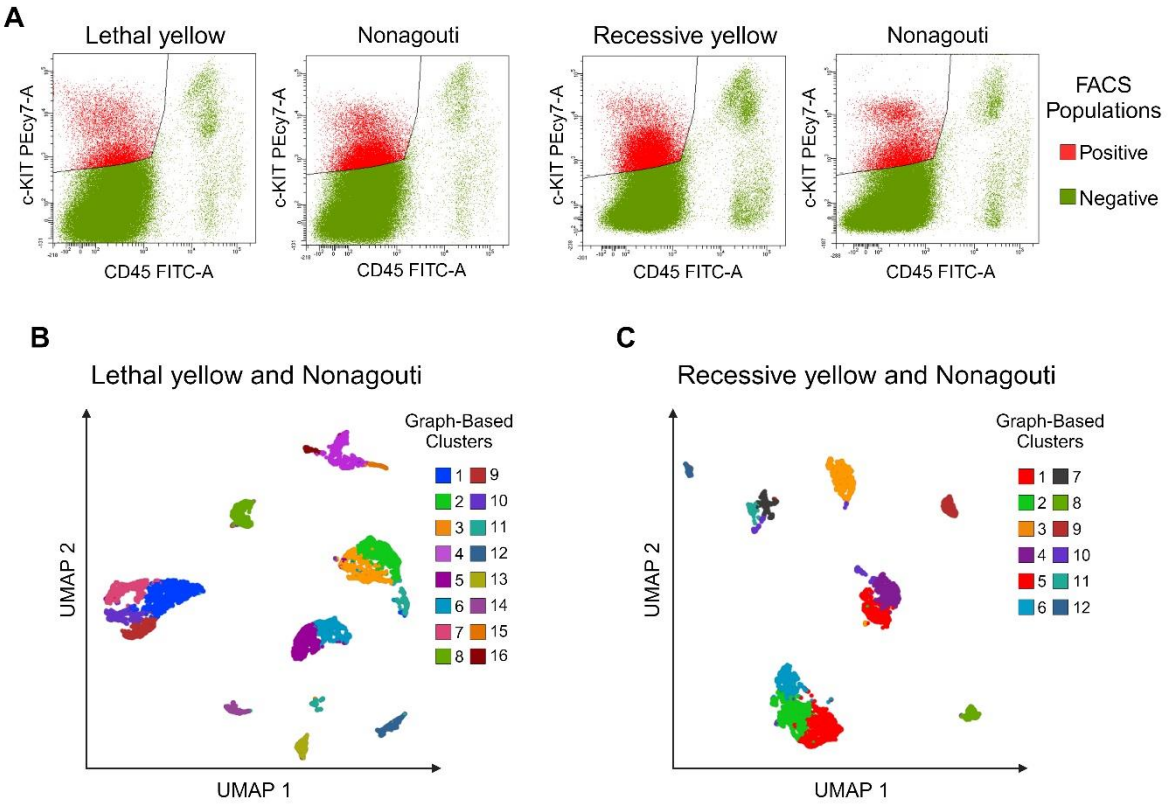


Figure 3. Overview of Single-cell Sequencing of Positive Selected FACS Population. (A) FACS enrichment of KIT^{+}/CD45^{-} 'positive' cells isolated from all samples (red). (B-C) Uniform Manifold Approximation and Projection (UMAP) plots of the sequenced cells that passed quality control for each pairwise experiment. Cells isolated from nonagouti and lethal yellow paired samples (6,413 cells in B) and nonagouti and recessive yellow paired samples (4645 cells in C) which passed quality control after sequencing and mapped by graph-based clusters.

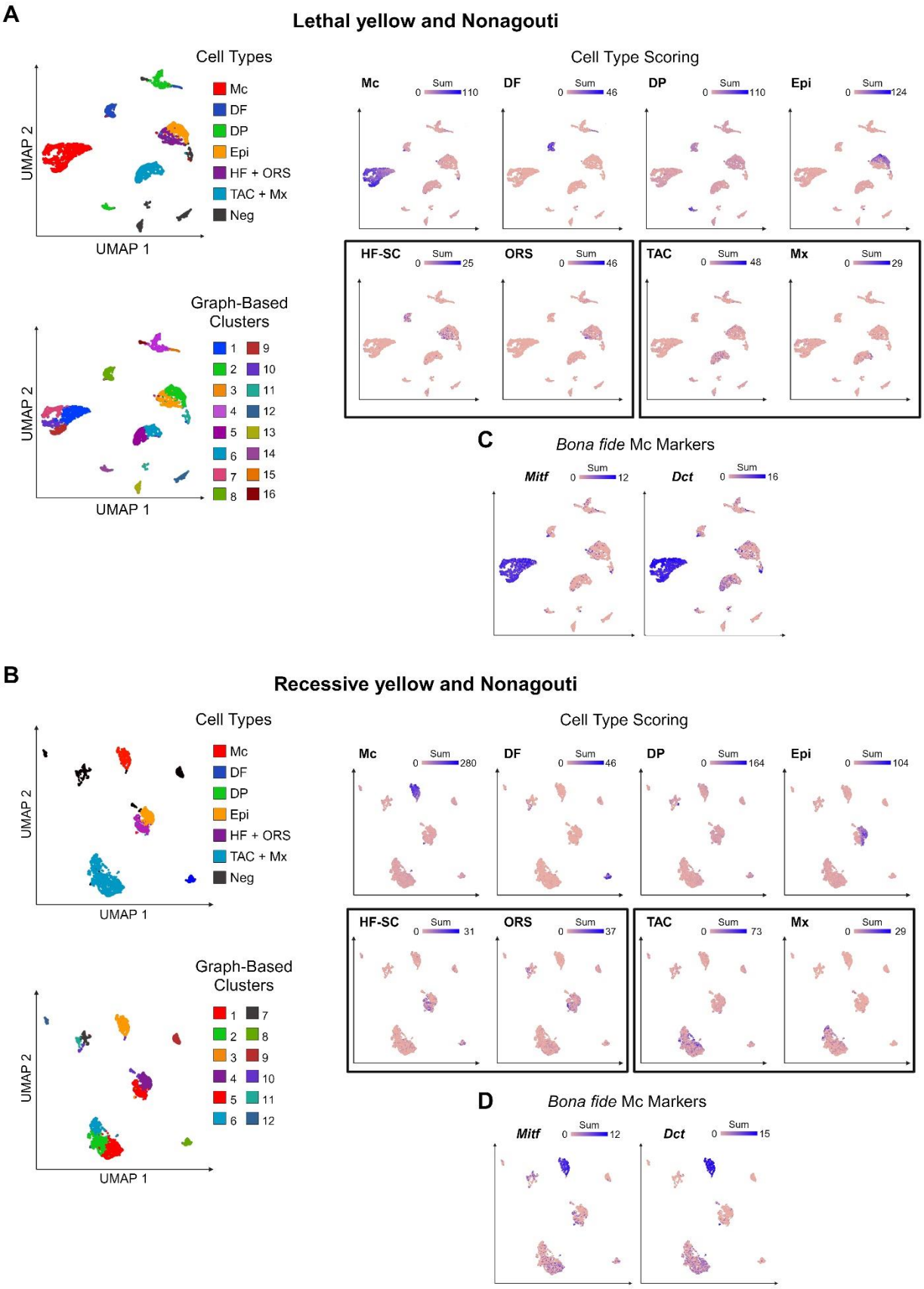

A
Lethal yellow and Nonagouti
Cell Types
Mc
DF
DP
Epi
HF + ORS
TAC + Mx
Neg
UMAP 2
UMAP 1
Graph-Based Clusters
1 9
2 10
3 11
4 12
5 13
6 14
7 15
8 16
Cell Type Scoring
Mc Sum 0 110
DF Sum 0 46
DP Sum 0 110
Epi Sum 0 124
HF-SC Sum 0 25
ORS Sum 0 46
TAC Sum 0 48
Mx Sum 0 29
C
Bona fide Mc Markers
Mitf Sum 0 12
Dct Sum 0 16
B
Recessive yellow and Nonagouti
Cell Types
Mc
DF
DP
Epi
HF + ORS
TAC + Mx
Neg
UMAP 2
UMAP 1
Graph-Based Clusters
1 7
2 8
3 9
4 10
5 11
6 12
Cell Type Scoring
Mc Sum 0 280
DF Sum 0 46
DP Sum 0 164
Epi Sum 0 104
HF-SC Sum 0 31
ORS Sum 0 37
TAC Sum 0 73
Mx Sum 0 29
D
Bona fide Mc Markers
Mitf Sum 0 12
Dct Sum 0 15

Figure 4. Identification and Classification of Sequenced Cells. (A,B) Uniform Manifold Approximation and Projection (UMAP) plots of the (A) lethal yellow and nonagouti cells and (B) recessive yellow and nonagouti cells classified by skin cell type: Melanocytes (Mc), Dermal fibroblasts (DF), Dermal papilla (DP), Epidermis (Epi), Hair follicle and Outer root sheath (HF + ORS), Transit amplifying and Matrix cells (TAC + Mx), and Negative (Neg) cells which could not be classified. (B) UMAP of cells classified by graph-based cluster. (C,D) UMAPs depicting scores of bona fide melanocyte genes for (C) lethal yellow and nonagouti cells and (D) recessive yellow and nonagouti cells.

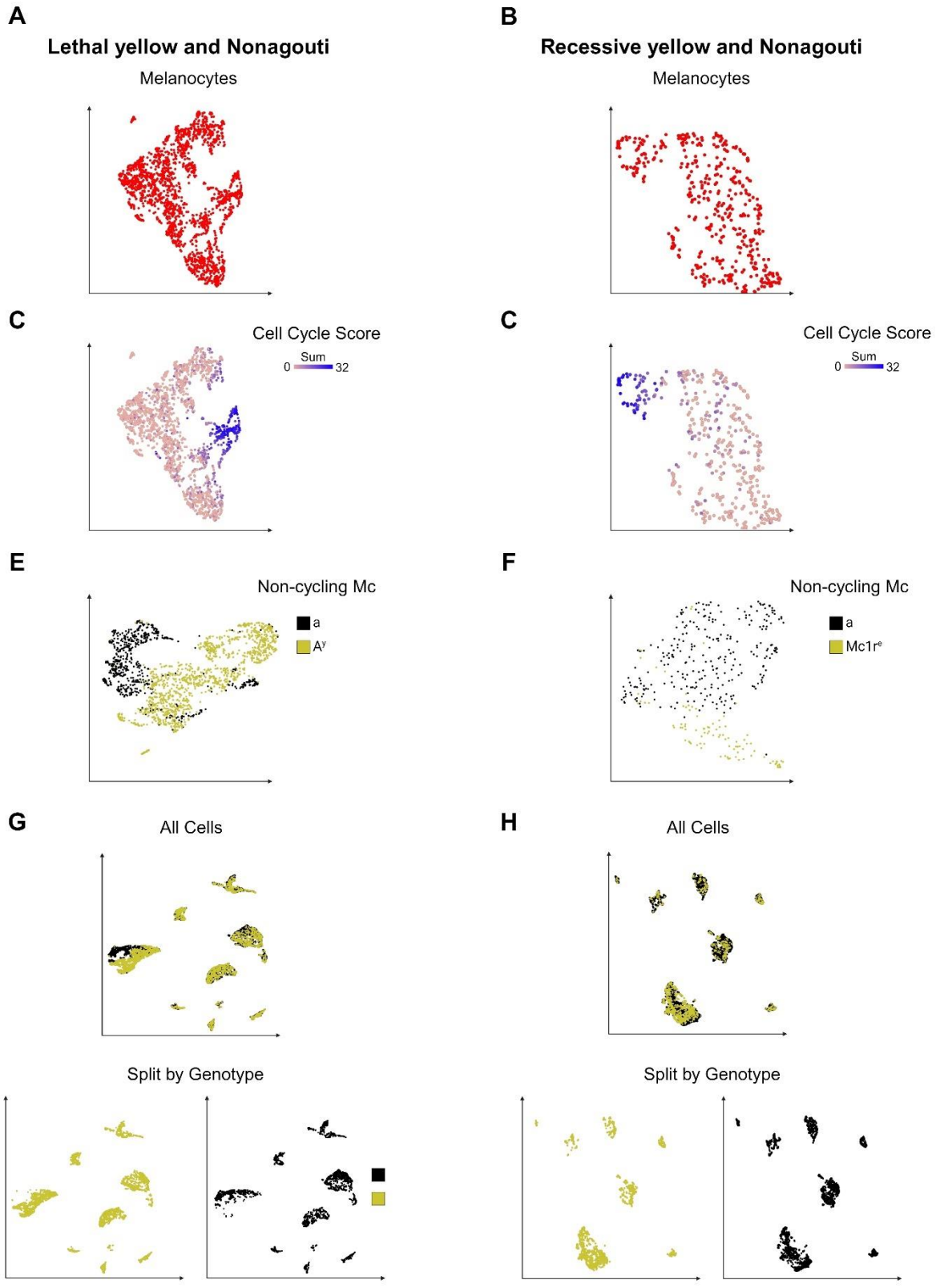


Figure 5. Identification of Analysis Ready Melanocytes. (A,B) Uniform Manifold Approximation and Projection (UMAP) plot of all melanocytes for (A) lethal yellow and nonagouti and (B) recessive yellow and nonagouti samples. (C,D) UMAPs

depicting heatmap of the cell cycle scoring for (C) lethal yellow and nonagouti and (D) recessive yellow and nonagouti samples cycle highlighted in blue. (E,F) UMAP plots of cells classified as non-cycling melanocytes. The nonagouti melanocytes (black) segregate from the recessive yellow and lethal yellow (gold) melanocytes consistent with a eumelanin and phaeomelanin producing melanocytes having distinct transcriptional profiles. (G,H) UMAPs of all sequenced cells from (F) lethal yellow and nonagouti and (G) recessive yellow highlighting that other skin cell types are not altered by intrinsic MC1R signalling loss.

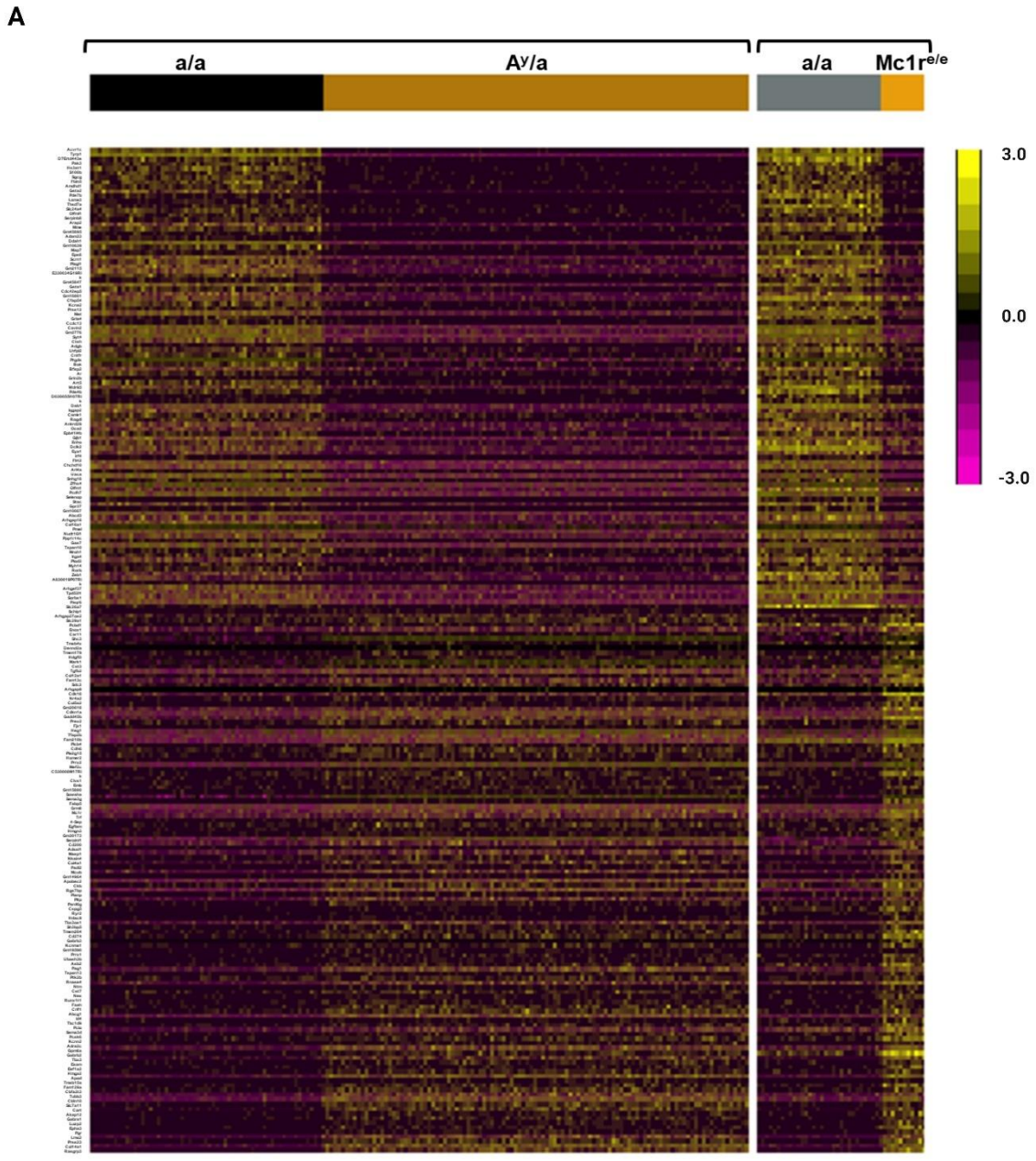


Figure 6. Heatmap of Scaled Expression Data from the 216 DEGs in Each Cell Grouped by Sample. (A) Samples harvested as experimental pairs are bracketed. Genes are ranked based on the lethal yellow vs nonagouti littermate fold change value with the genes significantly downregulated in the lethal yellow and recessive yellow samples shown at the top of the heatmap.

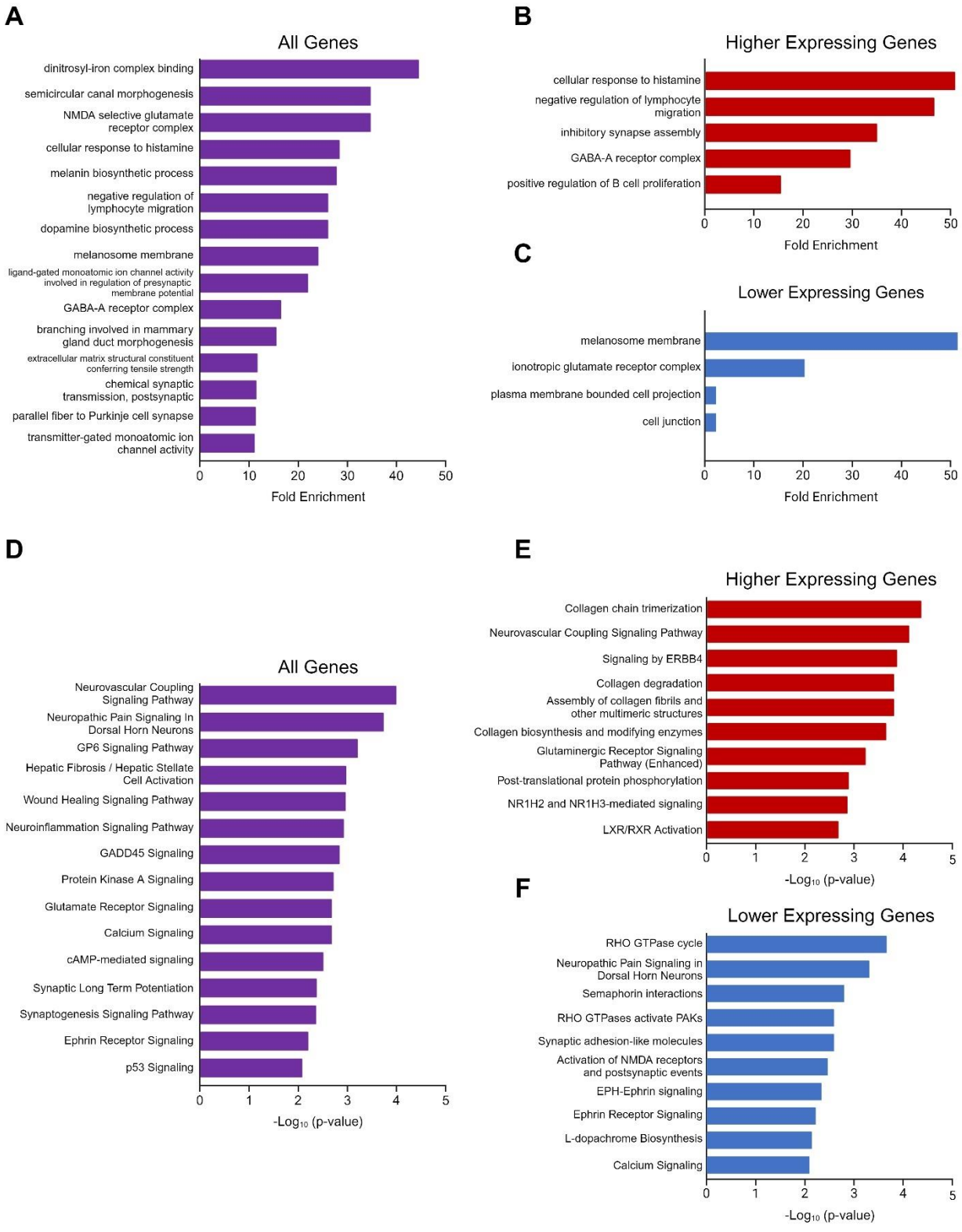


Figure 7. Enriched Processes and Pathways Found in the MiGS. (A-C) Top significant GO terms ranked by fold-enrichment (FDR < 0.05) for the entire MiGS (A), higher expressed genes (B), and lower expressed genes (C). (D-F) Top

significant pathway terms from IPA ranked by significance (p-value <0.05) for the entire MiGS (D), higher expressed genes (E), and lower expressed genes (F).

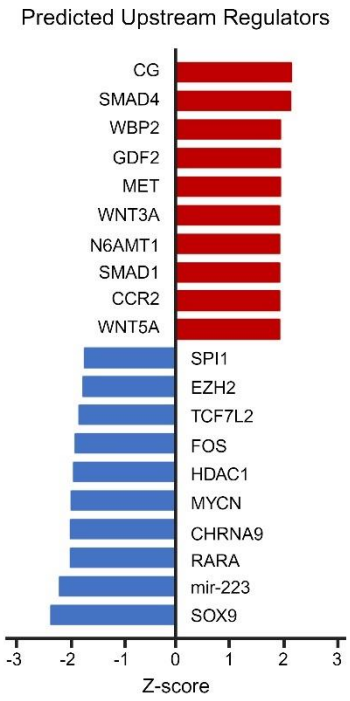


Figure 8. Predicted Upstream Regulators of MiGS Includes TGFβ Superfamily.

Top 10 predicted activated (red) and inhibited (blue) regulators of the MiGS gene list ranked by Z-score.

A

	Lethal yellow			Recessive yellow		
TF	FDR step up	Fold change	Normalized total counts	FDR step up	Fold change	Normalized total counts
Plagl1	7.02E-74	-4.95	75093.01	4.49E-16	-7.74	25407.16
Id4	9.10E-41	4.32	186906.13	1.12E-06	4.06	17478.45
Mef2c	8.98E-40	2.69	453242.33	1.93E-07	2.33	87371.49
Tfap2b	4.41E-26	2.56	584934.88	1.73E-05	2.30	83465.70
Zeb1	1.21E-24	-2.14	47523.38	9.35E-08	-2.50	48687.94
Tbx3	6.32E-20	5.62	46973.35	1.31E-24	16.73	5321.54
Irf4	1.32E-19	-3.02	36655.02	7.19E-03	-2.61	17344.66
Ar	1.02E-17	-3.49	26378.97	6.09E-05	-11.40	11661.52
Hmga2	1.34E-12	5.72	18179.50	2.41E-04	4.11	3286.45
Zfhx4	4.70E-11	-2.71	14529.54	4.77E-05	-23.02	8133.80
Rorb	8.80E-09	-2.17	18530.54	1.73E-02	-4.24	14844.71
Pgr	2.68E-08	10.98	13734.53	2.15E-10	15.85	2921.65
Prrx2	1.04E-04	2.65	11115.52	2.71E-03	3.57	2039.79
Nr4a2	1.06E-03	2.46	75427.14	1.96E-31	7.30	43090.94
Prrx1	4.02E-03	3.69	9610.96	1.76E-02	3.69	629.40
Co-TF						
Eya1	2.95E-37	-3.05	74686.22	2.38E-37	-11.24	84281.10
Lmo2	3.15E-36	11.61	82076.32	8.78E-15	6.91	7456.96
Padi2	2.86E-16	3.27	49814.38	3.51E-08	4.82	5252.94
Cbfa2t3	2.43E-16	5.94	37487.51	1.65E-06	3.72	2999.43
Pcbd1	1.25E-03	2.12	39324.37	2.37E-02	2.34	4546.95
Runx1t1	3.60E-03	4.19	10497.53	1.19E-09	10.85	3162.79
Hdac9	4.05E-02	3.47	5426.38	1.02E-02	7.52	6127.99

B

Known

Ar
Eya1
Id4
Irf4
Hmga2
Mef2c
Nr4a2
Tbx3
Tfap2b
Zeb1

Novel

Cbfa2t3
Hdac9
Lmo2
Padi2
Pcbd1
Pgr
Plagl1
Prrx1
Prrx2
Rorb
Runx1t1
Zfhx4

C

Neural Crest Development

Hmga2
Id4
Mef2c
Tbx3
Tfap2b

Melanocyte Differentiation

Mef2c

Pigmentation

Eya1
Id4
Irf4
Tbx3

Oxidative Stress Protection

Nr4a2

Melanoma

Ar
Eya1
Hmga2
Irf4
Nr4a2
Tbx3
Zeb1

Figure 9. Annotated TF/co-TFs Expressed in MiGS. (A) List of all differentially expressed transcription/co-transcription factors (TF/co-TF) found within the MiGS and ranked by FDR from the nonagouti/lethal yellow pairwise differential analysis. (B) TF and co-TFs divided by known or novel relationships with melanocyte and pigment cell biology. (C) Known TF/co-TFs delineated by association with melanocyte biology.

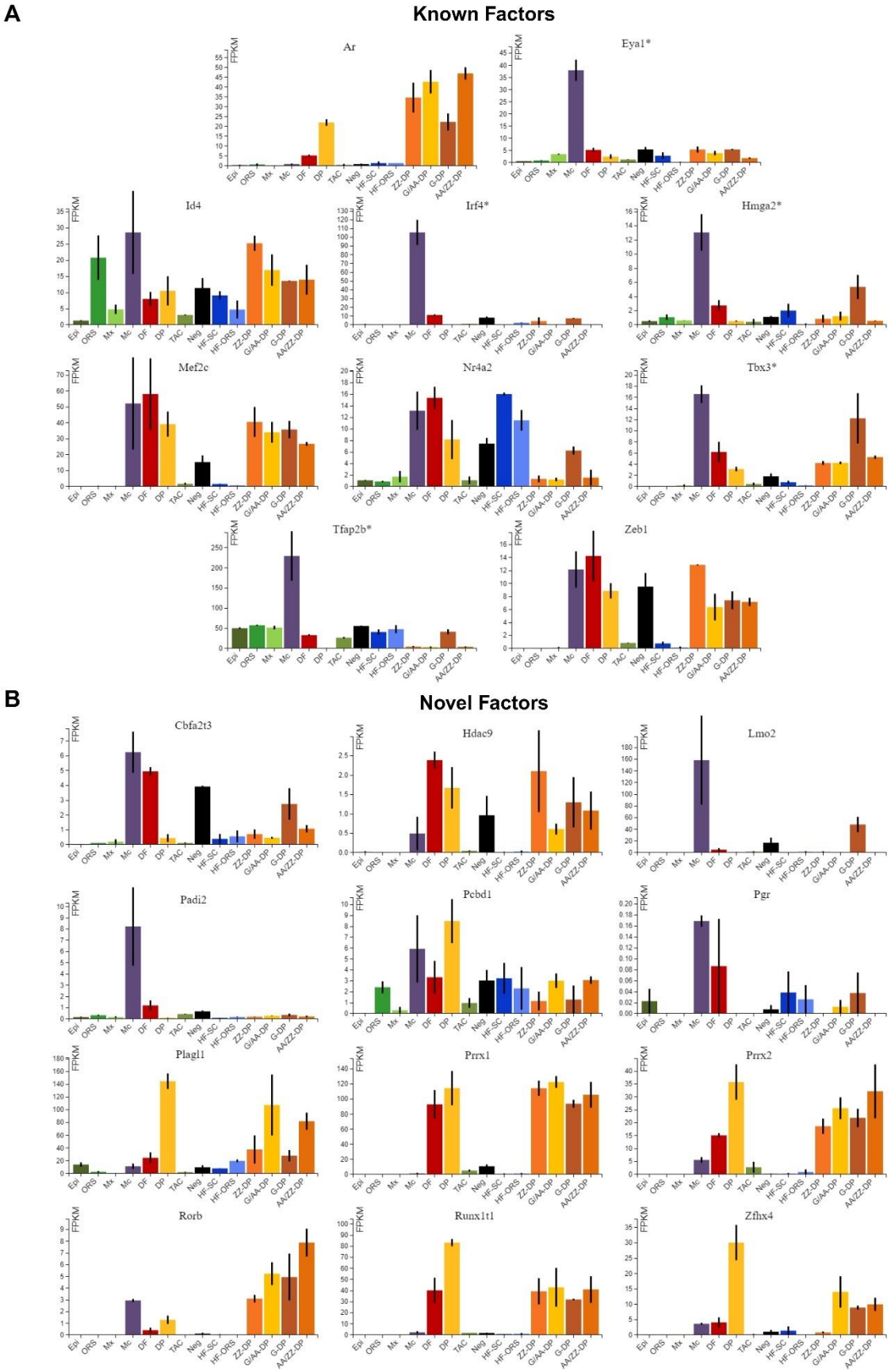

A
Known Factors
Ar
Eya1*
Id4
Irf4*
Hmga2*
Mef2c
Nr4a2
Tbx3*
Tfap2b*
Zeb1
B
Novel Factors
Cbfa2t3
Hdac9
Lmo2
Padi2
Pcbd1
Pgr
Plagl1
Prrx1
Prrx2
Rorb
Runx1t1
Zfhx4
FPKM
Epi
ORS
Mx
Mc
DF
DP
TAC
Neg
HF-SC
HF-ORS
ZZ-DP
G/AA-DP
G-DP
AAZZ-DP

Figure 10. MiGS TF/co-TF Expression from the Hair-GEL Database. (A-B) Bar chart depicting FPKM (Fragments Per Kilobase of transcript per Million mapped reads) values for skin cell types from Hair-GEL.net with melanocyte signature genes marked by an * (Rezza et al., 2016). (A) Expression values of known TF/co-TFs. (B) Expression values of unknown TF/co-TFs.

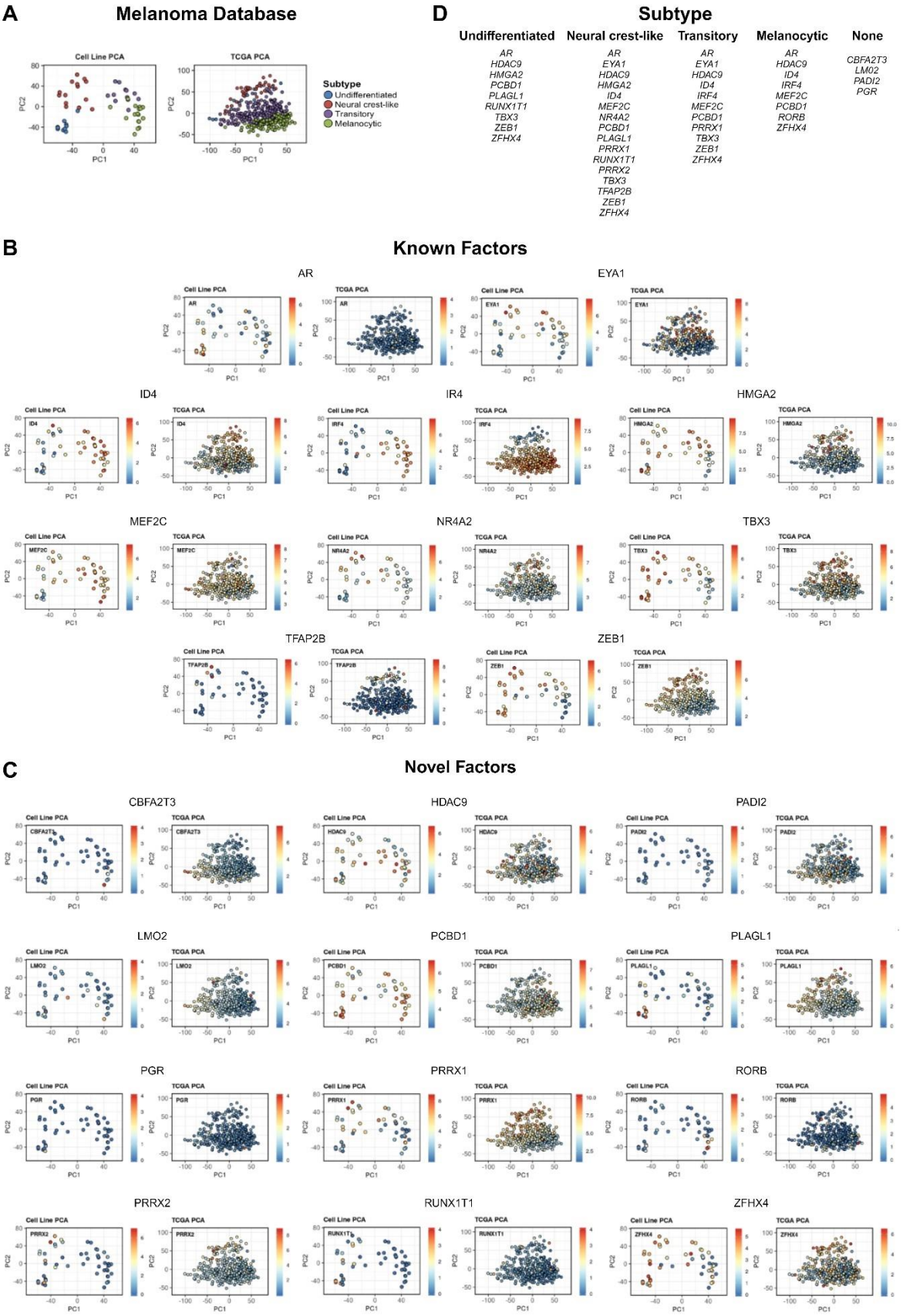


Figure 11. MiGS TF/co-TF Expression in Melanoma Cell Lines and Patient Samples. (A) PCA depicting melanoma subtype classification in cell lines and

TCGA samples. (B) PCA heatmap plots of gene expression of known MiGS TF/co-TFs. (C) PCA heatmap plots of gene expression of novel MiGS TF/co-TFs. (D) Table of MiGS TF/co-TFs which exhibit prominent expression within a given melanoma subtype.

Table 1. Pigmentation Associated Genes Found Within the MC1R-inhbited Gene Signature (MiGS). In each pairwise experiment a negative FC indicates reduced expression in the phaeomelanin producing melanocytes (RHC mice; lethal yellow, *A^{y}/a*; recessive yellow, *Mc1r^{e}/^{e}*) compared to the eumelanin producing melanocytes isolated from nonagouti littermates.

	Lethal yellow (*A^{y}/a*)			Recessive yellow (*Mc1r$^{e/e}$*)		
Gene	**FDR step up**	**Fold change**	**Normalized total counts**	**FDR step up**	**Fold change**	**Normalized total counts**
Tyrp1	0.00E+00	-19.31	775984.48	1.12E-67	-83.9	286332.60
Pmel	4.82E-46	-2.33	8214929.50	5.82E-16	-2.55	2144016.69
Mef2c	8.98E-40	2.69	453242.33	1.93E-07	2.33	87371.49
Oca2	1.77E-25	-3.16	1308.27	9.28E-05	-2.47	75510.26
Slc7a11	5.38E-23	7.72	92466.92	3.79E-03	3.92	7263.31
Irf4	1.32E-19	-3.02	36655.02	7.19E-03	-2.61	17344.66
Mc1r	2.58E-11	2.94	553621.06	3.64E-03	3.63	62970.90
Gas7	1.37E-07	-2.28	14496.09	1.05E-02	-8.57	3650.95
Sdc2	1.70E-07	2.39	56501.17	8.94E-13	4.29	12197.97
Pcbd1	1.25E-03	2.12	39324.37	2.37E-02	2.34	4546.95
Masp1	9.76E-03	3.11	8721.57	1.73E-02	2.69	3468.97

Chapter 4: TBX3 Binds and Regulates Genes in Melanogenesis and Senescence Bypass

Introduction

In the previous chapter, I used scRNA-seq to profile the transcriptomes of melanocytes isolated from RHC mouse models. From this, I identified the MiGS comprising genes which are differentially expressed in phaeomelanin (RHC), compared to eumelanin producing, melanocytes. This signature comprises genes which are both novel and known genes in terms of melanogenesis and oncogenic transformation. Furthermore, I discovered that ~10% (22/216) of MiGS genes encode TFs or co-TFs. Surprisingly, this list does not include prominent regulatory TFs of melanocytes, such as *Mitf*. Given this, it is likely that one or more of the MiGS TF/co-TFs directly regulate at least a subset of other MiGS genes. A potential functional role in melanocyte biology exists for all TF/co-TFs present in the MiGS and, therefore, each one merits further exploration. For initial follow-up work, which will be the basis of this chapter, I selected one TF gene, *Tbx3*, a T-box family member, to interrogate. This selection was made for several reasons including: (1) it is downstream of the TGFβ signalling pathway (Khan et al., 2019; J. Li et al., 2013), which was predicted to be a driver of MiGS expression, (2) it has high fold-enrichment in the melanocytes of both RHC mice, (3) this gene is present in many of the biologically enriched terms identified in my bioinformatic analyses, (4) TBX3 has known functional roles in development of the NC and its terminal derivatives (López et al., 2018; Mesbah et al., 2012; Willmer et al., 2017), and lastly (5) it is highly expressed in several cancers, especially melanoma (Boyd et al., 2013; Dong et al., 2018; Peres et al., 2010, 2021; Peres & Prince, 2013; Rodriguez et al., 2008). Given this, I reasoned that TBX3 binds and regulates (B&R) genes governing biological processes of melanocytes and therefore chose this candidate for initial exploratory work.

The T-box family comprises a group of 17 ancient and highly conserved TF encoding genes which share a common DNA-binding domain known as the T-box and is further divided into 5 sub-families largely based on sequence homology (Khan et al., 2019; Washkowitz et al., 2012). All family members can recognize and bind to DNA at the T-box element (AGGTGTGA) (Khan et al., 2019; Washkowitz et al., 2012). T-box TFs are expressed during development in several tissue and cell types with specific family members often showing restricted expression. For example, TBX3, is expressed in the heart (Mesbah et al., 2012; Mohan et al., 2020; Singh et al., 2012), lungs (Lüdtke et al., 2016), limbs (Frank et al., 2013; Sheeba & Logan, 2017), inner ear (Kaiser et al., 2021; Song & Morrow, 2023), and tissues derived from the NC (López et al., 2018; Mesbah et al., 2012; Willmer et al., 2017). Beyond development, T-box family members also regulate biological processes which include, but are not limited to, proliferation, differentiation, and EMT (F. Chang et al., 2016; Willmer et al., 2017).

Tbx3 is a member of the Tbx2 subfamily which also includes *Tbx2*, *Tbx4*, and *Tbx5* (Khan et al., 2019; Washkowitz et al., 2012). The Tbx2 subfamily arose from a common ancestral gene by two successive genomic events: (1) tandem duplication and (2) chromosomal duplication and dispersion (Washkowitz et al., 2012). Consequently, TBX2 and TBX3 share 90% amino acid identity within the T-box domain and they are often expressed concomitantly in multiple tissues during development (Washkowitz et al., 2012). Despite the similarity of all Tbx2 subfamily members, TBX2 and TBX3 are the only ones which have been described to primarily function in transcriptional repression (J. Lu et al., 2010). However, the Goding lab recently demonstrated that TBX2 can both activate and repress transcription of target genes in melanoma cells (S. Lu et al., 2021). Furthermore, its

function, be that activation or repression, is largely dictated by the type of binding motif present on the cis-regulatory element of a given target gene. For example, they showed that TBX2 facilitates genes expression when bound to an E-box, while repression primarily occurs when TBX2 is bound to the canonical T-box (S. Lu et al., 2021). Elevated levels of TBX2/3 are associated with tumorigenesis in several forms of carcinoma, including cutaneous melanoma (F. Chang et al., 2016; Khan et al., 2019; Papaioannou, 2014). For example, Rodriguez and colleagues showed that overexpression of TBX3 leads to down-regulation of E-cadherin, thereby promoting EMT, and thus enhanced melanoma invasiveness (Rodriguez et al., 2008). As mentioned, TBX2 and TBX3 exhibit a high degree of homology in their DNA binding domain; however, these two factors appear to have distinct roles in melanomagenesis whereby TBX2 promotes tumour growth while TBX3 functions in tumour formation and subsequent invasion (Peres et al., 2010).

Given the established role of TBX3 in melanomagenesis, its appearance in the MiGS, and the fact that it is a downstream target of TGFβ signaling, I propose that TBX3 is a novel mediator of canonical melanocyte functions. Therefore, in this chapter, I set out to test this experimentally. TBX3 is a TF, thus, I first evaluated chromatin occupancy in a melanocyte specific context. By doing this, I confirmed that TBX3, a MiGS and melanoma-associated TF, preferentially binds at two DNA binding motifs, the canonically associated T-box, and the E-box, which, to my knowledge, has not been previously reported. Furthermore, I show that TBX3 is a candidate to directly B&R the expression of MiGS genes as well as key genes associated with anti-senescence and melanogenesis. Lastly, I show that the highly homologous Tbx2 subfamily members, TBX2 and TBX3, B&R unique and independent targets within melanoma cells. Collectively, the results presented here

provide key insights into how RHC trait variants may increase melanoma risk via altered regulation of MiGS candidate genes downstream of MC1R.

Results

TBX3 Binds Genes Associated with Hypopigmentation

I hypothesized that TBX3 can bind, and therefore potentially regulate the expression of, MiGS genes. In the context of MC1R loss, this transcription program driven by TBX3 could promote a cellular state which is more favourable for phaeomelanogenesis by melanocytes. To test this notion, I first assessed TBX3 chromatin occupancy. To my knowledge, no global binding studies (i.e., Chromatin Immunoprecipitation-sequencing (ChIP-seq)) of TBX3 have been reported in a melanocyte specific context. Therefore, Goding lab members, Drs. Sizhu Lu and Pakavarin Louphrasitthiphol, performed a ChIP-seq experiment in the 501mel human melanoma cell line. Primary melanocytes are notoriously difficult to culture, likewise, in our hands, commercially available antibodies against TBX3 proved inadequate for IP-pulldown. Thus, we utilized a melanoma cell line for our experiment and created a sub-line whereby we could induce an epitope-tagged version of TBX3. To do this, Dr. Sizhu Lu developed a 3xHA-tagged TBX3 construct which could be induced by a tetracycline-transcriptional activation (Tet-on) system. In short, when doxycycline, a tetracycline derivative, is added to the culture medium it binds to reverse tetracycline transactivator (rtTA) which in turn allows this complex to bind, and promote expression of, a target gene (i.e., *TBX3*) under the control of the tetracycline response element (TRE). Using a PiggyBac integration approach, two plasmids with inverted terminal repeats, (1) iTBX3-3xHA-PuroR, containing the

TRE and TBX3 cDNA piggyBac transposase and (2) CAG-rtTA (rtTA), comprising the rtTA element, which is under the control of a constitutive CAG promoter, were transfected with a PiggyBac transposase to integrate these constructs at random TTAA sites in the genome (Figure 1A). Besides insufficient immunoprecipitation of TBX3 with commercial antibodies, we further chose to utilize this specific approach as it has been shown to produce high-quality ChIP-seq datasets (Laurette et al., 2015; Louphrasitthiphol et al., 2020; S. Lu et al., 2021). Furthermore, we chose the 501mel cell line as these cells have been used for previous ChIP analyses of other TFs, MITF, TBX2, and BRN2, by our lab and they are easy to transfect and, importantly, despite having functional MC1R, endogenously express TBX3 (Figure 1B). We also wanted to recapitulate the endogenous levels of TBX3 using the inducible expression system as this would avoid generating ChIP signals at non-physiological binding sites. Thus, we titrated the amount of doxycycline to match inducible expression with endogenous, and therefore physiologically relevant, levels by western blotting using an anti-TBX3 antibody to detect both endogenous and inducible protein (Figure 1C). GAPDH was used as a loading control. Western blotting of total cell extract, although a powerful tool for detection of protein, does not inherently assay for protein localization. Thus, to verify TBX3 nuclear localization, as well as protein level, we used immunofluorescence using anti-TBX3 and anti-HA antibodies and observed that the HA-tagged protein was indeed localized to the nucleus and was expressed at the expected levels (Figure 1D). Using an anti-TBX3 antibody we were also able to confirm that the expression of the ectopic HA-TBX3 did not substantially increase total TBX3 levels. With the cell line validated, we next performed ChIP-seq on two biological replicates. Significant called peaks were identified using MACS2 (q-value cutoff ≤ 0.01). Next, I identified

bound peaks which were common between the two replicates. To do this, an intersection filter was applied which stipulated an 80% overlap of coordinates between the two replicates. In total, this query identified 20,449 replicated peaks (Figure 1D).

Gene expression, or more precisely transcription, is regulated by a multitude of factors, such as TFs, which bind to, and exert their action at, gene regulatory elements, including promoters and enhancers (R. Andersson, 2015). Therefore, I next wanted to determine which of the common TBX3 peaks were associated with these regulatory features. To that end, I used the Genomic Regions Enrichment Annotation Tool (GREAT) to determine which peaks were associated with these elements and further assess their potential biological significance (McLean et al., 2010). In brief, GREAT identifies the called peaks which are found at annotated cis-regulatory regions (e.g., promoter, enhancer) of genes. In my query, GREAT identified that 10,000/20,449 peaks located at known cis-regulatory elements of 7,109 genes (Appendix B: Table S1). Distance between binding peaks and the TSS is an indicator of regulatory function, for example, proximal binding within ±5 kb of the TSS most likely indicated binding to a promoter region. Therefore, I next assessed the binding distribution of these 10,000 TBX3-bound peaks to evaluate to what extent TBX3 is located at proximal or distal regulatory elements. Of all replicated peaks, the majority were situated ≥ ±20 kb from the TSS; however, GREAT identified that 12.68% of replicated peals were located near the promoter (±5 kb of the TSS) (Figure 2A). For further validation, I repeated the assay with a similar but different tool, ChIP Seeker. Unlike GREAT, ChIP Seeker provides a more refined analysis which encompasses more genomic elements, such as 5’ UTR, and thus extends beyond the simpler definition of proximal and distal regulatory

elements. The ChIP Seeker results were consistent and identified the same promoter region peaks as GREAT (Figure 2B). Collectively, these data suggests that TBX3 binding peaks most frequently associated with distal enhancer elements in the context of *in vitro* melanoma cells (Figure 2A,B).

Our bioinformatic analysis with GREAT identified 10,000 peaks associated with cis-regulatory elements of 7,109 genes. Given this, I next wanted to know whether this gene set showed enrichment for any particular biological terms or pathways. GREAT has a built-in feature for GO analysis which elucidated several terms with the mostly highly enriched ones being those which included pigmentation/melanogenic pathways, such as ‘developmental pigmentation’ and ‘melanosome’, as well as multiple terms associated with EMT, including ‘positive regulation of EMT’, which is a well-described function of TBX3 (Boyd et al., 2013; F. Chang et al., 2016; Khan et al., 2019; Papaioannou, 2014; Rodriguez et al., 2008; Willmer et al., 2017) (Figure 2C). GREAT also assesses the gene set to determine significant ‘Phenotype Associations’ of which the result with the highest significance comprised pigmentation-related phenotypes, in both human and mouse, with a particular emphasis on hypopigmentation as highlighted by mouse phenotypes, such as, ‘hypopigmentation’, ‘diluted coat colour’, and ‘absent skin pigmentation’, as well as human pigmentation phenotypes, including ‘hypopigmentation of hair’ and ‘abnormality of dermal melanosome’ (Figure 2D). Collectively, these GO analyses were consistent with the hypothesized role for TBX3 in the regulation of melanogenic genes.

TBX3 ChIP Peaks Most Strongly Associate with T-box and E-box Motifs

TFs exert their influence by binding short and specific sequences of regulatory DNA known as motifs. For example, TBX3, a T-box family member, is known to bind the T-box element (AGGTGTGA) (Khan et al., 2019; Washkowitz et al., 2012). However, it is unclear if TBX3 can recognize and bind other DNA binding motifs. Therefore, I next used MEME-ChIP to assess motif enrichment within the sequences of shared TBX3 peaks (10,000/24,449) from our two biological replicates. Using *de novo* motif analysis, MEME identified the top 10 JASPAR CORE DNA binding sequences. This analysis showed enrichment for only two motif families, the T-box and E-box. Enrichment of the T-box element, which is the canonical recognition sequence for TBX3, was expected. However, the strong and significant association with the E-box was unexpected as this has, to the best of my knowledge, never been reported previously. Furthermore, T-box associated elements only constitute 20% (2/10) of the top motifs while the remainder are all E-box related (Figure 3A). The E-box motif sequence (CACGTG) is bound by bHLH and bHLH-LZ TFs (Pan et al., 2023). Importantly, this includes MITF, a master melanocyte regulator, and its related family members, such as TFEB and TFE3 (Goding & Arnheiter, 2019). Interestingly, the E-box sequence shares a 3 bp (GTG) region with the T-box element, which is bound by T-box family members (Khan et al., 2019; Washkowitz et al., 2012). This 3 bp region, bases 3-5 of the T-box element, is considered the core component for DNA recognition, and binding, by TBX3 whereas the flanking base pairs play a much less influential role (Coll et al., 2002). The core 'GTG' sequence more precisely comprises 5/8 bps within the T-box element (AG**GTGTG**A). Consistent with the notion that TBX3 may directly bind E-box

regions, TBX3 has previously been shown to repress the expression of *CDH1* by binding a **CA**G**GTGT** site which shares 5/6 bp with the canonical E-box motif (Rodriguez et al., 2008). A TBX3 peak was not called at this site in the 501mel ChIP dataset; however, TBX3 and MITF have three overlapping peaks within intron 2 of *CDH1* as well as a 4th peak is shared ~16 kb upstream of the promoter region (Figure 3C).

In summary, the MEME-ChIP analysis identified two binding motifs, the T-box and E-box elements, which constituted the vast majority of TBX3-bound input sequences (8,320/10,000; 83.20%). Within this set, E-box motifs occurred more frequently than T-box motifs (69.17% vs 45.92%, respectively) (Figure 3B). As mentioned previously, the E-box motif is the primary recognition sequence associated with MITF, a master melanocyte regulatory TF (Goding & Arnheiter, 2019). Therefore, I next wanted to interrogate the degree of shared genome-wide binding sites between TBX3 and MITF. To do this, I assessed the extent of common chromatin occupancy by intersecting the 20,449 TBX3 peaks, from our ChIP dataset, with 12,137 MITF peaks, from a previously published human MITF ChIP dataset in 501mel cells (Strub et al., 2011), to identify 4,758 common peaks. Importantly, both ChIP datasets were generated in the same cell line, 501mel, thus the overlap represents the greatest potential for biological significance as targets sites bound by both TBX3 and MITF are in melanocytes. I next used MEME-ChIP to query motif enrichment of the 4,758 common peaks. Interestingly, but perhaps not surprisingly, the top 10 sequences (JASPAR CORE vertebrates non-redundant v2), ranked by e-value, do not include any T-box related motifs but instead are all E-box related, except for 'USF1' (Figure 3D). However, the sequence TCAT**GTG**A, highlighted as a USF1 target contains the 3 bp 'GTG' core, and this sequence is recognized by

MITF, for example in the *TYR* enhancer, and USF1 is known to bind MITF recognition motifs (Louphrasitthiphol et al., 2020). Importantly, the top 9 motifs are centrally located within the TBX3 bound peaks consistent with TBX3 binding directly to these E-boxes (Figure 3E). The high frequency of centrally located E-box motifs bound independently by both TBX3 and MITF, suggests that TBX3 and MITF may regulate the same target genes. Furthermore, these two TFs may compete against each other to bind at the E-box of target genes, or they may bind cooperatively since MITF recognizes E-box elements in the major groove, whereas TBX3 binds T-box elements in the minor groove (Coll et al., 2002). However, it is yet undetermined as to whether TBX3 can bind E-boxes in the major groove.

Pigmentation Genes Regulated by MITF are also Bound by TBX3

Given the large overlap of E-box bound peaks, and the enrichment of pigmentation terms in the GREAT analysis, I hypothesized that TBX3 can bind at genomic loci of pigmentation genes which are regulated by MITF. To query this, I first used GREAT to screen a previously generated MITF ChIP dataset and elucidate candidate targets using the same analysis parameters as used for our TBX3 data (Strub et al., 2011) (Appendix B: Table S2). The GREAT analysis yielded a total of 7,096 genes associated with MITF binding. The two ChIP datasets were generated in human cells, whereas the MiGS is derived from mouse; therefore, I next identified the relevant mouse homologs for both the TBX3 and MITF target gene sets to allow for an easier comparison to the MiGS gene list (Appendix B: Table S3,S4). The list of mouse homologs, comprising TBX3 (6,499/7,109) and MITF (6,661/7,096) gene targets, were intersected to identify a shared set of 4,072 genes, that may be directly regulated by both TBX3 and MITF, representing 62.6%

of the TBX3 genome-wide target list (Figure 4A). Of these, 59 are MiGS (59/216; 27.3%) genes, thereby suggesting that these genes may be directly regulated by both TBX3 and MITF; furthermore, this proportion is slightly enriched (P=.04) relative to the entire genome wide portion of shared TBX3 and MITF targets (4,072 shared targets/18,778 annotated genes = 21.6% of genes genome wide) (Figure 4B). Importantly, my analysis revealed that TBX3 and MITF share binding sites at notable pigmentation genes, which include four genes, *IRF4*, *MC1R*, *OCA2*, and *TYRP1*, that have well-described cis-regulatory elements bound by MITF (Aoki & Moro, 2002; Gautron et al., 2020; Praetorius et al., 2013; Visser et al., 2012) (Figure 4C). Collectively, these data suggest that TBX3 can directly bind at E-box motifs targeted by MITF and that a set of these dual-targets are MiGS genes, thus indicating that they might be differentially regulated during melanin synthesis. Therefore, a potential regulatory role for TBX3 in melanogenesis may include modulation of MITF-mediated gene regulation either indirectly, by blocking MITF's ability to bind the E-box of target genes, for example, or directly, by actively repressing transcription of positively regulated MITF targets.

Transcriptional Regulation by TBX3 Includes Both Activation and Repression

ChIP-seq revealed extensive genome-wide binding of TBX3 with TBX3 peaks found at the cis-regulatory elements of 7,109 genes. Importantly, a subset of this total includes MiGS genes, which constitutes annotated genes implicated in melanogenesis. ChIP is useful for determining whether a given protein can bind specific regions DNA; however, it does not discern whether protein binding leads to

regulation of gene expression. Therefore, I sought additional experimental evidence to determine whether TBX3 can directly influence expression of these candidate genes, especially those within the MiGS. T-box TFs have been shown to activate and repress target genes; however, the Tbx2 subfamily members, TBX2 and TBX3, have traditionally been thought to function primarily as transcriptional repressors despite having an activator domain (Khan et al., 2019; Washkowitz et al., 2012). It is therefore unclear whether TBX3 acts to activate or repress specific candidate target genes within melanocytes. To address this uncertainty, I performed bulk RNA-seq in 501mel human melanoma cells, following transient reduction of TBX3, to (1) determine which putative target genes exhibit significant differential expression following loss of TBX3 and (2) determine whether TBX3 repressed or activated these targets, as indicated by positive or negative differential expression, respectively.

To do this, I first performed transient knockdown (KD) of *TBX3* in 501mels with two distinct small interfering RNAs (siRNA) (TBX3_13.6 and TBX3_13.8) and a non-targeting control. At the 24-hour time point I lysed the cells and harvested RNA from three independent replicates. For quality control, I confirmed KD by RT-qPCR and assessed RNA integrity using an Agilent TapeStation analysis prior to library synthesis and bulk RNA-seq. After sequencing, I performed differential expression analysis (siRNA vs non-targeting control) and identified significant DEGs ($padj < 0.05$) that were responsive to TBX3 depletion (Appendix B: Table S5). I next filtered out DEGs that exhibited contradictory directional FC as it is unlikely that these genes are biologically significant in this context. This yielded 1,420 positive FC genes (+FC) and 1,340 negative FC genes (-FC) (Figure 5A). I next wanted to identify the subset of these genes that were most likely to be directly regulated by

TBX3 binding. Therefore, I intersected the two DEG lists with my TBX3 ChIP-associated target genes to identify a total of 1,091 targets (623 +FC, 468 -FC). This list represents candidate genes which are bound and therefore likely directly regulated by TBX3 as they (1) show responsiveness to TBX3 depletion and (2) exhibit ChIP-seq identified peaks within cis-regulatory elements of those genes (Appendix B: Table S6).

MiGS and Cell Cycle Genes and Regulated by TBX3

With the B&R gene set identified, I next performed GSEA to identify significant KEGG terms (FDR < 0.05) associated with the +FC and -FC gene lists, with the top 20, as ranked by $-Log_{10}$ of the FDR, depicted in Figure 5B. Terms associated with the +FC list, or candidate genes of TBX3 mediated repression, include those related to TBX3's known role(s) in melanoma, such as, 'focal adhesion' and 'ECM receptor interaction', as well as, 'TGFβ signalling pathway', of which *TBX3* is a downstream target (Figure 5B, red). Importantly, 'melanogenesis' was one of the most significant enriched terms identified in the +FC list. In contrast, enriched terms for the -FC genes, or those which are candidates to be activated by TBX3, included those consistent with TBX3's pro-proliferative and anti-senescence functions, such as 'cell cycle', MAPK signalling pathway', and 'p53 signalling pathway' (Figure 5B, blue). More specifically, this includes cell cycle progression genes *CDK1* and *CDK2* (Appendix B: Table S6). Last, I wanted to assess the extent of MiGS targets which were specifically B&R in my *in vitro* assay. To do this, I first converted the candidate TBX3 B&R genes (1,091 +/- FC) to their known mouse homologs, yielding 1,041 genes. These were intersected with the MiGS to identify 23 candidate genes B&R by TBX3 in melanocytes (Figure 5C). Collectively, these

data highlight known functional roles of TBX3, such as anti-senescence, with an example being reduced expression of cell cycle progression genes, *CDK1* and *CDK2*, when TBX3 is diminished. Furthermore, these results suggest previously undescribed roles for TBX3, apart from potential modulation of MITF-mediated gene regulation, in the regulation of melanogenesis via transcriptional activation and/or repression of MiGS genes.

Comparison of TBX2/3 Bound and Regulated Genes in Melanoma Cells

As previously stated, the T-box family of TFs comprise five subfamilies, with TBX3 being a member of the TBX2 sub-group and TBX2 and TBX3 share 95% homology within the DNA binding domain (Washkowitz et al., 2012); therefore, it seems likely that TBX2/3 may B&R a large number of similar gene targets. The Goding group recently showed that TBX2, which canonically binds the T-box, can also bind the E-box motif in mouse melanoma cells (S. Lu et al., 2021). Additionally, they showed that TBX2 functions as an activator and repressor of transcription and that this function is largely dependent on which motif it binds to (S. Lu et al., 2021). Like that study, my data supports the idea that TBX3 binds to, and regulates gene expression via, the E-box motif. Given this, I asked whether TBX3 exhibits a similar pattern of activating E-box associated genes and repressing T-box associated genes. Using MEME-ChIP, I queried for motif enrichment on TBX3 peaks which were associated with B&R -FC and +FC gene lists, respectively. Interestingly, and unlike TBX2, the type of motif bound does not seem to influence the regulatory

action of TBX3 as both motifs are present in the activated and repressed gene lists (Figure 6A).

Given this finding, and the high extent of homology between TBX2 and TBX3, I was curious as to what extent these two TFs may B&R similar target genes in the melanocyte lineage. To address this question, I turned to TBX2 ChIP-seq and bulk RNA-seq datasets generated by Lu and colleagues in the B16-F10 mouse melanoma cell lines (S. Lu et al., 2021). Although they defined TBX2 B&R genes in their study, I decided to reperform the analysis using the same criteria as defined by our TBX3 datasets. Because the TBX2 ChIP study was done in mouse melanoma cells, while the TBX3 ChIP data was generated in human cells, I utilized the UCSC 'liftover' tool to map the mouse MACS2 called TBX2 binding peaks from 'clone 9' of Lu et al. to the human genome (hg38). I then intersected the two biological replicates to identify 2,150 shared peaks (Figure 7A) (Methods, clone 9, R1= 2,787, R2=6,677; 2150 shared).

With the total set of shared TBX2 peaks defined, I next wanted to determine to what extent these peaks associate with cis-regulatory elements of annotated genes. Therefore, I utilized GREAT to address this question by using the same analytical parameters as were used for the TBX3 only dataset. In total, GREAT found 1,705 peaks (1,705/2,150) located at cis-regulatory elements of 1,807 genes (Methods, Appendix B: Table S7). With this, I next wanted to define gene candidates which could be B&R by TBX2. To do this, I first determined the extent of significant differentially expressed genes, by bulk RNA-seq, in the siRNA mediated TBX2 KD dataset. To avoid any potential bias, I defined significant differentially expressed genes using the same threshold as used for the TBX3 dataset (padj < 0.05), which revealed a total of 4,286 DEGs (Appendix B: Table S8). So that all four datasets

could be easily compared, I converted this TBX2 gene set to their known human homologs, yielding 3,969 in total (3,969/4,286) (Appendix B: Table S9). With this, I determined the extent of TBX2 B&R genes by intersecting the ChIP associated genes, as defined by GREAT, and the significant DEGs, from the bulk RNA-seq experiment, giving a total of 586 genes (Figure 7B). The TBX2 B&R genes were then delineated by directional FC to define those which are repressed (+FC) or activated (-FC) by TBX2 (Appendix B: Table S10). With the total array of TBX2 and TBX3 B&R genes defined, I next queried to what extent these factors regulated the same gene targets. To do this, I intersected the respective B&R lists and found a total of 94 common genes, 63 of which have +FC and 31 with -FC in the TBX2 KD experiment, this representing 15.7% and 8.6% of all TBX2/3 B&R genes, respectively (Appendix B: Table S11). I then used the same intersection approach to determine what degree of the 94 TBX2/3 targets are (1) activated by both, have -FC (47/94), (2) repressed by both, have +FC (15/94), or (3) regulated in an opposing manner, +FC in one factor and -FC in the other (32/94) (Appendix B: Table S12). Collectively, the analysis suggests that TBX2 and TBX3 may share only a small subset of regulatory targets in melanocytes and that any dual-targets may not be consistently activated or repressed by each other. However, it is important to note that conclusions from this analysis may be limited given the difference in cell lines and species.

The previous analysis identified genes B&R by TBX2/3; however, it did not address whether or not regulation of these targets occurred at the same regulatory elements / DNA binding locations. To address this, I intersected TBX2/3 peaks which were associated with cis-regulatory elements, as defined by GREAT, which revealed 25 shared peaks which are associated with 25 genes. Therefore, of the 94

genes B&R by TBX2/3, only 25 are regulated at the same genomic elements with the majority (73%, 19/26) belonging to the ‘repressed by both’ group (Figure 7C). Given this majority, in conjunction with the known opposing action of TBX2 mediated gene expression based on DNA binding motif, I was curious if a bias existed in the DNA binding motif of these cis-regulatory elements. To address this question, I generated FASTA files from the TBX3 peaks summit files and then assessed them for motif enrichment. Using MEME-ChIP, I queried for motif enrichment of the 25 peaks and, interestingly, of the 5 motifs discovered, none were E- or T-boxes; however, motifs ‘2’ and ‘3’ contain the core 3bp nucleotide sequence ‘CAC/GTG’ of the E- and T-box (Figure 7D). In total, these data suggest, despite the significant homology that exists in their DNA binding domain, that the majority of genes B&R by TBX2/3 TFs are unique to each respective TF, at least in melanoma cells.

Discussion

In Chapter 3, I used scRNA-seq to identify the MiGS, a set of 216 genes showing significant differential expression in murine melanocytes with inhibited MC1R signalling. This gene signature contains 22 genes (22/216) which encode TF/co-TFs. Importantly, all 22 of these merit further scientific investigation; however, I initially selected one, *Tbx3*, for immediate follow-up studies. I choose to work on *Tbx3*/TBX3 for several reasons including the fact that it is a melanocyte signature gene, as defined by Rezza and colleagues, and is expressed normally in melanocytes; however, little to no work has investigated a functional role for TBX3 in melanocytes (Hair-GEL.net; (Rezza et al., 2016). Relatedly, it is often overexpressed in cancerous melanocytes, in the form of melanoma, where its

function is well-described in tumour growth and invasion whereby it promotes proliferation and EMT (Boyd et al., 2013; Dong et al., 2018; Peres et al., 2010, 2021; Peres & Prince, 2013; Rodriguez et al., 2008). In this chapter, we used ChIP-seq to define the genomic occupancy of TBX3 in human melanoma cells. Furthermore, I identified candidate genes which are most likely B&R by TBX3, including MiGS genes, and I show that TBX3 may mediate gene expression through both activation and repression of transcription. TBX2/3 are both members of the same T-box subfamily, sharing 95% sequence homology in their DNA binding sequence, and they are both expressed in melanocytes and melanoma (Hair-GEL.net; Graeber Lab, 2015). TBX2 has been shown to regulate transcription primarily at two DNA binding motifs in, the T- and E-box, in melanoma cells (S. Lu et al., 2021). Consistent with TBX2, I found that DNA binding by TBX3 occurs not only at the T-box motif, but also includes prominent binding of the canonical 'CACGTG' E-box, which is the main recognition sequence of the melanocyte master regulatory TF MITF. Despite these similarities, my data suggests, at least in melanoma cells, that these two TFs exhibit few shared binding sites across the genome and may therefore regulate their own unique gene targets.

The differential expression of *Tbx3* between wildtype and RHC / MC1R-inhibited melanocytes, along with genome-wide binding of TBX3 to T- and E-box elements in melanoma cells, suggested that TBX3 can regulate gene expression of MiGS genes. Given the binding of TBX3 at E-boxes, this regulation could include MITF-dependent target genes. Using a multi-omics approach, which included ChIP-seq and bulk RNA-seq, I identified a set of genes which are most likely B&R by TBX3 in the human 501mel melanoma cell line, including a subset of MiGS genes. Traditionally, the literature has classified the primary role of TBX3 as transcriptional

repression; however, at least one study has shown its ability to induce transcription of putative target genes (J. Lu et al., 2010). Supporting this notion, my data strongly suggests that TBX3 can both activate and/or repress putative target genes, including MiGS candidates which have known associations with melanogenesis and pigmentation phenotypes. One such intriguing target of TBX3 mediated activation is *Slc7a11*. This gene encodes the cystine/glutamate exchanger (xCT / SLC7A11), an antiporter, which imports cystine in exchange for glutamate at a 1:1 ratio (Chintala et al., 2005). Once inside the cell, cystine is reduced and proceeds to form two molecules of cysteine, a necessary component of phaeomelanin synthesis (Chintala et al., 2005; Fernandes et al., 2023; Hida et al., 2020; Hoekstra, 2006). An influx of intracellular cysteine in melanocytes creates a favourable environment for phaeomelanin synthesis; therefore, TBX3-mediated activation of *Slc7a11* / SLC7A11 represents the possibility of active promotion of phaeomelanin synthesis. Furthermore, this suggests that phaeomelanin synthesis might not inherently be a by-product of MITF inhibition or loss but rather, through promotion of gene expression, this process might be much more active than previously appreciated.

Beyond phaeomelanin, cysteine plays important roles in melanocytes by regulating oxidative stress response and inhibiting ferroptosis as it is an essential component of the glutathione system (Chintala et al., 2005; Poltorack & Dixon, 2022; Swanda et al., 2023; Wu et al., 2022). These functions are exemplified in my study; for example, following siRNA mediated KD of *TBX3* I observed a significant reduction of *SLC7A11* and associated enrichment, by GSEA, of pathways associated with ‘glutathione metabolism’ and ‘apoptosis’. This action, when comparing TBX2 and TBX3, is unique to TBX3, as TBX2 does not bind cis-regulatory elements found near *Slc7a11* nor is it differentially expressed after KD of

TBX2 in B16-F10 melanoma cells (Appendix B: Table S8, S9). The production of phaeomelanin by melanocytes is a somewhat perplexing phenomenon of evolutionary conservation given its association with cellular toxicity and oncogenic transformation (Mitra et al., 2012; Napolitano et al., 2014). What is clear, is that proper regulation of cysteine levels within melanocytes is critical and presents a paradox whereby too little cysteine inhibits appropriate function of the glutathione system, and thus promotes oxidative stress, yet too much, perhaps by means of overaccumulation of phaeomelanin, can exacerbate cell stress and disrupt cellular homeostasis.

TBX3 participates in senescence by-pass through, in part, repressing cell cycle checkpoint genes, such as *CDKN2B* (Khan et al., 2019). My *in vitro* study, with siRNA mediated KD of TBX3 in 501mel cells, further supports this as *CDKN2B* exhibits significantly higher levels of expression in the KD groups, as compared to the control (Appendix B: Table S6). In conjunction with this finding, my data further supports a role for TBX3 in senescence by-pass through activation of cell cycle progression genes. For example, *CDK1* and *CDK2* have TBX3 ChIP peaks at known cis-regulatory elements and exhibit diminished levels of expression in the TBX3 KD conditions (Appendix B: Table S6). A previous study, by Willmer and colleagues showed that TBX3 is a significant mediator of cell cycle progression, more specifically in S-phase transition, whereby TBX3 action is altered by post-translational modifications through phosphorylation via CDK2 (Willmer et al., 2015). In fact, more recent work from this group has revealed a more complex feedback relationship whereby TBX3 itself promotes the expression of *CDK2* (Damerell et al., 2022). In total, this data provides further support for this model and, importantly, reveals the context as to how TBX3 may contribute to oncogenic transformation and

facilitate senescence by-pass. These observations provide potential mechanistic insights into why diminished MC1R function, and the RHC phenotype, is associated with increased predisposition for melanoma.

As stated previously, T-box family members comprise five distinct sub-groups, with TBX2/3 both being members of the Tbx2 subfamily. *TBX2/3* derive from a common ancestral gene, consequently they share 95% sequence homology within their DNA binding domains (Washkowitz et al., 2012). The Goding lab recently showed that TBX2, which is most strongly associated with DNA binding at the T-box element, can also bind the E-box motif; furthermore, they demonstrated that TBX2 can function in both the activation and repression of gene expression (S. Lu et al., 2021). The data from this study strongly suggests that TBX3 can (1) bind the E-box motif of target genes and (2) promote or inhibit their expression. However, unlike TBX2, the type of motif bound does not seem to influence the function of TBX3. The role of TBX2, as either an activator or repressor, appears to be highly influenced by the motif to which it is bound to whereby the E-box promotes, and the T-box inhibits, gene expression (S. Lu et al., 2021). Interestingly, this observation was not found for TBX3 (Figure 6A). This would suggest that the DNA binding motif is not a primary component driving the functional action of TBX3.

The ability of TBX2/3 to recognize the E-box site might be explained by historical protein structural studies. As mentioned previously, the canonical E- and T-box elements share a 3 bp ‘GTG’ region which corresponds to bps 3-5 of the T-box element (AG**GTG**TGA). Importantly, this 3 bp ‘GTG’ core is considered the most significant component for DNA recognition, and binding, by TBX3 whereas the flanking base pairs play a much less influential role (Coll et al., 2002). TBX2/3 can bind DNA in a monomeric fashion; furthermore, TBX3 can bind as a monomer in

either the major or minor groove (Coll et al., 2002). Therefore, while bound in the minor grove, it is possible that the function of TBX3, and most likely TBX2, could be influenced by other TFs bound in the major grove, such as MITF itself.

The degree to which TBX2/3 modulate gene expression is most likely dependent on several factors, including, but not limited to, cell type, differentiation state, co-factor availability, chromatin accessibility, and biological state, such as post-translational modifications (e.g., methylated, acetylated). Collectively, these factors might explain why putative TBX3 genes targets, which are B&R *in vitro* in human melanoma cells, are not necessarily present (i.e., differentially expressed) in the MiGS which derives from *in vivo*, non-cancerous, murine melanocytes. This idea can also be applied to the identification of shared genes B&R by both TBX2/3. Commonalities do exist, for example, all bulk RNA-seq and ChIP-seq datasets were generated *in vitro* from melanoma (501mel and B16-F10) cell lines, but these are where the similarities stop. Although both cell lines are melanomas, the driving mutations, and subsequent burden of other somatic mutations are by no means the same. Likewise, a clear difference exists phenotypically in culture between these two. B16-F10s produce copious amounts of melanin which results in a change in the colour of the media to a dark black. In contrast, 501mels may produce melanin but not at the same extent as B16-F10s as evidenced by no change to the media colour. Likewise, differences in differentiation state, co-factor availability, chromatin accessibility, and biological state are not characterized or known. Of significance, the TBX2 data is derived from mouse cells whereas the TBX3 data was generated in human cells. Though these two species share substantial homology, and liftover to other genomic builds is possible, comparison of these datasets is not ideal. Lastly, there are 10x as many significant called peaks in the TBX3 dataset as compared to

the TBX2. The reasoning for this, whether technical or biological, is not readily apparent. It is therefore possible that many biologically relevant binding sites of TBX2 were not identified. However, it is equally possible that TBX2/3 do in fact share few genomic targets. For example, the binding could be highly dependent on the availability of specific co-factors which may not be present in one cell line or the other. Therefore, any future studies investigating this question should carefully consider these numerous complexities during experimental design and data interpretation.

In summary, I used ChIP-seq to explore the genomic occupancy of TBX3, a T-box TF family member, which exhibits pronounced expression in RHC melanocytes and is a known mediator of melanoma progression. I also showed that TBX3 can not only bind, but also most likely regulate expression of, a subset of MiGS genes, including those with well-described roles in pigmentation. Furthermore, my studies support the known literature regarding TBX3's role in senescence by-pass and proliferation. In conclusion, I propose that increased expression of *Tbx3*/*TBX3*/TBX3, and consequent suppression of senescence, in melanocytes lacking functional MC1R, and prior to the acquisition of activating mutations in pro-oncogenes, such as BRAF or NRAS, is a potential mechanism which could explain why people with the RHC phenotype have high a predisposition to melanoma. Further studies will be needed to confirm this potential mechanism. Relatedly, future experiments have been designed to address this hypothesis and are discussed in detail in Chapter 5 (pgs. 165 - 174).

Figures

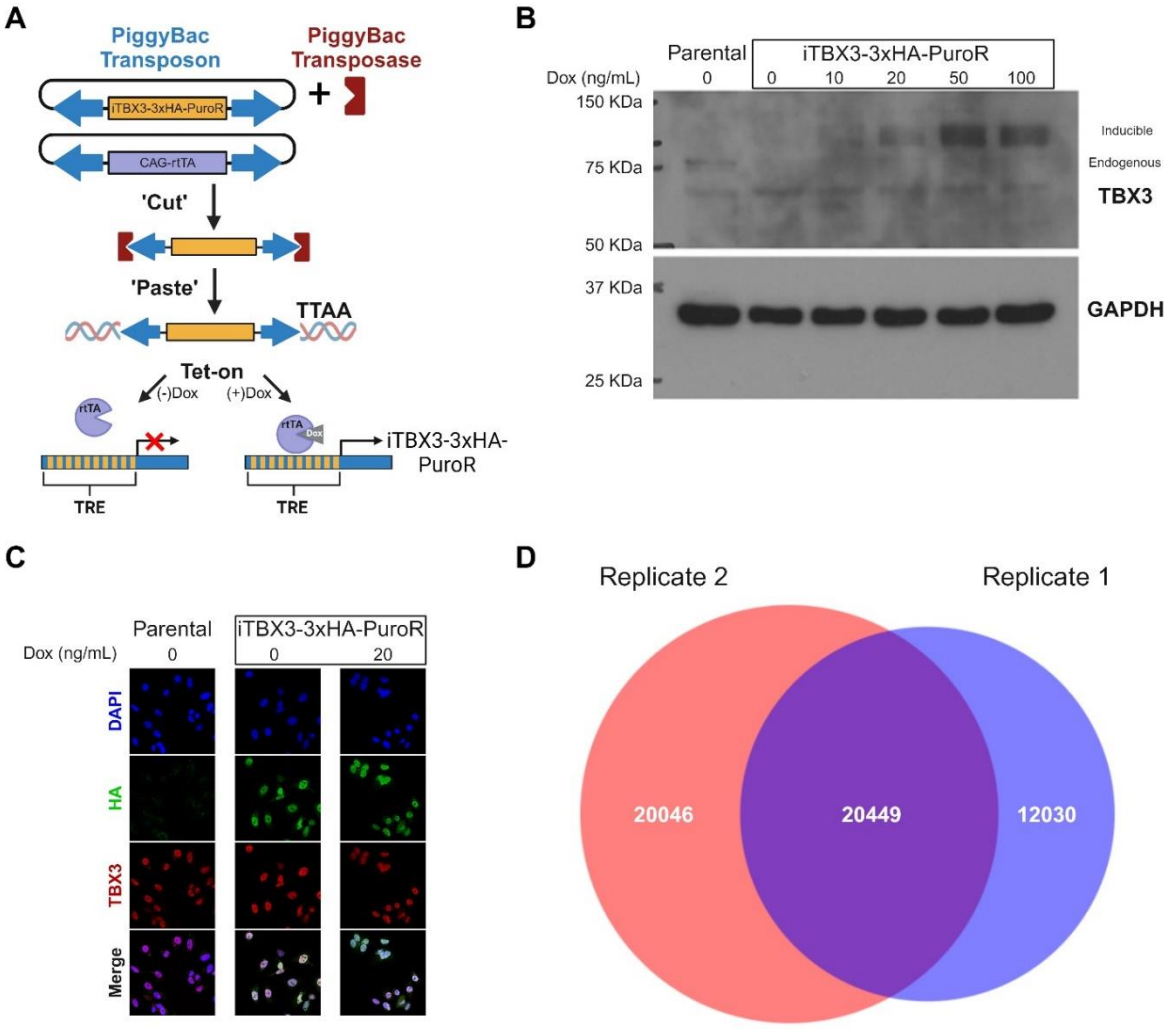


Figure 1. Validation of the Inducible TBX3 Cell Line. (A) Schematic of piggyBac transposase system with integration of CAG-rtTA and Tet-on inducible TBX3. Dox, doxycycline; TRE, tetracycline response element; rtTA, reverse tetracycline-controlled transactivator. (B) Western blot with dose titration of doxycycline in the polyclonal 501mel-iTBX3-3xHA-PuroR inducible and parental 501mel cells. Each condition was collected 24 h after treatment. (C) Immunofluorescence staining depicting expression and nuclear localization of HA and TBX3 in monolayers of polyclonal 501mel-iTBX3-3xHA-PuroR inducible and parental 501mel cells. (D)

Venn diagram depicting the shared peak intersection from both ChIP biological replicates.

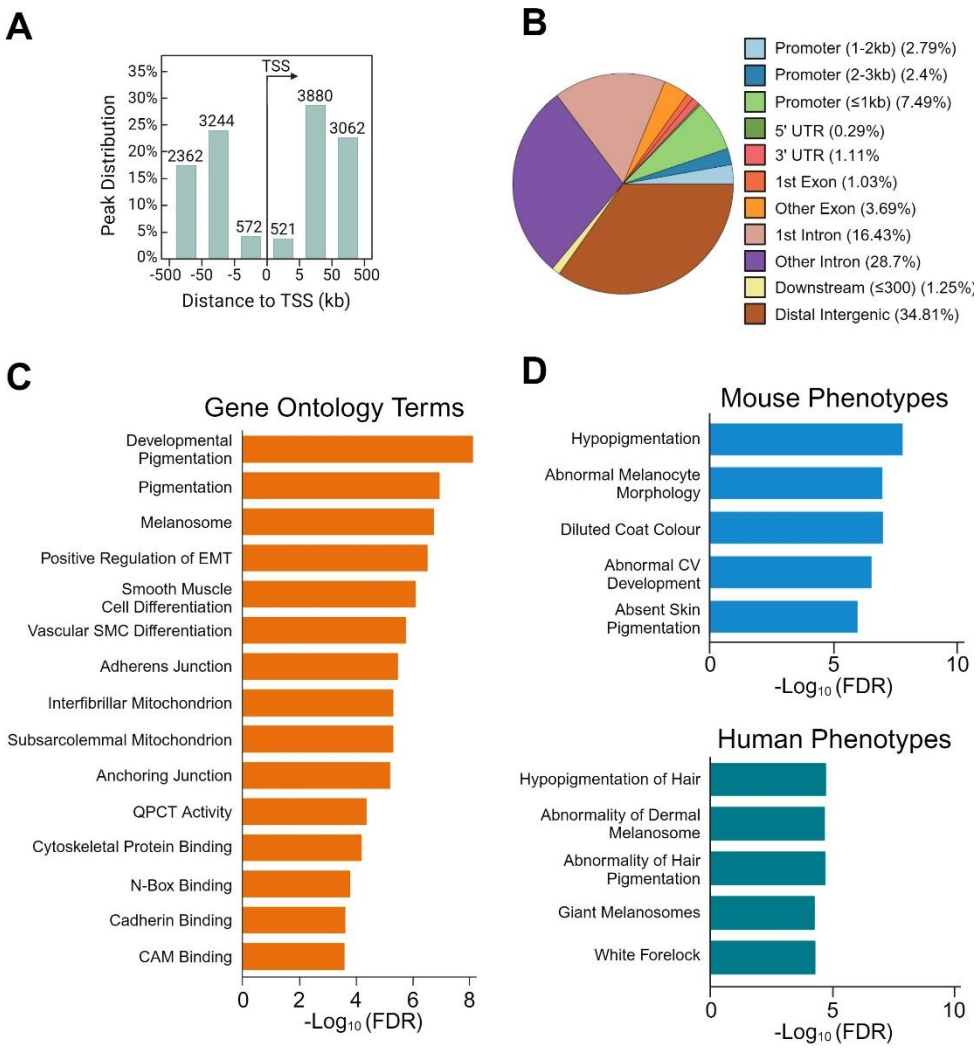


Figure 2. Chromatin Binding Analysis Implicates TBX3 as a Regulator of Melanogenesis. (A) Position and number of called TBX3 peaks relative to the TSS of genes across the entire genome. (B) ChIPseeker plot identifying the percentage of TBX3 bound peaks by genomic regions. (C) Top 15 GO enrichment terms associated with TBX3 ChIP target genes ranked by -Log_{10} of the FDR. (D) Top 5 predicted phenotype associations (human and mouse) from TBX3 bound genes which are ranked by -Log_{10} of the FDR.

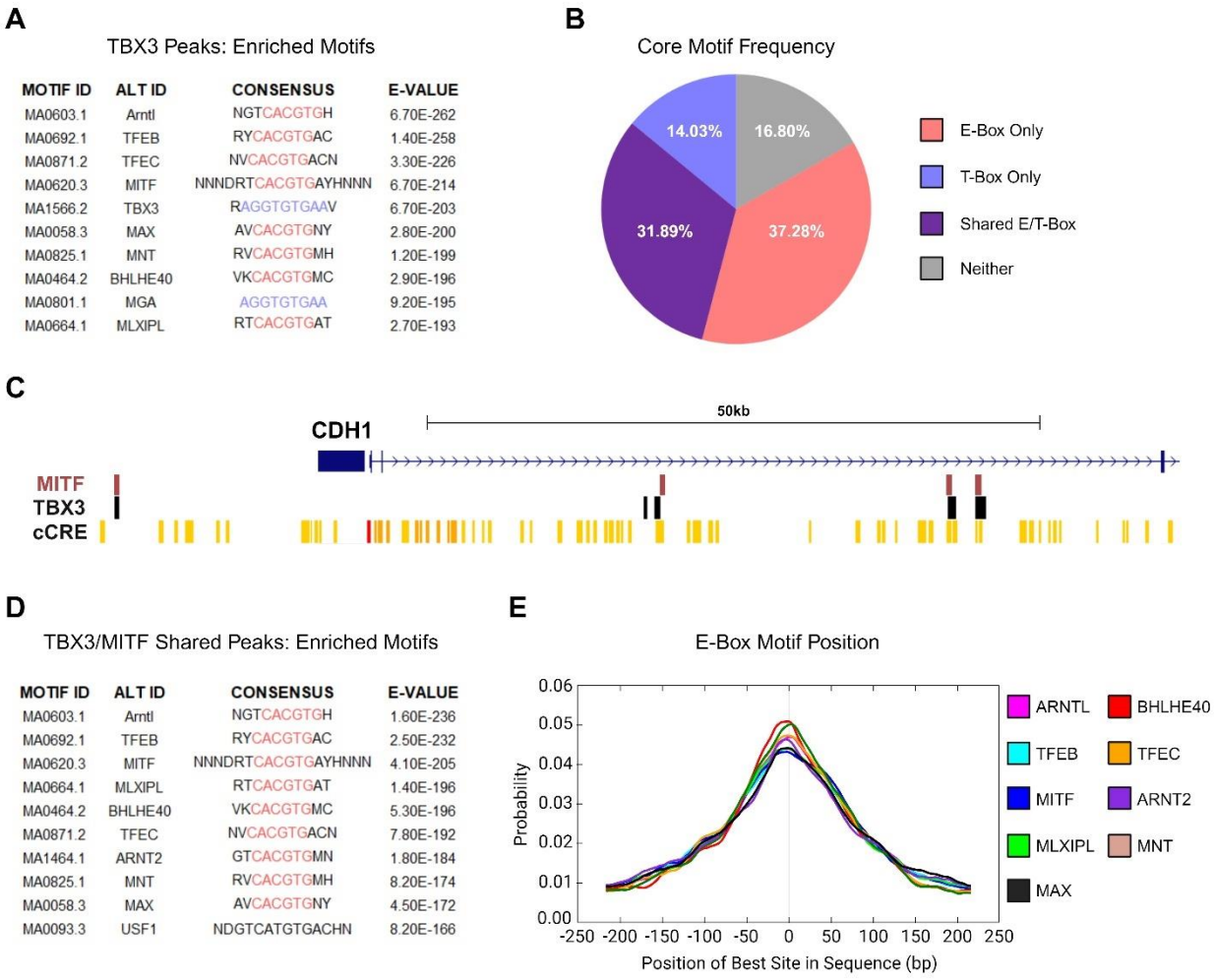


Figure 3. TBX3 Exhibits Enriched Binding at E-box Motifs. (A) The top 10 motifs enriched within TBX3 ChIP peaks which exhibit an over-representation of core E-box (red) and T-box (purple) sequences. (B) Pie chart depicting that the majority of TBX3 ChIP peaks contain either a T-box motif (14%), an E-box motif (27%), or both (32%). (C) UCSC browser track screen shot of TBX3 and MITF ChIP peaks associated with *CDH1*. Browser tracks are as follows: TBX3 = replicated binding sites in our dataset; MITF = ChIP peaks from Strub et al; cCRE = ENCODE annotated candidate cis-regulatory elements. (D) Top 10 motif sequences of shared MITF and TBX3 peak sites (E-box = red; T-box = purple). (D) CentriMo plot depicting central binding around the top 9 bound motifs.

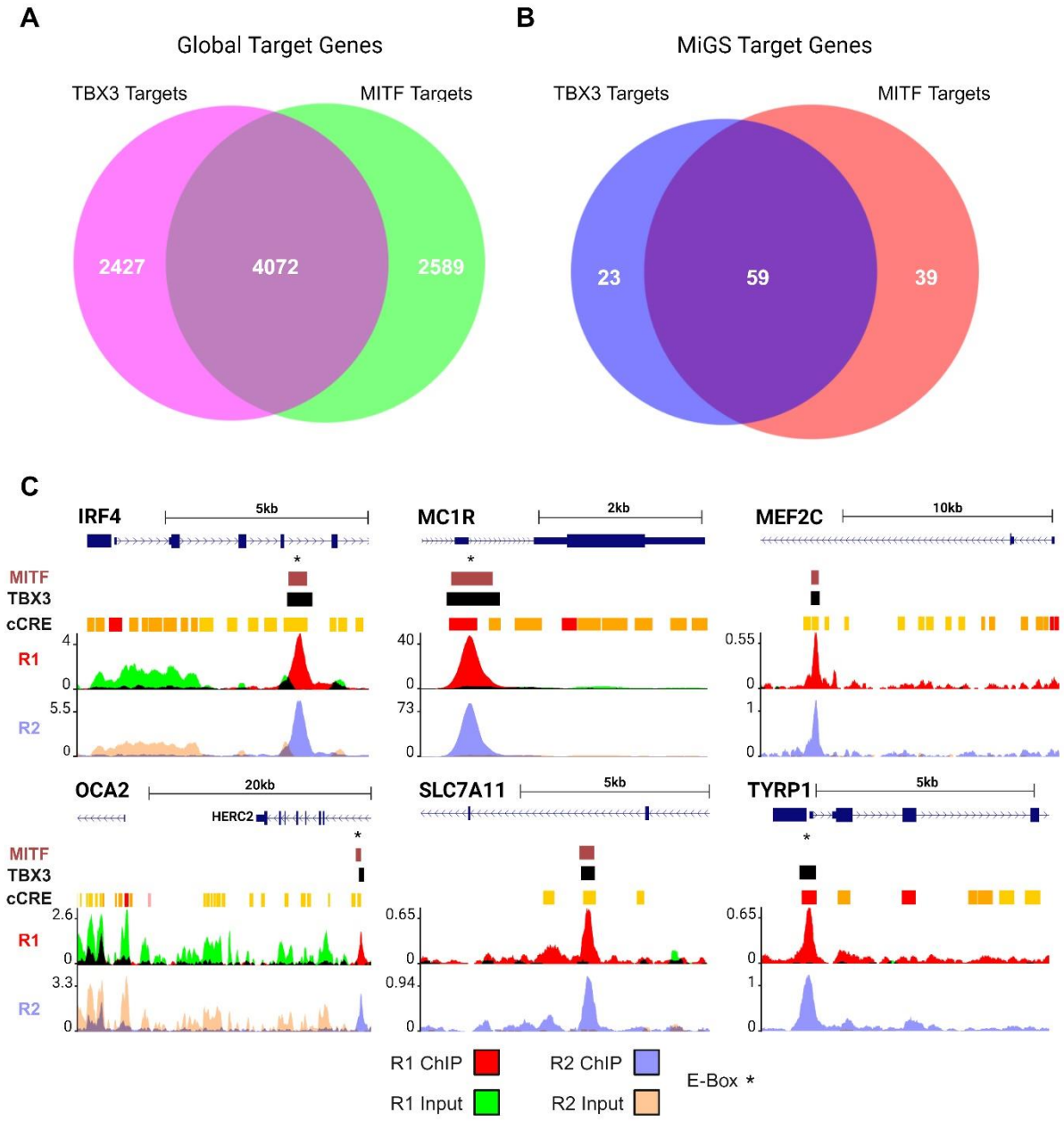


Figure 4. TBX3 Binds E-boxes of Pigmentation Genes Regulated by MITF. (A) Venn diagram depicting the intersection and number of murine genes (4072) associated with TBX3 and MITF ChIP peaks. (B) Intersection of MiGS genes which were identified as targets for both TBX3 and MITF. (C) UCSC browser view screen captures of TBX3 and MITF ChIP peaks which are associated with prominent pigmentation genes. Browser tracks are as follows: TBX3 = replicated binding sites in my dataset; MITF = ChIP peaks from Strub et al, 2011; cCRE = ENCODE

annotated candidate cis-regulatory elements. The location of verified MITF regulatory elements containing E-box motifs are indicated (*) (references in text).

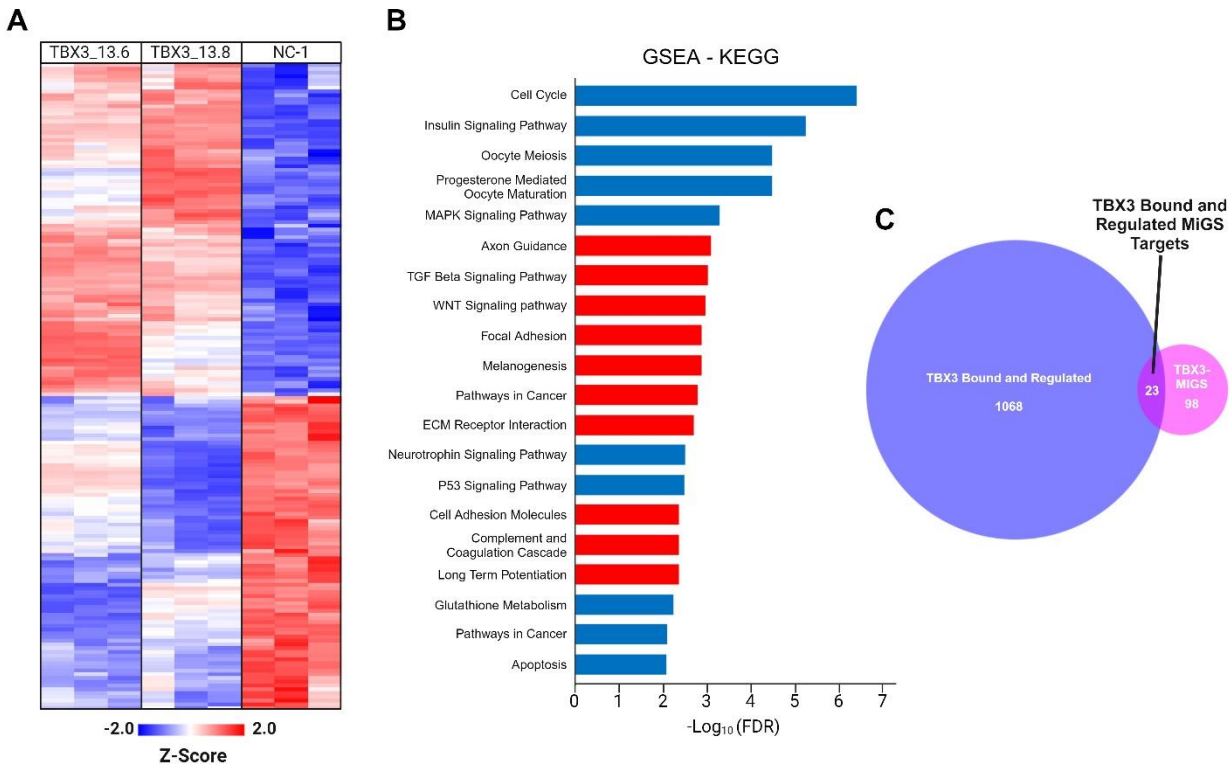


Figure 5. TBX3 Binds and Regulates MiGS genes. (A) Heatmap depicting relative gene expression of 2,760 DEGs (Adjusted p-value < 0.05) from the TBX3 knockdown (TBX3_13.6, TBX3_13.8) samples against a non-targeting control (NC-1). (B) Top KEGG terms ranked by -Log10 of the p-value for significant +FC (blue) and -FC (red) genes. (C) Intersection of differentially expressed TBX3 gene targets against MiGS TBX3 targets.

A

Motif Enrichment: Positive Fold Change

MOTIF ID	ALT ID	CONSENSUS	E-VALUE
MA0603.1	Arntl	NGTCACGTGH	8.90E-37
MA0801.1	MGA	AGGTGTGAA	4.40E-33
MA0871.2	TFEC	NVCACGTGACN	1.40E-31
MA1566.2	TBX3	RAGGTGTGAAV	1.20E-30
MA0800.1	EOMES	RAGGTGTGAAAWN	8.30E-30
MA0692.1	TFEB	RYCACGTGAC	1.10E-29
MA1464.1	TBX4	AGGTGTGA	1.20E-28
MA0825.1	TBR1	AGGTGTGAAA	9.50E-28
MA0058.3	TBX2	DAGGTGTGAAA	1.50E-27
MA0093.3	TFE3	GTCACGTGAC	2.80E-27

Motif Enrichment: Negative Fold Change

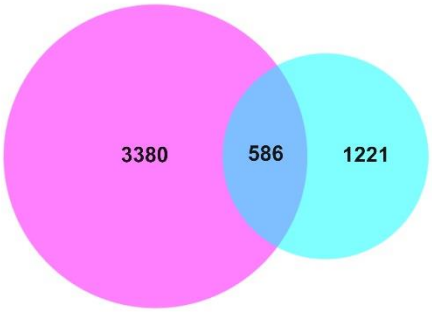
MOTIF ID	ALT ID	CONSENSUS	E-VALUE
MA0603.1	Arntl	NGTCACGTGH	2.90E-25
MA01464.1	ARNT2	GTCACGTGMN	3.40E-20
MA0692.1	TFEB	RYCACGTGAC	5.50E-20
MA01099.2	HES1	GGCRCGTGBC	6.00E-20
MA0058.3	TBX2	DAGGTGTGAAA	1.50E-19
MA0464.2	BHLHE40	VKCACGTGMC	2.30E-19
MA1566.2	TBX3	RAGGTGTGAAV	3.10E-19
MA0871.2	TFEC	NVCACGTGACN	1.20E-18
MA0825.1	MNT	RVCACGTGMH	5.30E-18
MA1464.1	TBX4	AGGTGTGA	6.70E-18

Figure 6. Motif enrichment by fold change direction in TBX3 KD studies. (A) Top 10 motifs, ranked by e-value, of TBX3 ChIP peaks associated with putative target genes with increased expression (left) or decreased expression (right) upon TBX3 knockdown.

A



B



C

Repressed by both TBX2/3		Repressed by TBX2 / Activated by TBX3	Activated by both TBX2/3	Activated by TBX2 / Repressed by TBX3
+FC in both KD experiments		TBX2 +FC and TBX3 -FC	Both -FC	TBX2 -FC and TBX3 +FC
MMP15	CITED2	PPARGC1A	RRM1	RDX
TLE1	DLC1	TANC1	PIK3R3	
CADM1	CHSY3	SASH1		
MEGF10	LRP6			
FZD2	ROCK2			
NFIX	EYA1			
GRIK2	EEF1A1			
PHLDA3	MBNL2			
PDZRN3	YAP1			
SOX5				

D

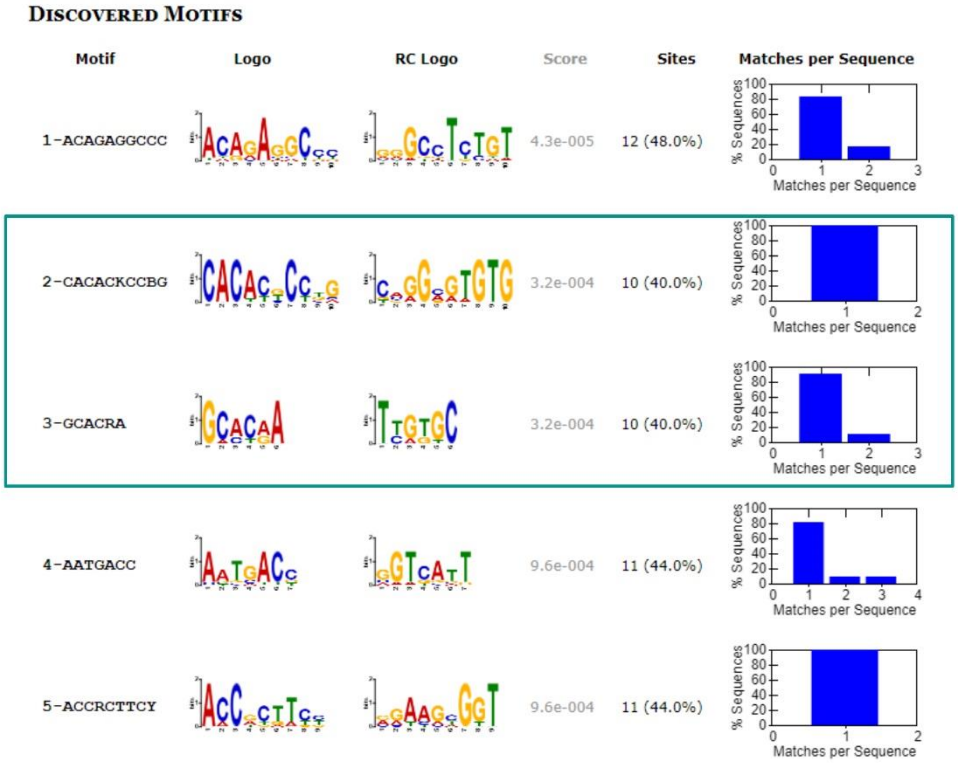


Figure 7. TBX2 and TBX3 Rarely Target the Same Cis-Regulatory Elements.

(A) Venn diagram depicting the shared peak intersection from both TBX2 ChIP

biological replicates. (B) Intersection defining TBX2 B&R genes by contrasting significant DEGs from the TBX2 KD against the TBX2 ChIP gene targets. (C) List of genes which are B&R at the same cis-regulatory elements by TBX2/3 with the respective functional consequence (i.e., activated or repressed) for each TF. (D) Top 5 motifs, ranked by e-value, of TBX2/3 peaks associated with the same cis-regulatory elements. The green box highlights motifs containing the core CAC/GTG sequence.

Chapter 5: Discussion

Summary of Major Findings

A major aim of this thesis was to use scRNA-seq to profile the transcriptomes of *in vivo*-derived murine melanocytes which produced eumelanin, had active MC1R signalling, versus those which produced phaeomelanin, had inactive MC1R signaling and concomitantly modelled the human RHC trait (Figure 1, Chapter 3: Figures 1-5). Once these transcriptomes were identified, I performed differential expression analyses between the eumelanin and phaeomelanin producing melanocytes and found that the two RHC model mice (lethal yellow, A^{y}/a; and recessive yellow, $Mc1r^{e}/^{e}$) shared 216 differentially expressed genes which I defined as the 'MC1R-inhibited Gene Signature' (MiGS). This set included genes with both known (~5%) and novel (~95%) associations with melanogenesis (Figure 1, Chapter 3: Figure 6, Appendix A: Table S4). Given this, I next used a series of bioinformatic techniques to investigate the biological significance of this gene signature. GO and IPA analyses revealed enrichment of several terms which collectively centred on three principal biological themes: 'morphogenesis', 'neurogenesis / neurotransmitter regulation', and 'melanogenesis' itself. Several genes were found to populate multiple terms related to morphogenesis; however, only one gene, *Tbx3*, was present in all terms of this theme (Chapter 3: Figure 7).

MC1R is considered a master regulator of pigment switching (Walker & Gunn, 2010). Surprisingly, bioinformatic based interrogation of the MiGS did not yield enrichment for terms commonly associated with the MC1R signalling pathway (Chapter 3: Figure 7). Relatedly, the transcriptomic results revealed that *Mitf*, which encodes for a melanocyte master regulatory TF, and is a downstream target of MC1R signalling (Goding & Arnheiter, 2019; Levy et al., 2006), was not differentially expressed between eumelanotic and phaeomelanotic melanocytes. This came as

a surprise given previous work which supports the notion that these two factors are major forces governing pigment-type switching (Walker & Gunn, 2010). Therefore, I wanted to identify what other signalling pathways and/or factors could be contributing to the pigmentation phenotype as well as differential expression of MiGS genes. To address this, I first turned to IPA to predict enrichment of possible upstream molecular regulators driving MiGS expression. From this query, I identified several factors predicted to be actively involved, including several related to the TGFβ signalling pathway (Chapter 3: Figure 8). Therefore, I hypothesized that the observed differential expression of MiGS genes is highly likely to be driven by TGFβ signalling *in vivo*.

TFs are key regulators of gene expression and mainly exert their actions once bound to cis-regulatory elements of a given gene, such as a promoter (Mitsis et al., 2020). Given the lack of differential expression in *Mitf*, as well as several other prominent melanocytes associated TF genes (e.g., *Sox10*), I explored the possibility that other differentially expressed TFs within MiGS were largely responsible for driving the observed differential expression of the genes within this signature and reasoned that the most likely candidates would be those which were under the influence of TGFβ signalling. To do this, I identified 22 genes encoding for TF/co-TFs in the MiGS and, following an extensive literature review, delineated them into known or novel regulators of melanocyte biology (Chapter 3: Figure 9-11). When combining the bioinformatic analyses and literature review findings I identified *Tbx3* as a prime candidate for MiGS regulation. I chose this factor for follow-up studies as it is downstream of TGFβ, has been implicated in pigmentation, and is often found to be highly expressed in melanoma where it functions in advancing the

disease state (Figure 1) (L. Andersson, 2020; Imsland et al., 2016; Khan et al., 2019; J. Li et al., 2013; Peres et al., 2010; Rodriguez et al., 2008; Wagstaff et al., 2022).

With the primary objective of profiling eumelanotic and phaeomelanotic melanocytes complete, I next set out to interrogate a possible functional role for TBX3, a MiGS-identified factor, in the regulation of melanogenesis and melanomagenesis. TBX3, a T-box TF, regulates gene expression by binding DNA at T-box motifs of cis-regulatory elements of target genes (Khan et al., 2019). To my knowledge, in the context of melanocytes, global DNA binding studies of TBX3 have never been reported. Therefore, I used ChIP-seq data to assess chromatin occupancy of TBX3 in a melanocyte specific context (Chapter 4: Figure 1). These experiments revealed two important and previously unknown findings, namely that (1) TBX3 binds the cis-regulatory elements of several genes which are implicated in melanogenesis and pigmentation phenotypes and (2) this binding primarily occurs at two DNA binding motifs, the T-box and the CACGTG-type E-box (Figure 1, Chapter 4: Figures 2-3). Crucially, the E-box is the main recognition sequence of MITF, which is considered a master regulatory TF of melanocyte biology and melanogenesis (Goding & Arnheiter, 2019; Levy et al., 2006). Given this, it stood to reason that TBX3 and MITF might regulate several similar target genes, including those implicated melanin synthesis. Therefore, I queried to what extent, if any, MITF and TBX3 shared gene targets and found that 62.6% of TBX3 bound genes are also bound by MITF (Chapter 4: Figure 4). Among these, 59 are also MiGS genes (59/216), encompassing a subset of prominent pigmentation genes that are bound by both MITF and TBX3 at E-boxes of the associated cis-regulatory elements. (Chapter 4: Figure 4).

Our ChIP-seq study revealed important findings related to TBX3's ability to bind specific target genes; however, this technique did not disclose whether TBX3 could directly regulate the expression of these associated genes. Therefore, to test the question of whether TBX3 could directly B&R ChIP identified gene targets I turned to bulk RNA-seq, in conjunction with siRNA mediated KD of TBX3, to identify differentially expressed genes which were responsive, either directly or indirectly, to reduction of TBX3 (Chapter 4: Figure 5). By intersecting the ChIP target genes with the differentially expressed genes identified by bulk RNA-seq, I found 1,091 (1,091/2,060) candidates for direct binding and subsequent expression regulation by TBX3 (Figure 1; Appendix B: Table S6).

Previous studies suggest that the main functional role TBX3 is in transcriptional repression (J. Lu et al., 2010); however, my data strongly suggests that TBX3 mediates both repression and activation of target genes. Likewise, several groups have determined significant functional roles for TBX3 in promoting cellular proliferation and inhibiting senescence (Bennett & Medrano, 2002; Ha et al., 2008; Khan et al., 2019; Lingbeek et al., 2002; Peres et al., 2010; Vredeveld et al., 2012; Wagstaff et al., 2022). Using the TBX3 B&R gene list, I performed GSEA and found enrichment of several terms which are consistent with these previously described functions (Figure 1, Chapter 4: Figure 5). Likewise, GSEA revealed increased expression of genes which are known to promote eumelanogenesis. This data supports the hypothesis that TBX3 is a novel regulator of melanogenesis and that it does this through suppression of eumelanogenesis and promotion of phaeomelanogenesis. In agreement with this assertion, my experiments and analysis show that TBX3 can B&R a subset of MiGS genes, including those which promote phaeomelanogenesis, such as *Slc7a11* whose protein product promotes

the import of cystine, a necessary component of phaeomelanin and a key mediator of the glutathione system and ferroptosis (Chintala et al., 2005; Poltorack & Dixon, 2022; Swanda et al., 2023; Wu et al., 2022) (Figure 1).

The final experimental efforts in this thesis examined the relationship of TBX2 and TBX3 mediated gene expression regulation in melanoma cells. As stated previously, TBX2/3 are paralog family members of the Tbx2 sub-family and share 95% amino acid sequence identify in their DNA binding domain (Washkowitz et al., 2012). The Goding lab recently demonstrated that TBX2 controls a pro-proliferative gene expression program in melanoma through activation, when bound to the E-box, and repression, when bound to the T-box, of target genes (S. Lu et al., 2021). The work in this thesis showed that TBX3, akin to TBX2, can bind T-box and E-box elements at cis-regulatory regions of target genes. Given this, I investigated whether TBX3, like TBX2, modulated target gene regulation in a motif dependent fashion. Findings from my bioinformatic analyses suggested that the motif type, at least in 501mel cells, is not a determinant in dictating the function of TBX3. Albeit, the data does trend in a manner which might suggest that motifs associated with TBX3 activated targets are indeed related to the T-box (6/10) while the majority of repressed targets contain E-box motifs (6/10) (Chapter 4: Figure 6). Future functional experiments could definitively address this question.

Given the high degree of homology which exists in the DNA binding domain of TBX2/3, coupled with their known associations in melanocyte biology, including melanoma, I was curious to what extent these two TFs B&R the same target genes. Using previously published TBX2 datasets, I first identified 586 genes which can be B&R by TBX2 (Chapter 4: Figure 7). Comparing this with my TBX3 data, I determined that 94 of these are also B&R by TBX3, wherein 47 are activated by

both, 15 are repressed by both, and 32 are regulated in an opposing manner (i.e., activated by one factor and repressed by the other) (Appendix B: Table S12). However, of these 94 genes, only 25 had ChIP binding peaks at the same cis-regulatory element for that given gene. Interestingly, each motif associated with those peaks shared the same 3 bp core (CAC/GTG), which represents the same 3 bps considered most critical for DNA binding of TBX3 (Coll et al., 2002) (Chapter 4: Figure 7). Therefore, my analysis suggests that TBX2/3 predominately B&R their own unique sets of target genes in melanoma; however, future work is needed to resolve several outstanding questions.

In total, the work presented in this thesis reveals several findings which apply to a broad array of scientific disciplines and will be of great interest to pigment cell biologists. The RHC trait, which is due to LOF coding variants in *MC1R*, consists of high phaeomelanin production, freckling, inability to tan, and is thought be an evolutionary colour adaption to allow for sufficient Vitamin D production of human populations in extreme latitudes; however, a significant tradeoff in this evolutionary trait is that people with RHC, by not fully understood mechanisms, are far more likely to develop melanoma as compared to the non-RHC population (D. Duffy, 2019). Thus, my model, which utilized a multi-omics approach, including scRNA-seq, bulk RNA-seq, and ChIP-seq, extends beyond transcriptomic differences of differential pigment producing melanocytes and critically provides a foundation for elucidating key mechanisms which regulate melanogenesis and melanoma predisposition in those possessing the RHC trait. The MiGS provides a springboard for further genetic studies which interrogate the regulation of melanogenesis and melanomagenesis. Relatedly, this work provides an insight into the transcriptional regulation of cellular pathways underlying melanoma risk, including the regulation

of oxidative stress, metabolism, and TGFβ signalling, and thus has broad relevance beyond pigment cells for cell and developmental biology, functional biochemistry, oncology, as well as evolutionary biology, as pigmentation genetics is often found to be highly conserved across vertebrates.

Proposed Mechanism of TBX3

Using differential gene expression analyses, I defined the gene MiGS and performed additional work on one particular gene, a melanoma-associated transcription factor encoding gene, *Tbx3*. Importantly, melanocytes from all three genotypes express *Tbx3*; however, melanocytes from both RHC mice (lethal yellow, A^y/a; recessive yellow, $Mc1r^e/^e$) express significantly more transcript. An obvious question therefore is how does MC1R inhibition lead to increased levels of *Tbx3*? One possibility is that, when active, the MC1R pathway inhibits, but does not completely abrogate, *Tbx3* expression. Thus, when MC1R signalling is shutoff, the inhibition of *Tbx3* is also lost (Figure 2A).

Does this sufficiently explain the subsequent rise of *Tbx3*? In other words, is inhibitor loss sufficient on its own to increase *Tbx3* to the levels observed in the RHC melanocytes, or are there other factors driving this increased expression? Bioinformatic analyses suggest the latter, and the increase in expression in RHC melanocytes is being driven, at least in part, by the TGFβ signalling pathway (Figure 2A). The hair follicle contains several cell types which secrete TGFβ family member ligands and normal melanocytes themselves express TGFβ in certain contexts and, importantly, melanocytes express TGFβ receptors, therefore, both paracrine and autocrine mediated activation of this pathway is likely to occur in melanocytes

(Krasagakis et al., 1994; Rezza et al., 2016; Rodeck et al., 1994). Relatedly, in the absence of sunlight and UVR, keratinocytes primarily secrete TGFβ to maintain melanocyte quiescence and reduce melanin synthesis in human epidermal melanocytes (Vandamme & Berx, 2019). Furthermore, TGFβ has been reported to regulate melanocyte maturation, melanogenesis, and melanomagenesis in several ways (Katkat et al., 2023; D.-S. Kim et al., 2004; H.-R. Moon et al., 2020; Moustakas, 2008; Nishimura et al., 2010; G. Yang et al., 2008); however, many of these reported findings present contradictory functional roles. Regardless, a universal takeaway from these studies is that TGFβ signalling can greatly affect melanocyte biology. Despite this, the cross-talk and interplay between the MC1R and TGFβ signalling pathways in melanocytes and melanoma is unknown despite the vast amount of literature which exists on the independent function of these two pathways. Therefore, future work in this field should aim to investigate the functional interplay which appears likely to exist between these two axes. Regardless, I propose that the TGFβ signalling pathway is a primary driving force of *Tbx3* expression in melanocytes which are in a state of MC1R signalling inhibition (Figure 2A).

My work revealed that TBX3 can B&R several known pigmentation genes in melanoma cells. As previously stated, melanocytes in the MC1R-inhibited state *in vivo*, exhibit higher levels of *Tbx3*. My data suggests that this observed difference may be due to the TGFβ pathway whereby SMADs, which are downstream mediators of the pathway bind to and induce transcription of *Tbx3*, amongst other downstream targets (Schmierer & Hill, 2007). This, subsequently, leads to a rise in the level of TBX3 resulting in TBX3 binding at E- and T-box to regulate expression of target genes which function to: (1) foster phaeomelanogenesis, (2) inhibit eumelanogenesis, (3) promote proliferation, and (4) prevent cellular senescence

(Figure 2B). These actions, in melanocytes lacking functional MC1R prior to the acquisition of activating mutations, such as BRAF or NRAS, promote the production of phaeomelanin, which itself is an oncogenic driver (Mitra et al., 2012; Napolitano et al., 2014), suppress senescence, inhibit the production of antioxidant eumelanin, and could therefore provide a potential mechanism by which people with RHC exhibit predisposition to melanoma.

Limitations and Future Directions

Translation to Humans

Model organisms are an essential means to study biological phenomena, and their underlying mechanisms, and without their help, we would not have the fundamental insights and comprehension of molecular mechanisms to understand and treat of human disease (P. Hunter, 2008). Several model organisms are in use, one such model organism is *Mus musculus* which is considered an ideal choice to study human disease as it exhibits a high degree of homology with *Homo sapiens* (Rydell-Törmänen & Johnson, 2019). Given this, I choose to use *in vivo* derived murine melanocytes to study the complexities which govern gene expression of eumelanotic and phaeomelanotic producing cells. An important, and age-old argument, which extends across all model organism-based studies, is whether the associated findings, derived from a model organism, will provide direct and translatable insights into human disease which is, ultimately, a major force driving molecular biology research (P. Hunter, 2008). The short answer is yes. For example, MC1R signalling is highly conserved among mammals and multiple well-characterized mouse strains exist which have both active and inhibited MC1R

signalling and mimic the resultant human phenotypes associated with those states, with a prime example being lethal yellow and recessive yellow, mice which both genotypically and phenotypically recapitulate the human RHC trait. Furthermore, the study of pigmentation genetics across several types of species has led to major scientific insights which greatly impact our understanding of human biology and disease (Hoekstra, 2006). Likewise, and as stated by Hunter, 'the paradox of model organisms seems to be that the need for them will only diminish once most of the fundamental mechanisms of biology have been solved to allow the greater use of both human tissue cultures and in silico methods for drug discovery. To reach that point, however, requires the extensive use of model organisms' (P. Hunter, 2008).

Multiple key points supporting the use of model organisms which extend to cost, time, availability of tissue/subjects, and ethics are missing from Hunter's argument. It could be argued that the ideal study design for the single-cell profiling experiments should have included human samples or human derived cell lines. There is merit to this point, and the possibility of this approach does exist. For example, I could have obtained melanocytes from human samples using the same digestion and FACS enrichment protocol of skin samples to profile eumelanotic melanocytes with functional MC1R variants against phaeomelanotic samples which comprised all known MC1R coding variants associated with RHC trait. However, at this moment in time I do not have access to these types of samples and establishing a protocol could take some years. Coupled with this, there is no guarantee that an IRB(s) would approve of the proposed study. Therefore, a reasonable alternative might have instead been to use primary melanocyte cell lines which are already established and/or commercially available. Much like human primary samples, this approach has limitations due to the fact that: (1) primary melanocytes are

notoriously difficult to culture, (2) commercially available RHC melanocyte cell lines are not available, (3) both somatic and germline variants which exist in human derived samples can greatly modify gene expressions programs, and (3) this *in vitro* approach takes away the complexity of the *in vivo* environment. Therefore, my choice of model possess several advantages which would have been difficult to adequately address with human cell line and tissues. Importantly these profiling experiments uncovered an extensive list of novel differentially expressed genes which may play critical roles in melanocyte biology and disease. With this information at hand, future studies can now take a much more directed, single gene approach, to understand the significance of MiGS genes in human biology.

Functional Validation of TBX3's Proposed Role in Melanocytes

Confirmation of TBX3 Expression in Melanocytes

Using scRNA-seq, I quantified relative transcript levels of all detectable genes from *in vivo* derived melanocytes. By doing this, I discovered that *Tbx3* is expressed in melanocytes from all murine samples tested but that significantly higher levels were found in the melanocytes from RHC mice. As external validation, I queried the Hair-GEL database, which is derived from bulk RNA-seq of individual skin cell types, to assess *Tbx3* mRNA levels of melanocytes from P5 mice (Hair-GEL.net; Rezza et al., 2016). I found that *Tbx3* is indeed normally expressed by melanocytes and that *Tbx3* is considered a 'melanocyte signature gene' (Chapter 3: Figure 10A). This provided further confidence that the transcript levels observed in my dataset were both real and valid. However, the possibility of inappropriately mapped reads, and therefore miscalculation of sequenced transcript levels,

although highly unlikely, does remain possible. Therefore, an orthogonal quantitative approach, such as in situ hybridization (ISH) / fluorescence in situ hybridization (FISH), should be further used to assay *Tbx3* expression levels and cellular localization. In short, ISH detects expression of target genes of interest through hybridization of a nucleic acid-based probe to a complementary sequence of mRNA which derives from the gene of interest (Sterchi, 2008). The probe contains an attached label, such as a fluorescent tag, which can be visualized and quantified by techniques such as fluorescence-based microscopy (Sterchi, 2008). The latest advent in this field relates to RNAscope which maximises the signal-to-noise ratio and therefore allows more accurate visualization of gene expression at the single cell level (Robles-Remacho et al., 2023). One or more of these related techniques should be used to (1) confirm expression of *Tbx3* in normal murine and human melanocytes, (2) validate increased levels of expression in murine RHC melanocytes, and (3) confirm whether human RHC melanocytes exhibit the same relative increase of TBX3 compared to *MC1R* wildtype.

A common question in the life sciences is how gene expression dictates biological phenotypes (Y. Liu et al., 2016). Recent advances, such as scRNA-seq, provide a powerful tool to investigate this question. For example, scRNA-seq allows for an unprecedented view of global gene expression across different cell types, states, and tissues which did not exist before its genesis (Jovic et al., 2022). Importantly, mRNA levels, the detected feature of scRNA-seq, do not inherently correlate to protein levels, which are the functional output of genes (Y. Liu et al., 2016). Thus, the biological significance of mRNA expression is almost impossible to determine without proteomic based studies. However, differential mRNA expression studies have shown that the called significant DEGs do tightly correlate

with changes in the level of protein product as compared to non-DEGs (Koussounadis et al., 2015). Therefore, the MiGS, even without robust proteomic studies, provides important biological insights governing phenotypic differences between eumelanin and phaeomelanin producing melanocytes.

Regardless, proteomic assays are needed to fully validate the interpretation of these findings. Given that TBX3 is a TF, the proteomic work in this thesis focused on chromatin binding and transcriptional regulation of target genes. This led to novel insights related to the action of TBX3 in melanocytes. Future work should aim to validate these findings through complementary assays and further refine the biological significance of elevated levels of TBX3 in melanocytes. An important first step might be to confirm the notion that the significant differential expression, as observed by mRNA in phaeomelanotic melanocytes is positively correlated with expected alterations in protein levels. There are multiple ways in which this could be achieved. One way would be to assess the quantity and localization of protein in melanocytes from all the mouse strains used in this thesis. For example, P3 melanocytes could be derived from the same FACS-based enrichment assay and then probed for TBX3 levels by Western Blot using an anti-TBX3 antibody. Alternatively, immunohistochemistry or immunofluorescence might be used on whole skins to detect TBX3 expression and nuclear localization of melanocytes *in situ*. Collectively, these two approaches could be used to validate the observed and expected levels of *Tbx3*/*TBX3*/TBX3 expression in melanocytes which are primarily eumelanotic or phaeomelanotic.

Conditional Modulation of TBX3 *in vivo* to Evaluate a Functional Role in Melanocyte Biology

Mechanistically, I propose that TBX3 functions to regulate multiple biological pathways in melanocytes, including melanogenesis. More specifically, I predict that TBX3 facilitates gene expression within melanocytes to promote phaeomelanogenesis and inhibit eumelanogenesis. Additional experimentation, especially *in vivo*, is needed to validate this hypothesis. For example, future mouse model-based studies might conditionally modulate TBX3 levels through cell specific deletion or overexpression to confirm the cell intrinsic effects of TBX3. The Cre recombinase-loxP system (Cre-lox) has been used with great effect to investigate the function of genes in a spatial, specific cell or tissue type, and/or temporal manner (H. Kim et al., 2018). In simple terms, Cre is a tyrosine site-specific recombinase enzyme that mediates site specific deletion of DNA between two loxP, also known as, flox or fl, sites (Figure 3A) (H. Kim et al., 2018). The following two principles of the system are key to spatial manipulation: first, loxP sites must be inserted in a such a manner that upon recombination by Cre the genetic deletion yields sufficient alteration in gene expression. For example, in the case of LOF, loxP sites should flank a significant area so that no active protein product is produced. Second, Cre induction should be connected to a cell type specific promoter so that recombination (i.e., genetic deletion) only occurs in the cell or tissue type of interest (H. Kim et al., 2018) (Figure 3B).

Lopez and colleagues used a *Tbx3 fl/fl; Wnt1-Cre* mouse model to investigate the function of TBX3 in the developing enteric nervous system (López et al., 2018). Importantly, *Wnt1* expression is restricted spatially to NCCs, which are precursors to enteric neurons and glia, amongst many other cell type derivatives

(Lewis et al., 2013). Therefore, their system allowed them to investigate the effect of tissue specific deletions of TBX3 in NCCs. Of note, melanocytes are also NC derivatives; therefore, the system developed by Lopez and colleagues could be of use for functional investigation of TBX3 in melanocytes. However, mice in their study die within 24 hours of birth and, therefore, the examination of melanin-based phenotypes would be less than ideal with how the model stands.

Despite the short comings of their model for my specific question, the basic study design can be altered so that recombination is under the control of a melanocyte specific-Cre. A prime candidate could be *Tyr-Cre* which was developed for use in mice by the lab of Lionel Laure (Delmas et al., 2003). In their model, recombination occurs in melanoblasts by E11.5 and, therefore, represents a good choice to assess the function of TBX3 on pigmentation as well as melanocyte maturation. Tyrosinase is a key melanogenic enzyme which converts Tyrosine to Dopaquinone, an essential precursor for both eumelanin and phaeomelanin (Fernandes et al., 2023; Hida et al., 2020). Crucially, this gene was not observed to be differentially expressed between the melanocytes of RHC and nonagouti mice. Thus, it is an optimal Cre driver for conditional studies of TBX3 function in melanocytes.

Using *Tbx3 fl/fl; Tyr-Cre* mice I could first assess the impact of TBX3 loss in melanocytes. First, recessive yellow, lethal yellow, and nonagouti animals would be engineered so that we could create the *Tbx3 fl/fl; Tyr-Cre* genotype in all three backgrounds (Figure 3C). In this state, RHC mice (recessive yellow and lethal yellow), with conditional loss of TBX3 (*Tbx3 fl/fl; Tyr-Cre*), would (1) have reduced levels of phaeomelanin, become paler, or (2) be more brown-black, due to a decrease in phaeomelanin coupled with an increase in eumelanin production, as

compared to the wildtype control (*Tbx3*$^{+/+}$*; Tyr-Cre*) (Figure 3C). For nonagouti, we would predict that, following melanocyte specific Cre mediated recombination and deletion of *Tbx3*, these nonagouti animals would either (1) show no alteration on coat colour or (2) they would present with an even darker coat colour, mimicking that of extreme nonagouti mouse (*a*^{e}*/a*^{e}) (Walker and Gunn et al., 2010) as compared to the wildtype condition (*Tbx3*$^{+/+}$*; Tyr-Cre*) (Figure 3C).

Instead of deleting TBX3, I could perform a contrasting experiment and investigate the effect of TBX3 overexpression in melanocytes. To do this, one possible approach might make use of a triple transgenic mouse system, first devised by Belteki and colleagues, which combines tissue specificity, via Cre-mediated recombination, with titratability, through induction of a *Tbx3* transgene using a tetracycline-transcriptional activation (Tet-on) system (Belteki et al., 2005). In the case of TBX3, mice would be engineered so that flox-STOP-flox rtTA and TRE-*Tbx3* transgenes would be inserted into the genome at a safe-harbour locus, such as *ROSA26*. In these mice the STOP site in front of the rtTA which would be removed following the expression of *Tyr-Cre*. This, in turn, would lead to ubiquitous expression of rtTA in all recombined cells. The induction of rtTA on its own would not lead to increased levels of *Tbx3*/TBX3 as rtTA-TRE binding only occurs once rtTA is bound by tetracycline. Once a tetracycline drug is delivered to the system, the newly formed tetracycline-rtTA complex can then bind the TRE of the *Tbx3* transgene and drive gene expression (Figure 3D). Thus, with this system I could control the level of *Tbx3* transgene expressed and regulate, temporally, when this occurs. Relatedly, I could further experimentally test whether the phenotype reverts to *status quo* following the withdrawal of tetracycline. With this overexpression model, I would predict that the observed phenotypes are directly contrary to those

predicted following TBX3 deletion. Namely, treated RHC mouse models (flox-STOP-flox rtTA; TRE-*Tbx3*; +Dox) would (1) exhibit no coat colour alteration or (2) become more yellow-red due to raised levels of phaeomelanin, as compared to non-treated animals (flox-STOP-flox rtTA; TRE-*Tbx3*; -Dox (Figure 3E). In the case of nonagouti animals, I would predict that they would display a lighter coat colour due to decreased levels of eumelanin and/or increased levels of phaeomelanin (Figure 3E). These theoretical animal models represent possible routes to functionally interrogate TBX3 mediated biology in melanocytes, especially as it relates to melanogenesis. Furthermore, these models can be easily adapted to test the function of TBX3 in the melanocyte lineage including in development and melanomagenesis.

Validating Candidate Bound and Regulated TBX3 Target Genes

In Chapter 4, we used ChIP-seq to evaluate genome-wide chromatin occupancy of TBX3 in the 501mel melanoma cell line. ChIP is a well-established technique which is used to capture and identify physiologically relevant protein-DNA interactions (Gade & Kalvakolanu, 2011). The typical procedure is as follows: first, cross-linking is performed with a fixative, such as formaldehyde, to preserve the in-situ state of protein-DNA interactions. Following this, chromatin is sheared into small fragments, typically within a range of 100-500 bps, to facilitate the ease of downstream analytic techniques such as sequencing or ChIP-PCR. Immunoprecipitation of protein bound DNA occurs using an antibody which targets an epitope of the specific protein of interest. Next, the protein is released from the bound portion of DNA through reverse cross-linking proteins. For ChIP-seq, the residual DNA is sequenced to determine the loci which were bound by the protein

of interest (Elnitski et al., 2006). With this TBX3 ChIP-seq data, I utilized MEME-ChIP, an oft-used bioinformatic tool to identify over-represented patterns in DNA binding and discovered that TBX3 binding peaks most associate with two motif types in 501mel cells, the T-box which has been previously reported, and the E-box, which was not previously reported (Chapter 4: Figure 3). However, a limitation of this approach is that I was unable to detect the exact location of DNA binding by TBX3. Therefore, it is impossible to conclusively say whether binding, and subsequent regulation, of TBX3 is through the identified motif.

To address this, future work should utilize techniques such as promoter, or enhancer-promoter, mutagenesis to verify site-specific DNA binding and subsequent regulation of gene expression. One way to address this would involve a firefly-luciferase reporter system. In this approach, a reporter gene (e.g., firefly-luciferase), downstream of a specific cis-regulatory element sequence, is induced, when bound by an activating TF, and its activity is measured against a baseline control (Wet et al., 1985, 1987; Wood et al., 1984). With this technique, I could confirm the degree to which TBX3 binds the predicted cis-regulatory elements of the several target genes identified by the GREAT analysis. Furthermore, I could use the same approach to identify the exact binding sequence. To do this, I would induce several different genetic alterations, via mutagenesis, at the cis-regulatory element bound by TBX3 so that I can query which nucleotides facilitate and are necessary for protein binding. In the case of TBX3, we could predict for a given target gene that binding is most likely at the T- or E-box. Thus, I would modulate the nucleotide sequence of these elements to confirm whether this hypothesis is true. For example, following deletion and/or alteration of the core ‘GTG’ site I would strongly suspect that TBX3 could no longer bind that region of DNA and, therefore, luciferase would

no longer be expressed. This system represents one method by which I can test binding, and subsequent regulation, of candidate B&R TBX3 gene targets.

Identifying Interacting Cofactors of TBX3

The extent to which TBX3 can regulate gene expression is most probably dependent on a number of factors and might include cell type, state of differentiation, chromatin accessibility, and/or co-factor availability. Therefore, our ChIP-seq experiment, which used a single human melanoma cell line, is not sufficient to fully address the complexities which most likely underlie TBX3's ability to B&R genes within the melanocyte lineage. TBX3 crystal structure studies suggest that this protein preferentially binds to DNA as a monomer; however, TBX3, and other T-box family members, can function as homo- or hetero-dimers, and the heterodimer can comprise a partner from an unrelated TF family, such as a homeobox (Coll et al., 2002). Likewise, TBX3 is known to interact with several cofactors, and it is most probable that the specific cofactor type works to modulate specific functional actions of TBX3 (Washkowitz et al., 2012). Given this, future studies should aim to experimentally evaluate the full spectrum of TBX3-interacting factors. For example, one possible technique would be the use of a BioID assay to examine proximity-based protein-protein interactions which has been done with successfully previously by the Goding lab (S. Lu et al., 2021). In brief, a biotin ligase would be fused to a protein of interest, in this case TBX3, and, when in close proximity to another protein, this biotin ligase would facilitate the attachment of biotin to the nearby protein through biotinylation. The biotinylated proteins would then be isolated via a biotin-affinity capture array with the use of streptavidin beads, which form a strong bond to biotin. The identity of the isolated biotinylated proteins would then be confirmed

by mass spectrometry (Roux et al., 2012) (Figure 4A). These experiments could be performed to determine the full repertoire of interacting factors in melanocytes across several differentiation and disease states (melanoblasts – melanocytes, healthy vs melanoma).

Protein-protein interactions identified by BioID could be further corroborated with ‘bait-prey’ live-cell nuclear tethering assays which have been used previously by our lab (S. Lu et al., 2021). In essence, a bait protein, in this case TBX3, would be fused to an mCherry-Lac repressor (LacR) vector construct, whereas a prey protein, X which represents any enriched protein identified by BioID, would be fused to a GFP reporter construct, and then these two plasmids would be transfected into U2OS cells containing an integrated Lac operator (U2OS-LacO) so that the TBX3-LacR-mCherry protein will bind to, and accumulate at, the LacO and, if TBX3 and Protein X interact, there will be a readily detectable co-localized yellow dot by fluorescence microscopy (Figure 4B, Top). Conversely, if the prey protein (or empty vector) does not interact with the bait there will be diffuse GFP signal and no yellow co-localization dot (Figure 4B. Bottom). With this approach I could orthogonally validate the entire list of BioID identified TBX3-interacting factors.

Conclusion

In this thesis, I set out to profile the transcriptomes of melanocytes which were in an active eumelanotic versus phaeomelanotic state so that we could gain an appreciation as to the GRNs which function, and possibly dictate, these two different melanocyte pigment producing states. To do this, I performed scRNA-seq on melanocytes from nonagouti mice, which primarily synthesize eumelanin, as well

as mice with inhibited MC1R signalling which predominately produce phaeomelanin and mimic the human RHC trait. From those experiments, I identified a set of differentially expressed genes which exists between those two states, and I have defined those genes as the MiGS. Remarkably, this gene signature overwhelmingly comprises a large set of genes which have never been studied in the context of melanogenesis. A functional role for these genes in melanogenesis is unknown and thus they all merit further investigation towards better understanding of the complex function of GRNs in melanocytes, and how these regulate melanogenesis and melanocyte function.

The MiGS contains several TF/co-TF encoding genes. This includes *Tbx3* which encodes for a melanoma-associated transcription factor. I showed that TBX3 can B&R the expression of putative target genes at the E- and T-box to regulate several biological processes of melanocytes, including melanogenesis. Follow-up experimental studies related to TBX3 should aim to orthogonally validate TBX3's ability to B&R target genes at T-box and E-box motifs across the several biological states which exist in both healthy and diseased melanocytes. Candidate TBX3 B&R targets include those associated with pigmentation, cell cycle regulation, EMT, and MiGS genes themselves. Thus, I hypothesize that increased levels of *TBX3*/TBX3 leads to suppression of senescence, promotion of oncogenic phaeomelanin and, in melanocytes lacking functional MC1R prior to acquisition of activating mutations in BRAF or NRAS, could thus provide a potential mechanism RHC trait possessing people exhibit increased predisposition to melanoma development. As mentioned, more work is needed to sufficiently test this hypothesis. In total, the MC1R-inhbited Gene Signature represents the first attempt, at single-cell resolution, to define to the transcriptomic state of melanocytes which are primarily eumelanotic or

phaeomelanotic. This list is dominated by genes which are not known to function in melanogenesis or even melanocyte biology generally. Thus, MiGS highlights the complex GRNs which exist between these states and provides an exciting foundation to direct future studies aimed at unravelling the complexities of melanocyte biology which include development, cell signalling, melanogenesis, and melanomagenesis.

Figures

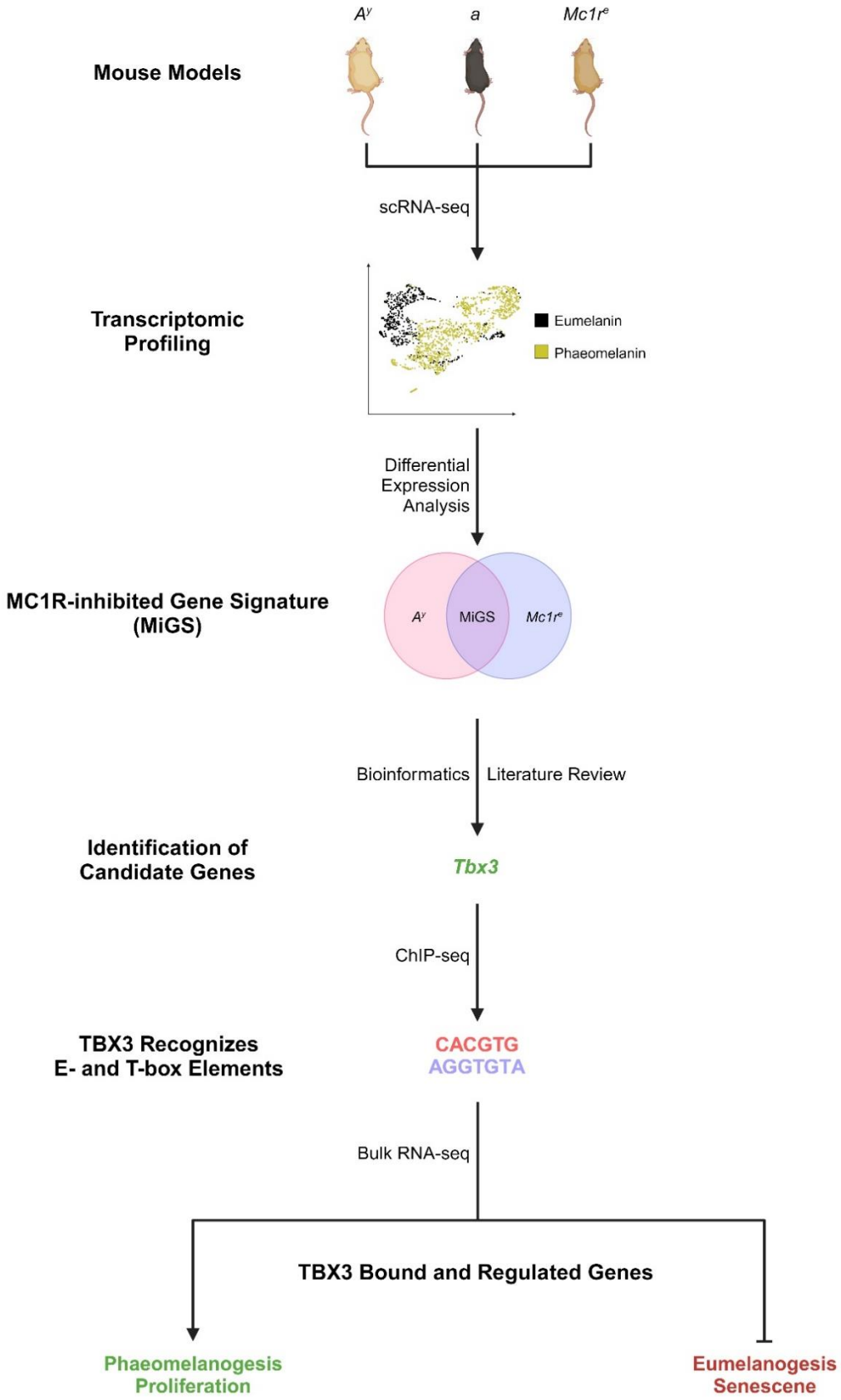

Mouse Models
A^y
a
$Mc1r^e$
scRNA-seq
Transcriptomic Profiling
Eumelanin
Phaeomelanin
Differential Expression Analysis
MC1R-inhibited Gene Signature (MiGS)
A^y
MiGS
$Mc1r^e$
Bioinformatics
Literature Review
Identification of Candidate Genes
Tbx3
ChIP-seq
TBX3 Recognizes E- and T-box Elements
CACGTG
AGGTGTA
Bulk RNA-seq
TBX3 Bound and Regulated Genes
Phaeomelanogesis Proliferation
Eumelanogesis Senescene

Figure 1. Summary of Work and Findings. Melanocytes which were eumelanotic (nonagouti, *a*) or phaeomelanotic (lethal yellow, A^{y} ;recessive yellow, $Mc1r^{e}$), and mimic human RHC trait, were isolated from mice and transcriptomically profiled using scRNA-seq. Using differential expression analyses, I found 216 common DEGs between melanocytes from the RHC mice and defined this gene set as the 'MC1R-inhibited Gene Signature' (MiGS). I utilized multiple techniques to interpret the biological significance of this signature and determine which might pose the most functional relevance in melanocytes. One such gene was *Tbx3*, which encodes a T-box TF known to have a functional role in melanoma. Using a multi-omics approach I showed that TBX3 can B&R gene targets through E-box and T-box elements. Subsequently, I found that activated genes were associated with cellular proliferation and phaeomelanogenesis while repressed genes were affiliated with senescence and eumelanogenesis.

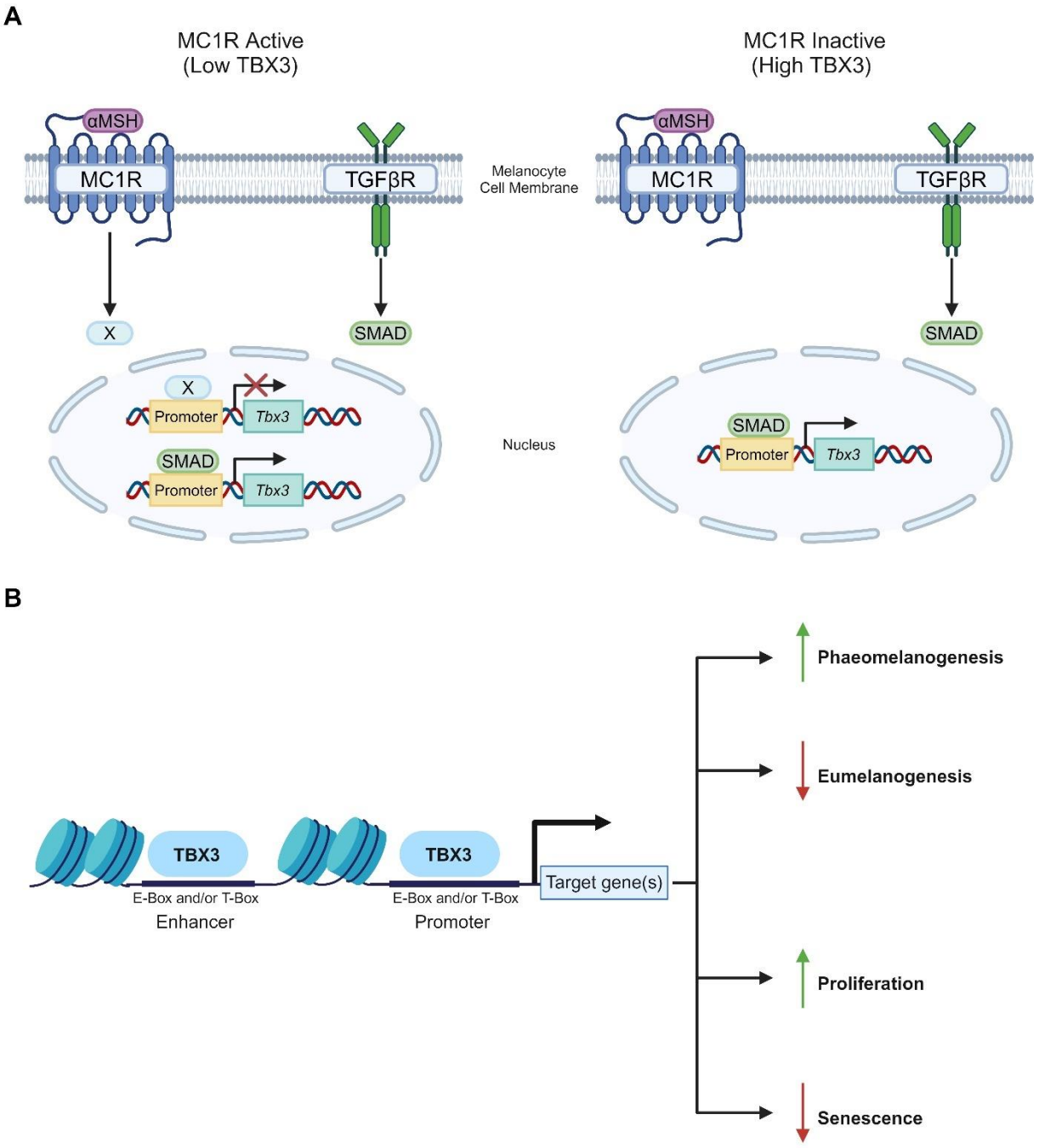
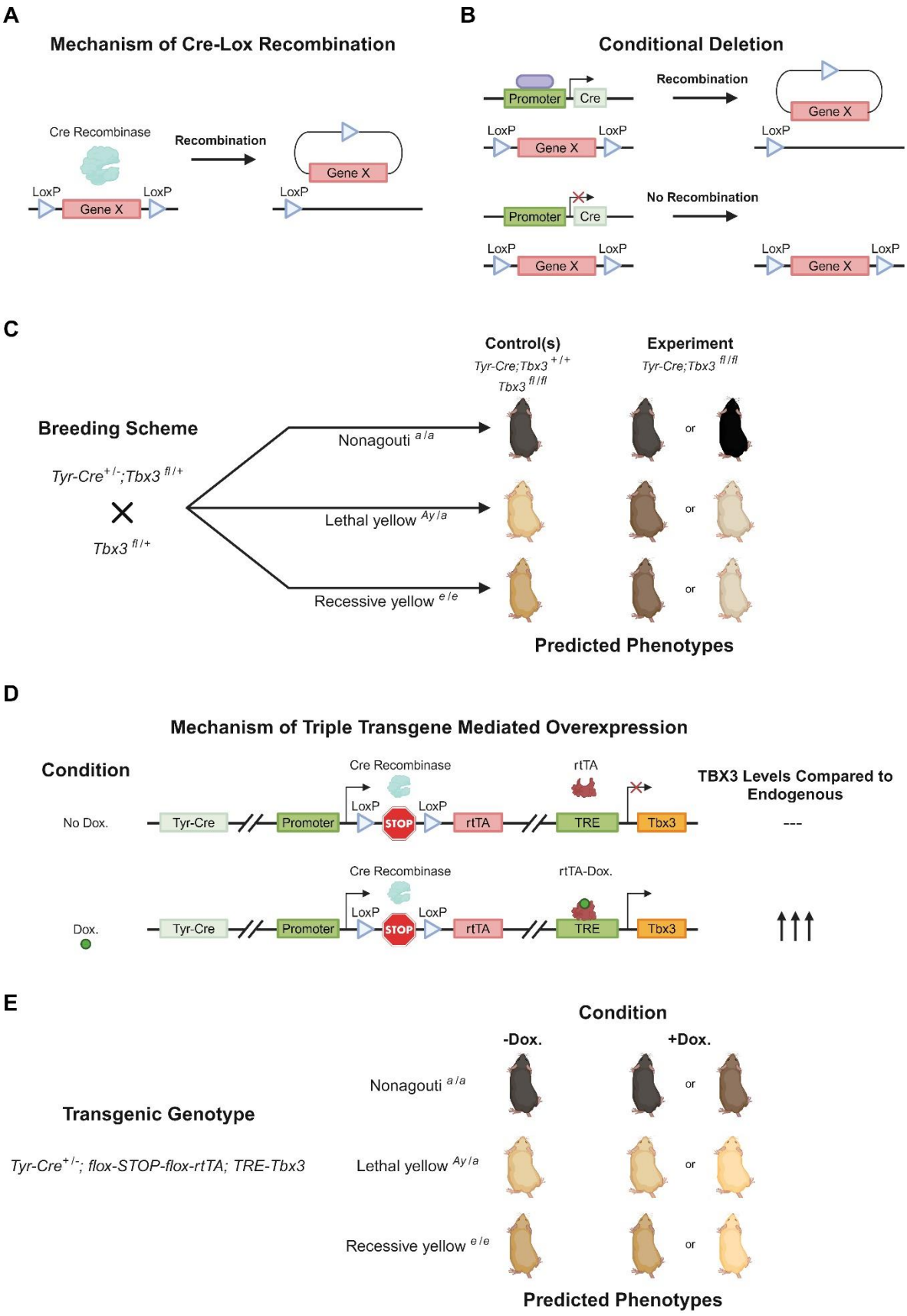


Figure 2. Expression and Proposed Role of TBX3 in Melanocytes. (A) When MC1R signalling is active, *Tbx3* is found at low levels (left). In contrast, when MC1R is inactive, inhibited, or non-functional, TGFβ, and its downstream mediators, is predicted to induce robust expression of *Tbx3* in melanocytes (right). (B) TBX3 binds to E-box and T-box elements found with cis-regulatory elements of target

genes and functions to promote phaeomelanogenesis and proliferation while concomitantly inhibiting eumelanogenesis and cellular senescence.


A
Mechanism of Cre-Lox Recombination
Cre Recombinase
Recombination
LoxP
Gene X
LoxP
LoxP
Gene X
B
Conditional Deletion
Promoter
Cre
Recombination
Gene X
LoxP
Gene X
LoxP
LoxP
Promoter
Cre
No Recombination
LoxP
Gene X
LoxP
LoxP
Gene X
C
Control(s)
Tyr-Cre;Tbx3 +/+
Tbx3 fl/fl
Experiment
Tyr-Cre;Tbx3 fl/fl
Breeding Scheme
Tyr-Cre+/-;Tbx3 fl/+
×
Tbx3 fl/+
Nonagouti a/a
Lethal yellow Ay/a
Recessive yellow e/e
or
Predicted Phenotypes
D
Mechanism of Triple Transgene Mediated Overexpression
Condition
Cre Recombinase
rtTA
TBX3 Levels Compared to Endogenous
No Dox.
Tyr-Cre
Promoter
LoxP
STOP
LoxP
rtTA
TRE
Tbx3

Cre Recombinase
rtTA-Dox.
Dox.
Tyr-Cre
Promoter
LoxP
STOP
LoxP
rtTA
TRE
Tbx3
E
Condition
-Dox.
+Dox.
Transgenic Genotype
Tyr-Cre+/-; flox-STOP-flox-rtTA; TRE-Tbx3
Nonagouti a/a
Lethal yellow Ay/a
Recessive yellow e/e
or
Predicted Phenotypes

Figure 3. *In vivo* Models for Future Functional Studies of TBX3 Function in Melanocytes. (A) Schematic depicting the basics of the Cre-Lox recombinase system with (B) highlighting recombination which leads to conditional deletion of genomic elements. (C) Overview of conditional mouse model generation with precited phenotypic outcomes. (D) Review of the triple transgene approach which leads to TBX3 overexpression. (E) Overview of conditional mouse model generation with precited phenotypic outcomes associated with TBX3 overexpression.

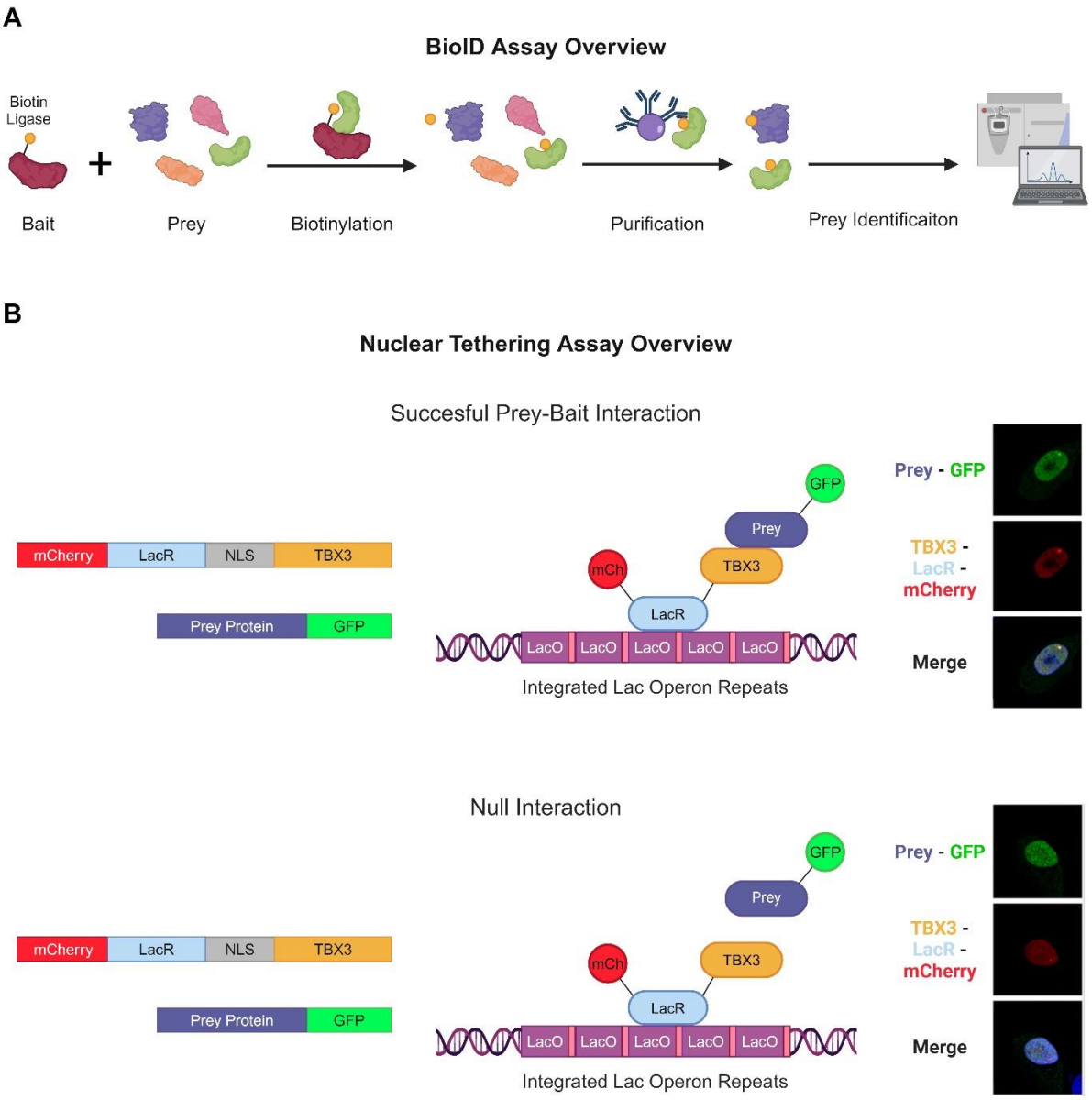


Figure 4. Future Experimental Techniques to Identify TBX3 Cofactors. (A) Schematic depicting the basics of a BioID assay. (B) Overview of nuclear tethering assay with positive (top) and negative (bottom) interactions associated with 'prey-bait' proteins.

Appendix A:

Supplemental Tables Associated with Chapter 3.

Table S1: Gene Signature of Murine Skin Cells from Rezza et al., 2016 (Hair-GEL.net)

Table S2: Significant Differentially Expressed Genes Between Lethal Yellow and Nonagouti Melanocytes

Table S3: Significant Differentially Expressed Genes Between Recessive Yellow and Nonagouti Melanocytes

Table S4: MC1R-inhibted Gene Signature

Appendix B:

Supplemental Tables Associated with Chapter 4.

Table S1: GREAT Output for TBX3 ChIP Dataset

Table S2: GREAT Output for MITF ChIP Dataset

Table S3: Human to Mouse Conversion of TBX3 Target Genes

Table S4: Human to Mouse Conversion of MITF Target Genes

Table S5: Significant Differentially Expressed Genes from TBX3 Knockdown

Table S6: Significant Differentially Expressed Genes from TBX3 Knockdown which are also Associated with TBX3 ChIP-seq Peaks

Table S7: GREAT Output for TBX2 ChIP Dataset

Table S8: Significant Differentially Expressed Genes from TBX2 Knockdown

Table S9: Mouse to Human Conversion of Significant Differentially Expressed Genes from TBX2 Knockdown

Table S10: Significant Differentially Expressed Genes from TBX2 Knockdown which are also Associated with TBX2 ChIP-seq Peaks

Table S11: Bound and Regulated Genes Which are Shared by TBX2/3

Table S12: Bound and Regulated Genes Which are Shared by TBX2/3 and Split by Action of Activation or Repression

Appendix C:

Manuscript by Berns et al., 2024. Downloaded from *Pigment Cell and Melanoma Research*.

https://onlinelibrary.wiley.com/doi/full/10.1111/pcmr.13141

H. Matthew Berns, Dawn E. Watkins-Chow, Sizhu Lu, Pakavarin Louphrasitthiphol, Tongwu Zhang, Kevin M. Brown, Pedro Moura-Alves, Colin R. Goding, William J. Pavan. 2024. Single-cell profiling of MC1R-inhibited melanocytes. *Pigment Cell and Melanoma Research*. DOI: 10.1111/pcmr.13141

References

Achkar, C. M. el, Harrer, M., Smith, L., Kelly, M., Iqbal, S., Maljevic, S., Niturad, C. E., Vissers, L. E. L. M., Poduri, A., Yang, E., Lal, D., Lerche, H., Møller, R. S., Olson, H. E., & Group, for the G. W. (2021). Characterization of the GABRB2-Associated Neurodevelopmental Disorders. *Annals of Neurology*, *89*(3), 573–586. https://doi.org/10.1002/ana.25985

Adameyko, I., Lallemend, F., Aquino, J. B., Pereira, J. A., Topilko, P., Müller, T., Fritz, N., Beljajeva, A., Mochii, M., Liste, I., Usoskin, D., Suter, U., Birchmeier, C., & Ernfors, P. (2009). Schwann Cell Precursors from Nerve Innervation Are a Cellular Origin of Melanocytes in Skin. *Cell*, *139*(2), 366–379. https://doi.org/10.1016/j.cell.2009.07.049

Adameyko, I., Lallemend, F., Furlan, A., Zinin, N., Aranda, S., Kitambi, S. S., Blanchart, A., Favaro, R., Nicolis, S., Lübke, M., Müller, T., Birchmeier, C., Suter, U., Zaitoun, I., Takahashi, Y., & Ernfors, P. (2011). Sox2 and Mitf cross-regulatory interactions consolidate progenitor and melanocyte lineages in the cranial neural crest. *Development*, *139*(2), 397–410. https://doi.org/10.1242/dev.065581

Adjeround, S., Tonon, M. C., Lamacz, M., Leneveu, E., Stoeckel, M. E., Tappaz, M. L., Cazin, L., Danger, J. M., Bernard, C., & Vaudry, H. (1986). GABA-ergic control of α-Melanocyte-Stimulating Hormone (α-MSH) release by frog neurointermediate lobe in vitro. *Brain Research Bulletin*, *17*(5), 717–723. https://doi.org/10.1016/0361-9230(86)90206-6

Agarwal, P., Verzi, M. P., Nguyen, T., Hu, J., Ehlers, M. L., McCulley, D. J., Xu, S.-M., Dodou, E., Anderson, J. P., Wei, M. L., & Black, B. L. (2011). The MADS box transcription factor MEF2C regulates melanocyte development and is a direct transcriptional target and partner of SOX10. *Development*, *138*(12), 2555–2565. https://doi.org/10.1242/dev.056804

Akison, L., & Robker, R. (2012). The Critical Roles of Progesterone Receptor (PGR) in Ovulation, Oocyte Developmental Competence and Oviductal Transport in Mammalian Reproduction. *Reproduction in Domestic Animals*, *47*(s4), 288–296. https://doi.org/10.1111/j.1439-0531.2012.02088.x

Allen, J. R., Skeath, J. B., & Johnson, S. L. (2019). Maintenance of Melanocyte Stem Cell Quiescence by GABA-A Signaling in Larval Zebrafish. *Genetics*, *213*(2), 555–566. https://doi.org/10.1534/genetics.119.302416

Andersson, L. (2020). Mutations in Domestic Animals Disrupting or Creating Pigmentation Patterns. *Frontiers in Ecology and Evolution*, *8*, 116. https://doi.org/10.3389/fevo.2020.00116

Andersson, R. (2015). Promoter or enhancer, what's the difference? Deconstruction of established distinctions and presentation of a unifying model. *BioEssays*, *37*(3), 314–323. https://doi.org/10.1002/bies.201400162

Aoki, H., & Moro, O. (2002). Involvement of microphthalmia-associated transcription factor (MITF) in expression of human melanocortin-1 receptor (MC1R). *Life Sciences*, *71*(18), 2171–2179. https://doi.org/10.1016/s0024-3205(02)01996-3

April, C. S., & Barsh, G. S. (2006). Skin layer-specific transcriptional profiles in normal and recessive yellow (Mc1re/Mc1re) mice. *Pigment Cell Research*, *19*(3), 194–205. https://doi.org/10.1111/j.1600-0749.2006.00305.x

Aramburu, T., Plucinsky, S., & Skordalakes, E. (2020). POT1-TPP1 telomere length regulation and disease. *Computational and Structural Biotechnology Journal*, *18*, 1939–1946. https://doi.org/10.1016/j.csbj.2020.06.040

Armstrong, B. K., & Kricker, A. (1993). How much melanoma is caused by sun exposure? *Melanoma Research*, *3*(6), 395–402. https://doi.org/10.1097/00008390-199311000-00002

Ayed, I. B., Bouzid, A., Kammoun, F., souissi, A., Jallouli, O., Mallouli, S., Guidara, S., Loukil, S., Aloulou, H., Jbeli, F., Aouichaoui, S., Abid, D., Abdelhedi, F., Triki, C., Kamoun, H., & Masmoudi, S. (2021). 8q21.11 microdeletion syndrome: Delineation of HEY1 as a candidate gene in neurodevelopmental and cardiac defects. *Molecular Genetics & Genomic Medicine*, *9*(11), e1811. https://doi.org/10.1002/mgg3.1811

Bailey, T. L., Johnson, J., Grant, C. E., & Noble, W. S. (2015). The MEME Suite. *Nucleic Acids Research*, *43*(W1), W39–W49. https://doi.org/10.1093/nar/gkv416

Bauer, J., Curtin, J. A., Pinkel, D., & Bastian, B. C. (2007). Congenital Melanocytic Nevi Frequently Harbor NRAS Mutations but no BRAF Mutations. *Journal of Investigative Dermatology*, *127*(1), 179–182. https://doi.org/10.1038/sj.jid.5700490

Baxter, L. L., Watkins-Chow, D. E., Pavan, W. J., & Loftus, S. K. (2019). A curated gene list for expanding the horizons of pigmentation biology. *Pigment Cell & Melanoma Research*, *32*(3), 348–358. https://doi.org/10.1111/pcmr.12743

Belote, R. L., Le, D., Maynard, A., Lang, U. E., Sinclair, A., Lohman, B. K., Planells-Palop, V., Baskin, L., Tward, A. D., Darmanis, S., & Judson-Torres, R. L. (2021). Human melanocyte development and melanoma dedifferentiation at single-cell resolution. *Nature Cell Biology*, 1–13. https://doi.org/10.1038/s41556-021-00740-8

Belote, R. L., Le, D., Maynard, A., Lang, U. E., Sinclair, A., Planells-Palop, V., Baskin, L., Tward, A. D., Darmanis, S., & Judson-Torres, R. L. (2020). Human melanocyte development and melanoma dedifferentiation at single cell resolution. *BioRxiv*, 2020.05.25.115287. https://doi.org/10.1101/2020.05.25.115287

Belteki, G., Haigh, J., Kabacs, N., Haigh, K., Sison, K., Costantini, F., Whitsett, J., Quaggin, S. E., & Nagy, A. (2005). Conditional and inducible transgene expression in mice through the combinatorial use of Cre-mediated recombination and tetracycline induction. *Nucleic Acids Research*, *33*(5), e51–e51. https://doi.org/10.1093/nar/gni051

Benito-Martinez, S., Salavessa, L., Raposo, G., Marks, M. S., & Delevoye, C. (2021). Melanin transfer and fate within keratinocytes in human skin pigmentation. *Integrative and Comparative Biology*. https://doi.org/10.1093/icb/icab094

Bennett, D. C., & Medrano, E. E. (2002). Molecular Regulation of Melanocyte Senescence. *Pigment Cell Research*, *15*(4), 242–250. https://doi.org/10.1034/j.1600-0749.2002.02036.x

Berwick, M., Erdei, E., & Hay, J. (2009). Melanoma Epidemiology and Public Health. *Dermatologic Clinics*, *27*(2), 205–214. https://doi.org/10.1016/j.det.2008.12.002

Blanchard, S. G., Harris, C. O., Ittoop, O., Nichols, J. S., Parks, D. J., Truesdale, A. T., & Wilkison, W. O. (1995). Agouti Antagonism of Melanocortin Binding and Action in the B16F10 Murine Melanoma Cell Line. *Biochemistry*, *34*(33), 10406–10411. https://doi.org/10.1021/bi00033a012

Boyd, S. C., Mijatov, B., Pupo, G. M., Tran, S. L., Gowrishankar, K., Shaw, H. M., Goding, C. R., Scolyer, R. A., Mann, G. J., Kefford, R. F., Rizos, H., & Becker, T. M. (2013). Oncogenic B-RAFV600E Signaling Induces the T-Box3 Transcriptional Repressor to Repress E-Cadherin and Enhance Melanoma Cell Invasion. *Journal of Investigative Dermatology*, *133*(5), 1269–1277. https://doi.org/10.1038/jid.2012.421

Brenner, M., & Hearing, V. J. (2008). The Protective Role of Melanin Against UV Damage in Human Skin†. *Photochemistry and Photobiology*, *84*(3), 539–549. https://doi.org/10.1111/j.1751-1097.2007.00226.x

Breslow, A. (1970). Thickness, Cross-Sectional Areas and Depth of Invasion in the Prognosis of Cutaneous Melanoma. *Annals of Surgery*, *172*(5), 902–908. https://doi.org/10.1097/00000658-197011000-00017

Brombin, A., Simpson, D. J., Travnickova, J., Brunsdon, H., Zeng, Z., Lu, Y., Young, A. I. J., Chandra, T., & Patton, E. E. (2022). Tfap2b specifies an embryonic melanocyte stem cell that retains adult multifate potential. *Cell Reports*, *38*(2), 110234. https://doi.org/10.1016/j.celrep.2021.110234

Bronner, M. E., & LeDouarin, N. M. (2012). Development and evolution of the neural crest: An overview. *Developmental Biology*, *366*(1), 2–9. https://doi.org/10.1016/j.ydbio.2011.12.042

Bultman, S. J., Michaud, E. J., & Woychik, R. P. (1992). Molecular characterization of the mouse agouti locus. *Cell*, *71*(7), 1195–1204. https://doi.org/10.1016/s0092-8674(05)80067-4

Cao, J., Wan, L., Hacker, E., Dai, X., Lenna, S., Jimenez-Cervantes, C., Wang, Y., Leslie, N. R., Xu, G. X., Widlund, H. R., Ryu, B., Alani, R. M., Dutton-Regester, K., Goding,

C. R., Hayward, N. K., Wei, W., & Cui, R. (2013). MC1R Is a Potent Regulator of PTEN after UV Exposure in Melanocytes. *Molecular Cell*, *51*(4), 409–422. https://doi.org/10.1016/j.molcel.2013.08.010

Castellani, G., Buccarelli, M., Arasi, M. B., Rossi, S., Pisanu, M. E., Bellenghi, M., Lintas, C., & Tabolacci, C. (2023). BRAF Mutations in Melanoma: Biological Aspects, Therapeutic Implications, and Circulating Biomarkers. *Cancers*, *15*(16), 4026. https://doi.org/10.3390/cancers15164026

Castro-Pérez, E., Singh, M., Sadangi, S., Mela-Sánchez, C., & Setaluri, V. (2023). Connecting the dots: Melanoma cell of origin, tumor cell plasticity, trans-differentiation, and drug resistance. *Pigment Cell & Melanoma Research*. https://doi.org/10.1111/pcmr.13092

Centeno, P. P., Pavet, V., & Marais, R. (2023). The journey from melanocytes to melanoma. *Nature Reviews Cancer*, *23*(6), 372–390. https://doi.org/10.1038/s41568-023-00565-7

Chambers, J., & Rabbitts, T. H. (2015). LMO2 at 25 years: a paradigm of chromosomal translocation proteins. *Open Biology*, *5*(6), 150062. https://doi.org/10.1098/rsob.150062

Chang, C., Murzaku, E. C., Penn, L., Abbasi, N. R., Davis, P. D., Berwick, M., & Polsky, D. (2014). More Skin, More Sun, More Tan, More Melanoma. *American Journal of Public Health*, *104*(11), e92–e99. https://doi.org/10.2105/ajph.2014.302185

Chang, F., Xing, P., Song, F., Du, X., Wang, G., Chen, K., & Yang, J. (2016). The role of T-box genes in the tumorigenesis and progression of cancer. *Oncology Letters*, *12*(6), 4305–4311. https://doi.org/10.3892/ol.2016.5296

Chang, H., & Nathans, J. (2013). Responses of hair follicle–associated structures to loss of planar cell polarity signaling. *Proceedings of the National Academy of Sciences*, *110*(10), E908–E917. https://doi.org/10.1073/pnas.1301430110

Chen, Y., Lu, X., Montoya-Durango, D. E., Liu, Y.-H., Dean, K. C., Darling, D. S., Kaplan, H. J., Dean, D. C., Gao, L., & Liu, Y. (2017). ZEB1 Regulates Multiple Oncogenic Components Involved in Uveal Melanoma Progression. *Scientific Reports*, *7*(1), 45. https://doi.org/10.1038/s41598-017-00079-x

Chhabra, Y., Yong, H. X. L., Fane, M. E., Soogrim, A., Lim, W., Mahiuddin, D. N., Kim, R. S. Q., Ashcroft, M., Beatson, S. A., Ainger, S. A., Smit, D. J., Jagirdar, K., Walker, G. J., Sturm, R. A., & Smith, A. G. (2018). Genetic variation in IRF4 expression modulates growth characteristics, tyrosinase expression and interferon-gamma response in melanocytic cells. *Pigment Cell & Melanoma Research*, *31*(1), 51–63. https://doi.org/10.1111/pcmr.12620

Chiba, K., Lorbeer, F. K., Shain, A. H., McSwiggen, D. T., Schruf, E., Oh, A., Ryu, J., Darzacq, X., Bastian, B. C., & Hockemeyer, D. (2017). Mutations in the promoter of the telomerase gene TERT contribute to tumorigenesis by a two-step mechanism. *Science*, *357*(6358), 1416–1420. https://doi.org/10.1126/science.aao0535

Chintala, S., Li, W., Lamoreux, M. L., Ito, S., Wakamatsu, K., Sviderskaya, E. V., Bennett, D. C., Park, Y.-M., Gahl, W. A., Huizing, M., Spritz, R. A., Ben, S., Novak, E. K., Tan, J., & Swank, R. T. (2005). Slc7a11 gene controls production of pheomelanin pigment and proliferation of cultured cells. *Proceedings of the National Academy of Sciences of the United States of America*, *102*(31), 10964–10969. https://doi.org/10.1073/pnas.0502856102

Cho, K.-W., Kim, J.-Y., Song, S.-J., Farrell, E., Eblaghie, M. C., Kim, H.-J., Tickle, C., & Jung, H.-S. (2006). Molecular interactions between Tbx3 and Bmp4 and a model for dorsoventral positioning of mammary gland development. *Proceedings of the National Academy of Sciences*, *103*(45), 16788–16793. https://doi.org/10.1073/pnas.0604645103

Cicek, E., Monard, G., & Sungur, F. A. (2022). Molecular Mechanism of Protein Arginine Deiminase 2: A Study Involving Multiple Microsecond Long Molecular Dynamics Simulations. *Biochemistry*, *61*(13), 1286–1297. https://doi.org/10.1021/acs.biochem.2c00158

Coll, M., Seidman, J. G., & Müller, C. W. (2002). Structure of the DNA-Bound T-Box Domain of Human TBX3, a Transcription Factor Responsible for Ulnar-Mammary Syndrome. *Structure*, *10*(3), 343–356. https://doi.org/10.1016/s0969-2126(02)00722-0

Colombo, S., Berlin, I., Delmas, V., & Larue, L. (2011). *Melanins and Melanosomes*. 21–61. https://doi.org/10.1002/9783527636150.ch2

Corre, S., Tardif, N., Mouchet, N., Leclair, H. M., Boussemart, L., Gautron, A., Bachelot, L., Perrot, A., Soshilov, A., Rogiers, A., Rambow, F., Dumontet, E., Tarte, K., Bessede, A., Guillemin, G. J., Marine, J.-C., Denison, M. S., Gilot, D., & Galibert, M.-D. (2018). Sustained activation of the Aryl hydrocarbon Receptor transcription factor promotes resistance to BRAF-inhibitors in melanoma. *Nature Communications*, *9*(1), 4775. https://doi.org/10.1038/s41467-018-06951-2

Cui, R., Widlund, H. R., Feige, E., Lin, J. Y., Wilensky, D. L., Igras, V. E., D'Orazio, J., Fung, C. Y., Schanbacher, C. F., Granter, S. R., & Fisher, D. E. (2007). Central Role of p53 in the Suntan Response and Pathologic Hyperpigmentation. *Cell*, *128*(5), 853–864. https://doi.org/10.1016/j.cell.2006.12.045

Cust, A. E., Armstrong, B. K., Goumas, C., Jenkins, M. A., Schmid, H., Hopper, J. L., Kefford, R. F., Giles, G. G., Aitken, J. F., & Mann, G. J. (2011). Sunbed use during adolescence and early adulthood is associated with increased risk of early-onset melanoma. *International Journal of Cancer*, *128*(10), 2425–2435. https://doi.org/10.1002/ijc.25576

Dąbrowska, A. K., Spano, F., Derler, S., Adlhart, C., Spencer, N. D., & Rossi, R. M. (2018). The relationship between skin function, barrier properties, and body-dependent factors. *Skin Research and Technology*, *24*(2), 165–174. https://doi.org/10.1111/srt.12424

D'Alba, L., & Shawkey, M. D. (2019). Melanosomes: Biogenesis, Properties, and Evolution of an Ancient Organelle. *Physiological Reviews*, *99*(1), 1–19. https://doi.org/10.1152/physrev.00059.2017

Damerell, V., Ambele, M. A., Salisbury, S., Neumann-Mufweba, A., Durandt, C., Pepper, M. S., & Prince, S. (2022). The c-Myc/TBX3 Axis Promotes Cellular Transformation of Sarcoma-Initiating Cells. *Frontiers in Oncology*, *11*, 801691. https://doi.org/10.3389/fonc.2021.801691

Davey, R. A., & Grossmann, M. (2016). Androgen Receptor Structure, Function and Biology: From Bench to Bedside. *The Clinical Biochemist. Reviews*, *37*(1), 3–15.

Davis, L. E., Shalin, S. C., & Tackett, A. J. (2019). Current state of melanoma diagnosis and treatment. *Cancer Biology & Therapy*, *20*(11), 1366–1379. https://doi.org/10.1080/15384047.2019.1640032

Dekoninck, S., Hannezo, E., Sifrim, A., Miroshnikova, Y. A., Aragona, M., Malfait, M., Gargouri, S., Neunheuser, C. de, Dubois, C., Voet, T., Wickström, S. A., Simons, B. D., & Blanpain, C. (2020). Defining the Design Principles of Skin Epidermis Postnatal Growth. *Cell*, *181*(3), 604-620.e22. https://doi.org/10.1016/j.cell.2020.03.015

Delmas, V., Martinozzi, S., Bourgeois, Y., Holzenberger, M., & Larue, L. (2003). Cre-mediated recombination in the skin melanocyte lineage. *Genesis*, *36*(2), 73–80. https://doi.org/10.1002/gene.10197

Denda, M., Inoue, K., Inomata, S., & Denda, S. (2002). γ-Aminobutyric Acid (A) Receptor Agonists Accelerate Cutaneous Barrier Recovery and Prevent Epidermal Hyperplasia Induced by Barrier Disruption. *Journal of Investigative Dermatology*, *119*(5), 1041–1047. https://doi.org/10.1046/j.1523-1747.2002.19504.x

DiVito, K. A., Trabosh, V. A., Chen, Y., Simbulan-Rosenthal, C. M., & Rosenthal, D. S. (2015). Inhibitor of differentiation-4 (Id4) stimulates pigmentation in melanoma leading to histiocyte infiltration. *Experimental Dermatology*, *24*(2), 101–107. https://doi.org/10.1111/exd.12582

D'Mello, S. A. N., Finlay, G. J., Baguley, B. C., & Askarian-Amiri, M. E. (2016). Signaling Pathways in Melanogenesis. *International Journal of Molecular Sciences*, *17*(7), 1144. https://doi.org/10.3390/ijms17071144

Dobin, A., Davis, C. A., Schlesinger, F., Drenkow, J., Zaleski, C., Jha, S., Batut, P., Chaisson, M., & Gingeras, T. R. (2013). STAR: ultrafast universal RNA-seq aligner. *Bioinformatics*, *29*(1), 15–21. https://doi.org/10.1093/bioinformatics/bts635

Dong, L., Dong, Q., Chen, Y., Li, Y., Zhang, B., Zhou, F., Lyu, X., Chen, G. G., Lai, P., Kung, H., & He, M.-L. (2018). Novel HDAC5-interacting motifs of Tbx3 are essential for the suppression of E-cadherin expression and for the promotion of metastasis in hepatocellular carcinoma. *Signal Transduction and Targeted Therapy*, *3*(1), 22. https://doi.org/10.1038/s41392-018-0025-6

D'Orazio, J., Jarrett, S., Amaro-Ortiz, A., & Scott, T. (2013). UV Radiation and the Skin. *International Journal of Molecular Sciences*, *14*(6), 12222–12248. https://doi.org/10.3390/ijms140612222

Du, W., Liu, X., Yang, M., Wang, W., & Sun, J. (2021). The Regulatory Role of PRRX1 in Cancer Epithelial-Mesenchymal Transition. *OncoTargets and Therapy*, *14*, 4223–4229. https://doi.org/10.2147/ott.s316102

Dubucs, C., Chassaing, N., Sergi, C., Aubert-Mucca, M., Attié-Bitach, T., Lacombe, D., Thauvin-Robinet, C., Arpin, S., Perez, M. J., Cabrol, C., Chen, C. P., Aziza, J., Colin, E., Martinovic, J., Calvas, P., & Plaisancié, J. (2021). Re-focusing on Agnathia-Otocephaly complex. *Clinical Oral Investigations*, *25*(3), 1353–1362. https://doi.org/10.1007/s00784-020-03443-w

Duffy, D. (2019). MC1R minor variants and the multiple pathways to melanoma. *The Lancet Child & Adolescent Health*, *3*(5), 287–288. https://doi.org/10.1016/s2352-4642(19)30026-4

Duffy, D. L., Lee, K. J., Jagirdar, K., Pflugfelder, A., Stark, M. S., McMeniman, E. K., Soyer, H. P., & Sturm, R. A. (2019). High naevus count and MC1R red hair alleles contribute synergistically to increased melanoma risk. *British Journal of Dermatology*, *181*(5), 1009–1016. https://doi.org/10.1111/bjd.17833

Duhl, D. M. J., Stevens, M. E., Vrieling, H., Saxon, P. J., Miller, M. W., Epstein, C. J., & Barsh, G. S. (1994). Pleiotropic effects of the mouse lethal yellow (Ay) mutation explained by deletion of a maternally expressed gene and the simultaneous production of agouti fusion RNAs. *Development*, *120*(6), 1695–1708. https://doi.org/10.1242/dev.120.6.1695

Dujon, A. M., Capp, J.-P., Brown, J. S., Pujol, P., Gatenby, R. A., Ujvari, B., Alix-Panabières, C., & Thomas, F. (2021). Is There One Key Step in the Metastatic Cascade? *Cancers*, *13*(15), 3693. https://doi.org/10.3390/cancers13153693

Dupin, E., & Douarin, N. M. L. (2003). Development of melanocyte precursors from the vertebrate neural crest. *Oncogene*, *22*(20), 3016–3023. https://doi.org/10.1038/sj.onc.1206460

Durand, S., Tang, Y., Pommier, R. M., Benboubker, V., Grimont, M., Boivin, F., Barbollat-Boutrand, L., Cumunel, E., Dupeuble, F., Eberhardt, A., Plaschka, M., Dalle, S., & Caramel, J. (2023). ZEB1 controls a lineage-specific transcriptional program essential for melanoma cell state transitions. *BioRxiv*, 2023.02.10.526467. https://doi.org/10.1101/2023.02.10.526467

Dyck, F. V., Declercq, J., Braem, C. V., & Ven, W. J. M. V. de. (2007). PLAG1, the prototype of the PLAG gene family: versatility in tumour development (review). *International Journal of Oncology*, *30*(4), 765–774.

Dzierżęga-Lęcznar, A., Kurkiewicz, S., Tam, I., Marek, Ł., & Stępień, K. (2017). Pheomelanin content of cultured human melanocytes from lightly and darkly pigmented skin: A pyrolysis-gas chromatography/tandem mass spectrometry study. *Journal of Analytical and Applied Pyrolysis*, *124*, 349–354. https://doi.org/10.1016/j.jaap.2017.01.009

Eddy, K., & Chen, S. (2021). Glutamatergic Signaling a Therapeutic Vulnerability in Melanoma. *Cancers*, *13*(15), 3874. https://doi.org/10.3390/cancers13153874

Eddy, K., Shah, R., & Chen, S. (2021). Decoding Melanoma Development and Progression: Identification of Therapeutic Vulnerabilities. *Frontiers in Oncology*, *10*, 626129. https://doi.org/10.3389/fonc.2020.626129

Elnitski, L., Jin, V. X., Farnham, P. J., & Jones, S. J. M. (2006). Locating mammalian transcription factor binding sites: A survey of computational and experimental techniques. *Genome Research*, *16*(12), 1455–1464. https://doi.org/10.1101/gr.4140006

Enkhtaivan, E., & Lee, C. H. (2021). Role of Amine Neurotransmitters and Their Receptors in Skin Pigmentation: Therapeutic Implication. *International Journal of Molecular Sciences*, *22*(15), 8071. https://doi.org/10.3390/ijms22158071

Erickson, C. A., Duong, T. D., & Tosney, K. W. (1992). Descriptive and experimental analysis of the dispersion of neural crest cells along the dorsolateral path and their entry into ectoderm in the chick embryo. *Developmental Biology*, *151*(1), 251–272. https://doi.org/10.1016/0012-1606(92)90231-5

Ernfors, P. (2010). Cellular origin and developmental mechanisms during the formation of skin melanocytes. *Experimental Cell Research*, *316*(8), 1397–1407. https://doi.org/10.1016/j.yexcr.2010.02.042

Fargnoli, M. C., Gandini, S., Peris, K., Maisonneuve, P., & Raimondi, S. (2010). MC1R variants increase melanoma risk in families with CDKN2A mutations: A meta-analysis. *European Journal of Cancer*, *46*(8), 1413–1420. https://doi.org/10.1016/j.ejca.2010.01.027

Feng, S., XU, S., WEN, Z., & ZHU, Y. (2015). Retinoic acid-related orphan receptor RORβ, circadian rhythm abnormalities and tumorigenesis (Review). *International Journal of Molecular Medicine*, *35*(6), 1493–1500. https://doi.org/10.3892/ijmm.2015.2155

Fernandes, B., Cavaco-Paulo, A., & Matamá, T. (2023). A Comprehensive Review of Mammalian Pigmentation: Paving the Way for Innovative Hair Colour-Changing Cosmetics. *Biology*, *12*(2), 290. https://doi.org/10.3390/biology12020290

Ferrara, G., & Argenziano, G. (2021). The WHO 2018 Classification of Cutaneous Melanocytic Neoplasms: Suggestions From Routine Practice. *Frontiers in Oncology*, *11*, 675296. https://doi.org/10.3389/fonc.2021.675296

Ferrè, S., Baaij, J. H. F. de, Ferreira, P., Germann, R., Klerk, J. B. C. de, Lavrijsen, M., Zeeland, F. van, Venselaar, H., Kluijtmans, L. A. J., Hoenderop, J. G. J., & Bindels, R. J. M. (2014). Mutations in PCBD1 Cause Hypomagnesemia and Renal Magnesium Wasting. *Journal of the American Society of Nephrology*, *25*(3), 574–586. https://doi.org/10.1681/asn.2013040337

Frank, D. U., Emechebe, U., Thomas, K. R., & Moon, A. M. (2013). Mouse Tbx3 Mutants Suggest Novel Molecular Mechanisms for Ulnar-Mammary Syndrome. *PLoS ONE*, *8*(7), e67841. https://doi.org/10.1371/journal.pone.0067841

Gade, P., & Kalvakolanu, D. V. (2011). Transcriptional Regulation, Methods and Protocols. *Methods in Molecular Biology*, *809*, 85–104. https://doi.org/10.1007/978-1-61779-376-9_6

García-Borrón, J. C., Abdel-Malek, Z., & Jiménez-Cervantes, C. (2014). MC1R, the cAMP pathway, and the response to solar UV: extending the horizon beyond pigmentation. *Pigment Cell & Melanoma Research*, *27*(5), 699–720. https://doi.org/10.1111/pcmr.12257

Gautron, A., Migault, M., Bachelot, L., Corre, S., Galibert, M., & Gilot, D. (2020). Human TYRP1: two functions for a single gene? *Pigment Cell & Melanoma Research*. https://doi.org/10.1111/pcmr.12951

Ghit, A., Assal, D., Al-Shami, A. S., & Hussein, D. E. E. (2021). GABAA receptors: structure, function, pharmacology, and related disorders. *Journal of Genetic Engineering and Biotechnology*, *19*(1), 123. https://doi.org/10.1186/s43141-021-00224-0

Goding, C. R., & Arnheiter, H. (2019). MITF—the first 25 years. *Genes & Development*, *33*(15–16), 983–1007. https://doi.org/10.1101/gad.324657.119

Guida, S., Guida, G., & Goding, C. R. (2021). MC1R Functions, Expression, and Implications for Targeted Therapy. *Journal of Investigative Dermatology*. https://doi.org/10.1016/j.jid.2021.06.018

Ha, L., Merlino, G., & Sviderskaya, E. V. (2008). Melanomagenesis: Overcoming the barrier of melanocyte senescence. *Cell Cycle*, *7*(13), 1944–1948. https://doi.org/10.4161/cc.7.13.6230

Haltaufderhyde, K. D., & Oancea, E. (2014). Genome-wide transcriptome analysis of human epidermal melanocytes. *Genomics*, *104*(6), 482–489. https://doi.org/10.1016/j.ygeno.2014.09.010

Harris, M. L., Fufa, T. D., Palmer, J. W., Joshi, S. S., Larson, D. M., Incao, A., Gildea, D. E., Trivedi, N. S., Lee, A. N., Day, C.-P., Michael, H. T., Hornyak, T. J., Merlino, G., Program, N. C. S., & Pavan, W. J. (2018). A direct link between MITF, innate immunity, and hair graying. *PLOS Biology*, *16*(5), e2003648. https://doi.org/10.1371/journal.pbio.2003648

Healy, E., Flannagan, N., Ray, A., Todd, C., Jackson, I. J., Matthews, J. N., Birch-Machin, M. A., & Rees, J. L. (2000). Melanocortin-1-receptor gene and sun sensitivity in individuals without red hair. *The Lancet*, *355*(9209), 1072–1073. https://doi.org/10.1016/s0140-6736(00)02042-0

Heppt, M. V., Wang, J. X., Hristova, D. M., Wei, Z., Li, L., Evans, B., Beqiri, M., Zaman, S., Zhang, J., Irmler, M., Berking, C., Besch, R., Beckers, J., Rauscher, F. J., Sturm, R.

A., Fisher, D. E., Herlyn, M., & Fukunaga-Kalabis, M. (2018). MSX1-Induced Neural Crest-Like Reprogramming Promotes Melanoma Progression. *Journal of Investigative Dermatology*, *138*(1), 141–149. https://doi.org/10.1016/j.jid.2017.05.038

Herring, J. A., Elison, W. S., & Tessem, J. S. (2019). Function of Nr4a Orphan Nuclear Receptors in Proliferation, Apoptosis and Fuel Utilization Across Tissues. *Cells*, *8*(11), 1373. https://doi.org/10.3390/cells8111373

Hida, T., Kamiya, T., Kawakami, A., Ogino, J., Sohma, H., Uhara, H., & Jimbow, K. (2020). Elucidation of Melanogenesis Cascade for Identifying Pathophysiology and Therapeutic Approach of Pigmentary Disorders and Melanoma. *International Journal of Molecular Sciences*, *21*(17), 6129. https://doi.org/10.3390/ijms21176129

Hoek, K. S., Eichhoff, O. M., Schlegel, N. C., Döbbeling, U., Kobert, N., Schaerer, L., Hemmi, S., & Dummer, R. (2008). In vivo Switching of Human Melanoma Cells between Proliferative and Invasive States. *Cancer Research*, *68*(3), 650–656. https://doi.org/10.1158/0008-5472.can-07-2491

Hoek, K. S., & Goding, C. R. (2010). Cancer stem cells versus phenotype-switching in melanoma. *Pigment Cell & Melanoma Research*, *23*(6), 746–759. https://doi.org/10.1111/j.1755-148x.2010.00757.x

Hoek, K. S., Schlegel, N. C., Brafford, P., Sucker, A., Ugurel, S., Kumar, R., Weber, B. L., Nathanson, K. L., Phillips, D. J., Herlyn, M., Schadendorf, D., & Dummer, R. (2006). Metastatic potential of melanomas defined by specific gene expression profiles with no BRAF signature. *Pigment Cell Research*, *19*(4), 290–302. https://doi.org/10.1111/j.1600-0749.2006.00322.x

Hoek, K. S., Schlegel, N. C., Eichhoff, O. M., Widmer, D. S., Praetorius, C., Einarsson, S. O., Valgeirsdottir, S., Bergsteinsdottir, K., Schepsky, A., Dummer, R., & Steingrimsson, E. (2008). Novel MITF targets identified using a two-step DNA microarray strategy. *Pigment Cell & Melanoma Research*, *21*(6), 665–676. https://doi.org/10.1111/j.1755-148x.2008.00505.x

Hoekstra, H. E. (2006). Genetics, development and evolution of adaptive pigmentation in vertebrates. *Heredity*, *97*(3), 222–234. https://doi.org/10.1038/sj.hdy.6800861

Hoogaars, W. M. H., Barnett, P., Rodriguez, M., Clout, D. E., Moorman, A. F. M., Goding, C. R., & Christoffels, V. M. (2008). TBX3 and its splice variant TBX3 + exon 2a are functionally similar. *Pigment Cell & Melanoma Research*, *21*(3), 379–387. https://doi.org/10.1111/j.1755-148x.2008.00461.x

Hoogaars, W. M. H., Tessari, A., Moorman, A. F. M., Boer, P. A. J. de, Hagoort, J., Soufan, A. T., Campione, M., & Christoffels, V. M. (2004). The transcriptional repressor Tbx3 delineates the developing central conduction system of the heart. *Cardiovascular Research*, *62*(3), 489–499. https://doi.org/10.1016/j.cardiores.2004.01.030

Hou, L., & Pavan, W. J. (2008). Transcriptional and signaling regulation in neural crest stem cell-derived melanocyte development: do all roads lead to Mitf? *Cell Research*, *18*(12), 1163–1176. https://doi.org/10.1038/cr.2008.303

Hsiao, C. J., Tung, P., Blischak, J. D., Burnett, J. E., Barr, K. A., Dey, K. K., Stephens, M., & Gilad, Y. (2020). Characterizing and inferring quantitative cell cycle phase in single-cell RNA-seq data analysis. *Genome Research*, *30*(4), 611–621. https://doi.org/10.1101/gr.247759.118

Hu, J., Verzi, M. P., Robinson, A. S., Tang, P. L.-F., Hua, L. L., Xu, S.-M., Kwok, P.-Y., & Black, B. L. (2015). Endothelin signaling activates Mef2c expression in the neural crest through a MEF2C-dependent positive-feedback transcriptional pathway. *Development*, *142*(16), 2775–2780. https://doi.org/10.1242/dev.126391

Hu, J.-S., Olson, E. N., & Kingston, R. E. (1992). HEB, a Helix-Loop-Helix Protein Related to E2A and ITF2 That Can Modulate the DNA-Binding Ability of Myogenic Regulatory Factors. *Molecular and Cellular Biology*, *12*(3), 1031–1042. https://doi.org/10.1128/mcb.12.3.1031-1042.1992

Hu, N., Zou, L., Wang, C., & Song, G. (2022). RUNX1T1 function in cell fate. *Stem Cell Research & Therapy*, *13*(1), 369. https://doi.org/10.1186/s13287-022-03074-w

Hu, S., & Zhu, L. (2018). Semaphorins and Their Receptors: From Axonal Guidance to Atherosclerosis. *Frontiers in Physiology*, *9*, 1236. https://doi.org/10.3389/fphys.2018.01236

Huber, W. E., Price, E. R., Widlund, H. R., Du, J., Davis, I. J., Wegner, M., & Fisher, D. E. (2003). A Tissue-restricted cAMP Transcriptional Response SOX10 MODULATES α-MELANOCYTE-STIMULATING HORMONE-TRIGGERED EXPRESSION OF MICROPHTHALMIA-ASSOCIATED TRANSCRIPTION FACTOR IN MELANOCYTES*. *Journal of Biological Chemistry*, *278*(46), 45224–45230. https://doi.org/10.1074/jbc.m309036200

Huizing, M., Helip-Wooley, A., Westbroek, W., Gunay-Aygun, M., & Gahl, W. A. (2008). Disorders of Lysosome-Related Organelle Biogenesis: Clinical and Molecular Genetics*. *Annual Review of Genomics and Human Genetics*, *9*(1), 359–386. https://doi.org/10.1146/annurev.genom.9.081307.164303

Hunter, K. W., Crawford, N. P., & Alsarraj, J. (2008). Mechanisms of metastasis. *Breast Cancer Research*, *10*(Suppl 1), S2. https://doi.org/10.1186/bcr1988

Hunter, P. (2008). The paradox of model organisms. *EMBO Reports*, *9*(8), 717–720. https://doi.org/10.1038/embor.2008.142

Hutchins, E. J., Kunttas, E., Piacentino, M. L., Howard, A. G. A., Bronner, M. E., & Uribe, R. A. (2018). Migration and diversification of the vagal neural crest. *Developmental Biology*, *444*, S98–S109. https://doi.org/10.1016/j.ydbio.2018.07.004

Imsland, F., McGowan, K., Rubin, C.-J., Henegar, C., Sundström, E., Berglund, J., Schwochow, D., Gustafson, U., Imsland, P., Lindblad-Toh, K., Lindgren, G., Mikko,

S., Millon, L., Wade, C., Schubert, M., Orlando, L., Penedo, M. C. T., Barsh, G. S., & Andersson, L. (2016). Regulatory mutations in TBX3 disrupt asymmetric hair pigmentation that underlies Dun camouflage color in horses. *Nature Genetics*, *48*(2), 152–158. https://doi.org/10.1038/ng.3475

Ito, S., & Wakamatsu, K. (2008). Chemistry of Mixed Melanogenesis—Pivotal Roles of Dopaquinone†. *Photochemistry and Photobiology*, *84*(3), 582–592. https://doi.org/10.1111/j.1751-1097.2007.00238.x

Jagirdar, K., Yin, K., Harrison, M., Lim, W., Muscat, G. E. O., Sturm, R. A., & Smith, A. G. (2013). The NR4A2 Nuclear Receptor Is Recruited to Novel Nuclear Foci in Response to UV Irradiation and Participates in Nucleotide Excision Repair. *PLoS ONE*, *8*(11), e78075. https://doi.org/10.1371/journal.pone.0078075

Janes, P. W., Slape, C. I., Farnsworth, R. H., Atapattu, L., Scott, A. M., & Vail, M. E. (2014). EphA3 biology and cancer. *Growth Factors*, *32*(6), 176–189. https://doi.org/10.3109/08977194.2014.982276

Jin, C., Luo, Y., Liang, Z., Li, X., Kołat, D., Zhao, L., & Xiong, W. (2023). Crucial role of the transcription factors family activator protein 2 in cancer: current clue and views. *Journal of Translational Medicine*, *21*(1), 371. https://doi.org/10.1186/s12967-023-04189-1

Jovic, D., Liang, X., Zeng, H., Lin, L., Xu, F., & Luo, Y. (2022). Single-cell RNA sequencing technologies and applications: A brief overview. *Clinical and Translational Medicine*, *12*(3), e694. https://doi.org/10.1002/ctm2.694

Juang, Y., Jeng, Y., Chen, C., & Lien, H. (2016). PRRX2 as a novel TGF-β-induced factor enhances invasion and migration in mammary epithelial cell and correlates with poor prognosis in breast cancer. *Molecular Carcinogenesis*, *55*(12), 2247–2259. https://doi.org/10.1002/mc.22465

Kaiser, M., Wojahn, I., Rudat, C., Lüdtke, T. H., Christoffels, V. M., Moon, A., Kispert, A., & Trowe, M.-O. (2021). Regulation of otocyst patterning by Tbx2 and Tbx3 is required for inner ear morphogenesis in the mouse. *Development*, *148*(8), dev.195651. https://doi.org/10.1242/dev.195651

Kanetsky, P. A., Swoyer, J., Panossian, S., Holmes, R., Guerry, D., & Rebbeck, T. R. (2002). A Polymorphism in the Agouti Signaling Protein Gene Is Associated with Human Pigmentation. *The American Journal of Human Genetics*, *70*(3), 770–775. https://doi.org/10.1086/339076

Karras, P., Bordeu, I., Pozniak, J., Nowosad, A., Pazzi, C., Raemdonck, N. V., Landeloos, E., Herck, Y. V., Pedri, D., Bervoets, G., Makhzami, S., Khoo, J. H., Pavie, B., Lamote, J., Marin-Bejar, O., Dewaele, M., Liang, H., Zhang, X., Hua, Y., … Marine, J.-C. (2022). A cellular hierarchy in melanoma uncouples growth and metastasis. *Nature*, 1–9. https://doi.org/10.1038/s41586-022-05242-7

Katkat, E., Demirci, Y., Heger, G., Karagulle, D., Papatheodorou, I., Brazma, A., & Ozhan, G. (2023). Canonical Wnt and TGF-β/BMP signaling enhance melanocyte

regeneration but suppress invasiveness, migration, and proliferation of melanoma cells. *Frontiers in Cell and Developmental Biology*, *11*, 1297910. https://doi.org/10.3389/fcell.2023.1297910

Kee, Y., & Bronner-Fraser, M. (2001). Id4 expression and its relationship to other Id genes during avian embryonic development. *Mechanisms of Development*, *109*(2), 341–345. https://doi.org/10.1016/s0925-4773(01)00576-7

Kempf, E., Landgraf, K., Stein, R., Hanschkow, M., Hilbert, A., Jamra, R. A., Boczki, P., Herberth, G., Kühnapfel, A., Tseng, Y.-H., Stäubert, C., Schöneberg, T., Kühnen, P., Rayner, N. W., Zeggini, E., Kiess, W., Blüher, M., & Körner, A. (2022). Aberrant expression of agouti signaling protein (ASIP) as a cause of monogenic severe childhood obesity. *Nature Metabolism*, 1–16. https://doi.org/10.1038/s42255-022-00703-9

Kenny, C., Dilshat, R., Seberg, H. E., Otterloo, E. V., Bonde, G., Helverson, A., Franke, C. M., Steingrímsson, E., & Cornell, R. A. (2022). TFAP2 paralogs facilitate chromatin access for MITF at pigmentation and cell proliferation genes. *PLOS Genetics*, *18*(5), e1010207. https://doi.org/10.1371/journal.pgen.1010207

Khan, S. F., Damerell, V., Omar, R., Toit, M. D., Khan, M., Maranyane, H., Mlaza, M., Bleloch, J., Bellis, C., Sahm, B. D. B., Peres, J., KN, A., & Prince, S. (2019). The roles and regulation of TBX3 in development and disease. *Gene*, *726*, 144223. https://doi.org/10.1016/j.gene.2019.144223

Khoshnoodi, J., Pedchenko, V., & Hudson, B. G. (2008). Mammalian collagen IV. *Microscopy Research and Technique*, *71*(5), 357–370. https://doi.org/10.1002/jemt.20564

Kim, D.-S., Park, S.-H., & Park, K.-C. (2004). Transforming growth factor-β1 decreases melanin synthesis via delayed extracellular signal-regulated kinase activation. *The International Journal of Biochemistry & Cell Biology*, *36*(8), 1482–1491. https://doi.org/10.1016/j.biocel.2003.10.023

Kim, H., Kim, M., Im, S.-K., & Fang, S. (2018). Mouse Cre-LoxP system: general principles to determine tissue-specific roles of target genes. *Laboratory Animal Research*, *34*(4), 147–159. https://doi.org/10.5625/lar.2018.34.4.147

Kolberg, L., Raudvere, U., Kuzmin, I., Adler, P., Vilo, J., & Peterson, H. (2023). g:Profiler—interoperable web service for functional enrichment analysis and gene identifier mapping (2023 update). *Nucleic Acids Research*, *51*(W1), W207–W212. https://doi.org/10.1093/nar/gkad347

Koussounadis, A., Langdon, S. P., Um, I. H., Harrison, D. J., & Smith, V. A. (2015). Relationship between differentially expressed mRNA and mRNA-protein correlations in a xenograft model system. *Scientific Reports*, *5*(1), 10775. https://doi.org/10.1038/srep10775

Krasagakis, K., Garbe, C., Schrier, P. I., & Orfanos, C. E. (1994). Paracrine and autocrine regulation of human melanocyte and melanoma cell growth by transforming growth factor beta in vitro. *Anticancer Research*, *14*(6B), 2565–2571.

Kubic, J. D., Young, K. P., Plummer, R. S., Ludvik, A. E., & Lang, D. (2008). Pigmentation PAX-ways: the role of Pax3 in melanogenesis, melanocyte stem cell maintenance, and disease. *Pigment Cell & Melanoma Research*, *21*(6), 627–645. https://doi.org/10.1111/j.1755-148x.2008.00514.x

Kumar, R., Cheney, K. M., McKirdy, R., Neilsen, P. M., Schulz, R. B., Lee, J., Cohen, J., Booker, G. W., & Callen, D. F. (2008). CBFA2T3-ZNF652 Corepressor Complex Regulates Transcription of the E-box Gene HEB *. *Journal of Biological Chemistry*, *283*(27), 19026–19038. https://doi.org/10.1074/jbc.m709136200

Kunishige, J. H., Brodland, D. G., & Zitelli, J. A. (2013). Margins for standard excision of melanoma in situ. *Journal of the American Academy of Dermatology*, *69*(1), 164. https://doi.org/10.1016/j.jaad.2013.01.040

Langmead, B., & Salzberg, S. L. (2012). Fast gapped-read alignment with Bowtie 2. *Nature Methods*, *9*(4), 357–359. https://doi.org/10.1038/nmeth.1923

Larue, L., Vuyst, F. de, & Delmas, V. (2013). Modeling melanoblast development. *Cellular and Molecular Life Sciences*, *70*(6), 1067–1079. https://doi.org/10.1007/s00018-012-1112-4

Laurette, P., Strub, T., Koludrovic, D., Keime, C., Gras, S. L., Seberg, H., Otterloo, E. V., Imrichova, H., Siddaway, R., Aerts, S., Cornell, R. A., Mengus, G., & Davidson, I. (2015). Transcription factor MITF and remodeller BRG1 define chromatin organisation at regulatory elements in melanoma cells. *ELife*, *4*, e06857. https://doi.org/10.7554/elife.06857

Le, L., Sirés-Campos, J., Raposo, G., Delevoye, C., & Marks, M. S. (2021). Melanosome biogenesis in the pigmentation of mammalian skin. *Integrative and Comparative Biology*. https://doi.org/10.1093/icb/icab078

Lee, C., Collichio, F., Ollila, D., & Moschos, S. (2013). Historical review of melanoma treatment and outcomes. *Clinics in Dermatology*, *31*(2), 141–147. https://doi.org/10.1016/j.clindermatol.2012.08.015

Lee, K.-W., Yeo, S.-Y., Gong, J.-R., Koo, O.-J., Sohn, I., Lee, W. Y., Kim, H. C., Yun, S. H., Cho, Y. B., Choi, M.-A., An, S., Kim, J., Sung, C. O., Cho, K.-H., & Kim, S.-H. (2022). PRRX1 is a master transcription factor of stromal fibroblasts for myofibroblastic lineage progression. *Nature Communications*, *13*(1), 2793. https://doi.org/10.1038/s41467-022-30484-4

Levy, C., Khaled, M., & Fisher, D. E. (2006). MITF: master regulator of melanocyte development and melanoma oncogene. *Trends in Molecular Medicine*, *12*(9), 406–414. https://doi.org/10.1016/j.molmed.2006.07.008

Lewis, A. E., Vasudevan, H. N., O'Neill, A. K., Soriano, P., & Bush, J. O. (2013). The widely used Wnt1-Cre transgene causes developmental phenotypes by ectopic activation of Wnt signaling. *Developmental Biology*, *379*(2), 229–234. https://doi.org/10.1016/j.ydbio.2013.04.026

Li, J., Weinberg, M. S., Zerbini, L., & Prince, S. (2013). The oncogenic TBX3 is a downstream target and mediator of the TGF-β1 signaling pathway. *Molecular Biology of the Cell*, *24*(22), 3569–3576. https://doi.org/10.1091/mbc.e13-05-0273

Li, M., Knapp, S. K., & Iden, S. (2020). Mechanisms of melanocyte polarity and differentiation: What can we learn from other neuroectoderm-derived lineages? *Current Opinion in Cell Biology*, *67*, 99–108. https://doi.org/10.1016/j.ceb.2020.09.001

Lin, J. Y., & Fisher, D. E. (2007). Melanocyte biology and skin pigmentation. *Nature*, *445*(7130), 843–850. https://doi.org/10.1038/nature05660

Lingbeek, M. E., Jacobs, J. J. L., & Lohuizen, M. van. (2002). The T-box Repressors TBX2 and TBX3Specifically Regulate the Tumor Suppressor Genep14 ARF via a Variant T-site in the Initiator*. *Journal of Biological Chemistry*, *277*(29), 26120–26127. https://doi.org/10.1074/jbc.m200403200

Liu, J., Zheng, R., Zhang, Y., Jia, S., He, Y., & Liu, J. (2023). The Cross Talk between Cellular Senescence and Melanoma: From Molecular Pathogenesis to Target Therapies. *Cancers*, *15*(9), 2640. https://doi.org/10.3390/cancers15092640

Liu, X., Ding, J., & Meng, L. (2018). Oncogene-induced senescence: a double edged sword in cancer. *Acta Pharmacologica Sinica*, *39*(10), 1553–1558. https://doi.org/10.1038/aps.2017.198

Liu, Y., Beyer, A., & Aebersold, R. (2016). On the Dependency of Cellular Protein Levels on mRNA Abundance. *Cell*, *165*(3), 535–550. https://doi.org/10.1016/j.cell.2016.03.014

Long, E., Yin, J., Funderburk, K. M., Xu, M., Feng, J., Kane, A., Zhang, T., Myers, T., Golden, A., Thakur, R., Kong, H., Jessop, L., Kim, E. Y., Jones, K., Chari, R., Machiela, M. J., Yu, K., Consortium, M. M.-A., Iles, M. M., … Choi, J. (2022). Massively parallel reporter assays and variant scoring identified functional variants and target genes for melanoma loci and highlighted cell-type specificity. *The American Journal of Human Genetics*. https://doi.org/10.1016/j.ajhg.2022.11.006

Long, G. V., Swetter, S. M., Menzies, A. M., Gershenwald, J. E., & Scolyer, R. A. (2023). Cutaneous melanoma. *The Lancet*, *402*(10400), 485–502. https://doi.org/10.1016/s0140-6736(23)00821-8

López, S. H., Avetisyan, M., Wright, C. M., Mesbah, K., Kelly, R. G., Moon, A. M., & Heuckeroth, R. O. (2018). Loss of Tbx3 in murine neural crest reduces enteric glia and causes cleft palate, but does not influence heart development or bowel transit. *Developmental Biology*, *444*, S337–S351. https://doi.org/10.1016/j.ydbio.2018.09.017

Loring, J. F., & Erickson, C. A. (1987). Neural crest cell migratory pathways in the trunk of the chick embryo. *Developmental Biology*, *121*(1), 220–236. https://doi.org/10.1016/0012-1606(87)90154-0

Louphrasitthiphol, P., Siddaway, R., Loffreda, A., Pogenberg, V., Friedrichsen, H., Schepsky, A., Zeng, Z., Lu, M., Strub, T., Freter, R., Lisle, R., Suer, E., Thomas, B.,

Schuster-Böckler, B., Filippakopoulos, P., Middleton, M., Lu, X., Patton, E. E., Davidson, I., … Goding, C. R. (2020). Tuning Transcription Factor Availability through Acetylation-Mediated Genomic Redistribution. *Molecular Cell*, *79*(3), 472-487.e10. https://doi.org/10.1016/j.molcel.2020.05.025

Love, M. I., Huber, W., & Anders, S. (2014). Moderated estimation of fold change and dispersion for RNA-seq data with DESeq2. *Genome Biology*, *15*(12), 550. https://doi.org/10.1186/s13059-014-0550-8

Lu, J., Li, X.-P., Dong, Q., Kung, H., & He, M.-L. (2010). TBX2 and TBX3: The special value for anticancer drug targets. *Biochimica et Biophysica Acta (BBA) - Reviews on Cancer*, *1806*(2), 268–274. https://doi.org/10.1016/j.bbcan.2010.07.001

Lu, L., Wang, J., Fang, F., Guo, A., Jiang, S., Tao, Y., Zhang, Y., Li, Y., Zhang, K., Zhang, Z., Zhuo, R., Chu, X., Li, X., Tian, Y., Ma, L., Sang, X., Chen, Y., Yu, J., Yang, Y., … He, H. (2023). LMO2 promotes the development of AML through interaction with transcription co-regulator LDB1. *Cell Death & Disease*, *14*(8), 518. https://doi.org/10.1038/s41419-023-06039-w

Lu, S., Louphrasitthiphol, P., Goradia, N., Lambert, J.-P., Schmidt, J., Chauhan, J., Rughani, M. G., Larue, L., Wilmanns, M., & Goding, C. R. (2021). TBX2 controls a proproliferative gene expression program in melanoma. *Genes & Development*, *35*(23–24), 1657–1677. https://doi.org/10.1101/gad.348746.121

Luciani, F., Champeval, D., Herbette, A., Denat, L., Aylaj, B., Martinozzi, S., Ballotti, R., Kemler, R., Goding, C. R., Vuyst, F. D., Larue, L., & Delmas, V. (2011). Biological and mathematical modeling of melanocyte development. *Development*, *138*(18), 3943–3954. https://doi.org/10.1242/dev.067447

Lüdtke, T. H., Rudat, C., Wojahn, I., Weiss, A.-C., Kleppa, M.-J., Kurz, J., Farin, H. F., Moon, A., Christoffels, V. M., & Kispert, A. (2016). Tbx2 and Tbx3 Act Downstream of Shh to Maintain Canonical Wnt Signaling during Branching Morphogenesis of the Murine Lung. *Developmental Cell*, *39*(2), 239–253. https://doi.org/10.1016/j.devcel.2016.08.007

Ma, J., Weng, L., Bastian, B. C., & Chen, X. (2021). Functional characterization of uveal melanoma oncogenes. *Oncogene*, *40*(4), 806–820. https://doi.org/10.1038/s41388-020-01569-5

Ma, M., Ghosh, S., Tavernari, D., Katarkar, A., Clocchiatti, A., Mazzeo, L., Samarkina, A., Epiney, J., Yu, Y.-R., Ho, P.-C., Levesque, M. P., Özdemir, B. C., Ciriello, G., Dummer, R., & Dotto, G. P. (2020). Sustained androgen receptor signaling is a determinant of melanoma cell growth potential and tumorigenesis. *Journal of Experimental Medicine*, *218*(2), e20201137. https://doi.org/10.1084/jem.20201137

Macrì, S., Simula, L., Pellarin, I., Pegoraro, S., Onorati, M., Sgarra, R., Manfioletti, G., & Vignali, R. (2016). Hmga2 is required for neural crest cell specification in Xenopus laevis. *Developmental Biology*, *411*(1), 25–37. https://doi.org/10.1016/j.ydbio.2016.01.014

Mansoori, B., Mohammadi, A., Ditzel, H. J., Duijf, P. H. G., Khaze, V., Gjerstorff, M. F., & Baradaran, B. (2021). HMGA2 as a Critical Regulator in Cancer Development. *Genes*, *12*(2), 269. https://doi.org/10.3390/genes12020269

Martin, M. (2011). *TECHNICAL NOTES*. https://doi.org/10.14806/ej.17.1.200

Marusyk, A., Almendro, V., & Polyak, K. (2012). Intra-tumour heterogeneity: a looking glass for cancer? *Nature Reviews Cancer*, *12*(5), 323–334. https://doi.org/10.1038/nrc3261

McLean, C. Y., Bristor, D., Hiller, M., Clarke, S. L., Schaar, B. T., Lowe, C. B., Wenger, A. M., & Bejerano, G. (2010). GREAT improves functional interpretation of cis-regulatory regions. *Nature Biotechnology*, *28*(5), 495–501. https://doi.org/10.1038/nbt.1630

Mesbah, K., Rana, M. S., Francou, A., Duijvenboden, K. van, Papaioannou, V. E., Moorman, A. F., Kelly, R. G., & Christoffels, V. M. (2012). Identification of a Tbx1/Tbx2/Tbx3 genetic pathway governing pharyngeal and arterial pole morphogenesis. *Human Molecular Genetics*, *21*(6), 1217–1229. https://doi.org/10.1093/hmg/ddr553

Michaud, E. J., Bultman, S. J., Klebig, M. L., Vugt, M. J. van, Stubbs, L. J., Russell, L. B., & Woychik, R. P. (1994). A molecular model for the genetic and phenotypic characteristics of the mouse lethal yellow (Ay) mutation. *Proceedings of the National Academy of Sciences*, *91*(7), 2562–2566. https://doi.org/10.1073/pnas.91.7.2562

Millar, S. E., Miller, M. W., Stevens, M. E., & Barsh, G. S. (1995). Expression and transgenic studies of the mouse agouti gene provide insight into the mechanisms by which mammalian coat color patterns are generated. *Development*, *121*(10), 3223–3232. https://doi.org/10.1242/dev.121.10.3223

Miller, A. J., & Mihm, M. C. (2006). Melanoma. *The New England Journal of Medicine*, *355*(1), 51–65. https://doi.org/10.1056/nejmra052166

Miskolczi, Z., Smith, M. P., Rowling, E. J., Ferguson, J., Barriuso, J., & Wellbrock, C. (2018). Collagen abundance controls melanoma phenotypes through lineage-specific microenvironment sensing. *Oncogene*, *37*(23), 3166–3182. https://doi.org/10.1038/s41388-018-0209-0

Mitra, D., Luo, X., Morgan, A., Wang, J., Hoang, M. P., Lo, J., Guerrero, C. R., Lennerz, J. K., Mihm, M. C., Wargo, J. A., Robinson, K. C., Devi, S. P., Vanover, J. C., D'Orazio, J. A., McMahon, M., Bosenberg, M. W., Haigis, K. M., Haber, D. A., Wang, Y., & Fisher, D. E. (2012). An ultraviolet-radiation-independent pathway to melanoma carcinogenesis in the red hair/fair skin background. *Nature*, *491*(7424), 449–453. https://doi.org/10.1038/nature11624

Mitsis, T., Efthimiadou, A., Bacopoulou, F., Vlachakis, D., Chrousos, G., & Eliopoulos, E. (2020). Transcription factors and evolution: An integral part of gene expression (Review). *World Academy of Sciences Journal*. https://doi.org/10.3892/wasj.2020.32

Mohan, R. A., Bosada, F. M., Weerd, J. H. van, Duijvenboden, K. van, Wang, J., Mommersteeg, M. T. M., Hooijkaas, I. B., Wakker, V., Vries, C. de G., Coronel, R., Boink, G. J. J., Bakkers, J., Barnett, P., Boukens, B. J., & Christoffels, V. M. (2020). T-box transcription factor 3 governs a transcriptional program for the function of the mouse atrioventricular conduction system. *Proceedings of the National Academy of Sciences*, *117*(31), 18617–18626. https://doi.org/10.1073/pnas.1919379117

Molagoda, I. M. N., Kavinda, M. H. D., Ryu, H. W., Choi, Y. H., Jeong, J.-W., Kang, S., & Kim, G.-Y. (2021). Gamma-Aminobutyric Acid (GABA) Inhibits α-Melanocyte-Stimulating Hormone-Induced Melanogenesis through GABAA and GABAB Receptors. *International Journal of Molecular Sciences*, *22*(15), 8257. https://doi.org/10.3390/ijms22158257

Moon, H., Donahue, L. R., Choi, E., Scumpia, P. O., Lowry, W. E., Grenier, J. K., Zhu, J., & White, A. C. (2017). Melanocyte Stem Cell Activation and Translocation Initiate Cutaneous Melanoma in Response to UV Exposure. *Cell Stem Cell*, *21*(5), 665-678.e6. https://doi.org/10.1016/j.stem.2017.09.001

Moon, H.-R., Jung, J. M., Kim, S. Y., Song, Y., & Chang, S. E. (2020). TGF-β3 suppresses melanogenesis in human melanocytes cocultured with UV-irradiated neighboring cells and human skin. *Journal of Dermatological Science*, *99*(2), 100–108. https://doi.org/10.1016/j.jdermsci.2020.06.007

Moreiras, H., Seabra, M. C., & Barral, D. C. (2021). Melanin Transfer in the Epidermis: The Pursuit of Skin Pigmentation Control Mechanisms. *International Journal of Molecular Sciences*, *22*(9), 4466. https://doi.org/10.3390/ijms22094466

Morgan, M. D., Pairo-Castineira, E., Rawlik, K., Canela-Xandri, O., Rees, J., Sims, D., Tenesa, A., & Jackson, I. J. (2018). Genome-wide study of hair colour in UK Biobank explains most of the SNP heritability. *Nature Communications*, *9*(1), 5271. https://doi.org/10.1038/s41467-018-07691-z

Mort, R. L., Jackson, I. J., & Patton, E. E. (2015). The melanocyte lineage in development and disease. *Development*, *142*(4), 620–632. https://doi.org/10.1242/dev.106567

Motahari, Z., Luna, R. I. M.-D., Viczian, A. S., & Zuber, M. E. (2016). Tbx3 represses bmp4 expression and, with Pax6, is required and sufficient for retina formation. *Development*, *143*(19), 3560–3572. https://doi.org/10.1242/dev.130955

Mountjoy, K. G., Robbins, L. S., Mortrud, M. T., & Cone, R. D. (1992). The Cloning of a Family of Genes That Encode the Melanocortin Receptors. *Science*, *257*(5074), 1248–1251. https://doi.org/10.1126/science.1325670

Moustakas, A. (2008). TGF-β Targets PAX3 to Control Melanocyte Differentiation. *Developmental Cell*, *15*(6), 797–799. https://doi.org/10.1016/j.devcel.2008.11.009

Murakami, M., Matsuzaki, F., & Funaba, M. (2009). Regulation of melanin synthesis by the TGF-β family in B16 melanoma cells. *Molecular Biology Reports*, *36*(6), 1247–1250. https://doi.org/10.1007/s11033-008-9304-6

Nam, S., & Lim, J.-S. (2016). Essential role of interferon regulatory factor 4 (IRF4) in immune cell development. *Archives of Pharmacal Research*, *39*(11), 1548–1555. https://doi.org/10.1007/s12272-016-0854-1

Napolitano, A., Panzella, L., Monfrecola, G., & d'Ischia, M. (2014). Pheomelanin-induced oxidative stress: bright and dark chemistry bridging red hair phenotype and melanoma. *Pigment Cell & Melanoma Research*, *27*(5), 721–733. https://doi.org/10.1111/pcmr.12262

Ni, J., Wang, N., Gao, L., Li, L., Zheng, S., Liu, Y., Ozukum, M., Nikiforova, A., Zhao, G., & Song, Z. (2016). The effect of the NMDA receptor-dependent signaling pathway on cell morphology and melanosome transfer in melanocytes. *Journal of Dermatological Science*, *84*(3), 296–304. https://doi.org/10.1016/j.jdermsci.2016.08.534

Nikolopoulou, E., Galea, G. L., Rolo, A., Greene, N. D. E., & Copp, A. J. (2017). Neural tube closure: cellular, molecular and biomechanical mechanisms. *Development*, *144*(4), 552–566. https://doi.org/10.1242/dev.145904

Nishimura, E. K., Suzuki, M., Igras, V., Du, J., Lonning, S., Miyachi, Y., Roes, J., Beermann, F., & Fisher, D. E. (2010). Key Roles for Transforming Growth Factor β in Melanocyte Stem Cell Maintenance. *Cell Stem Cell*, *6*(2), 130–140. https://doi.org/10.1016/j.stem.2009.12.010

Nordlund, J. J. (2007). The Melanocyte and the Epidermal Melanin Unit: An Expanded Concept. *Dermatologic Clinics*, *25*(3), 271–281. https://doi.org/10.1016/j.det.2007.04.001

Ollmann, M. M., Lamoreux, M. L., Wilson, B. D., & Barsh, G. S. (1998). Interaction of Agouti protein with the melanocortin 1 receptor in vitro and in vivo. *Genes & Development*, *12*(3), 316–330. https://doi.org/10.1101/gad.12.3.316

Olsen, B. R. (2014). Principles of Tissue Engineering (Fourth Edition). *Part 1: The Basis of Growth and Differentiation*, 189–208. https://doi.org/10.1016/b978-0-12-398358-9.00010-0

Opdecamp, K., Nakayama, A., Nguyen, M.-T. T., Hodgkinson, C. A., Pavan, W. J., & Arnheiter, H. (1997). Melanocyte development in vivo and in neural crest cell cultures: crucial dependence on the Mitf basic-helix-loop-helix-zipper transcription factor. *Development*, *124*(12), 2377–2386. https://doi.org/10.1242/dev.124.12.2377

Orkin, S. H. (1995). Hematopoiesis: how does it happen? *Current Opinion in Cell Biology*, *7*(6), 870–877. https://doi.org/10.1016/0955-0674(95)80072-7

Palmer, J. W., Kumar, N., An, L., White, A. C., Mukhtar, M. S., & Harris, M. L. (2023). Molecular heterogeneity of quiescent melanocyte stem cells revealed by single-cell RNA-sequencing. *BioRxiv*, 2023.12.19.571712. https://doi.org/10.1101/2023.12.19.571712

Palumbo, A. (2003). Melanogenesis in the Ink Gland of Sepia officinalis. *Pigment Cell Research*, *16*(5), 517–522. https://doi.org/10.1034/j.1600-0749.2003.00080.x

Pan, Y., Watt, P. J. van der, & Kay, S. A. (2023). E-box binding transcription factors in cancer. *Frontiers in Oncology*, *13*, 1223208. https://doi.org/10.3389/fonc.2023.1223208

Papaioannou, V. E. (2014). The T-box gene family: emerging roles in development, stem cells and cancer. *Development*, *141*(20), 3819–3833. https://doi.org/10.1242/dev.104471

Pape, E. L., Passeron, T., Giubellino, A., Valencia, J. C., Wolber, R., & Hearing, V. J. (2009). Microarray analysis sheds light on the dedifferentiating role of agouti signal protein in murine melanocytes via the Mc1r. *Proceedings of the National Academy of Sciences*, *106*(6), 1802–1807. https://doi.org/10.1073/pnas.0806753106

Pape, E. L., Wakamatsu, K., Ito, S., Wolber, R., & Hearing, V. J. (2008). Regulation of eumelanin/pheomelanin synthesis and visible pigmentation in melanocytes by ligands of the melanocortin 1 receptor. *Pigment Cell & Melanoma Research*, *21*(4), 477–486. https://doi.org/10.1111/j.1755-148x.2008.00479.x

Park, S.-Y., & Kim, J.-S. (2020). A short guide to histone deacetylases including recent progress on class II enzymes. *Experimental & Molecular Medicine*, *52*(2), 204–212. https://doi.org/10.1038/s12276-020-0382-4

Patel, D., Morton, D. J., Carey, J., Havrda, M. C., & Chaudhary, J. (2015). Inhibitor of differentiation 4 (ID4): From development to cancer. *Biochimica et Biophysica Acta (BBA) - Reviews on Cancer*, *1855*(1), 92–103. https://doi.org/10.1016/j.bbcan.2014.12.002

Pavan, W. J., & Sturm, R. A. (2019). The Genetics of Human Skin and Hair Pigmentation. *Annual Review of Genomics and Human Genetics*, *20*(1), 1–32. https://doi.org/10.1146/annurev-genom-083118-015230

Peres, J., Damerell, V., Chauhan, J., Popovic, A., Desprez, P.-Y., Galibert, M.-D., Goding, C. R., & Prince, S. (2021). TBX3 promotes melanoma migration by transcriptional activation of ID1 which prevents activation of E-cadherin by MITF. *Journal of Investigative Dermatology*. https://doi.org/10.1016/j.jid.2021.02.740

Peres, J., Davis, E., Mowla, S., Bennett, D. C., Li, J. A., Wansleben, S., & Prince, S. (2010). The Highly Homologous T-Box Transcription Factors, TBX2 and TBX3, Have Distinct Roles in the Oncogenic Process. *Genes & Cancer*, *1*(3), 272–282. https://doi.org/10.1177/1947601910365160

Peres, J., & Prince, S. (2013). The T-box transcription factor, TBX3, is sufficient to promote melanoma formation and invasion. *Molecular Cancer*, *12*(1), 117. https://doi.org/10.1186/1476-4598-12-117

Perfetto, S. P., Chattopadhyay, P. K., Lamoreaux, L., Nguyen, R., Ambrozak, D., Koup, R. A., & Roederer, M. (2010). Amine-Reactive Dyes for Dead Cell Discrimination in

Fixed Samples. *Current Protocols in Cytometry*, *53*(1), 9.34.1-9.34.14. https://doi.org/10.1002/0471142956.cy0934s53

Perrot, C. Y., Gilbert, C., Marsaud, V., Postigo, A., Javelaud, D., & Mauviel, A. (2013). GLI2 cooperates with ZEB1 for transcriptional repression of CDH1 expression in human melanoma cells. *Pigment Cell & Melanoma Research*, *26*(6), 861–873. https://doi.org/10.1111/pcmr.12149

Pollock, P. M., Harper, U. L., Hansen, K. S., Yudt, L. M., Stark, M., Robbins, C. M., Moses, T. Y., Hostetter, G., Wagner, U., Kakareka, J., Salem, G., Pohida, T., Heenan, P., Duray, P., Kallioniemi, O., Hayward, N. K., Trent, J. M., & Meltzer, P. S. (2003). High frequency of BRAF mutations in nevi. *Nature Genetics*, *33*(1), 19–20. https://doi.org/10.1038/ng1054

Poltorack, C. D., & Dixon, S. J. (2022). Understanding the role of cysteine in ferroptosis: progress & paradoxes. *The FEBS Journal*, *289*(2), 374–385. https://doi.org/10.1111/febs.15842

Praetorius, C., Grill, C., Stacey, S. N., Metcalf, A. M., Gorkin, D. U., Robinson, K. C., Van Otterloo, E., Kim, R. S. Q., Bergsteinsdottir, K., Ogmundsdottir, M. H., Magnusdottir, E., Mishra, P. J., Davis, S. R., Guo, T., Zaidi, M. R., Helgason, A. S., Sigurdsson, M. I., Meltzer, P. S., Merlino, G., … Steingrimsson, E. (2013). A Polymorphism in IRF4 Affects Human Pigmentation through a Tyrosinase-Dependent MITF/TFAP2A Pathway. *Cell*, *155*(5), 1022–1033. https://doi.org/10.1016/j.cell.2013.10.022

Quinlan, A. R., & Hall, I. M. (2010). BEDTools: a flexible suite of utilities for comparing genomic features. *Bioinformatics*, *26*(6), 841–842. https://doi.org/10.1093/bioinformatics/btq033

Rabbie, R., Ferguson, P., Molina-Aguilar, C., Adams, D. J., & Robles-Espinoza, C. D. (2019). Melanoma subtypes: genomic profiles, prognostic molecular markers and therapeutic possibilities. *The Journal of Pathology*, *247*(5), 539–551. https://doi.org/10.1002/path.5213

Raimondi, S., Sera, F., Gandini, S., Iodice, S., Caini, S., Maisonneuve, P., & Fargnoli, M. C. (2008). MC1R variants, melanoma and red hair color phenotype: A meta-analysis. *International Journal of Cancer*, *122*(12), 2753–2760. https://doi.org/10.1002/ijc.23396

Raimondi, S., SUPPA, M., & GANDINI1, S. (2020). Melanoma Epidemiology and Sun Exposure. *Acta Dermato-Venereologica*, *100*(11), 5746. https://doi.org/10.2340/00015555-3491

Rambow, F., Job, B., Petit, V., Gesbert, F., Delmas, V., Seberg, H., Meurice, G., Van Otterloo, E., Dessen, P., Robert, C., Gautheret, D., Cornell, R. A., Sarasin, A., & Larue, L. (2015). New Functional Signatures for Understanding Melanoma Biology from Tumor Cell Lineage-Specific Analysis. *Cell Reports*, *13*(4), 840–853. https://doi.org/10.1016/j.celrep.2015.09.037

Rambow, F., Marine, J.-C., & Goding, C. R. (2019). Melanoma plasticity and phenotypic diversity: therapeutic barriers and opportunities. *Genes & Development*, *33*(19–20), 1295–1318. https://doi.org/10.1101/gad.329771.119

Rambow, F., Rogiers, A., Marin-Bejar, O., Aibar, S., Femel, J., Dewaele, M., Karras, P., Brown, D., Chang, Y. H., Debiec-Rychter, M., Adriaens, C., Radaelli, E., Wolter, P., Bechter, O., Dummer, R., Levesque, M., Piris, A., Frederick, D. T., Boland, G., … Marine, J.-C. (2018). Toward Minimal Residual Disease-Directed Therapy in Melanoma. *Cell*, *174*(4), 843-855.e19. https://doi.org/10.1016/j.cell.2018.06.025

Raposo, G., & Marks, M. S. (2007). Melanosomes — dark organelles enlighten endosomal membrane transport. *Nature Reviews Molecular Cell Biology*, *8*(10), 786–797. https://doi.org/10.1038/nrm2258

Raposo, G., Tenza, D., Murphy, D. M., Berson, J. F., & Marks, M. S. (2001). Distinct Protein Sorting and Localization to Premelanosomes, Melanosomes, and Lysosomes in Pigmented Melanocytic Cells✪. *The Journal of Cell Biology*, *152*(4), 809–824. https://doi.org/10.1083/jcb.152.4.809

Raskin, L., Fullen, D. R., Giordano, T. J., Thomas, D. G., Frohm, M. L., Cha, K. B., Ahn, J., Mukherjee, B., Johnson, T. M., & Gruber, S. B. (2013). Transcriptome Profiling Identifies HMGA2 as a Biomarker of Melanoma Progression and Prognosis. *Journal of Investigative Dermatology*, *133*(11), 2585–2592. https://doi.org/10.1038/jid.2013.197

Rayner, J. E., McMeniman, E. K., Duffy, D. L., De'Ambrosis, B., Smithers, B. M., Jagirdar, K., Lee, K. J., Soyer, H. P., & Sturm, R. A. (2019). Phenotypic and genotypic analysis of amelanotic and hypomelanotic melanoma patients. *Journal of the European Academy of Dermatology and Venereology*, *33*(6), 1076–1083. https://doi.org/10.1111/jdv.15446

Rebecca, V. W., Sondak, V. K., & Smalley, K. S. M. (2012). A brief history of melanoma. *Melanoma Research*, *22*(2), 114–122. https://doi.org/10.1097/cmr.0b013e328351fa4d

Rees, J. L. (2000). The Melanocortin 1 Receptor (MC1R): More Than Just Red Hair. *Pigment Cell Research*, *13*(3), 135–140. https://doi.org/10.1034/j.1600-0749.2000.130303.x

Rezza, A., Wang, Z., Sennett, R., Qiao, W., Wang, D., Heitman, N., Mok, K. W., Clavel, C., Yi, R., Zandstra, P., Ma'ayan, A., & Rendl, M. (2016). Signaling Networks among Stem Cell Precursors, Transit-Amplifying Progenitors, and their Niche in Developing Hair Follicles. *Cell Reports*, *14*(12), 3001–3018. https://doi.org/10.1016/j.celrep.2016.02.078

Rhodes, A. R., Weinstock, M. A., Fitzpatrick, T. B., Mihm, M. C., & Sober, A. J. (1987). Risk Factors for Cutaneous Melanoma: A Practical Method of Recognizing Predisposed Individuals. *JAMA*, *258*(21), 3146–3154. https://doi.org/10.1001/jama.1987.03400210088032

Robbins, L. S., Nadeau, J. H., Johnson, K. R., Kelly, M. A., Roselli-Rehfuss, L., Baack, E., Mountjoy, K. G., & Cone, R. D. (1993). Pigmentation phenotypes of variant

extension locus alleles result from point mutations that alter MSH receptor function. *Cell*, *72*(6), 827–834. https://doi.org/10.1016/0092-8674(93)90572-8

Robles-Remacho, A., Sanchez-Martin, R. M., & Diaz-Mochon, J. J. (2023). Spatial Transcriptomics: Emerging Technologies in Tissue Gene Expression Profiling. *Analytical Chemistry*, *95*(42), 15450–15460. https://doi.org/10.1021/acs.analchem.3c02029

Rodeck, U., Bossler, A., Graeven, U., Fox, F. E., Nowell, P. C., Knabbe, C., & Kari, C. (1994). Transforming growth factor beta production and responsiveness in normal human melanocytes and melanoma cells. *Cancer Research*, *54*(2), 575–581.

Rodriguez, M., Aladowicz, E., Lanfrancone, L., & Goding, C. R. (2008). Tbx3 Represses E-Cadherin Expression and Enhances Melanoma Invasiveness. *Cancer Research*, *68*(19), 7872–7881. https://doi.org/10.1158/0008-5472.can-08-0301

Rossetti, S., Hoogeveen, A. T., Esposito, J., & Sacchi, N. (2010). Loss of MTG16a (CBFA2T3), a novel rDNA repressor, leads to increased ribogenesis and disruption of breast acinar morphogenesis. *Journal of Cellular and Molecular Medicine*, *14*(6a), 1358–1370. https://doi.org/10.1111/j.1582-4934.2009.00982.x

Rossi, M., Pellegrini, C., Cardelli, L., Ciciarelli, V., Nardo, L. D., & Fargnoli, M. C. (2019). Familial Melanoma: Diagnostic and Management Implications. *Dermatology Practical & Conceptual*, *9*(1), 10–16. https://doi.org/10.5826/dpc.0901a03

Rousseau, K., Kauser, S., Pritchard, L. E., Warhurst, A., Oliver, R. L., Slominski, A., Wei, E. T., Thody, A. J., Tobin, D. J., & White, A. (2007). Proopiomelanocortin (POMC), the ACTH/ melanocortin precursor, is secreted by human epidermal keratinocytes and melanocytes and stimulates melanogenesis. *The FASEB Journal*, *21*(8), 1844–1856. https://doi.org/10.1096/fj.06-7398com

Roux, K. J., Kim, D. I., Raida, M., & Burke, B. (2012). A promiscuous biotin ligase fusion protein identifies proximal and interacting proteins in mammalian cells. *Journal of Cell Biology*, *196*(6), 801–810. https://doi.org/10.1083/jcb.201112098

Rydell-Törmänen, K., & Johnson, J. R. (2019). Mouse Cell Culture, Methods and Protocols. *Mouse Cell Culture*, *1940*, 3–22. https://doi.org/10.1007/978-1-4939-9086-3_1

Safe, S., Jin, U.-H., Morpurgo, B., Abudayyeh, A., Singh, M., & Tjalkens, R. B. (2016). Nuclear receptor 4A (NR4A) family – orphans no more. *The Journal of Steroid Biochemistry and Molecular Biology*, *157*, 48–60. https://doi.org/10.1016/j.jsbmb.2015.04.016

Saginala, K., Barsouk, A., Aluru, J. S., Rawla, P., & Barsouk, A. (2021). Epidemiology of Melanoma. *Medical Sciences*, *9*(4), 63. https://doi.org/10.3390/medsci9040063

Sakai, C., Ollmann, M., Kobayashi, T., Abdel-Malek, Z., Muller, J., Vieira, W. D., Imokawa, G., Barsh, G. S., & Hearing, V. J. (1997). Modulation of murine melanocyte

function in vitro by agouti signal protein. *The EMBO Journal*, *16*(12), 3544–3552. https://doi.org/10.1093/emboj/16.12.3544

Salaverria, I., Akasaka, T., Gesk, S., Szczepanowski, M., Burkhardt, B., Harder, L., Damm-Welk, C., Oschlies, I., Klapper, W., Dyer, M. J. S., & Siebert, R. (2012). The CBFA2T3/ACSF3 locus is recurrently involved in IGH chromosomal translocation t(14;16)(q32;q24) in pediatric B-cell lymphoma with germinal center phenotype. *Genes, Chromosomes and Cancer*, *51*(4), 338–343. https://doi.org/10.1002/gcc.21919

Samarkina, A., Youssef, M. K., Ostano, P., Ghosh, S., Ma, M., Tassone, B., Proust, T., Chiorino, G., Levesque, M. P., Goruppi, S., & Dotto, G. P. (2023). Androgen receptor is a determinant of melanoma targeted drug resistance. *Nature Communications*, *14*(1), 6498. https://doi.org/10.1038/s41467-023-42239-w

Sauka-Spengler, T., & Bronner-Fraser, M. (2008). A gene regulatory network orchestrates neural crest formation. *Nature Reviews Molecular Cell Biology*, *9*(7), 557–568. https://doi.org/10.1038/nrm2428

Schiöth, H. B., Phillips, S. R., Rudzish, R., Birch-Machin, M. A., Wikberg, J. E. S., & Rees, J. L. (1999). Loss of Function Mutations of the Human Melanocortin 1 Receptor Are Common and Are Associated with Red Hair. *Biochemical and Biophysical Research Communications*, *260*(2), 488–491. https://doi.org/10.1006/bbrc.1999.0935

Schmierer, B., & Hill, C. S. (2007). TGFβ–SMAD signal transduction: molecular specificity and functional flexibility. *Nature Reviews Molecular Cell Biology*, *8*(12), 970–982. https://doi.org/10.1038/nrm2297

Searle, A. G. (1968). An Extension Series in the Mouse. *Journal of Heredity*, *59*(6), 341–342. https://doi.org/10.1093/oxfordjournals.jhered.a107739

Seberg, H. E., Otterloo, E. V., Loftus, S. K., Liu, H., Bonde, G., Sompallae, R., Gildea, D. E., Santana, J. F., Manak, J. R., Pavan, W. J., Williams, T., & Cornell, R. A. (2017). TFAP2 paralogs regulate melanocyte differentiation in parallel with MITF. *PLoS Genetics*, *13*(3), e1006636. https://doi.org/10.1371/journal.pgen.1006636

Sensi, M., Nicolini, G., Petti, C., Bersani, I., Lozupone, F., Molla, A., Vegetti, C., Nonaka, D., Mortarini, R., Parmiani, G., Fais, S., & Anichini, A. (2006). Mutually exclusive NRASQ61R and BRAFV600E mutations at the single-cell level in the same human melanoma. *Oncogene*, *25*(24), 3357–3364. https://doi.org/10.1038/sj.onc.1209379

Serrano, M., Hannon, G. J., & Beach, D. (1993). A new regulatory motif in cell-cycle control causing specific inhibition of cyclin D/CDK4. *Nature*, *366*(6456), 704–707. https://doi.org/10.1038/366704a0

Seyfried, T. N., & Huysentruyt, L. C. (2012). On the Origin of Cancer Metastasis. *Critical Reviews in Oncogenesis*, *18*(1–2), 43–73. https://doi.org/10.1615/critrevoncog.v18.i1-2.40

Shain, A. H., & Bastian, B. C. (2016). From melanocytes to melanomas. *Nature Reviews Cancer*, *16*(6), 345–358. https://doi.org/10.1038/nrc.2016.37

Sheeba, C. J., & Logan, M. P. O. (2017). Chapter Twelve The Roles of T-Box Genes in Vertebrate Limb Development. *Current Topics in Developmental Biology*, *122*, 355–381. https://doi.org/10.1016/bs.ctdb.2016.08.009

Shin, H.-J., Gil, M., & Lee, I.-S. (2022). Association of Elevated Expression Levels of COL4A1 in Stromal Cells with an Immunosuppressive Tumor Microenvironment in Low-Grade Glioma, Pancreatic Adenocarcinoma, Skin Cutaneous Melanoma, and Stomach Adenocarcinoma. *Journal of Personalized Medicine*, *12*(4), 534. https://doi.org/10.3390/jpm12040534

Silvers, W. K. (1979). *The Coat Colors of Mice, A Model for Mammalian Gene Action and Interaction*. 6–44. https://doi.org/10.1007/978-1-4612-6164-3_2

Singh, R., Hoogaars, W. M., Barnett, P., Grieskamp, T., Rana, M. S., Buermans, H., Farin, H. F., Petry, M., Heallen, T., Martin, J. F., Moorman, A. F. M., Hoen, P. A. C. 't, Kispert, A., & Christoffels, V. M. (2012). Tbx2 and Tbx3 induce atrioventricular myocardial development and endocardial cushion formation. *Cellular and Molecular Life Sciences*, *69*(8), 1377–1389. https://doi.org/10.1007/s00018-011-0884-2

Slominski, A., Plonka, P. M., Pisarchik, A., Smart, J. L., Tolle, V., Wortsman, J., & Low, M. J. (2005). Preservation of Eumelanin Hair Pigmentation in Proopiomelanocortin-Deficient Mice on a Nonagouti (a/a) Genetic Background. *Endocrinology*, *146*(3), 1245–1253. https://doi.org/10.1210/en.2004-0733

Smith, A. G., Lim, W., Pearen, M., Muscat, G. E. O., & Sturm, R. A. (2011). Regulation of NR4A nuclear receptor expression by oncogenic BRAF in melanoma cells. *Pigment Cell & Melanoma Research*, *24*(3), 551–563. https://doi.org/10.1111/j.1755-148x.2011.00843.x

Smith, A. G., Luk, N., Newton, R. A., Roberts, D. W., Sturm, R. A., & Muscat, G. E. O. (2008). Melanocortin-1 Receptor Signaling Markedly Induces the Expression of the NR4A Nuclear Receptor Subgroup in Melanocytic Cells*. *Journal of Biological Chemistry*, *283*(18), 12564–12570. https://doi.org/10.1074/jbc.m800480200

Snodgrass, S. R. (1992). GABA and Epilepsy: Their Complex Relationship and the Evolution of Our Understanding. *Journal of Child Neurology*, *7*(1), 77–86. https://doi.org/10.1177/088307389200700114

Song, H., & Morrow, B. E. (2023). Tbx2 and Tbx3 regulate cell fate progression of the otic vesicle for inner ear development. *Developmental Biology*, *494*, 71–84. https://doi.org/10.1016/j.ydbio.2022.12.003

Sterchi, D. L. (2008). Theory and Practice of Histological Techniques (Sixth Edition). *Theory and Practice of Histological Techniques*, 537–558. https://doi.org/10.1016/b978-0-443-10279-0.50033-6

Steudle, F., Rehman, S., Bampali, K., Simeone, X., Rona, Z., Hauser, E., Schmidt, W. M., Scholze, P., & Ernst, M. (2020). A novel de novo variant of GABRA1 causes increased sensitivity for GABA in vitro. *Scientific Reports*, *10*(1), 2379. https://doi.org/10.1038/s41598-020-59323-6

Strub, T., Giuliano, S., Ye, T., Bonet, C., Keime, C., Kobi, D., Gras, S. L., Cormont, M., Ballotti, R., Bertolotto, C., & Davidson, I. (2011). Essential role of microphthalmia transcription factor for DNA replication, mitosis and genomic stability in melanoma. *Oncogene*, *30*(20), 2319–2332. https://doi.org/10.1038/onc.2010.612

Su, L., Deng, Z., & Leng, F. (2020). The Mammalian High Mobility Group Protein AT-Hook 2 (HMGA2): Biochemical and Biophysical Properties, and Its Association with Adipogenesis. *International Journal of Molecular Sciences*, *21*(10), 3710. https://doi.org/10.3390/ijms21103710

Sulem, P., Gudbjartsson, D. F., Stacey, S. N., Helgason, A., Rafnar, T., Jakobsdottir, M., Steinberg, S., Gudjonsson, S. A., Palsson, A., Thorleifsson, G., Pálsson, S., Sigurgeirsson, B., Thorisdottir, K., Ragnarsson, R., Benediktsdottir, K. R., Aben, K. K., Vermeulen, S. H., Goldstein, A. M., Tucker, M. A., … Stefansson, K. (2008). Two newly identified genetic determinants of pigmentation in Europeans. *Nature Genetics*, *40*(7), 835–837. https://doi.org/10.1038/ng.160

Sulem, P., Gudbjartsson, D. F., Stacey, S. N., Helgason, A., Rafnar, T., Magnusson, K. P., Manolescu, A., Karason, A., Palsson, A., Thorleifsson, G., Jakobsdottir, M., Steinberg, S., Pálsson, S., Jonasson, F., Sigurgeirsson, B., Thorisdottir, K., Ragnarsson, R., Benediktsdottir, K. R., Aben, K. K., … Stefansson, K. (2007). Genetic determinants of hair, eye and skin pigmentation in Europeans. *Nature Genetics*, *39*(12), 1443–1452. https://doi.org/10.1038/ng.2007.13

Sun, Q., Lee, W., Hu, H., Ogawa, T., Leon, S. D., Katehis, I., Lim, C. H., Takeo, M., Cammer, M., Taketo, M. M., Gay, D. L., Millar, S. E., & Ito, M. (2023). Dedifferentiation maintains melanocyte stem cells in a dynamic niche. *Nature*, 1–9. https://doi.org/10.1038/s41586-023-05960-6

Swanda, R. V., Ji, Q., Wu, X., Yan, J., Dong, L., Mao, Y., Uematsu, S., Dong, Y., & Qian, S.-B. (2023). Lysosomal cystine governs ferroptosis sensitivity in cancer via cysteine stress response. *Molecular Cell*. https://doi.org/10.1016/j.molcel.2023.08.004

Switonski, M., Mankowska, M., & Salamon, S. (2013). Family of melanocortin receptor (MCR) genes in mammals—mutations, polymorphisms and phenotypic effects. *Journal of Applied Genetics*, *54*(4), 461–472. https://doi.org/10.1007/s13353-013-0163-z

Tadjuidje, E., & Hegde, R. S. (2013). The Eyes Absent proteins in development and disease. *Cellular and Molecular Life Sciences*, *70*(11), 1897–1913. https://doi.org/10.1007/s00018-012-1144-9

Tagore, M., Hergenreder, E., Perlee, S. C., Cruz, N. M., Menocal, L., Suresh, S., Chan, E., Baron, M., Melendez, S., Dave, A., Chatila, W. K., Nsengimana, J., Koche, R. P., Hollmann, T. J., Ideker, T., Studer, L., Schietinger, A., & White, R. M. (2023). GABA regulates electrical activity and tumor initiation in melanoma. *Cancer Discovery*, *13*(10), 2270–2291. https://doi.org/10.1158/2159-8290.cd-23-0389

Tamate, H. B., & Takeuchi, T. (1984). Action of the e Locus of Mice in the Response of Phaeomelanic Hair Follicles to α-Melanocyte-Stimulating Hormone in Vitro. *Science*, *224*(4654), 1241–1242. https://doi.org/10.1126/science.6328651

Tang, Y., Durand, S., Dalle, S., & Caramel, J. (2020). EMT-Inducing Transcription Factors, Drivers of Melanoma Phenotype Switching, and Resistance to Treatment. *Cancers*, *12*(8), 2154. https://doi.org/10.3390/cancers12082154

Theveneau, E., & Mayor, R. (2012a). Neural crest delamination and migration: From epithelium-to-mesenchyme transition to collective cell migration. *Developmental Biology*, *366*(1), 34–54. https://doi.org/10.1016/j.ydbio.2011.12.041

Theveneau, E., & Mayor, R. (2012b). Neural crest migration: interplay between chemorepellents, chemoattractants, contact inhibition, epithelial–mesenchymal transition, and collective cell migration. *Wiley Interdisciplinary Reviews: Developmental Biology*, *1*(3), 435–445. https://doi.org/10.1002/wdev.28

Thomas, A. J., & Erickson, C. A. (2009). FOXD3 regulates the lineage switch between neural crest-derived glial cells and pigment cells by repressing MITF through a non-canonical mechanism. *Development*, *136*(11), 1849–1858. https://doi.org/10.1242/dev.031989

Torre, L. A., Bray, F., Siegel, R. L., Ferlay, J., Lortet-Tieulent, J., & Jemal, A. (2015). Global cancer statistics, 2012. *CA: A Cancer Journal for Clinicians*, *65*(2), 87–108. https://doi.org/10.3322/caac.21262

Tsao, H., Chin, L., Garraway, L. A., & Fisher, D. E. (2012). Melanoma: from mutations to medicine. *Genes & Development*, *26*(11), 1131–1155. https://doi.org/10.1101/gad.191999.112

Tsoi, J., Robert, L., Paraiso, K., Galvan, C., Sheu, K. M., Lay, J., Wong, D. J. L., Atefi, M., Shirazi, R., Wang, X., Braas, D., Grasso, C. S., Palaskas, N., Ribas, A., & Graeber, T. G. (2018). Multi-stage Differentiation Defines Melanoma Subtypes with Differential Vulnerability to Drug-Induced Iron-Dependent Oxidative Stress. *Cancer Cell*, *33*(5), 890-904.e5. https://doi.org/10.1016/j.ccell.2018.03.017

Vandamme, N., & Berx, G. (2019). From neural crest cells to melanocytes: cellular plasticity during development and beyond. *Cellular and Molecular Life Sciences*, *76*(10), 1919–1934. https://doi.org/10.1007/s00018-019-03049-w

Vega-Benedetti, A. F., Saucedo, C., Zavattari, P., Vanni, R., Zugaza, J. L., & Parada, L. A. (2017). PLAGL1: an important player in diverse pathological processes. *Journal of Applied Genetics*, *58*(1), 71–78. https://doi.org/10.1007/s13353-016-0355-4

Vega-Lopez, G. A., Cerrizuela, S., Tribulo, C., & Aybar, M. J. (2018). Neurocristopathies: New Insights 150 Years After the Neural Crest Discovery. *Developmental Biology*, *444*, S110–S143. https://doi.org/10.1016/j.ydbio.2018.05.013

Visser, M., Kayser, M., & Palstra, R.-J. (2012). HERC2 rs12913832 modulates human pigmentation by attenuating chromatin-loop formation between a long-range enhancer and the OCA2 promoter. *Genome Research*, *22*(3), 446–455. https://doi.org/10.1101/gr.128652.111

Voisey, J., Gomez-Cabrera, M. del C., Smit, D. J., Leonard, J. H., Sturm, R. A., & Daal, A. V. (2006). A polymorphism in the agouti signalling protein (ASIP) is associated with decreased levels of mRNA. *Pigment Cell Research*, *19*(3), 226–231. https://doi.org/10.1111/j.1600-0749.2006.00301.x

Vredeveld, L. C. W., Possik, P. A., Smit, M. A., Meissl, K., Michaloglou, C., Horlings, H. M., Ajouaou, A., Kortman, P. C., Dankort, D., McMahon, M., Mooi, W. J., & Peeper, D. S. (2012). Abrogation of BRAFV600E-induced senescence by PI3K pathway activation contributes to melanomagenesis. *Genes & Development*, *26*(10), 1055–1069. https://doi.org/10.1101/gad.187252.112

Wagstaff, W., Mwamba, R. N., Grullon, K., Armstrong, M., Zhao, P., Hendren-Santiago, B., Qin, K. H., Li, A. J., Hu, D. A., Youssef, A., Reid, R. R., Luu, H. H., Shen, L., He, T.-C., & Haydon, R. C. (2022). Melanoma --- Molecular genetics, metastasis, targeted therapies, immunotherapies, and therapeutic resistance. *Genes & Diseases*, *9*(6), 1608–1623. https://doi.org/10.1016/j.gendis.2022.04.004

Walker, W. P., & Gunn, T. M. (2010). Shades of meaning: the pigment-type switching system as a tool for discovery. *Pigment Cell & Melanoma Research*, *23*(4), 485–495. https://doi.org/10.1111/j.1755-148x.2010.00721.x

Wang, C., Li, H., Guo, Y., Huang, J., Sun, Y., Min, J., Wang, J., Fang, X., Zhao, Z., Wang, S., Zhang, Y., Liu, Q., Jiang, Q., Wang, X., Guo, Y., Yang, C., Wang, Y., Tian, F., Zhuang, G., … Zhong, J. (2020). Donkey genomes provide new insights into domestication and selection for coat color. *Nature Communications*, *11*(1), 6014. https://doi.org/10.1038/s41467-020-19813-7

Wang, L., Yao, Z. Q., Moorman, J. P., Xu, Y., & Ning, S. (2014). Gene Expression Profiling Identifies IRF4-Associated Molecular Signatures in Hematological Malignancies. *PLoS ONE*, *9*(9), e106788. https://doi.org/10.1371/journal.pone.0106788

Wansleben, S., Peres, J., Hare, S., Goding, C. R., & Prince, S. (2014). T-box transcription factors in cancer biology. *Biochimica et Biophysica Acta (BBA) - Reviews on Cancer*, *1846*(2), 380–391. https://doi.org/10.1016/j.bbcan.2014.08.004

Washkowitz, A. J., Gavrilov, S., Begum, S., & Papaioannou, V. E. (2012). Diverse functional networks of Tbx3 in development and disease. *Wiley Interdisciplinary Reviews: Systems Biology and Medicine*, *4*(3), 273–283. https://doi.org/10.1002/wsbm.1162

Wehrle-Haller, B. (2003). The Role of Kit-Ligand in Melanocyte Development and Epidermal Homeostasis. *Pigment Cell Research*, *16*(3), 287–296. https://doi.org/10.1034/j.1600-0749.2003.00055.x

Wehrle-Haller, B., & Weston, J. A. (1995). Soluble and cell-bound forms of steel factor activity play distinct roles in melanocyte precursor dispersal and survival on the lateral neural crest migration pathway. *Development*, *121*(3), 731–742. https://doi.org/10.1242/dev.121.3.731

Weston, J. A. (1991). 6 Sequential Segregation and Fate of Developmentally Restricted Intermediate Cell Populations in the Neural Crest Lineage. *Current Topics in Developmental Biology*, *25*, 133–153. https://doi.org/10.1016/s0070-2153(08)60414-7

Wet, J. R. de, Wood, K. V., DeLuca, M., Helinski, D. R., & Subramani, S. (1987). Firefly Luciferase Gene: Structure and Expression in Mammalian Cells. *Molecular and Cellular Biology*, *7*(2), 725–737. https://doi.org/10.1128/mcb.7.2.725-737.1987

Wet, J. R. de, Wood, K. V., Helinski, D. R., & DeLuca, M. (1985). Cloning of firefly luciferase cDNA and the expression of active luciferase in Escherichia coli. *Proceedings of the National Academy of Sciences*, *82*(23), 7870–7873. https://doi.org/10.1073/pnas.82.23.7870

Whiteman, D. C., Green, A. C., & Olsen, C. M. (2016). The Growing Burden of Invasive Melanoma: Projections of Incidence Rates and Numbers of New Cases in Six Susceptible Populations through 2031. *Journal of Investigative Dermatology*, *136*(6), 1161–1171. https://doi.org/10.1016/j.jid.2016.01.035

Willmer, T., Cooper, A., Peres, J., Omar, R., & Prince, S. (2017). The T-Box transcription factor 3 in development and cancer. *BioScience Trends*, *11*(3), 2017.01043. https://doi.org/10.5582/bst.2017.01043

Willmer, T., Peres, J., Mowla, S., Abrahams, A., & Prince, S. (2015). The T-Box factor TBX3 is important in S-phase and is regulated by c-Myc and cyclin A-CDK2. *Cell Cycle*, *14*(19), 3173–3183. https://doi.org/10.1080/15384101.2015.1080398

Wong, R. W. J., Ong, J. Z. L., Theardy, M. S., & Sanda, T. (2022). IRF4 as an Oncogenic Master Transcription Factor. *Cancers*, *14*(17), 4314. https://doi.org/10.3390/cancers14174314

Wood, K. V., Wet, J. R. de, Dewji, N., & DeLuca, M. (1984). Synthesis of active firefly luciferase by in vitro translation of RNA obtained from adult lanterns. *Biochemical and Biophysical Research Communications*, *124*(2), 592–596. https://doi.org/10.1016/0006-291x(84)91595-x

Wu, X., Jin, S., Yang, Y., Lu, X., Dai, X., Xu, Z., Zhang, C., & Xiang, L. F. (2022). Altered expression of ferroptosis markers and iron metabolism reveals a potential role of ferroptosis in vitiligo. *Pigment Cell & Melanoma Research*. https://doi.org/10.1111/pcmr.13032

Yang, C., Croteau, S., & Hardy, P. (2021). Histone deacetylase (HDAC) 9: versatile biological functions and emerging roles in human cancer. *Cellular Oncology*, *44*(5), 997–1017. https://doi.org/10.1007/s13402-021-00626-9

Yang, G., Li, Y., Nishimura, E. K., Xin, H., Zhou, A., Guo, Y., Dong, L., Denning, M. F., Nickoloff, B. J., & Cui, R. (2008). Inhibition of PAX3 by TGF-β Modulates Melanocyte Viability. *Molecular Cell*, *32*(4), 554–563. https://doi.org/10.1016/j.molcel.2008.11.002

Yin, K., Chhabra, Y., Tropée, R., Lim, Y. C., Fane, M., Dray, E., Sturm, R. A., & Smith, A. G. (2017). NR4A2 Promotes DNA Double-strand Break Repair Upon Exposure to UVR. *Molecular Cancer Research*, *15*(9), 1184–1196. https://doi.org/10.1158/1541-7786.mcr-17-0002

Yin, K., Sturm, R. A., & Smith, A. G. (2014). MC1R and NR4A receptors in cellular stress and DNA repair: implications for UVR protection. *Experimental Dermatology*, *23*(7), 449–452. https://doi.org/10.1111/exd.12420

Yokoyama, S., Takahashi, A., Kikuchi, R., Nishibu, S., Lo, J. A., Hejna, M., Moon, W. M., Kato, S., Zhou, Y., Hodi, F. S., Song, J. S., Sakurai, H., Fisher, D. E., & Hayakawa, Y. (2021). SOX10 regulates melanoma immunogenicity through an IRF4-IRF1 axis. *Cancer Research*, *81*(24), canres.2078.2021. https://doi.org/10.1158/0008-5472.can-21-2078

Yu, G., Wang, L.-G., & He, Q.-Y. (2015). ChIPseeker: an R/Bioconductor package for ChIP peak annotation, comparison and visualization. *Bioinformatics*, *31*(14), 2382–2383. https://doi.org/10.1093/bioinformatics/btv145

Zhang, M., Du, S., Ou, H., Cui, R., Jiang, N., Lin, Y., Ge, R., Ma, D., & Zhang, J. (2021). Ablation of Zfhx4 results in early postnatal lethality by disrupting the respiratory center in mice. *Journal of Molecular Cell Biology*, *13*(3), 210–224. https://doi.org/10.1093/jmcb/mjaa081

Zhang, T., Choi, J., Kovacs, M. A., Shi, J., Xu, M., Program, N. C. S., Consortium, M. M.-A., Goldstein, A. M., Trower, A. J., Bishop, D. T., Iles, M. M., Duffy, D. L., MacGregor, S., Amundadottir, L. T., Law, M. H., Loftus, S. K., Pavan, W. J., Brown, K. M., Lee, J. E., … Young, A. C. (2018). Cell-type–specific eQTL of primary melanocytes facilitates identification of melanoma susceptibility genes. *Genome Research*, *28*(11), 1621–1635. https://doi.org/10.1101/gr.233304.117

Zhang, Y., Liu, T., Meyer, C. A., Eeckhoute, J., Johnson, D. S., Bernstein, B. E., Nusbaum, C., Myers, R. M., Brown, M., Li, W., & Liu, X. S. (2008). Model-based Analysis of ChIP-Seq (MACS). *Genome Biology*, *9*(9), R137. https://doi.org/10.1186/gb-2008-9-9-r137

Zhang, Y., Xiong, Y., & Yarbrough, W. G. (1998). ARF Promotes MDM2 Degradation and Stabilizes p53: ARF-INK4a Locus Deletion Impairs Both the Rb and p53 Tumor Suppression Pathways. *Cell*, *92*(6), 725–734. https://doi.org/10.1016/s0092-8674(00)81401-4

Zhou, J. J., Huang, Y., Zhang, X., Cheng, Y., Tang, L., & Ma, X. (2017). Eyes absent gene (EYA1) is a pathogenic driver and a therapeutic target for melanoma. *Oncotarget*, *8*(62), 105081–105092. https://doi.org/10.18632/oncotarget.21352

Zhou, Q., Liu, M., Xia, X., Gong, T., Feng, J., Liu, W., Liu, Y., Zhen, B., Wang, Y., Ding, C., & Qin, J. (2017). A mouse tissue transcription factor atlas. *Nature Communications*, *8*(1), 15089. https://doi.org/10.1038/ncomms15089

Zhu, C., Liu, C., & Chai, Z. (2023). Role of the PADI family in inflammatory autoimmune diseases and cancers: A systematic review. *Frontiers in Immunology*, *14*, 1115794. https://doi.org/10.3389/fimmu.2023.1115794